Dissertation

submitted to the
Combined Faculties for the Natural Sciences and for Mathematics
of the Ruprecht – Karls University of Heidelberg, Germany
for the degree of

Doctor of Natural Sciences

Agnieszka Religa

born in Wroclaw, Poland

April 2010

The expected and unexpected roles of *Plasmodium* telomere-associated proteins; Telomerase, SIR2A and SIR2B

Agnieszka Religa

Supervisors:

Prof. dr. M. Lanzer
University of Heidelberg, Heidelberg

Prof. dr. A.P. Waters
University of Glasgow, Glasgow

The work described was carried out at the Leiden University Medical Centre, Leiden, the Netherlands and at the Glasgow Biomedical Research Centre, University of Glasgow, Scotland, UK, under the supervision of Prof. Andy Waters and Dr. Chris Janse, between November 2006 and March 2010.

Author’s declaration

I hereby declare that I have written the submitted dissertation myself and in this process have used no other sources or materials than those expressly indicated. I have not applied to be examined at any other institution, nor have I used the dissertation in this or any other form at any other institution as an examination paper, nor submitted it to any other faculty as a dissertation.

Agnieszka Religa

Summary

Telomeres define the ends of eukaryotic chromosomes, and are covered by a number of proteins (collectively called the telosome), which protect the telomeres from degradation, thereby ensuring genome stability. One highly conserved telosome protein identified in *Plasmodium* is a histone (protein) deacetylase silent information regulator 2 (PfSIR2A) and its distant homologue SIR2B (PfSIR2B). The *P. falciparum* SIR2A appears crucial in the regulation of multigene families (e.g. *var* genes) involved in a process called antigenic variation, which is the mechanism in which pathogenic organisms alter their surface antigens in order to evade the host immune system. Deletion of either *Pfsir2a* or *Pfsir2b* causes transcriptional up-regulation of distinct types of *var* genes in the early asexual blood stages.

Orthologues of the two *P. falciparum sir2* genes have been identified in all genome-sequenced *Plasmodium* species, including the rodent malaria parasite *P. berghei*. Three *P. berghei* lines lacking *Pbsir2a*, *Pbsir2b* and uniquely lacking *sir2a* and *sir2b* genes were obtained and cloned. When propagated in mouse infections no gross alterations were observed in asexual blood stage growth, multiplication or virulence of all 3 parasite mutants. Global transcriptome analysis of asexual blood stages of the double deletion mutant (*Pbsir2a*$^{-}$/*Pbsir2b*$^{-}$) demonstrated deregulation of subtelomeric gene families (*bir, Pb-fam*) implicated in the process of antigenic variation, confirming the mode of gene regulation exercised by SIR2 shown in *P. falciparum. Pbsir2b* deletion had no effect on parasite growth throughout the complete life cycle excluding an essential role for SIR2B in parasite development in the mosquito and host liver. Unexpectedly, development of parasites lacking PbSIR2A was completely blocked in the mosquito host at the ookinete-to-oocyst transition. Using transgenic parasites expressing a GFP-tagged PbSIR2A protein we found a hitherto uncharacterised non-nuclear localisation focused to the apical end of the ookinete. Moreover, morphological analysis and examination of the distribution and concentration of several micronemal proteins as well as a preliminary examination of general protein acetylation status in mutant ookinetes suggests an aberrant functioning of the apical apparatus that might minimally affect ookinete motility. These results imply that SIR2A might play a role during attachment/invasion/traversal of the ookinete of the mosquito midgut wall.

Another protein of crucial importance to telomere biology is the highly conserved telomerase holoenzyme, which functions as “telomere length guard”. With each cell division telomeres shorten due to the so-called end-replication problem. The ribonucleoprotein telomerase reverse transcriptase (TERT) – the core subunit of the telomerase complex adds new telomeric repeats to the 3’ G-rich chromosome end, preventing premature cell senescence and eventual death (the delayed death phenotype), observed in TERT- and TR-deficient cells of plants, yeast, protozoa and mammals, in which telomerase is the major player in telomere maintenance pathway. *Plasmodium* telomere length is stably maintained during blood stage proliferation, and TERT activity is detectable at the trophozoite and schizont blood stages where DNA replication occurs. TERT has been widely explored as a drug target in e.g. cancer cells, and was shown to effectively inhibit cancer growth. Unpublished preliminary data from the nucleoside analogue drug testing on *P. falciparum in vitro* culture show parasites are killed after 3 – 5 blood stage cycles at micromolar concentrations (A. Scherf, Institute Pasteur). A recently published evaluation of several compounds indicated that delavirdine (a non-nucleoside reverse transcriptase inhibitor) has high anti-malarial activity *in vitro* against liver stage of *P. yoelii*. In support of these data, negative effects of TERT absence can be seen from attempts to delete *P. berghei tert*. Despite the presence of *tert*$^{-}$ parasites in the initial transfection population, the *tert*$^{-}$ clones could not be obtained, which is in agreement with the expected delayed death phenotype, observed in other organisms. A more extensive cloning of the parasites revealed no positive clones. The obtained results prove TERT to be essential in *Plasmodium* development and designate anti-telomerase drugs as plausible auxiliaries in the treatment of malaria infections.

Zusammenfassung

Telomere begrenzen die Enden eukaryotischer Chromosomen und sind mit einer als Telosomen bezeichneten Gruppe von Proteinen bedeckt, die die Telomere vor deren Abbau schützen und somit die Stabilität des Genoms sicherstellen. In *Plasmodium* wurde ein hoch konserviertes Telosom Protein identifiziert, das *histone (protein) deacetylase silent information regulator 2* Protein (PfSIR2A) und sein Homolog SIR2B. Das *P. falciparum* SIR2A Protein scheint eine kritische Rolle bei der Regulation von Multigen Familien (z. B. *var* Gene) zu spielen, die in den Prozess der Antigenvariation involviert sind, ein Mechanismus der es pathogenen Organismen erlaubt ihre Oberflächenantigene zu verändern um dem Immunsystem ihres Wirts zu entgehen. Eine Deletion von *Pfsir2a* oder *Pfsir2b* führt zur Hochregulierung der Transkription bestimmter *var* Gene in den jungen asexuellen Blutstadien.

Orthologe der beiden *sir2* Gene von *P. falciparum* wurden in allen *Plasmodium* Arten gefunden, deren Genome bis dato sequenziert wurden, einschliesslich dem des Nagerparasiten *P. berghei*. Drei *P. berghei* Zelllinien wurden generiert und geklont, denen entweder *Pbsir2a* oder *Pbsir2b* oder sowohl *Pbsir2a* als auch *Pbsir2b* fehlen. In der Maus wurden keine Veränderungen beim Wachstum der asexuellen Blutstadien, der Vermehrungsrate oder der Virulenz der drei mutierten Parasitenlinien beobachtet. Die Analyses des Transkriptoms der asexuellen Blutstadien der Doppel-Nullmutante (*Pbsir2a*$^{-}$*/Pbsir2b*$^{-}$) zeigte eine Deregulierung von Genfamilien in der sub-telomer Region (*bir*, *Pb-fam*), die mit dem Prozess der Antigenvariation in Verbindung stehen und bestätigte die Art der Genregulation durch SIR2, die für *P. falciparum* gezeigt wurde. Die Deletion von *Pbsir2b* hatte keinerlei Effekt auf das Wachstum der Parasiten während des gesamten Lebenszyklus, weshalb eine essenzielle Rolle des SIR2B Proteins für die Entwicklung der Moskito und Leberstadien ausgeschlossen werden kann. Die Deletion des *Pbsir2a* Gens führte jedoch zu einer unerwarteten Blockade der Entwicklung der Parasiten im Moskito beim Übergang vom Ookineten zum Oozysten Stadium. Bei der Analyse transgener Parasiten die eine GFP-markierte Form von PbSIR2A exprimieren, beobachteten wir eine bisher nicht charakterisierte Lokalisierung ausserhalb des Zellkerns am apikalen Pol der Ookinete. Morphologische Studien und die Untersuchung der Verteilung und Konzentration mehrerer micronemaler Proteine sowie einleitende Untersuchungen des Acetylierungsstatus von Proteinen in den mutierten Ookineten deuten auf eine aberrante Funktion des apikallen Apparates hin, welche womöglich einen minimalen Effekt auf die Motilität der Ookinete hat. Diese Ergebnisse weisen auf eine mögliche Funktion von SIR2A während der Anheftung/ Invasion/ Durchquerung der Ookinete durch die Mitteldarmwand des Moskitos hin.

Ein weiteres Protein das für die Funktion der Telomere kritisch ist, ist das hoch konservierte Telomerase Holoenzym, welches für den Erhalt der Länge der Telomere wichtig ist. Bei jeder Zellteilung werden die Telomere aufgrund des Problems der End-Replikation verkürzt. Die Ribonukleoprotein Telomerase Reverse Transkriptase (TERT) ist die zentrale Untereinheit des Telomerase Komplexes und fügt den G-reichen 3' Enden der Chromosomen neue repetitive Oligomere hinzu. Dadurch wird ein vorzeitiges Altern und letztendlich der Zelltod (verzögerter lethaler Phenotyp) verhindert, wie er in TERT und TR- defizienten Pflanzenzellen, Hefen, Protozoen und Säugerzellen beschrieben wurde, bei denen die Telomerase in erster Linie für den Erhalt funktioneller Telomere verantwortlich ist. Die Länge der Telomere in *Plasmodium* ist stabil während der Blutzellstadien und die Aktivität der TERT ist nachweisbar während der Trophozoiten- und Schizontenstadien, in denen die Replikation der DNA stattfindet. TERT wurde weithin als mögliches Zielmolekül für die Entwicklung von Medikamenten beispielsweise gegen Krebszellen untersucht und eine Inhibierung des Tumorwachstums konnte gezeigt werden. Vorläufige, bisher nicht publizierte Daten über den Effekt von Nucleosid-Analogen auf *in vitro* Kulturen von *P. falciparum* zeigen einen lethalen Effekt auf die Blutstadien der Parasiten nach 3-5 Zyklen bei micromolaren Konzentrationen (A. Scherf, Institute Pasteur). Eine kürzlich veröffentlichte Evaluierung verschiedener Komponenten deutet auf eine hohe anti-plasmodiale Aktivität von Delarvidine in vitro gegen Leberstadien von *P. yoelii* hin.

Zusätzlich zu diesen Daten kann ein negativer Effekt durch das Fehlen von TERT bei Deletionsversuchen in *P. berghei* beobachtet werden. Obwohl die Anwesenhiet von *tert*$^{-}$ Parasiten in der anfänglichen Population direkt nach der Transfektion beobachtet wurde, konnten keine tert^{-} Klone gewonnen werden. Dies ist in Übereinstimmung mit dem verzögerten lethalen Phenotyp, der in anderen Organismen beobachtet wurde. Auch nach einer ausgedehnten Klonierungsprozedur konnten keine postiven Klone gefunden werden. Die gewonnenen Resultate zeigen das TERT für die Entwicklung von *Plasmodium* essentiell ist und kennzeichnen Anti-Telomerase Medikamente als mögliche Hilfsmittel bei der Behandlung von Malaria Erkrankungen.

Abbreviations

Å	Angstrom
°C	Celsius degree
aa	amino acids
ADP	Adenosine Diphosphate
ADPR	Adenosine Diphosphate Ribose
ATP	Adenosine Triphosphate
bp	base pairs
BSA	bovine serum albumin
cDNA	complementary DNA
CSP	circumsporozoite protein
C-terminal	carboxy-terminal
CTRP	Circumsporozoite- and TRAP-related protein
DHFR	dihydrofolate reductase
DMEM	Dulbecco's Modified Eagle Medium
DNA	Deoxyribonuclotide acid
dNTP	Deoxyribonucleoside Triphosphate
FCS	fetal calf serum
g	gram
h	hour
IFA	Immnuofluorescence assay
IL-6	Interleukin-6
kb	kilo base pairs
kDa	kilo Dalton
kDa	kilo dalton
kg	kilogram
l	liter
m	meter, or mili
M	molar
mg	milligram
min	minute
ml	milliliter
mM	millimolar
mRNA	messenger RNA
NAD	Nicotinamide Adenine Dinucleotide
N-terminal	amino-terminal
P. berghei	*Plasmodium berghei*
P. chabaudi	*Plasmodium* chabaudi
P. falciparum	*Plasmodium* falciparum
P. gallinaceum	*Plasmodium* gallinaceum
P. knowlesi	*Plasmodium* knowlesi
P. vivax	*Plasmodium* vivax

P. yoelii	*Plasmodium yoelii*
PBS	Phosphate buffered saline
PCR	Polymerase chain reaction
pH	potentia hydrogenii
pI	isoelectric point
PVM	parasitophorous vacuolar membrane
RMS	Root Mean Squared
RNA	ribonucleic acid
RNA-seq	RNA sequencing
rpm	revolutions per minute
RPMI medium	Rosewell Park Memorial Institute medium
RT	Reverse Transcriptase
sec	second
SIR2	Silent Information Regulator 2
Taq	Thermus aquaticus
TERT	Telomerase Reverse Trasncriptase
TNF	Tumor necrosis factor
TRAP	Thrombospondin-related-adhesive protein
U	Unit
V	Volt
WT	wild type
α	anti, or alpha
µ	micron
µg	micro gram
µl	micro liter
µm	micro meter
µM	micro molar

Table of Contents

AUTHOR'S DECLARATION **4**

SUMMARY **5**

ZUSAMMENFASSUNG **6**

ABBREVIATIONS **8**

I. INTRODUCTION **17**

I.1 Chromosome structure **17**

I.2 Telomeres **17**
I.2.1 Telomere structure in *Plasmodium* 22

I.3 Telomerase complex and interacting proteins **25**
Telomerase mechanism of action 26
I.3.1 Telomerase Reverse Transcriptase (TERT) 27
Telomerase RNA (TR) 30
I.3.2 The effects of telomerase absence 31
I.3.3 Telomerase Reverse Transcriptase in *Plasmodium* 32

I.4 Chromatin structure and gene regulation. **36**
I.4.1 Histones as major structural components of chromatin. 36
I.4.1.1 Deciphering the histone code 37
I.4.2 Factors in epigenetic regulation 38
I.4.2.1 HATs and HDACs in *Plasmodium* 39
I.4.2.2 Spatial distribution and influence on gene transcription 40
I.4.2.3 Role of nuclear pore complex in transcriptional regulation 41

I.5 Telomere position effect **42**
I.5.1 TPE, epigenetics and antigen expression regulation in *Plasmodium* 43

I.6 The composite roles of SIR2 proteins **45**
I.6.1 Introducing a family of sirtuins 45
I.6.2 Sirtuin structure 45
I.6.3 Sirtuin mechanism of action 46
I.6.4 SIR2 diverse functions 47
I.6.4.1 Sirtuins play many parts in histone and other protein acetylation. 47
I.6.4.2 SIR2 proteins as ADP-ribosyltransferases 49
I.6.5 Function-dependent localisation 50
I.6.6 Biological roles of SIR2s – from calorie uptake through gene regulation to aging 51
I.6.7 Two SIR2 proteins in *Plasmodium* 52
I.6.7.1 *Plasmodium* SIR2A 53
I.6.7.2 *Plasmodium* SIR2B 56

I.7 The malaria parasite **58**
Plasmodium berghei 60
I.7.1 Anti-parasite response in mouse and Brown Norway (BN) rat models 61
I.7.2 Anti-parasite response in *Anopheles* spp. 61
I.7.3 Parasite invasion of the mosquito vector 62

II. MATERIALS AND METHODS 64

II.1 *P. berghei* transfection. 64
II.1.1 Selection of transformed parasites 64
II.1.2 Cryopreservation of blood stage parasites 65

II.2 Cloning of the transfected parasites by limiting dilution 65

II.3 Negative selection (5-Fluorocytosine treatment) 66

II.4 Field Inversion Gel Electrophoresis (FIGE) 66

II.5 Removal of leucocytes from infected blood. 66

II.6 Purification of gametocytes. 67

II.7 *In vitro* fertilisation/zygote development assay 67

II.8 Ookinete culture *in vitro* 67

II.9 Preparation of DNA constructs for transfection. 68

II.10 Genomic DNA extraction 69

II.11 Plasmid rescue from gDNA 69

II.12 Total RNA extraction 70

II.13 Southern/Northern analysis 70

II.14 Telomere Restriction Fragment (TRF) analysis 71

II.15 Western analysis 71
II.15.1 Sodium dodecyl sulphate polyacrylamide gel electrophoresis (SDS-PAGE) 72
II.15.2 Protein transfer onto a membrane 72
II.15.3 Immuno-detection 73

II.16 Immunofluorescence assay (IFA) 74

II.17 Fluorescent in situ hybridization (FISH)$^{DNA-DNA}$ 74

II.18 Matrigel™ ookinete motility assay. 76

II.19 Mosquito haemocoel injections of mature ookinetes. 76

II.20 Mosquito midguts dissections 76

II.21 Preparation of midguts for electron microscopy and paraffin embedding. 77

II.22 Toluidine blue-staining of midgut sections. 77

II.23 Chitinase assay 77

III. RESULTS..... 78

III.1 Generation of the *sir2a*, *sir2b* single and *sir2a/b* double deletion cloned parasite lines. 78
III.1.1 Silent Information Regulator 2 b (Sir2b) knockout. 78
III.1.1.1 Analysis of the *Pbsir2b* knockout transfection population 81
III.1.1.2 Negative selection of the 5-FC treated *sir2b* knockout parasites..... 82
III.1.1.3 Cloning of the *Pbsir2b* knockout parasites 84
III.1.1.4 Second negative selection and cloning of the *Pbsir2b* mutant line. 85

III.2 Generation of the *Pbsir2a*$^{-}$ line..... 88
III.2.1 Generation of the *Pbsir2a/sir2b* double knockout parasites. 89

III.3 Generation of parasite lines expressing tagged PbSIR2A and PbSIR2B 91
III.3.1 SIR2A::GFP line 91
III.3.2 SIR2B::MYC line 96

III.4 Assessment of *PbSir2a/b* double knockout parasites survival in Brown Norway rats compared to a wild type GFP-LUC expressing line 98
III.4.1 Average telomere length measurement in 1184 *Pbsir2a/Pbsir2b*$^{-/-}$ parasites..... 101

III.5 Global transcriptome analysis of *Pbsir2a/b* double deletion line versus wild type line102
III.5.1 Microarray analysis of 4 asexual parasite stages 102

III.6 Analysis of the effect of absence of PBSIR2A and PBSIR2B in sexual stages of *Plasmodium berghei*. 114
III.6.1 Mosquito passage of the *Pbsir2* mutants. 114
III.6.2 *sir2a*$^{-}$ and *sir2a/b*$^{-/-}$ ookinetes arrest at an ookinete-to-oocyst stage. 115
III.6.3 *sir2a*$^{-}$ and *sir2a/b*$^{-/-}$ ookinetes are not able to cross the mosquito midgut epithelium 117
III.6.3.1 *Δsir2a* parasites cannot penetrate the peritrophic membrane 120
III.6.1 *sir2a*-deficient ookinete stage morphology 123
III.6.2 SIR2A is not essential for oocyst formation. 124
III.6.3 Analysis of possible causes of *Δpbsir2* ookinete deficiencies. 126
III.6.3.1 SIR2A contributes to ookinete motility 126
III.6.3.2 Investigation of microneme proteins. 127
III.6.3.3 Acetylation level analysis 132
III.6.3.4 Gametocyte transcriptome analysis of sir2a/b double deletion parasites by RNA-sequencing 134

III.7 The average telomere length measurement 146

III.8 Fluorescence *in situ* hybridisation with telomere-specific probe 147

III.9 Completing the *P. berghei* Telomerase Reverse Transcriptase gene structure..... 148

III.10 The *P.berghei* TERT knockout 149
III.10.1 Vector design and *P. berghei* transfection..... 150
III.10.2 Diagnostic analysis of the TERT transfection population 152
III.10.3 Cloning of the TERT knockout parasites. 155
III.10.4 Extensive cloning of the TERT mutant population. 160

III.11 Telomerase RNA (TR) analysis 161

III.12 Immunodetection of *P. berghei* TERT using PfTERT antibody. 162

IV. DISCUSSION AND FUTURE PERSPECTIVES 164

IV.1 SIR2 proteins 164
IV.1.1 Can SIR2s have combined action of its several counterparts in mammals? 164
IV.1.1.1 *Plasmodium* SIR2A affects telomere length 165
IV.1.2 Does Sir2 affect cellular localisation of genes within the nucleus by altering their transcriptional status? 167
IV.1.3 PbSIR2A and PbSIR2B interaction partners 167
IV.1.4 *In vivo* effects of *sir2a* and *sir2b* deletion 169
IV.1.4.1 Brown Norway rat experiments 169
IV.1.4.2 Mosquito development 170
IV.1.5 Analysis of acetylation status of putative substrates of sirtuins in *P. berghei sir2a*$^-$ and *sir2b*$^-$ clones. 173
IV.1.6 Sirtuins influence transcription of a number of genes 175
IV.1.7 Are sirtuin inhibitors/activators potential anti-malarials? 178
IV.1.7.1 Inhibitors 178
IV.1.7.2 Activators 179

IV.2 TERT protein 180
IV.2.1 TERT has an evolutionary conserved function in *Plasmodium* 180
IV.2.2 TR subunit mutagenesis and deletion 180
IV.2.3 Shelterin complex protein identification 181
IV.2.4 Anti-telomerase drugs as auxiliary treatment to existing therapies? 181

REFERENCE LIST 183

APPENDIX 207

ACKNOWLEDGMENTS 213

Figures

Fig. 1 The structure of a mitotic chromosome 17
Fig. 2 Metaphase chromosomes with visualized telomeres (yellow) at their ends. 18
Fig. 3 The end-replication problem. 20
Fig. 4 T-loop and D-loop structures at a telomere end. 21
Fig. 5 Schematic representation of chromosome end structure of several malaria species. 23
Fig. 6 Schematic illustration of the telomerase core subunit 25
Fig. 7 Telomerase mechanism of action. 27
Fig. 8 Sequence motifs common to eukaryotic Telomerase Reverse Transcriptases. 29
Fig. 9 Secondary structures of telomerase RNA (TR) from Tetrahymena, human (TERC) and yeast (TLC1). 31
Fig. 10 Multi-way alignment of available, complete *Plasmodium* TERT DNA and protein sequences. 34
Fig. 11 Multi-way protein alignment of PbTERT partial amino acid sequences with the other *Plasmodium* TERTs 35
Fig. 12 The nucleosome structure. 36
Fig. 13 Structure of the core histones. 37
Fig. 14 HATs and HDACs in Acetylation/deacetylation pathway in *P. falciparum*. 40
Fig. 15 Models for nuclear pore complex-mediated gene activation and silencing within the nuclear periphery 42
Fig. 16 Sirtuin domain. 46
Fig. 17 A simplified mechanism of sirtuin reaction. 47
Fig. 18 General function and localisation of sirtuins 51
Fig. 19 A proposed model for SIR2-mediated silencing of *var* genes at subtelomeric regions. 54
Fig. 20 PfSIR2A has a conserved structure of a sirtuin. 56
Fig. 21 Multi-way alignment of available, complete *Plasmodium* SIR2B protein sequences. 57
Fig. 22 The malaria parasite life cycle (see text for details). 59
Fig. 23 *Pbsir2b* homology arms 78
Fig. 24 The pL0035 plasmid was used for generation of the pL1325 *sir2b* knockout construct 79
Fig. 25 Schematic representation of the recombination event leading to the deletion of the *Pbsir2b* gene. 80
Fig. 26 Positive/negative selection cassette removal 81
Fig. 27 Analysis of *Pbsir2* k.o. uncloned 1079 population by PCR and FIGE. 82
Fig. 28 Analysis of the negatively selected parasites by Southern blotting. 84
Fig. 29 *Pbsir2b* knockout clones analysis by PCR. 85
Fig. 30 Analysis of the 5-FC 1079 clones by Southern blotting. 86
Fig. 31 1079 clones analysis. 87
Fig. 32 *Δsir2a* generation. 89
Fig. 33 *Δsir2a/b* analysis. 90
Fig. 34 Analysis of PbSIR2A::GFP expressing parasite line 92
Fig. 35 SIR2A::GFP expression and localisation. 95
Fig. 36 *Pbsir2b::myc* tagging construct 96
Fig. 37 Analysis of the *Pbsir2b::myc* tagging construct integration. 97
Fig. 38 Western analysis of the PbSIR2B::MYC (1209 cl1). 97
Fig. 39 Bioluminescence measurements of 676-infected BN rats 100

Fig. 40 Average telomere length measurement of the 1184 samples. 102
Fig. 41 RNA samples analysis. 104
Fig. 42 RNA degradation plot of the HP and *Δsir2a/b* (1184) samples 106
Fig. 42 PCA plot of the *Δsir2a/b* 1184 and HP 10 and 16 hpi samples. 107
Fig. 43 The heatmap representation of 188 differentially expressed genes 111
Fig. 44 Total number of 124 genes deregulated solely in the long oligo DNA array (Singapore) 113
Fig.45 *P. falciparum* expression data deposited on PlasmoDB 115
Fig. 46 Ookinete and oocyst production in *sir2*-modified lines 116
Fig. 47 Mosquito midgut analysis by fluorescence stereomicroscopy. 118
Fig.48 Blood meal and epithelium wild type and *Δsir2a* parasite numbers in *Anopheles* midguts 119
Fig. 49 Assessment of *A. stephensi* mosquito midgut invasion ability of wild type, *Δsir2a* and *Δsir2a/b* ookinetes. 121
Fig.50 Giemsa-stained *in vitro* ookinetes of *Δsir2a/b*, *Δsir2a* and *sir2a::gfp* clones. 123
Fig. 51. TEM of *Δsir2a* (1022 cl2) and wt ookinetes. 124
Fig. 52 Ookinete motility assay in Matrigel™. 126
Fig. 53 Chitinase assay results *in vitro*. 128
Fig. 54 Western analysis of three parasite lines for CTRP and P28 expression. 129
Fig. 55 CTRP and P28 IFA on mature wild type, *sir2a-* and *sir2a/b*$^{-/-}$ ookinetes. 131
Fig. 56 Plasmepsin 4 IFA on mature wild type, *sir2a*$^{-}$ and *sir2a/b*$^{-/-}$ ookinetes. 132
Fig. 57 Immunofluorescence assay using anti-acetylation 133
Fig. 58. A general overview of transcriptional changes at 14 chromosomes 140
Fig. 59 Top 50 up- and down-regulated genes categorised according to the GeneDB newest release annotation 141
Fig. 60 Top 100 deregulated genes assorted according to GO ontology, predicted gene function clusters, GeneDB and PlasmoDB annotation. 142
Fig. 61 A. Sequence reads levels at *sir2a* and *sir2b* loci 145
Fig. 62 Telomere length measurement by Telomere Restriction Fragment analysis 147
Fig. 63 Fluorescence in situ hybridization with a telomere-specific probe 148
Fig. 64 The alignment of the P. chabaudi tert-containing 1026 contig and the P. berghei available genomic sequences 149
Fig. 65 The two homology arms for *Pbtert* DXO 150
Fig. 66 Design of the TERT double cross-over knockout plasmid 151
Fig. 67 Schematic representation of the tert knockout generation by homologous double cross-over integration. 152
Fig. 68 Analysis of the tert k.o. transfection populations by PCR and FIGE. 154
Fig. 69 PCR analysis of 1065 clones 1 – 9. 156
Fig. 70 FIGE of 1065 clones 1, 2 and 4 – 9. 157
Fig. 71 Determination of *Tgdhfr-ts* presence in chromosome 7 by PCR 158
Fig. 72 Analysis for pL1324 TERT plasmid presence in 1065 clones 1- 3 and 1065 uncloned. 159
Fig. 73 Analysis of the three uncloned populations collected after transfection 160
Fig. 74 Analysis of the tert k.o. transfection populations. 161
Fig. 75 Northern blot for the TR presence in several *P. berghei* life cycle stages 162
Fig. 76 Western analysis of PfTERT antibody 163
Fig. 77 Schematic represenatation of a condensed and “open” chromatin structure at telomere-proximal regions 166
Fig. 78 SIR2 possible mode of action. SIR2 deacetylates ALBA proteins 168
Fig. 79. Model for SIR2A action at the apical end. 175

Tables

Table 1 Telomeric sequences in various organisms. 19
Table 2 *Plasmodium* gene families....24
Table 3. SDS-PAGE resolving and stacking gel preparation 72
Table 4 *P. berghei* ANKA HP and P. berghei *Δpbsir2a/b* RNA samples....104
Table 5. Comparison of an extent of up- and down-regulation in 10 versus 16 hpi. 107
Table 6. Differentially expressed genes in the 1184 *Pbsir2a/Pbsir2b*$^{-/-}$ at 10 hours post infection.....110
Table 7. Samples collected for an extended second microarray analysis.....112
Table 8. A summary of genes at least 2 fold deregulated in the Sanger and Singapore data sets.....114
Table 9 Mosquito haemocoel micro-injections. 125
Table 10. Optimisation of tag length and respective changes in the percentage of uniquely mapped tags.....137
Table. 11 Merozoite-specific gene transcription levels.....138
Table 12 Down-regulated genes common to SIR2A/B- and DOZI-null gametocytes.....143

I. INTRODUCTION

I.1 Chromosome structure

In eukaryotic cells DNA is found in the form of a nucleoprotein complex called chromatin. In human diploid cells, if one would combine all the DNA end-to-end it would be around 2 metres long! Therefore, the DNA must be compacted by several orders of magnitude to fit into a tiny nucleus (for human cell typically 10-15 μm in size). The necessity of DNA packing in the cells is not only due to its size. Other reasons include protection of DNA from damage and efficient division of the DNA "package" between two daughter cells in a process of cell division. Last but not least, the organized structure of each chromosome facilitates gene expression and its control.

There are several levels of DNA packing in the cell, and the most compact form of DNA found in the cell – the mitotic chromosome (Fig. 1), reduces the linear length of DNA by 10,000-fold. Each mitotic chromosome comprises two sister chromatids (or two chromosomes), held together by a centromere. Each of the two chromatids are two DNA molecules resulting from DNA replication process, and each of the molecules has two arms – a short, p arm (p from "petit"), and a long, q arm ("q" simply because it is the next letter in the alphabet). The ends of each DNA molecule are defined as telomeres.

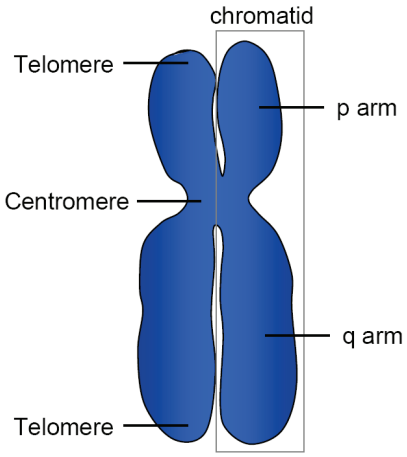

Fig. 1 The structure of a mitotic chromosome. Each mitotic chromosome is composed of two sister chromatids (= two DNA molecules), which are held together by a centromere. Each chromatid has a short (p) arm, and a long (q) arm. The ends of each DNA molecule are called telomeres.

I.2 Telomeres

Telomeres are specialized DNA-protein complexes which define the ends of eukaryotic chromosomes (Fig. 2). The DNA at the telomere is composed of a specialised sequence generally not found

elsewhere in the genome that consists of a number of tandemly arranged G-rich repeats (strand oriented 5' – 3' toward the chromosome terminus). The repeat in most species is six or seven base pairs long, with minor variations in the sequence, though with conserved triple or quadruple (or in some cases more) guanidine block. The telomeric sequence was first determined in a ciliated protozoan *Tetrahymena thermophila*, with a hexanucleotide repeat sequence GGGGTT (Blackburn and Gall, 1978; Blackburn et al., 1983). Before the end of 1990's the telomeric sequence was known for several other organisms, including slime molds *Physarum* and *Dictyostelium*, ciliate *Oxytricha*, *Trypanosome* parasite and several vertebrates including mouse and human. The summary of telomeric sequences in different organisms is shown in table 1.

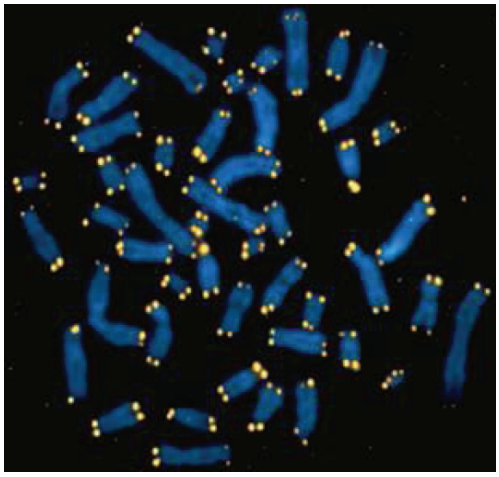

Fig. 2 Metaphase chromosomes with visualized telomeres (yellow) at their ends. Fluorescent *in situ* hybridization (FISH) technique with telomeric probe was used to obtain this image; taken by Peter M. Lansdorp, BC Cancer Research Centre, Vancouver, Canada; http://www.bccrc.ca/tfl/people_plansdor.html.

The function of telomeres has been shown to be mainly preservation of genome integrity and stability, since the telomeric DNA repeats and a number of proteins associated with them act against chromosome end-to-end fusions and degradation by double-stranded DNA breaks recognition mechanisms. However, they also serve as organisation points in certain organisms from which the transcriptional status of proximal genes might be determined (Baur et al., 2004; Aparicio et al., 1991; recent review O'Sullivan and Karlseder, 2010).

Organism	Telomeric repeat sequence	Telomere length (bases)	References
Protozoa			
Holotrichous ciliates			
Tetrahymena, Paramecium	T_2G_4	250 – 900	(Blackburn and Gall, 1978)
Hypotrichous ciliates			
Oxytricha, Euplotes	T_4G_4	100 – 150	(Klobutcher et al., 1981)
Plasmodium spp.	T_2T/CAG_3	850 – 6700	(Figueiredo et al., 2002; Ponzi et al., 1985)
Trypanosoma	T_2AG_3	<1000 – 15000	(Dreesen et al., 2005)
Yeast			
Saccharomyces cerevisiae	$TG_{2–3}(TG)_{1–6}$	275 – 400	(Shampay et al., 1984)
Schizosaccharomyces pombe	$GGTTAC(X)_{0–8}$	70 – 350	(Trujillo et al., 2005)
Slime molds			
Dictyostelium	AG_{1-8}	n.d.	(Emery and Weiner, 1981)
Didymium	T_2AG_3	n.d.	(Forney et al., 1987)
Plants			
Arabidopsis, Triticum	T_3AG_3	2000 – 4000	(Richards and Ausubel, 1988)
Animals			
Insects			
Drosophila	non-telomerase HeT-A and TART*	average 46000	(Rubin, 1978; George et al., 2006; Mason and Biessmann, 1995; Okazaki et al., 1993)
Anopheles gambiae	satellite sequences$	500 – 3500	(Roth et al., 1997; Walter et al., 2001)
Bombyx, Locusta	T_2AG_2, non-telomerase TRAS, SART*	8000 (TERT-derived) – 300000 (TRAS- and SART-derived)	(Kubo et al., 2001; Osanai et al., 2006)
Vertebrates			
Mus musculus	T_2AG_3	4000 – 150000#	(Hemann and Greider, 2000; Kipling and Cooke, 1990)
Homo sapiens	T_2AG_3	4000 – 14000	(de Lange et al., 1990; Moyzis et al., 1988)

Table 1 Telomeric sequences in various organisms. n.d. – not determined.

* Telomere-specific LINE-like transposable elements.

$ Non-telomerase like repeats, recombination-based telomere maintenance.

For laboratory strains 30 – 150 kb, for wild-derived strains 4 – 15 kb.

Previous studies have demonstrated that telomere dynamics are linked to aging and senescence, the most direct evidence coming from research on the human disease dyskeratosis congenita (DC) characterized by mutation in genes related to telomere maintenance (Dokal, 2001; Vulliamy et al., 2001; for a recent review see Oeseburg et al., 2010). Another argument came from studies on

replication of several types of cells, including yeast, *Tetrahymena* and mammalian cells (Lundblad and Szostak, 1989; Yu et al., 1990; for review see Stewart and Weinberg, 2006) Replication was shown to be abolished after several cycles when telomere maintenance processes are inactive. Research on the mechanism leading to replicative cell senescence events (the Hayflick limit) and eventual cell death pinpointed telomere length to be the critical determinant of a cell's replicative life span. It has been demonstrated that with each cell division the telomeres shorten due to the so called end-replication problem (depicted in Fig. 3), first recognized by Watson in the early 1970's (Watson, 1972). DNA replication is semi-conservative, which means each of the separated DNA strands is a template for a new strand of DNA. All known DNA polymerases synthesise DNA in a 5' – 3' direction. What is more they require a primer with a 3'-hydroxyl group for initiation of strand elongation. Due to the fact the one of the "mother" strands is 5' – 3', the "daughter" strand is synthesised in 3' – 5' direction in small fragments, called Okazaki fragments, which are subsequently ligated to create a single strand. Synthesis of each DNA piece needs to be initiated with a primer. Once an RNA primer is removed, the end portion of the newly synthesised molecule (5' end) will be shorter than the template strand, by the length of the dissociated primer. It means the DNA replication during mitosis is incomplete. In the next round of replication the cycle repeats, which signifies that with each DNA replication process DNA molecules get shorter. Temporarily or permanently circular genomes of bacteria and viruses clearly bypass the end-replication problem. For organisms with linear genomes there are several solutions to the incomplete DNA replication. For instance, mammalian adenoviruses utilize a protein covalently attached to the 5' end of the synthesised DNA strand, which circumvents the need for a terminal primer. In other organisms the telomere problem is handled by a specialized DNA polymerase complex called telomerase, which extends the "mother" strand's 3' end providing necessary template for completing the synthesis of the lagging strand by DNA polymerase.

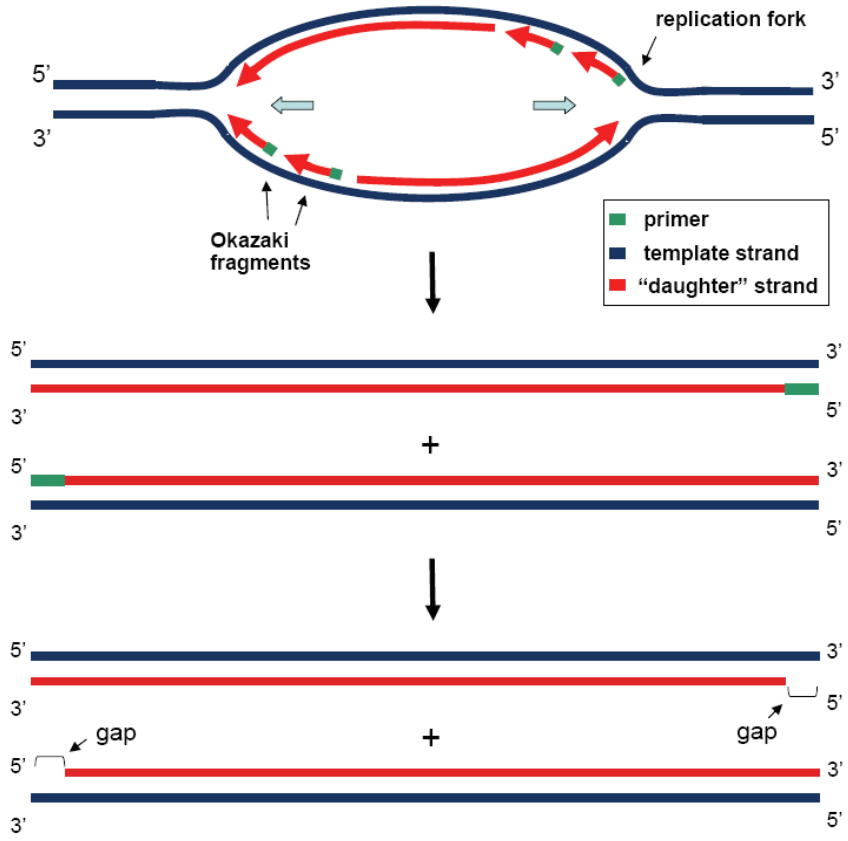

Fig. 3 The end-replication problem.
Due to the 5'-3' direction of action of DNA polymerase the leading strand is synthesised in a continuous fashion, whereas the lagging strand is ligated from smaller pieces called Okazaki fragments. DNA polymerase needs to utilise an RNA primer (green), which is later removed, leaving a gap at the 5' end of the newly synthesised DNA strand. Therefore the replication process leads to loss of sequence from opposite strands at both ends.

Cells that do not have an active telomerase complex (e.g. human somatic cells) experience telomere shortening. The average telomeric sequence loss in distinct types of human cells varies between 30 and 200 bp per cell division (Hayflick, 1965; Allsopp et al., 1995). However some cell types, like vertebrate embryonic stem cells, some highly proliferative cells, e.g. haematopoietic cells or intestinal crypts cells (for review see Forsyth et al., 2002; Serakinci et al., 2008), germline cells, and most cancer cells (85 – 90%), as well as most of lower eukaryotes, do possess active telomerase, which enables them to grow and replicate indefinitely. Clearly such a function has implications for studies on aging as well as cancer chemotherapy.

Telomeres are not naked DNA but instead are covered by a number of different proteins, which have multiple functions. Telomere-associated proteins (TAPs) as a part of the telosome (telomeric DNA + telomeric proteins) protect telomeres from degradation, regulate (positively or negatively) their length through protein-protein and protein-DNA interactions, regulate the transcriptional status of subtelomeric genes. The first protein ever identified bound to a telomere was the transcriptional activator/repressor protein Rap1p in yeast (Berman et al., 1986; Buchman et al., 1988), which was shown to be associated with telomeres *in vivo* and to negatively regulate telomere length (Conrad et al., 1990). Human telomeres have been shown to interact with, amongst others, two distinct TAPs, namely TRF1 and TRF2 (for telomeric repeat binding factor 1 and 2 respectively). TRFs have homology to DNA-binding domain of the Myb family of transcription factors. TRFs both bind selectively to the duplex telomeric DNA *in vitro* and *in vivo* (Broccoli et al., 1997) and were shown to stabilise the T-loop structure which indicates a “closed” state of telomeres. The closed state arises when the 3’ telomeric overhang bends back on itself, invades the telomeric duplex tract and anneals with the complementary sequences in the 5’ end of the opposite strand (D-loop) (Griffith et al., 1999) (Fig. 4). The human TAP POT1 (for protection of telomeres-1) is a ssDNA-binding protein, which associates with TRF1 and TRF2 through additional TAPs, including TPP1 and TIN2. Together this TAP complex regulates telomere length and capping (for review see de Lange, 2004). TAPs that are part of the telomerase-mediated telomere maintenance and regulation mechanisms are collectively called the shelterin complex, and are described below (section I.3)

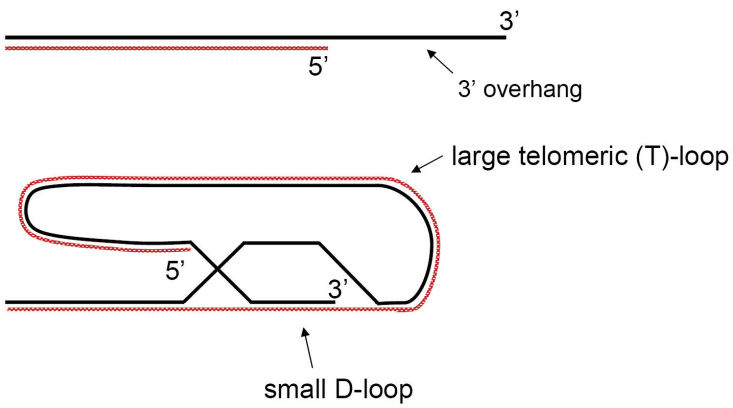

Fig. 4 T-loop and D-loop structures at a telomere end. The 3’ G-rich overhang loops back on itself (creating T-loop), invades the double stranded DNA region, and anneals with the complementary bases in the opposite strand (D-loop).

I.2.1 Telomere structure in *Plasmodium*

The *Plasmodium* genome is arranged into 14 linear chromosomes, which have a similar organisation like most eukaryotic chromosomes. The end portion of each chromosome comprises of a variable number of telomeric repeats, which are essential for chromosome function. Telomeric sequence was first identified in *Plasmodium berghei* by Clara Frontali's laboratory in 1985 (Ponzi et al., 1985). The 7-bp telomere repeat sequence (TTT/CAGGG) is universal across *Plasmodium* species (Dore et al., 1986), though the average telomere length per species varies, ranging from 850 bp in *P. falciparum* Sbd27 strain to 6700 bp in *P. vivax* (Figueiredo et al., 2002). The structure of the *Plasmodium* telomere and subtelomeric region (or Telomere Associated Sequence – TAS) differs significantly among various species (Fig. 5). In *P. falciparum* the subtelomeric region of each chromosome comprises six Telomere-Associated Repetitive Elements (TAREs), which are non-coding and polymorphic in nature. TARE6, also called Rep20, is implicated in chromosome clustering at the nuclear periphery, which should facilitate ectopic recombination events (Figueiredo et al., 2002). Further towards the centromere multigene families, such as *var, rifin, Pf60.1, stevor* are located, of which most are implicated in the ability of the parasite to evade for the most part the host immune system. Telomeres facilitate enhanced rates of recombination and the subtelomeric location of the mentioned multigene families enables the continual generation of the diversity necessary for continued avoidance of the immune system. Other malaria species, though do not contain *var*-like gene family, possess other multigene families implicated in host immune system interactions. Relatively recently a variant gene superfamily has been identified in six species of *Plasmodium*. The *pir* superfamily (for *Plasmodium* interspersed repeats) includes *rif* in *P. falciparum*, *vir* in *P. vivax*, *kir* in *P. knowlesi* and the *cir/yir/bir* family in three rodent species (*P. chabaudi*, *P. yoelii* and *P. berghei*, respectively) (Janssen et al., 2004). Other *Plasmodium* gene families identified to date include 235KDa rhoptry protein, HAD-Hydrolase, *pst-a* and *etramp*, all common to several *Plasmodium* species, including *P. falciparum*. For a list of common and species-specific gene families see Table 2 below. All gene families can be predominantly found in subtelomeric regions. *P. berghei* has estimated ~180 *bir* genes in the genome located in the telomeres vicinity (Hall et al., 2005). *P. ber*ghei chromosome ends contain no TAREs, but the subtelomeric region is composed of a tandem array of 2.3 kb units present in several hundred copies in the parasite genome. The 2.3 kb units consist of 2.1 kb repeat fragments separated by ~160-bp stretches of the telomeric or telomeric-like sequence (Dore et al., 1990). Interestingly, a *bir* pseudogene was found in the 2.1 kb element. In *P. vivax*, apart from telomeric repeat sequences there are no other repetitive elements present in the genome. Downstream of the telomere on possibly all *P. vivax* chromosomes a previously mentioned *vir* family (*P. vivax* variant genes) is located. *P. yoelii* chromosome ends are highly polymorphic, with some chromosomes containing short stretches of non-telomeric repeats. For *P. chabaudi* limited sequence data is available. However, study by Fischer et al. (2003) revealed that all chromosomes share a common

structure. The multicopy gene families (including *cir*) are present exclusively in subtelomeric regions of numerous chromosomes

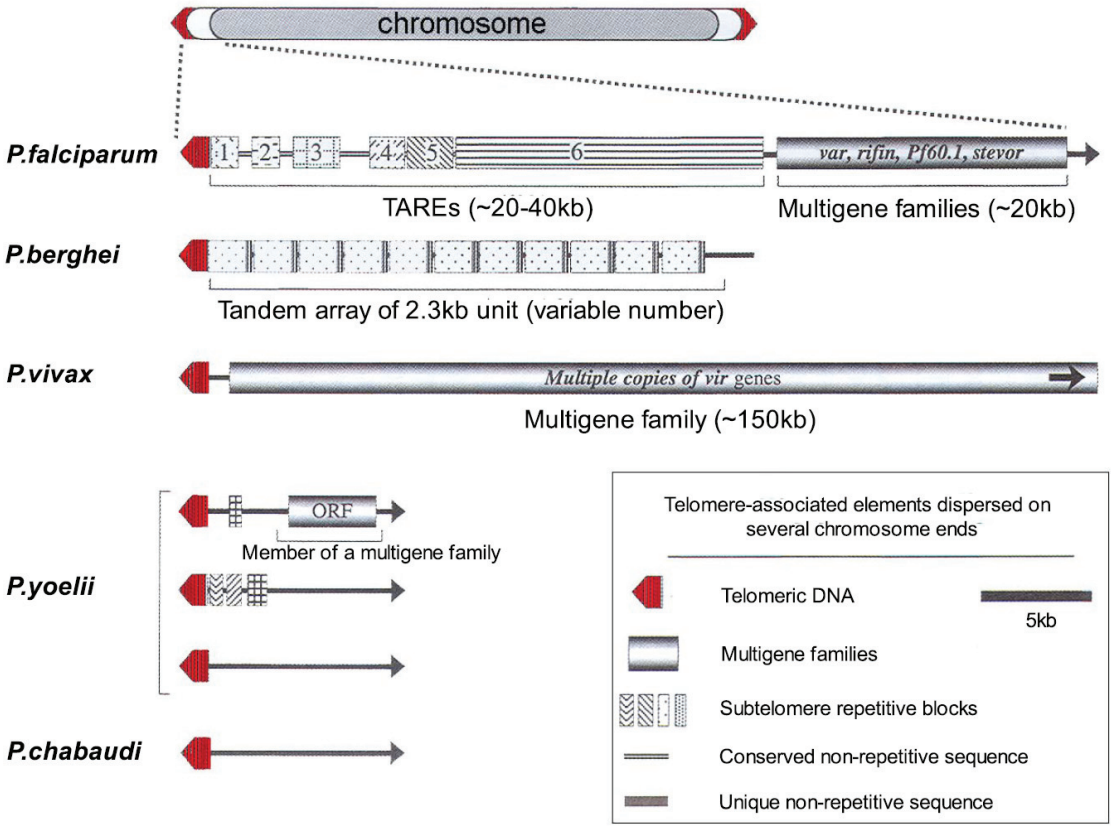

Fig. 5 Schematic representation of chromosome end structure of several malaria species. The subtelomeric region is located downstream from telomere (red). This region is greatly polymorphic among *Plasmodium* species. In *P. falciparum* the subtelomeric region (also called TAS) contains six Telomere Associated Repetitive Elements (TAREs). Further downstream multigene families (including *var* and *rifin* encoding virulence factors) are located. In *P. berghei* the subtelomeric region is composed of a variable number of 2.3 kb units. *P. vivax* contains no repetitive blocks, only long stretch occupied by *vir* gene family. *P. yoelii* chromosome ends exhibit highly polymorphic subtelomeric regions within heterologous chromosomes. For *P. chabaudi* still limited sequence data is available. However, it is known that chromosome ends share a common structure, and contain multigene families, including *cir*.
Modified from Scherf et al., Malaria Parasites, Genomes and Molecular Biology.

References
1. J. M. Carlton *et al.*, *Nature* **419**, 512 (2002). 2. K. Fischer *et al.*, *Mol Microbiol* **48**, 1209 (2003). 3. M. J. Gardner *et al.*, *Nature* **419**, 498 (2002). 4. E. Lasonder *et al.*, *Nature* **419**, 537 (2002). 5. L. Florens *et al.*, *Nature* **419**, 520 (2002).

	Sub telomeric family	*P. falciparum*	*P. chabaudi*	*P. berghei*	*P. yoelii*	Function	Protein Expression
Common gene families	235KDa rhoptry protein	4	4	10	14	Reticulocyte binding protein	OCY/SPZ
	HAD-Hydrolase	5	19	3	5	HAD hydrolase	ASX/GCT/OKN
	pst-a	10	41	6	12	Alpha beta hydrolase	GCT/OKN
	etramp	11	3	7	11	Early transcribed membrane protein	ASX/GCT/GAM
Rodent malaria Gene families	yir/cir/bir	0	138	180	838	Variant antigen?	ASX/GCT/OKN OCY/SPZ
	pyst-a	1	108	45	168	Unknown	ASX/SPZ
	pyst-b	0	10	34	57	Unknown	ASX/SPZ
	pyst-c	0	5	4	21	Unknown	ND
	pyst-d	0	0	1	17	Unknown	ND
	pcst-f	0	10	2	1	Unknown	ASX/GCT/OKN
	pcst-g	0	75	11	7	Unknown	SPZ
	pcst-h	1	5	6	4	Unknown	ND
P.falciparum gene families	Var	59	0	0	0	Erythrocyte membrane antigen (PfEMP1)	ASX/GAM/SPZ
	Rifin/stevor	177	0	0	0	variant RBC surface antigen	ASX/GAM/SPZ
	rhoph1/clag	4	1	1	2	Cytoadherence linked asexual protein	ASX/GAM/SPZ
	Pf-fam-a	35	0	0	0	DNAJ domain protein	SPZ /ASX/GAM
	Pf-fam-b	11	0	0	0	Unknown	SPZ/ASX
	Pf-fam-c	20	0	1	1	ser/thr kinase	SPZ/ASX/GAM
	Pf-fam-d	17	0	0	0	Unknown	ND
	Pf-fam-e	6	0	0	0	Unknown	SPZ/ASX/GCT/GAM
	Pf-fam-f	10	0	0	0	Unknown	SPZ/ASX/GCT
	Pf-fam-g	13	0	0	0	Unknown	SPZ/ASX/GCT/GAM
	Pf-fam-h	19	0	0	0	Unknown	SPZ/ASX/GCT/GAM
	Pf-fam-i	11	2	1	1	acyl-Co A sythetase	SPZ/ASX/GCT/GAM

Table 2 *Plasmodium* gene families. ASX – asexual blood stage; GCT – gametocyte; OKN – ookinete; OCY – oocyst; SPZ – sporozoite; ND – Not Determined. Table from Hall et al. (2005).

In *Plasmodium* it has been shown that during blood stage proliferation telomeres are maintained within a specific range of lengths and that they are found as clusters of 4 – 7 chromosome ends at the nuclear periphery (Figueiredo et al., 2002; Freitas-Junior et al., 2005). The fact that *Plasmodium* multiplies rapidly at several points in its life cycle (see Fig. 22 in “The malaria parasite” section), as well as the finding that telomere length is stably maintained throughout the life span meant that *Plasmodium* needs to utilise a mechanism to prevent telomere attrition in order to survive. This prompted a search for *Plasmodium* telomerase (Bottius et al., 1998), which is described below (point I.3.3).

I.3 Telomerase complex and interacting proteins

Telomerase is an RNA-dependent DNA polymerase complex, belonging to the reverse transcriptase family, which synthesises terminal telomeric repeats using an RNA template. Its function is therefore telomere maintenance, thus compensating for the telomere loss occurring with each cell division. Telomerase was first described in 1985 in the holotrichous ciliate *Tetrahymena thermophila* (Greider and Blackburn, 1985), as an activity that "synthesises tandem TTGGGG repeats *de novo*". It was the long sought after explanation to the end-replication problem.

Telomerase holoenzyme comprises several subunits: Telomerase Reverse Transcriptase (TERT), together with its RNA component, which specifies the sequence of telomeric repeats (Yu et al., 1990), is the core subunit (Fig. 6), and it is essential for telomerase activity. In all organisms where telomerase was found, the core subunit contains universally conserved reverse transcriptase sequence motifs.

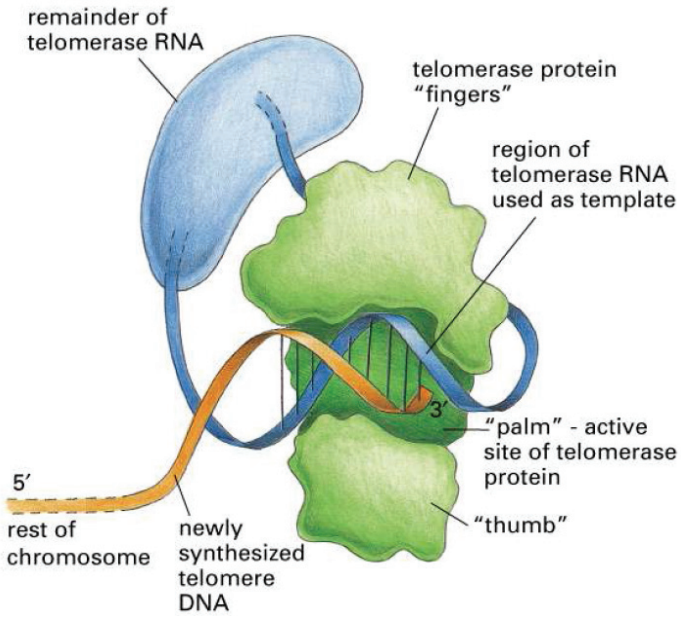

Fig. 6 Schematic illustration of the telomerase core subunit - Telomerase Reverse Transcriptase (TERT) and its RNA component. Molecular Biology of the Cell, Alberts et al., 4th edition.

Other components of telomerase ribonucleoprotein (RNP) complex have been found mainly through genetic screens in yeast (Lendvay et al., 1996), though they are less conserved than the core subunit. These proteins generically referred to as shelterin proteins, play essential roles in the biogenesis of the telomerase complex, recruitment to the telomere, regulation of telomerase activity and interaction of the holoenzyme with telomere sequence (e.g. Bednenko et al., 1997; Greene and Shippen, 1998; for a review see Palm and de, 2008). The first subunit identified was found in yeast – Est1p (for ever-

shortening telomeres) (Lundblad and Szostak, 1989). It binds to a bulged stem in TLC1 (yeast telomerase RNA) (Seto et al., 2002), and in *S. pombe* it was found to protect telomeric repeats from deletion (Beernink et al., 2003). Est1p interacts with another protein Cdc13p (called Est4p in yeast), which is a single-stranded binding protein (Pennock et al., 2001). Together they recruit telomerase to the ends of chromosomes. Cdc13p interacts with telomerase but it is not permanently associated with it. Other telomerase-associated proteins described include p43 in Euplotes (Aigner et al., 2000) and its orthologue p65 in *Tetrahymena* (Witkin and Collins, 2004), which have considerable homology to RNA-binding proteins (both contain three potential RNA-binding domains referred to as the La motif). It has been shown that both proteins interact with telomerase RNA (TR), which implies they might function in telomerase assembly and activity (Aigner and Cech, 2004). A La domain-containing protein was found in the human telomerase complex and it was shown to influence telomere length *in vivo* (Ford et al., 2001). Moreover, the p43 *Euplotes* telomerase subunit and the human POT1 (defined in earlier section) were shown to influence enzyme activity and processivity *in vitro* (Aigner and Cech, 2004; Lei et al., 2005). Ku protein which binds to telomeres as a heterodimer is another protein of the shelterin complex. It was found to recruit telomerase RNP to telomeres and damaged chromosome ends (Fisher et al., 2004; Stellwagen et al., 2003), though its activity has been shown to be non-essential for telomerase activity *in vivo* (Boulton and Jackson, 1998). Ku was also shown to regulate silencing of the HML and HMR loci (Vandre et al., 2008), as well as act as an anchor of telomeres to the nuclear periphery which partially blocks relocalisation-initiated telomere replication (Ebrahimi and Donaldson, 2008). A novel recently identified telomerase-associated protein is MOV10, a single- and double-stranded DNA binding protein, which possibly enhances telomerase activity on telomeric DNA (Nakano et al., 2009).

An active telomerase was found in distinct organisms, such as *Tetrahymena*, *Saccharomyces spp.* (Shampay and Blackburn, 1988), mouse (Prowse et al., 1993) and human (Morin, 1989) but was absent or inactive in normal adult human cells, a fact that has potential implications for anti-telomerase therapies against cancer cells and human parasites. This matter will be described later in more detail.

Telomerase mechanism of action

As mentioned before, telomerase adds new telomeric repeats to the 3' chromosome end to enable completion of DNA replication in eukaryotic cells. A model for processive elongation of 3' telomeric DNA was developed based on studies in *Tetrahymena*, yeast and humans (Baran et al., 2002; Collins and Greider, 1993; Collins, 1999; Greider, 1991; Lue and Peng, 1997; Lue, 2004; Melek et al., 1994; Morin, 1991). Telomerase acts by a "slippage" mechanism, depicted in Fig. 7. First telomeric DNA is recognized by the telomerase RNP, which consists of at least the TERT protein with its RNA component. The telomerase RNA (TR) template aligns with the complementary telomeric DNA bases at the 3' end. Addition of nucleotides to the telomere end is directed by the RNA template

(polymerization step). When the 5' end of the template is reached telomerase translocates so that another set of nucleotides can be added to the 3' end of DNA. Several rounds of this cycle result in the addition of multiple repeats.

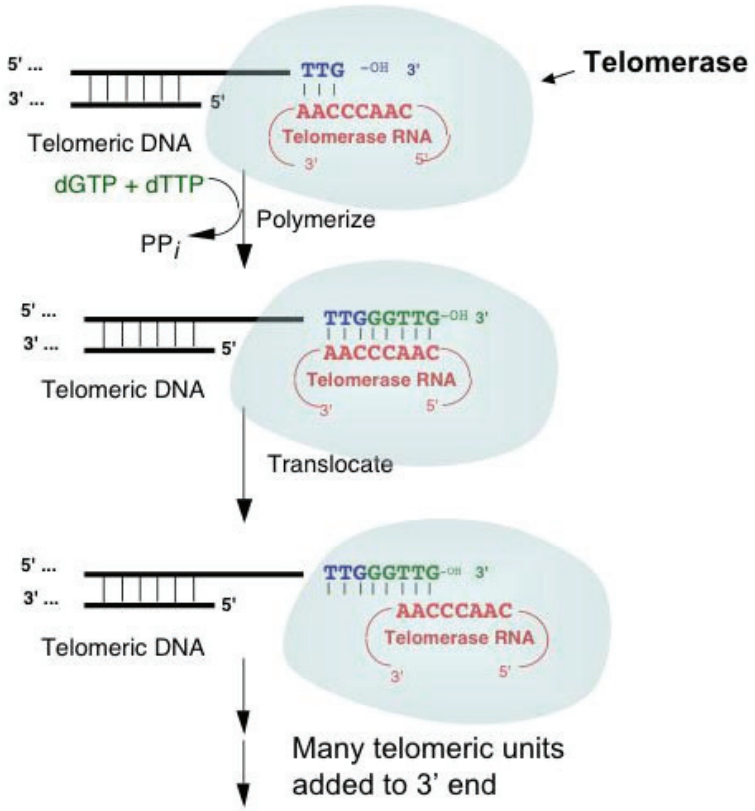

Fig. 7 Telomerase mechanism of action. Telomerase, composed at least of TERT and its RNA subunit, is recruited to the 3' end of a chromosome. Upon alignment telomerase adds nucleotides to the 3' end of telomeric DNA using the template of TR (polymerisation step). When the 5' end of the template is reached translocation of the enzyme occurs and the cycle is repeated multiple times. Telomerase activity is regulated by several factors, including TERT and TR intra- and intermolecular interaction.

I.3.1 Telomerase Reverse Transcriptase (TERT)

Telomerase Reverse Transcriptase, as mentioned before, is the core subunit of telomerase RNP. It was first identified in 1997 (Lingner et al., 1997) and since has been found in a number of organisms ranging from protozoa through yeast and slime molds to plants and mammals, including human (for a comprehensive review see Autexier and Lue, 2006), indicating that telomerase is a highly conserved feature of eukaryotic cells. The C-terminal end of all TERT sequences share homology with reverse transcriptases (RTs) from retrotransposons and retroviruses (Fig. 8), in particular the seven RT-specific motifs – 1, 2, A, B', C, D and E. The C-terminal part of TERT is responsible for the catalytic activity and processivity (Nakayama et al., 1998 and references therein; Huard et al., 2003); three aspartic acid residues located in the A and C motifs are particularly important. The crystal structure of the RT domain of TERT has not yet been solved. However based on homology with other RTs it is believed that the three-dimensional structure of the telomerase core subunit resembles a right hand

with fingers, where the palm contains C to E motifs, the fingers are motifs 1 to B' and the thumb is carboxy-terminal extension (CTE) domain (see Fig. 8 top and Fig. 6). The N-terminal portion of telomerase reverse transcriptase is relatively conserved amongst TERTs yet shows no homology either to the N terminus of other RTs such as L1 non-LTR retrotransposon ORF2, or to other proteins. However it has been postulated that the telomerase-specific half could originate from Gag/ORF1 proteins that function as RNA chaperones (Cristofari and Darlix, 2002). In retroviruses and the majority of retrotransposones Gag/ORF1 proteins are located on the same RNA molecule like reverse transcriptases. The 3D structure of the N-terminal TERT sequence would certainly be useful in answering this hypothesis. The function of N-terminal half of TERT is related to its RNA template perhaps explaining the lack of similarity to other RT-like enzymes: several conserved motifs – CP, QFP and T (green in Fig. 8) form telomerase RNA binding sites (TRBDs), as shown in *Tetrahymena thermophila* and yeast (Bryan et al., 2000; Bosoy et al., 2003). The TRBD interacts with the RNA template upstream of the template near the 5' end of TR (Lai et al., 2001). In human TERT (hTERT) the TRBDs are called RID1 and RID2, where RID1 binds the human TR (hTR) pseudoknot-template region, whereas RID2 interacts with CR4/CR5 domain of TR (Moriarty et al., 2004). The N-terminal part of TERT also functions in multimerisation and interactions with other proteins. Recently, the amino-terminal half of hTERT has been shown to comprise a DNA-binding domain, which is necessary for telomerase activity (Sealey et al., 2010).

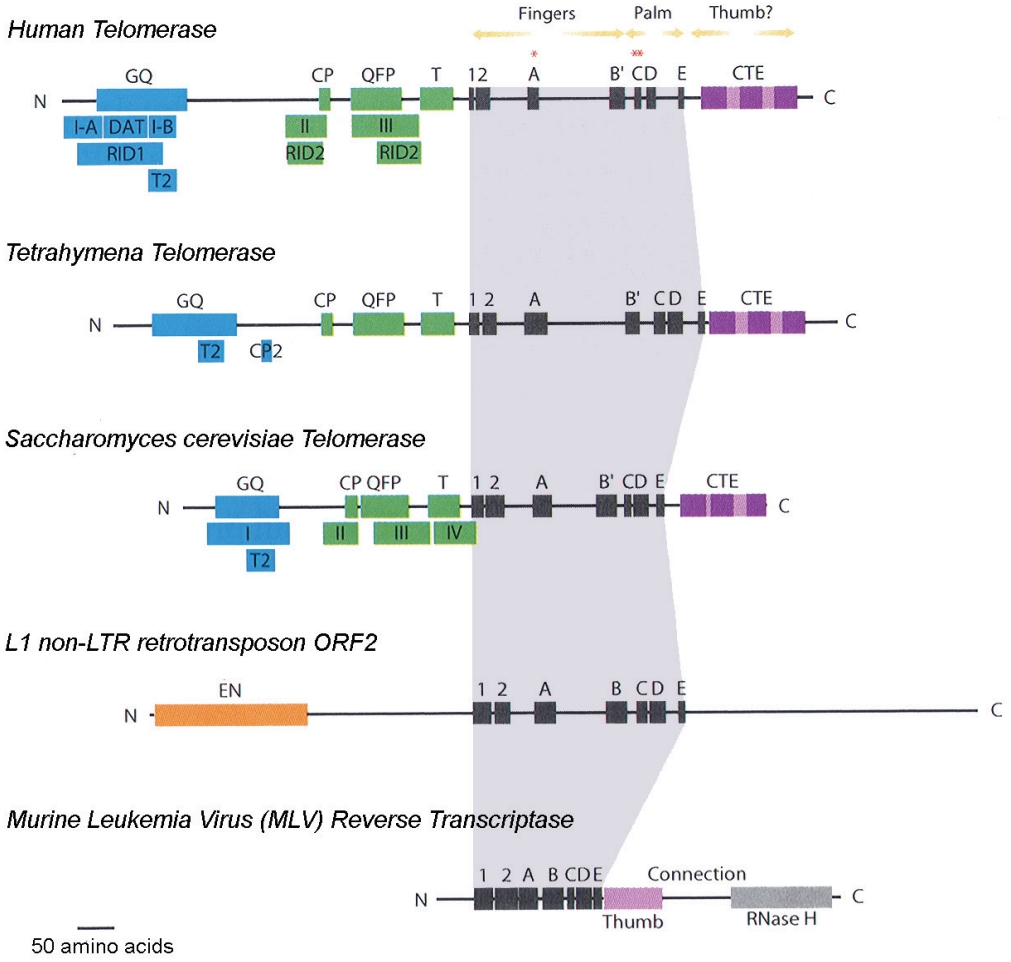

Fig. 8 Sequence motifs common to eukaryotic Telomerase Reverse Transcriptases. In the N terminus, which is essential for efficient binding of telomerase RNA (TR), the telomerase-specific motifs are shown. The C terminus, which shares homology with reverse transcriptases from retrotransposons and retroviruses, contains the RT-specific conserved motifs (1 to E) (highlighted in grey). The RNase H domain in MLV is not found in TERTs. Figure from "Telomeres", Blackburn et al., 2nd edition.

Telomerase activity can be reconstituted *in vitro* in cell-free systems from TERT and human TR (hTR or TERC) solely, confirming that together they form the core subunit, although reconstitution is dependent on the presence of chaperone proteins, such as Hsp90 (Masutomi et al., 2000; Weinrich et al., 1997; Collins and Gandhi, 1998; Holt et al., 1999). In a typical 60-minute reaction *in vitro*, products greater than 2000 nucleotides can be synthesised by *Tetrahymena* TERT (Greider, 1991). Although *Tetrahymena* and human telomerase are highly processive *in vitro*, telomerases from mouse and yeast (with the exception of *Saccharomyces castelli*) generate only short products in standard reactions (Cohn and Blackburn, 1995; Fulton and Blackburn, 1998; Lue and Peng, 1997; Prowse et al., 1993).

Telomerase RNA (TR)

TR is the RNA component of Telomerase Reverse Transcriptase (see Fig. 6) and in yeast called TLC1 that contains a short segment complementary to telomeric repeat sequence, which serves as template for reverse transcription by TERT at the 3' chromosome end. Despite its conserved function in different organisms, the TR sequence varies greatly, indicating it diverged early in evolution. The sequence length of TR ranges from 150 nucleotides in ciliates, through approx. 450 in vertebrates to around 1.2 kb in *S. cerevisiae*. However, several common structural features were found that are conserved among a number of diverse organisms, including ciliates, yeast and human (Romero and Blackburn, 1991; Dandjinou et al., 2004; Chen et al., 2000). For instance, the template region (marked in yellow in Fig. 9) is always single stranded and around 1.5 – 2 times the size of the telomeric repeat length of a particular organism (this feature is useful for the alignment and polymerisation steps of telomerase action). The template is flanked by elements which specify the 5' boundary of the template. The template boundary element (TBE) has different forms in various organisms; yet they all play a role in the polymerisation/translocation step of TERT activity (Seto et al., 2003; Lai et al., 2002; Chen and Greider, 2003; and references therein). A segment immediately downstream (3') of the template is known as template recognition element (TRE).

Secondary structure models for TR were derived through phylogenetic comparison of different groups (Chen et al., 2000; Lingner et al., 1994; Romero and Blackburn, 1991; Zappulla and Cech, 2004; Kachouri-Lafond et al., 2009; Copeland et al., 2009). Those models are utilised for TR screens in organisms whose genomes have been sequenced or whose partial sequence data is available. Validation of the models was performed using chemical probes and structure-specific RNases, mutational studies and recently nuclear magnetic resonance (NMR) analysis (Bhattacharyya and Blackburn, 1994; Dandjinou et al., 2004; Leeper et al., 2005; Lingner et al., 1994; Sperger and Cech, 2001; Nagata et al., 2008; Drosopoulos and Prasad, 2010; Xie et al., 2008).

Mutations in TR that disrupt its structural equilibrium are associated with the previously mentioned sever disease dyskeratosis congenita (autosomal and X-linked) (Theimer et al., 2003; Vulliamy et al., 2008), where either dyskerin – a protein binding and stabilising TR, or the TR itself is mutated.

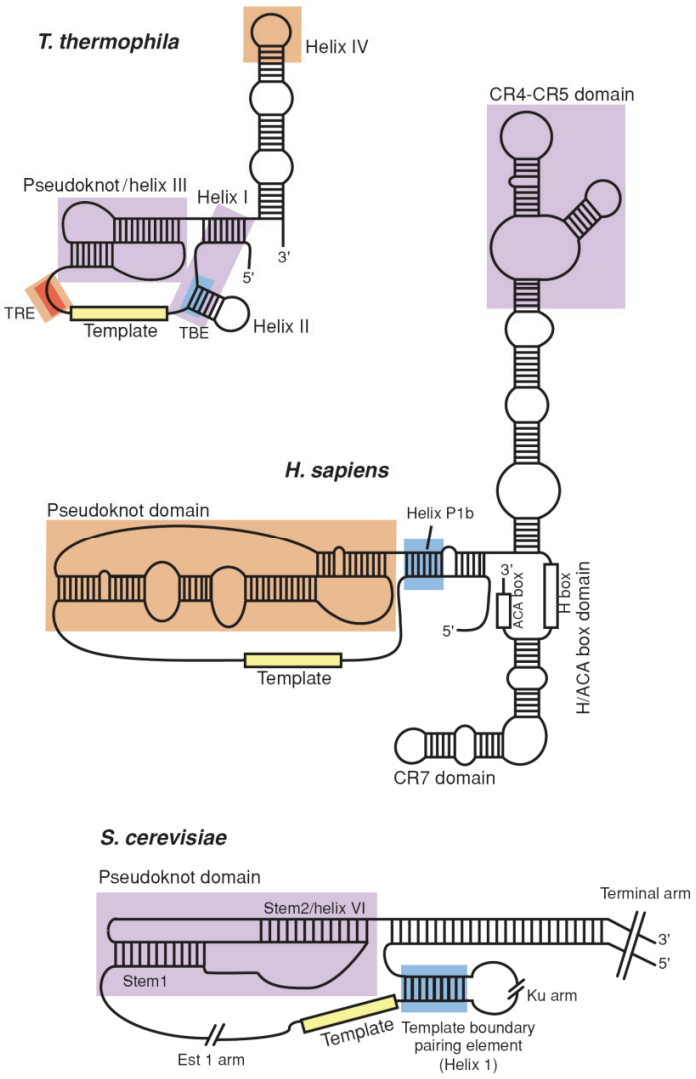

Fig. 9 Secondary structures of telomerase RNA (TR) from Tetrahymena, human (TERC) and yeast (TLC1). Despite divergent sequences and sizes, several TR elements are conserved among species. The template region (always single stranded), which is complementary to telomeric sequence at the 3' telomeric end is highlighted in yellow. Upstream of the template the 5' boundary element is located (blue), called template boundary element (TBE). The target recognition element (TRE) is located 3' from the template region. Main TERT-binding regions are highlighted in purple and low-affinity TERT-binding structures in orange. Only part of *S. cervisiae* TR is shown.
Image from (Autexier and Lue, 2006).

I.3.2 The effects of telomerase absence

The TERT gene has been deleted or mutated in a number of organisms. The TERT deficient phenotype, taking into consideration telomerase function, should initially show cell senescence and eventually result in cell death (the so-called delayed death phenotype) and indeed, this phenotype was observed in yeast, *Tetrahymena* and mammalian cells. In yeast cells Est mutants progressively lose telomeric DNA and exhibit increased frequency of chromosome loss (Lundblad and Szostak, 1989). Mutant cells have a senescence phenotype, due to a gradual decrease in telomere length, resulting in decreased chromosomal stability and subsequent cell death. Also, studies on *Tetrahymena*

telomerase-defect mutants showed abnormalities in nuclear and cell division (Yu et al., 1990), which eventually led to cell senescence and premature apoptosis.

Due to the complexity of vertebrates, theoretically telomerase absence should result in multiple abnormalities, interfering with proper organism functions, eventually greatly decreasing its survival time. Therefore, the effects of the absence of telomerase have been studied *in vitro* in a number of human cell lines. All cell types exhibit replicative senescence after a certain number of cell divisions, depending on initial telomere length implying that telomerase is necessary for the unlimited proliferation of human somatic cell *in vitro* (Bodnar et al., 1998; Funk et al., 2000). In whole organism the effects of telomerase dysfunction can be seen in the man in individuals with DC disease where defects are mostly seen in tissues with cells undergoing rapid turnover, such as skin and haematopoietic adult stem cell (for a recent review see Kirwan and Dokal, 2009 and references therein). In contrast to human cells, rodent cells have detectable telomerase activity in their somatic cells (Prowse and Greider, 1995), yet the defects are similar in human and mouse. Both show abnormalities in the production of blood cells and in the gut, as well as poor wound healing. The consequences of telomerase absence are therefore global and apply to all tissues of the body. In mouse both TERT and TR knockouts have been performed (Yuan et al., 1999; Blasco et al., 1997). The mouse TR (mTR) absence resulted in chromosomal abnormalities in the sixth generation. The phenotypic effects such as sterility, splenic atrophy, reduced proliferative capacity of B and T cells, abnormal haematological parameters, and progressive loss of organism viability were observed (Herrera et al., 1999). In mTR-/- mice telomeres shortened at an increased rate resulting in a dramatically decreased survival rate of the later generations. TERT knockout mice showed similar phenotype like the mTR-/- mice. However anaphylactic response defects were observed in TERT k.o. mice even in early generations, indicating a role for this enzyme in allergic reactions (Ujike-Asai et al., 2007). People with DC, as well as late-generation telomerase-deficient mice, also suffer from a higher rate of carcinomas (Artandi et al., 2000) as a result of unstable chromosomes with many chromosomes undergoing end-to-end fusions (Dokal, 2000) probably because their telomeres are terminally eroded.

I.3.3 Telomerase Reverse Transcriptase in *Plasmodium*

Since the completion of *Plasmodium falciparum* strain 3D7 genome project (Gardner et al., 2002), partially completed genomes of other *Plasmodium* species, including *P. vivax* (infectious to man), P. *knowlesi* (infectious to man and primates), *P. reichenowi* (primate parasite), *P. berghei*, *P. chabaudi* and *P. yoelii* (the rodent malaria species) (Carlton et al., 2002; Hall et al., 2005) and *P. gallinaceum* (avian parasite) are freely accessible online from several databases, e.g. PlasmoDB (Aurrecoechea et al., 2009), GeneDB (Bahl et al., 2002; Hertz-Fowler et al., 2004). This sequence data allowed for more

rapid gene function analysis uncovering both orthologues genes as well as malaria pathogen-specific genes.

Telomerase activity in malaria parasite was first identified in semi-purified extracts of *P. falciparum* blood stages by the group of Artur Scherf in 1998 (Bottius et al., 1998). Using a modified PCR-based telomere repeat amplification protocol (TRAP) they were able to show that telomeric sequences were added to the 3' end of primers, in an RNase A-sensitive manner. Later, taking advantage of the available genome sequences, they were able to find both reverse transcriptase- and telomerase-specific motifs in the *P. falciparum* TERT (PfTERT; PlasmoDB ID PF13_0080) gene, and TERTs of other *Plasmodium* species, including *P.knowlesi*, *P.yoelii* and *P.berghei* partial TERT sequences. The catalytic subunit of *Plasmodium* telomerase is approximately 280 kDa (~2500 amino acids) making it three times larger than all other eukaryotic TERTs. All *Plasmodium* TERTs have large sequence variations outside the conserved motifs and the protein appears to be evolving relatively rapidly. Even within *Plasmodium* the non-motif sequence is not well conserved (Fig. 10, on the right). However the conserved motifs (blue homology blocks in Fig. 10 on the right) containing all the conserved telomerase- and reverse transcriptase-motifs (Figueiredo et al., 2005) reach more than 90% sequence identity between the closely related species. PfTERT, in global two-sequence alignments (data not shown), shares 40, 41 and 42% amino acid identity with PvTERT, PyTERT and PkTERT, respectively. Surprisingly, PcTERT shows the highest 47% homology with the PfTERT aa sequence. Although the *P. berghei* complete TERT sequence is currently not available online, the partial PbTERT protein sequences exhibit relatively high 83% protein sequence homology both with PyTERT and PcTERT over a stretch of more than 1000 amino acids. When compared to the PfTERT, the same region shows less than 60% homology. The alignment of the *Plasmodium* TERTs with the partial PbTERT sequences is depicted in Fig. 11. The partial PbTERT protein aligns well with the other TERTs, sharing at least 60% identity within the conserved blocks. The TERT protein contains several nuclear localisation signal (NLS) – like motifs (identified with bioinformatics tools). Immune co-localisation studies have shown that PfTERT is found in the nucleus, but generally not at the telomere clusters. Instead it localises into a discrete nucleolar compartment, together with nucleolus-specific Nop1 protein (Figueiredo et al., 2005). However, separate locations of telomeres and TERT might be misleading. Low concentration of TERT molecules at telomeres, as well as current limited sensitivity of laboratory instruments might be the reason for this observation. In fact studies in yeast have demonstrated that telomerase co-precipitates telomeric repeats *in vivo* (Taggart et al., 2002).

Multi-way DNA alignment
Scoring matrix: Linear (Mismatch 2, OpenGap 4, ExtGap 1)

Sequence	Length (bp)	Match	NonMatch	%Match
Pftert	7557	4994	2860	63
Pvtert	7251	4430	3161	58
Pktert	6855	4634	2712	63
Pytert	6337	4826	2480	66
Pctert	6780	5173	2082	71

Multi-way protein alignment
Scoring matrix: BLOSUM 62

Sequence	Length (aa)	Match	NonMatch	%Match
PfTERT	2518	1267	1354	48
PvTERT	2416	1220	1322	47
PkTERT	2284	1254	1199	51
PyTERT	2111	1230	1190	50
PcTERT	2250	1376	1039	56

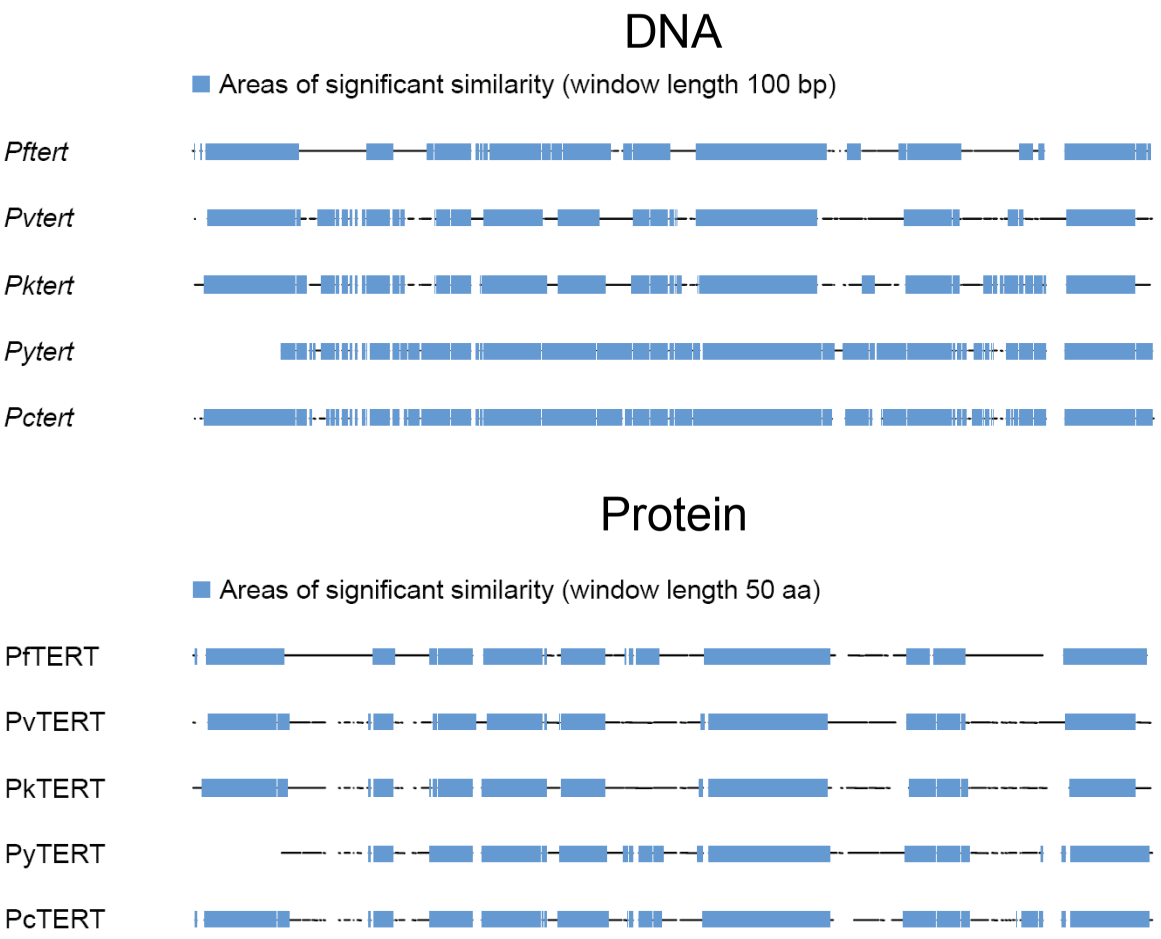

Fig. 10 Multi-way alignment of available, complete *Plasmodium* TERT DNA and protein sequences. TERTs of several *Plasmodium* species were aligned by pairwise alignment of all sequences and progressive assembly of alignments using Neighbour-Joining phylogeny. The DNA sequence and the protein sequence alignments are shown on the top and bottom, respectively. The length, number of matching and non-matching bp (for DNA) or amino acids (for protein) and the % identity of the particular sequence to all other sequences for each *Plasmodium* specie, is summarized in the tables on the left. Schematic representation of the alignments is depicted on the right. The longest protein sequence (of PfTERT) is 2518 amino acids long. The conserved regions, indicated in blue (60% similarity in 100 bp or 50 aa window length) contain all telomerase- and reverse-transcriptase-specific motifs, identified by Figueiredo et al. The black lines show sequence conservation between two species within the alignment. The white spaces symbolize no significant sequence homology. Note: the *P. yoelii* sequence is not complete at the N terminus. The analysis was performed in Clone Manager 9 Professional Edition.

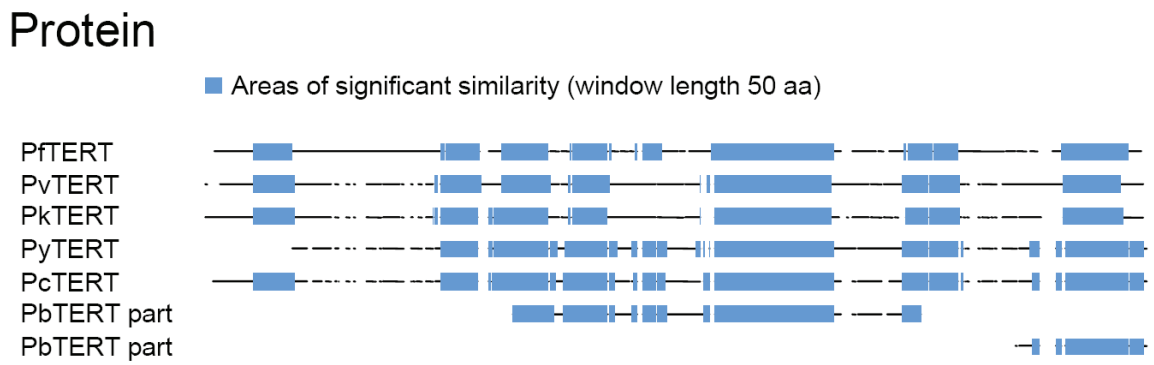

Fig. 11 Multi-way protein alignment of PbTERT partial amino acid sequences with the other *Plasmodium* TERTs shows the conserved regions specific to TERT. A significant part of the N terminus is missing in the PbTERT sequence. The *P. yoelii* TERT is not fully complete. The blue blocks indicate 60% or more sequence identity in windows of 50 amino acids.

PfTERT is capable of *de novo* synthesis of telomeric repeats both to the 3' telomeric overhang and to nontelomeric 3' ends, thus contributing not only to telomere maintenance but also to new telomere formation on broken chromosomes (Bottius et al., 1998) which has been shown to occur in cultured *P. falciparum* (Mattei and Scherf, 1994). Telomerase activity in *P. falciparum* is detectable at the trophozoite and schizont blood stages where DNA replication occurs (Bottius et al., 1998; Figueiredo et al., 2005). Not much is known about the RNA component of *Plasmodium* telomerase which has been identified only recently *in silico* in several species of *Plasmodium* (Chakrabarti et al., 2007) based on structural comparisons of conserved TR domains from other organisms. The *P. berghei* TERT RNA is predicted to be 2027 bp long, the *P. chabaudi* TR 1947 bp and *P. yoelii* 1999 bp. According to the rodent malaria species synteny map (Kooij et al., 2005) in all the three species the TR is located on chromosome 8 in the three species. Alignments with *P. falciparum* genome revealed that the PfTR is syntenic and located on chromosome 9, and is approximately 45% identical to the *P. berghei* TR, with several regions of homology higher than 60%. All the putative TRs are AT-rich (more than 70%). Secondary structure model of the *P. falciparum* TR showed a presence of several conserved regions (A, B, C, D, E, Pk-1 and Pk-2). The TR presence in *Plasmodium* was detected by Northern analysis though several the exact TR size could not be determined (Chakrabarti et al., 2007).

Initial drug tests *in vitro* using commonly used reverse transcriptase inhibitors such as dideoxy GTP in the TRAP (Telomere Repeat Amplification Protocol) assays for telomerase activity showed telomerase inhibition at micromolar concentrations. Additionally, preliminary studies on *in vitro P. falciparum* culture showed that these drugs can efficiently inhibit telomerase activity, killing the parasites after 3 – 5 blood stage cycles (Bottius et al., 1998).

I.4 Chromatin structure and gene regulation.

The basic unit of chromatin, the nucleosome, plays a substantial role in gene regulation. Nucleosome composition is conserved throughout all eukaryotic species - 147 base pairs of DNA wrapped in a left-handed superhelix around the histone octamer composed of two copies of each of core histones (Fig. 12). The “free” DNA fragment between nucleosomes is called linker DNA and its length varies among species and cell types. Both histones and DNA are subject to epigenetic modifications (explained later in this chapter).

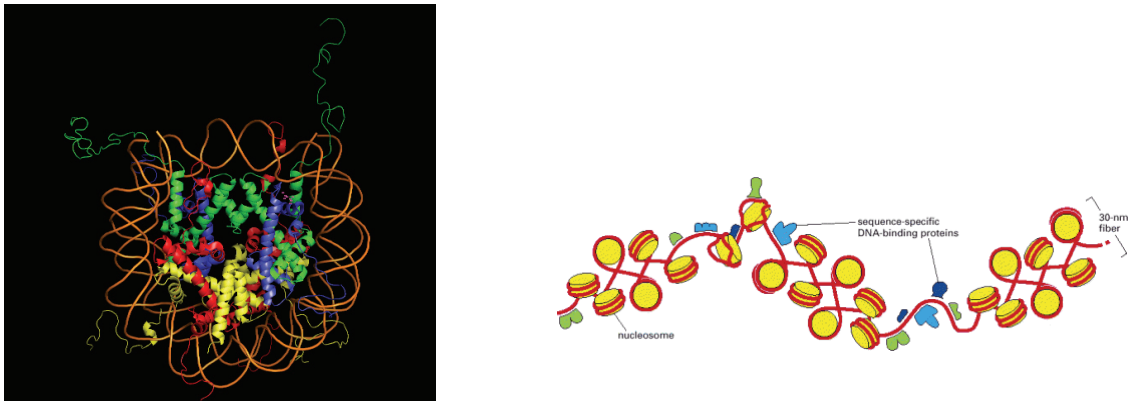

Fig. 12 The nucleosome structure. Histone core consists of two H2A • H2B dimers (red and yellow) and a H3 • H4 tetramer (green and blue). 147 bp of DNA (shown in orange) are wrapped around the histone octamer in 1.65 turns of a left-handed superhelix. The “beads on a string” model of chromatin compaction is shown on the right (from Molecular Biology of the Cell, Alberts et al., 2002).

Chromatin structure in the cell can be functionally divided into euchromatin – loosely packed chromatin considered transcriptionally active, and heterochromatin, which is a densely packed transcriptionally inactive form of chromatin. The densely packed form of DNA is inaccessible to regulatory factors, including DNA-binding proteins, and basal transcriptional machinery (Collingwood et al., 1999; Johnson et al., 2009; Orphanides and Reinberg, 2000). Therefore, usually for a gene to be transcribed the region must first become accessible. For that the chromatin must undergo temporal or stable structural changes by means of DNA-protein interactions and alterations of chromatin constituents, including exchange and/or incorporation of histone variants, histone modifications and DNA modifications.

I.4.1 Histones as major structural components of chromatin.

As already mentioned, the packing of genetic material in cells is possible thanks to small basic proteins called histones. Eukaryotic cells contain five abundant histones: the linker histone H1, and the highly conserved core histones H2A, H2B, H3 and H4. The core histones share a common histone-

fold domain (Fig. 13), which mediates the assembly of the histone octamer present in the nucleosome structure. Each of the core histones contains an N-terminal “tail”, which stabilises DNA wrapping around the histone octamer. Additionally the histone tails are a subject to numerous modifications, discussed below.

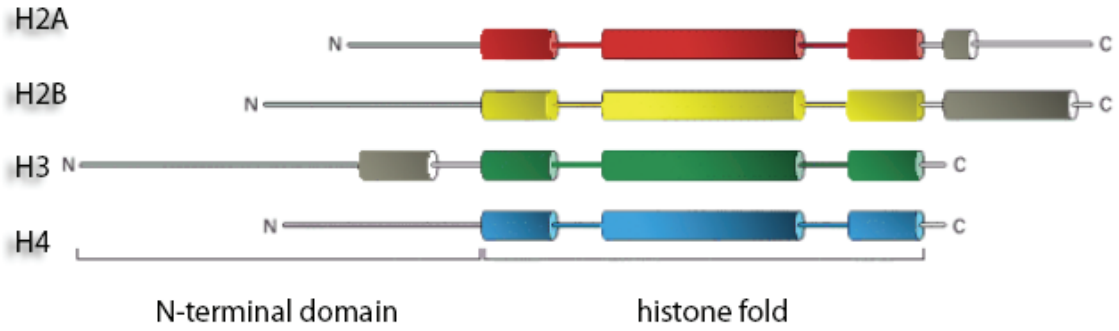

Fig. 13 Structure of the core histones. N-terminal tails and histone fold domains are indicated. Modified from Molecular Biology of the Cell, Alberts et al., 4th edition.

Linker histones, including histone H1 variants and histone H5, are composed of central globular domain and long N- and C-terminal tails, which are rich in basic amino acids. In higher organisms each histone is represented by a family of genes encoding multiple non-allelic primary-sequence variants. It is thought that histone variants serve two main purposes in the cell. First, the histone-exchange removes epigenetic marks on core histones and facilitates reprogramming of the particular gene. Second, their incorporation permits effectuation of various functions. The most studied histone variants are different histones H3 and H2A. These include H3.3, which functions in transcriptional activation (Ahmad and Henikoff, 2002) and CENPA - centromeric histone H3 (Sullivan et al., 1994), H2AZ, which plays a role in gene expression and chromosome segregation (Allis et al., 1986; Rangasamy et al., 2004; Wu et al., 2009), H2AX, which acts in DNA repair and recombination (de la Barre et al., 2001; Lee et al., 2010; Rogakou et al., 1998), macro H2A – transcriptional repression and X chromosome inactivation (Angelov et al., 2003; Chakravarthy and Luger, 2006; Costanzi and Pehrson, 1998) and H2ABBD possibly functioning in transcriptional activation (Bao et al., 2004; Gautier et al., 2004; for a recent H2A review see Altaf et al., 2009). The structural and functional roles of the linker histones still remain uncertain. *In vitro* studies show that loss of histone H1 leads to chromatin decondensation to the beads-on-a-string form at low ionic strength (e.g. Carruthers et al., 1998; recent review by Happel and Doenecke, 2009). General depletion of the linker histone usually takes place in transcriptionally active chromatin compared to inactive chromatin (Schlissel and Brown, 1984; Smith and Hager, 1997)

I.4.1.1 Deciphering the histone code

Introduction of a stable histone amino-terminal modification can influence interactions with chromatin-associated proteins. The combinatorial histone tail modifications, the so called histone code, working

through the concerted action of “translators” or effector proteins, regulatory and remodelling factors, dictate and determine the transitions of chromatin between transcriptionally active or silent states. Furthermore, the histone code provides an additional level for information storage, extending the capacity of the genetic code. Complex modifications of histones within chromatin have been recognised as an important mechanism of gene regulation, and even if it has been recently a subject of extensive research, our current knowledge is only the tip of the iceberg. Multiple signalling pathways converge on histones and their effects or “marks” are represented by covalent modifications of histone tail domains, which include acetylation, phosphorylation, methylation, ubiquitination and sumoylation. Each of enzymes performing these modifications is specific for particular amino acid positions in particular histones, and each combination of these modifications may be interpreted differently resulting in distinct downstream effects. Despite its complicated nature, extensive studies have already provided some insights into the relationship between histone tail modifications and their possible functions. For instance, acetylation is thought to directly facilitate transcription, both by weakening histone-DNA contacts (the positive charge on a lysine residue is neutralised) and by recruitment of transcriptional activators by hyperacetylated histones themselves. Methylation, which occurs at lysine and arginine residues, may exert either a positive or negative effect on gene transcription. Active genes are enriched for methylation at histone H3 Lys4 (H3-K4), H3-K36 and H3-K79. However trimethylation of K9 at histone H3, K20 at histone H4 and monomethylation of H3-K27 are marks of constitutive heterochromatin (e.g. Rice et al., 2003; Henckel et al., 2009). Another example is phosphorylation of serine 10 of histone H3, which is crucial for chromosomal condensation and cell cycle progression during mitosis and meiosis (Nowak and Corces, 2004; Jeong et al., 2010). Ubiquitination of Lys119 of histone H2A has been found to play a role in Polycomb silencing and X-chromosome inactivation (Fang et al., 2004; Wang et al., 2004). Additionally, methylation of histones was found to cross-talk with ubiquitination events at histone H2A (Wang et al., 2004; Shukla et al., 2009). Lastly histones may also be sumoylated and histone H4 sumoylation has been reported to be associated with transcriptional repression (Shiio and Eisenman, 2003) but also activation (for a review see Lyst and Stancheva, 2007).

I.4.2 Factors in epigenetic regulation

Chromatin compaction and expansion requires a multitude of chromatin-remodelling complexes. These multi-protein complexes act in concert with many other proteins present in the cell that take part in the induction or repression of transcription. There are two broad classes of chromatin-remodelling complexes – covalently modifying and transiently modifying complexes. The first class includes proteins which acetylate, methylate, phosphorylate and ubiquitinate the chromatin. Histone acetylation (MacDonald and Howe, 2009), phosphorylation (e.g. Nowak and Corces, 2004) and methylation (a recent review by Fingerman et al., 2008) modification systems have been characterised in detail. Probably the most studied representative of covalently modifying proteins is the family of histone acetyltransferase (HATs), which include complexes such as SAGA, PCAF, P300/CBP, etc. Histone

deacetylation is performed by histone deacetyltransferases (HDACs): the Sin3 (all eukaryotes), NuRD (higher eukaryotes) and SIR2 complexes (in yeast it is SIR2, SIR3 and SIR4) are exemplar members of this family. The second class of chromatin remodelling complexes perform ATP-dependent nucleosome or DNA alterations, and include ySWI/SNF (mating-type switching/sucrose non-fermenting) and SWI/SNF related complexes in higher eukaryotes (e.g. SMARC in humans), NuRD (nucleosome remodelling and deacetylation), CHRAC (chromatin accessibility complex) in higher eukaryotes, the *Drosophila* nucleosome remodelling factor (NURF), human Williams syndrome transcription factor (WSTF) and several others.

I.4.2.1 HATs and HDACs in *Plasmodium*

The acetylation status of a given histone will depend upon the balance of locale specific HAT and HDAC activity which is determined by accessory proteins. Several HDACs and HATs have been identified in e.g. *P. falciparum* genome (based on a recent review by Horrocks et al., 2009 and PlasmoDB search) indicating the expected presence of functional acetylation/deacetylation processes similar to those found in other organisms (see Fig. 14, modified from Malaria Parasite Metabolic Pathways database). HATs (Fig. 14 middle panel – Effectors) require Acetyl-CoA, a protein substrate and an adaptor protein SIN3. The product of HAT action, the acetylated histone is in turn a substrate for HDACs and *vice versa*. PlasmoDB annotation points to five HDACs in the *Plasmodium* genome, including two NAD^+-dependent deacetylases (Fig. 14, middle panel). The final products of deacetylation – nicotinamide, acetyl-ADP-ribose (for sirtuins), acetyl (for the remaining HDACs) and a deacetylated histone may convey further functions to the cell affecting for instance metabolic pathways. Deacetylated histones can be ADP-ribosylated upon deacetylation (Fig. 14 bottom, red panel), though deacetylation-independent ADP-ribosylation (top green panel) can also occur (see section “SIR2 diverse functions”).

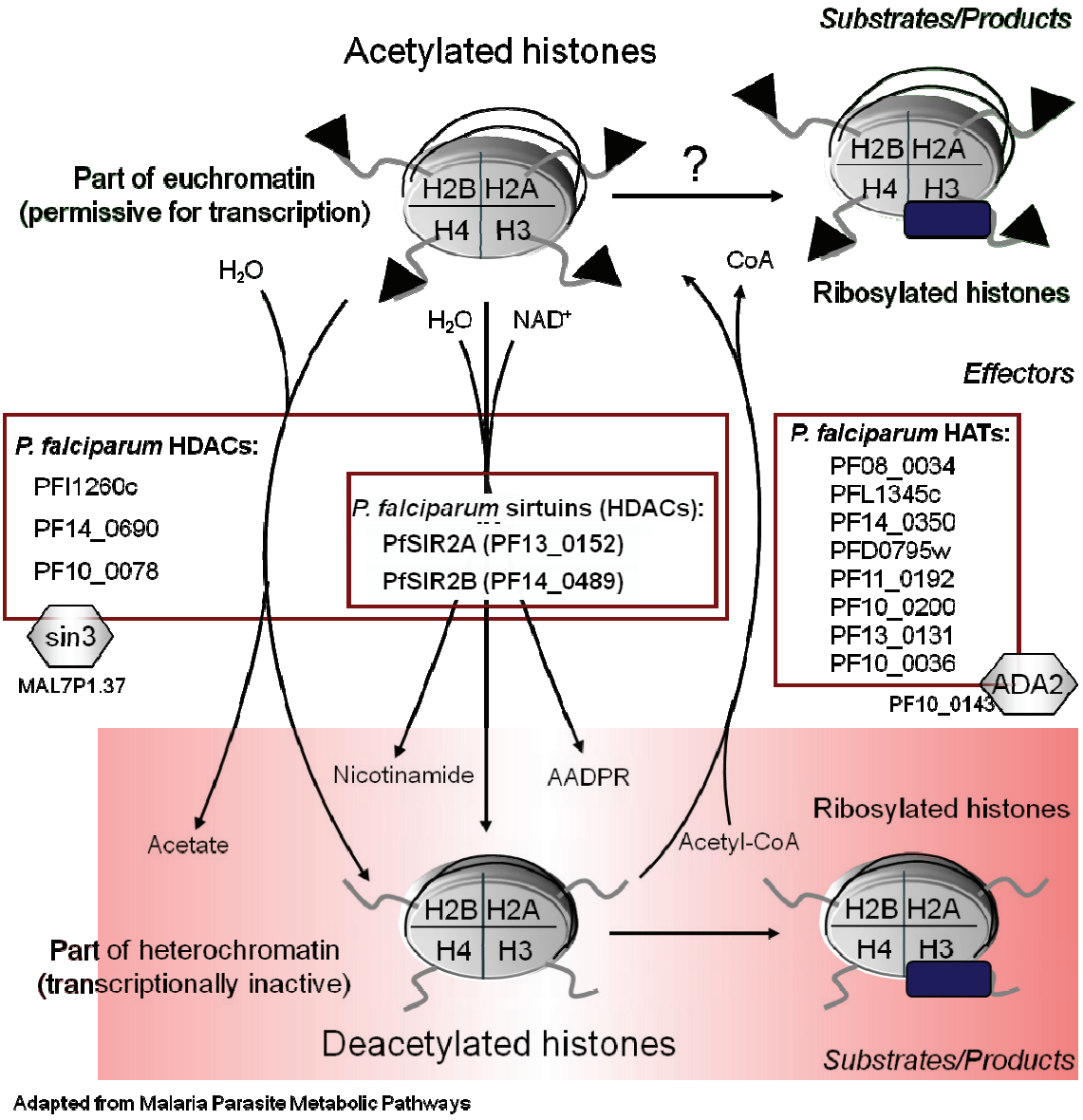

Fig. 14 HATs and HDACs in Acetylation/deacetylation pathway in *P. falciparum*. Acetylated (black triangles) histone tails (specifically Lys residues) are usually a part of transcriptionally-permissive chromatin (top green panel). On these histones DNA is usually less "tightly" wrapped enhancing transcription machinery accessibility. Histones (like other proteins in a cell) can also be ribosylated. Collected data suggests that in *Plasmodium* ADP-ribosylation can be performed by sirtuins following deacetylation (bottom red panel). However ADP-ribosylation can occur independently of the deacetylation reaction. Additionally to NAD^+-dependent sirtuins (middle panel – *Effectors*) *P. falciparum* genome contains other histone deacetylases (HDACs). The Sin3 protein, which serves an adaptor function for the non-sirtuin HDACs is shown. The product of deacetylation by any of the HDACs is a non-acetylated histone residue. Global deacetylation usually leads to chromatin condensation yielding a particular chromatin region transcriptionally inactive. Additional deacetylation products are nicotinamide and 2'-O-acetyl-ADP ribose (AADPR) in case of sirtuins and acetate for the remaining HDACs. Histone acetylases (HATs; middle pannel), with ADA2 as an adaptor protein, complete the cycle by performing histone acetylation using Acetyl-CoA as a co-substrate.

I.4.2.2 Spatial distribution and influence on gene transcription

Spatial distribution of a eukaryotic genome within the cell nucleus plays a substantial role in transcriptional regulation, adding an extra level of control to eukaryotic gene expression. A number of

studies suggest that a nucleus is divided into regions promoting transcription – thought to be the nuclear interior, and those that block gene activation, seemingly the nuclear periphery. However recent findings imply that domains for gene expression and silencing exist within both of these sites, suggesting that a concerted action of several factors is needed to determine the transcriptional status of a gene. In yeast, subtelomeric regions and silent mating-type loci localise to the nuclear periphery (Gotta and Gasser, 1996; Gotta et al., 1996a; Maillet et al., 1996; Gotta and Gasser, 1996; Towbin et al., 2009), forming foci or clusters of chromosome ends. These chromosome regions show typical characteristics of heterochromatin – gene silencing, late S-phase replication, depletion of active histone marks (such as H3 K4 trimethylation and H4 K16 acetylation). A similar pattern of telomere clustering was also observed in a human malaria parasite *P. falciparum* (Freitas-Junior et al., 2000) and was implicated in a mutually exclusive expression of the *var* antigen family, which localises to the nuclear periphery (both chromosome-internal and subtelomeric v*a*r genes) (Ralph et al., 2005). Curiously the telomeric clusters promoted ectopic recombination within the *var* members indicating formation of a temporary, recombination-permissive environment. Initially activation of a specific *var* gene was thought to be induced by repositioning of the *var*-contained telomere away from the telomere bundle (Duraisingh et al., 2005; Ralph et al., 2005). However it was recently shown that nuclear re-localisation was in fact not necessary, since a *var* gene remained within telomere clusters regardless of its transcriptional status (Marty et al., 2006). Another example is a well studied multigene rRNA family, silenced by their localisation to the so called nucleolus organiser regions (NORs) (McClintock, 1934; Ritossa and Spiegelman, 1965) where rRNA genes are tandemly arrayed. The silencing is restricted to rRNA genes and does not spread to or from neighbouring genes (Lewis and Pikaard, 2001; Silva et al., 2008).

I.4.2.3 Role of nuclear pore complex in transcriptional regulation

Recently some evidence has emerged as to possible mechanisms and players at the gene activating domains within repressive regions. In a number of recent studies e.g. in *S. cerevisiae* the nuclear pore complex (NPC) has been implicated in gene transcription regulation (for a review see Akhtar and Gasser, 2007; Hetzer and Wente, 2009). NPCs are thought to cause local compartmentalisation of the nuclear periphery, creating a transcriptionally permissive environment for a specific gene, simultaneously silencing all other genes in its vicinity. One obvious benefit of this mode of transcriptional control at the nuclear periphery is the facilitation of transport of transcripts from the nucleus operated directly by nuclear pore complexes (nuclear export).

The first evidence of a role for NPCs in transcriptional regulation came from work by Ishii et al. (2002), which identified proteins limiting spreading of activating or silencing factors to neighbouring genes. In subsequent studies a direct link between active transcription, mRNA export and NPC was found by showing the Sac3-Thp1 mRNA export complex interactions with Nup1, Sus1 and the SAGA complex (see Fig. 15b) (Fischer et al., 2002; Rodriguez-Navarro et al., 2004).

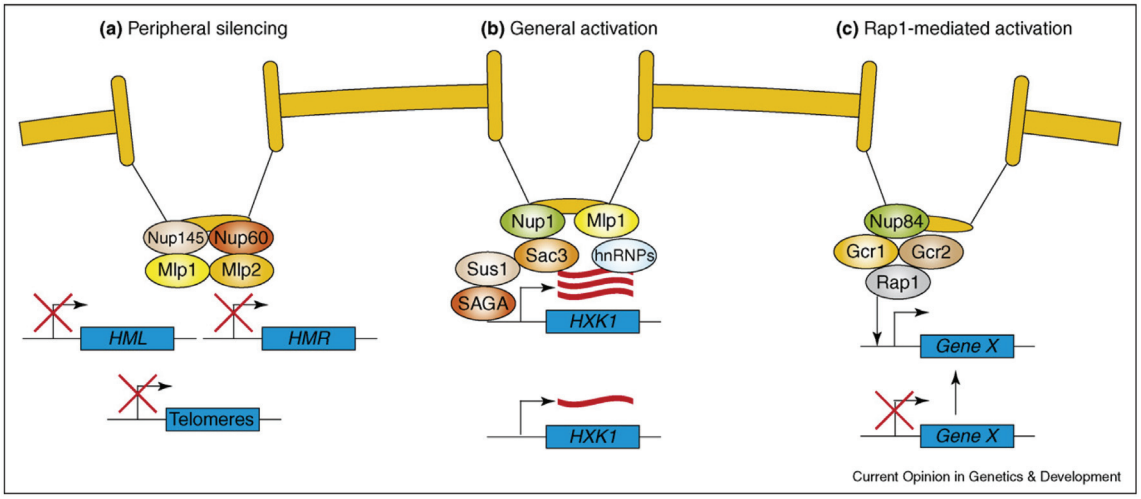

Fig. 15 Models for nuclear pore complex-mediated gene activation and silencing within the nuclear periphery in *S. cerevisiae*. Source: review by Brown and Silver (2007).

Another way of gene activation at the nuclear periphery might be through Rap1 protein (see Fig. 15c). In yeast the anchored Nup84 complex binds Rap1 resulting in gene tethering to the nuclear pore complex and subsequent transcription (Menon et al., 2005). Notably, Rap1 is a transcription factor recruiting SIR2 histone deacetylase in yeast, as well as a regulator of highly transcribed ribosomal protein genes and glycolysis genes (Miyoshi et al., 2003; Moehle and Hinnebusch, 1991). Recent studies implicate that untranslated regions might play a role in positioning of genes in the vicinity of NPCs through DNA-binding of various nuclear pore proteins, as shown for Nup116 and Nup2 (de la et al., 2002; Schmid et al., 2006).

I.5 Telomere position effect

Telomere position effect (TPE) has been first described in *S. cerevisiae* as reversible silencing of genes located near a telomere (Gottschling et al., 1990). It was shown that this phenomenon is dependent on telomere length and on the distance of the gene to the telomere (Renauld et al., 1993; Kyrion et al., 1993; Gottschling et al., 1990; Baur et al., 2001). In general the longer the telomere the stronger silencing effect it exerts. It was postulated that due to shortening of telomeres with age in human somatic cells, TPE could be a mechanism to gradually alter phenotype with cellular age (Wright and Shay, 1992). Near-telomere silencing results from changes in chromatin conformation. Several factors such as sirtuin family proteins (SIR2, SIR3 and SIR4; see further sections in this chapter; (Aparicio et al., 1991), Rap1 protein, Rif1p, Rif2p (Kyrion et al., 1993), HDF1 and HDF2 (Boulton and Jackson, 1998), histone modifications and histone variants, all conspire to alter the access of transcription machinery to the particular subtelomeric region (reviewed in Tham and Zakian, 2002; Baur et al., 2004). Some studies have demonstrated that cells with active ALT (alternative lengthening of telomeres) mechanism might not exhibit TPE (Sprung et al., 1996; Wiley and Zakian, 1995). Interestingly a recent finding proved that despite local heterochromatin structure the

subtelomeric regions are not as transcriptionally silent as it had previously been considered. Telomeric repeat-containing RNA (TERRA) are heterogeneous in size RNA molecules, which were found transcribed from subtelomeric locations and localised to telomeres where they contribute to establishment of heterochromatin (Azzalin et al., 2007). TERRA was shown to co-precipitate a number of telomeric proteins, including TRF1, TRF2, ORC1, HP1, H3K9me (Deng et al., 2009), thereby confirming its function is compact chromatin formation.

I.5.1 TPE, epigenetics and antigen expression regulation in *Plasmodium*

In order to evade the host immune system the malaria parasite uses switchable and clonal successful variants of a surface antigen; the phenomenon is known as antigenic variation (Hernandez-Rivas et al., 1997; Rubio et al., 1996). Successful switching of an antigen to a form immunologically cryptic in the ongoing malaria infection is thought to result from the selective pressure brought to bear by recognition of the iRBC surface components by the host immune system (Warimwe et al., 2009). Selection acts upon a population of parasites which have a low background rate of antigen switching and is a crucial survival strategy for the parasite (Hernandez-Rivas et al., 1997; Rubio et al., 1996). The *Plasmodium* genome contains a number of gene families that encode potential variant antigens families and most can be found in subtelomeric regions of the 14 linear, nuclear chromosomes. This sub-telomeric locale offers a number of advantages to the parasite including enhanced rates of recombination to maintain diversity in the repertoire and ease of regulation since they might be subject to TPE.

To date the best studied *Plasmodium* multigene family is *var* gene family in *Plasmodium falciparum*, which in a single genome encodes ~60 variants of highly-polymorphic *Plasmodium falciparum* erythrocyte membrane protein 1 (PfEMP1). PfEMP1 are large, structurally related, multi-domain proteins expressed on the surface of the iRBC and individual domains may act as adhesins conferring distinct binding profiles to a number of host receptors present in serum or on several host cell types, such as dendritic cells (DCs), B and T cells, platelets, red blood cells (RBCs), endothelial cells and syncytiotrophoblasts. The host receptors identified so far include CD36, ICAM-1, VCAM-1, CD31/PECAM-1, complement receptor 1, chondroitin sulphate A, heparan sulphate (for review see Flick and Chen, 2004 and references therein). *var* genes are currently classified into 7 groups based on *var*-specific *ups* promoter types (*upsA, B, C, D, E, BA, BC*). *UpsA* and *upsB* type *vars* localise mainly to subtelomeric regions (around two-thirds of the total *var* population in the 3D7 strain) while *upsC* types are mainly chromosome-internal. The remaining classes include *upsE* regulating *var2csa*, a predominant antigen expressed during pregnancy-associated malaria (Salanti et al., 2003), and *var* genes controlled by *upsBA* and *upsBC* promoter chimeras. Importantly severe malaria in children has been associated with *Plasmodium* expressing type *upsA* and *upsB var* genes (Kaestli et al., 2006; Rottmann et al., 2006).

First shown by Scherf et al. the expression of *var* genes is mutually exclusive, which means only one PfEMP1 variant is present at the iRBC surface at a time (Scherf et al., 1998; for review see Deitsch and Hviid, 2004). Switching from one *var* form to another has not yet been shown to involve DNA rearrangements (Scherf et al., 1998; Deitsch et al., 1999), as can happen with the *Trypanosoma brucei* variant surface glycoprotein (VSG) family (for review see Taylor and Rudenko, 2006), but is instead controlled epigenetically. The mutually exclusive expression pattern of *var* genes has been shown to be dependent on a *var* gene promoter (Voss et al., 2006), and a promoter activity in its vicinity (Dzikowski et al., 2007). Furthermore, the *var* intron was proposed to limit the spread of *var* promoter activity and affect the epigenetic status of its surroundings (Frank et al., 2006; Calderwood et al., 2003; Voss et al., 2006). Recently the 3' untranslated region has been shown to participate in *var* gene regulation as well (Muhle et al., 2009).

Epigenetic modifications, including at least acetylation and methylation of histones have been shown to be widespread in *Plasmodium*. The distribution of epigenetic euchromatin-associated modifications of histones, including at least acetylation of H3K9 and tri-methylation of H3K4 is biased and found across the entire *P. falciparum* genome with the exception of telomeric- and several chromosome-internal regions (Salcedo-Amaya et al., 2009; Lopez-Rubio et al., 2009). Interestingly at variant silent antigens (VSAs), including *var* genes H3K9me3 (silent chromatin mark) is highly over-represented, whereas H3K9ac is basically excluded (Freitas-Junior et al., 2005; Chookajorn et al. 2007; Lopez-Rubio et al. 2007, 2009; Salcedo-Amaya et al., 2009).
Not surprisingly, epigenetic mechanisms emerged as one way of controlling the mutually exclusive *var* gene expression. Freitas-Junior et al. showed that telomere-proximal regions consist mainly of densely packed, usually transcriptionally inactive chromatin – heterochromatin (Freitas-Junior et al., 2005). In parallel with Duraisingh and colleagues (2005) they showed that silencing of *var* genes is a result of heterochromatin formation at the subtelomeres. They demonstrated that silencing, in inverse relation, is mediated by covalent histone modification, namely acetylation, and *P. falciparum* Silent Information Regulator 2 homologue (PfSIR2). Recently, histone methylation was also shown to play a crucial role in *var* gene expression regulation (Chookajorn et al., 2007). In the study a blasticidin drug-resistance marker recombinant *var* gene (*varBSD*) was used, of which activation was dependent on blasticidin appliance. It was shown by Chromatin Immunoprecipitation (ChIP) with antibodies against H3K9 trimethylation that silent *var* loci are significantly enriched in the H3K9me3 silence chromatin mark (as described for instance in fission yeast Nakayama et al., (2001). In a study by Lopez-Rubio et al. (2007) *var2sca* was used to investigate histone modifications at the *var2csa* 5' flanking region. The upstream region of the active *var2csa* gene was enriched in histone H3 lysine 4 di- and tri-methylation, as well as H3K9 acetylation. H3K9 trimethylation was observed at the C-terminal part of exon 1 at *var2csa* in both poised (non-transcribed phase of *var* genes during the asexual life cycle) and "ON" states. Trimethyl H3K9 was found also on 5' flanking regions of genes other than *var* genes. However the H3K9me3 presence along a complete gene seems to be *var* gene specific and parasite stage independent. Furthermore H3K9 methylation and acetylation appear to be competitive processes. The

same study indicated H3K4 dimethylation as a possible mark for epigenetic memory essential for maintenance of an active *var* gene in subsequent parasite generations, and most probably required for efficient *var* gene switching.

It is now evident that the transcriptional activity of a *var*, or for that matter any other gene, is not solely determined by its associated cis- or trans-factors (e.g. regulatory proteins, DNA sequence). Spatial distribution of a gene within the cell nucleus plays a substantial role in transcriptional regulation, adding an extra level of control to eukaryotic gene expression (see previous section "Factors in epigenetic silencing). Telomere clustering in *Plasmodium* (Freitas-Junior et al., 2000) was implicated in a mutually exclusive expression of the *var* antigen family (Ralph et al., 2005). Constant ectopic recombination within the *var* members indicates formation of a temporary, recombination-permissive environment. In fact it has been recently demonstrated that various histone methylation modifications show specific differential distributions within the cell nucleus (Issar et al., 2009), thereby defining transcription-permissive and silent nuclear compartments.

I.6 The composite roles of SIR2 proteins

I.6.1 Introducing a family of sirtuins

The SIR2 and SIR2-like family of proteins are commonly called sirtuins, are highly conserved from archea to higher eukaryotes and are arguably most renowned for their role in cellular longevity. Having a wide scope of cellular actions sirtuins are often found at interconnections of a plenitude of cellular pathways. The sirtuin family has been in the spotlight of aging, life-span and metabolism studies and is linked to a number of diseases, including Alzheimer's disease, obesity, type II diabetes, neurodegenerative disorders and cancer. According to the Kyoto Encyclopedia of Genes and Genomes (KEGG) and UniProt, sirtuins collectively participate in gene silencing, cell cycle progression, chromosome segregation, microtubule organisation, genome stability and DNA repair (for a recent review see li-Youcef et al., 2007; Taylor et al., 2008b).
Sirtuins are central to proper cell functioning and proliferative life span therefore their role in pathogenic organisms such as Apicomplexa is intriguing.

I.6.2 Sirtuin structure

Sirtuin family members share a catalytic domain that allows the majority of sirtuins to function as NAD^+-dependent protein deacetylases, however the same domain generally acts as ADP-ribosyltransferase which in some cases can be the only activity of the sirtuin. A typical sirtuin (shown in Fig. 16) largely consists of a sirtuin catalytic domain which in turn comprises both a NAD-binding and acetyl-lysine-binding domain (red boxes in Fig. 16). The PFAM database defines the canonical sirtuin

domain (PFAM PF02146) consisting of several highly conserved regions stretching over 181 amino acids. Sirtuin domains of *Plasmodium* conform to the canonical sirtuin domain, with several highly conserved regions (Fig. 15, black boxes). Residues perfectly conserved within Apicomplexa are indicated with asterisks.

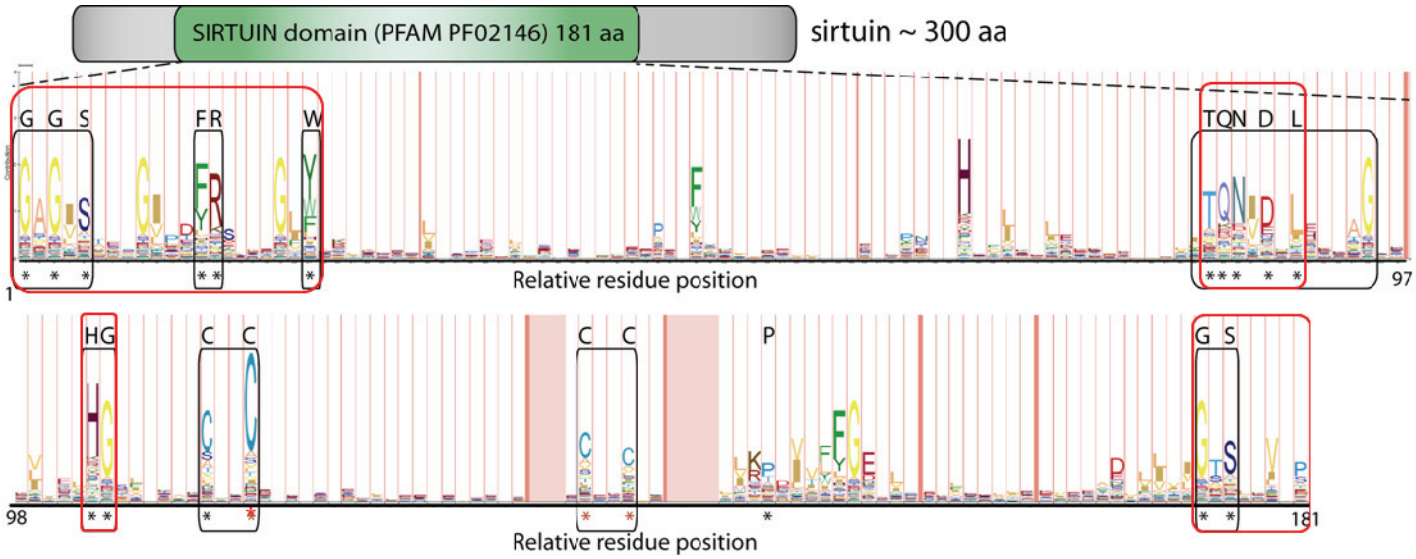

Fig. 16 Sirtuin domain. The average sirtuin of approximately 300 amino acids contains the canonical sirtuin domain (PFAM model PF02146) of 181 aa with several conserved regions (lower panel). Asterisks indicate residues conserved among Apicomplexa.

The portions of particular members of the sirtuin family that flank the sirtuin domain impose their possible additional functions and different subcellular localisations. For instance, mammalian SIRT1 exhibits different modes of nucleo-cytoplasmic shuttling depending on tissue or cell type. Two N-terminal nuclear localisation signals (NLS) and two nuclear export signals (NES) identified in mouse SIRT1 (Tanno et al., 2007) and found in SIRT1 from other organisms (nematodes, flies, other mammals) dictate various SIRT1 localisations and thus actions, such as protection from apoptosis (when nuclear) or induction of cell motility (when cytoplasmic). Another sirtuin, mitochondrial SIRT5 contains a cleavable N-terminal extension harbouring mitochondrial localisation signal (MLS) which also imposes auto-inhibition of the protein (Gertz and Steegborn, 2009). Biochemical studies on yeast SIR2 proteins have shown that ySIR2 undergoes homotrimerisation, which is required for efficient rDNA repression (Cubizolles et al., 2006), whereas SIR2, SIR3 and SIR4 heterotrimerisation is a prerequisite to telomeric silencing and heterochromatin formation.

I.6.3 Sirtuin mechanism of action

The mechanism by which sirtuins perform the deacetylation reaction is conserved and well-established (Landry et al., 2000). Despite this fact the exact sequence of chemical events is still under debate, with some reports supporting the presence of an intermediate compound (S_N1 reaction type) and others pointing to direct conversion of the substrates into reaction products (S_N2 type). Nevertheless,

deacetylation of an acetyl-lysine residue and NAD+ hydrolysis occurs in the same pocket of the enzyme, yielding a lysine (K) residue, nicotinamide and O-acetyl-ADP-ribose (*O*AADPr) as the final three products (Fig. 17, products I). Although sirtuins are most commonly thought of as protein deacetylases they are generally bifunctional and possess protein ADP-ribosyltransferase (ADPRT) activity. ADP-ribosylation can occur simultaneously with the initial target K residue either eventually deacetylated, or left acetyled (Fig. 17 products II and III, respectively). Nicotinamide is produced independent of the reaction type performed by a sirtuin.

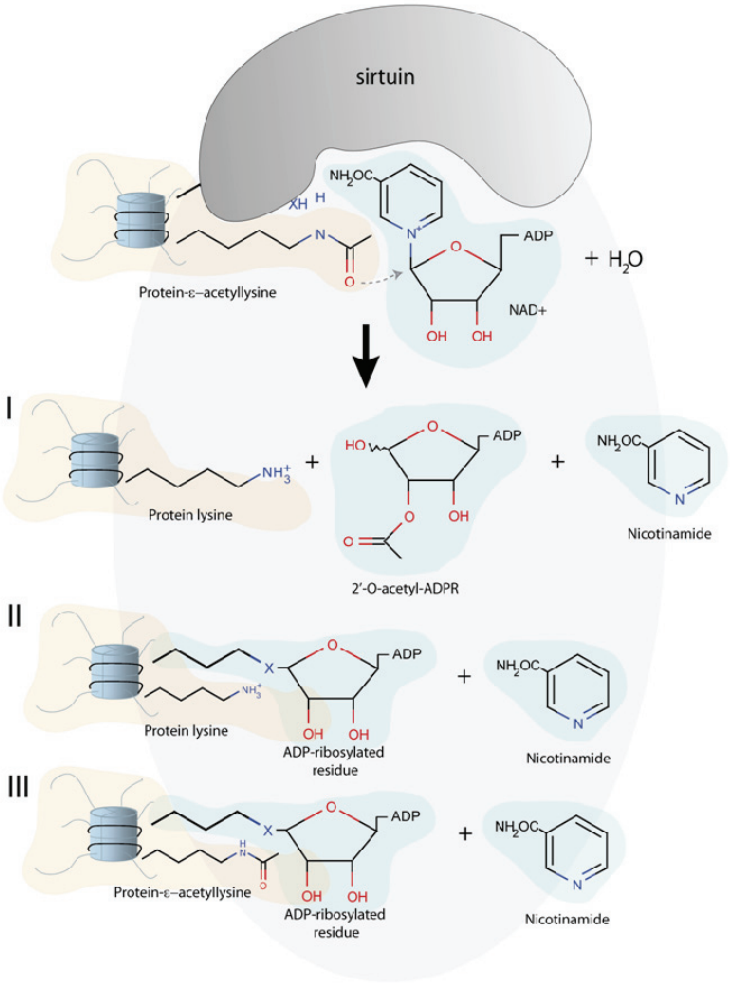

Fig. 17 A simplified mechanism of sirtuin reaction. Acetylated Lysine (K) residue on a histone protein (red background) is a sirtuin substrate. Nicotinamide adenine dinucleotide (NAD^+; blue background) and H_2O molecule are necessary for the reaction. (I) Deacetylation occurs within a sirtuin active site yielding (I) deacetylated K residue, nicotinamide and 2'-O-acetyl-ADP-ribose, a potential second messenger or (II) an ADP-ribosylated residue, deacetylated Lys residue and nicotinamide or (III) an ADP-ribosylated residue, K residue which remains acetylated and nicotinamide.

I.6.4 SIR2 diverse functions

I.6.4.1 Sirtuins play many parts in histone and other protein acetylation.

Protein acetylation is one of the best studied post translational modifications and occurs as a modification of Lysine (K) residues at the ε-methyl position of the side chain. It is currently suspected that lysine modification by acetylation/deacetylation occurs on a much greater scale than previously anticipated; and that it has a powerful influence on a wide variety of cellular processes in diverse

cellular compartments. For instance Kim et al. showed that as many as 195 mitochondria-localised proteins are post-translationally modified by acetylation at one or more sites within a particular protein (Kim et al., 2006). A very recent comprehensive global proteome study demonstrated that a vast number of 1750 proteins in a human acute myeloid leukemia cell line, are subjects of acetylation, of which at least 80% were previously unknown (Choudhary et al., 2009). The acetylation targets are highly overrepresented in chromatin modifying enzyme complexes (which are also subject to other post-translational modifications) and all major nuclear processes, e.g. DNA damage repair, transcription, nuclear ubiquitination, RNA splicing, nuclear transport. Furthermore, many acetylated proteins participate in protein folding, signal transduction, cell cycle control and cytoskeletal regulation. The acetylation status of a target protein is determined by the equilibrium of protein acetyltransferases acting as either acetylases or deacetylases. These acetyltransferases are many in number and diverse in location and members may have broad or highly focussed target specificity. Sirtuins are a subclass of the deacetylases and an individual sirtuin may act in a highly specific manner, such as the seven sirtuin family members (SIRT1-7) in humans where each possesses discrete target specificity that are often resident in distinct subcellular compartments. However, where sirtuin types are limited members may multitask as do the orthologous proteins in bacteria (*cobB* and *cobT* gene products) and seemingly some eukaryotic sirtuins. For instance *Escherichia coli* CobB deacetylates a variety of both cognate and non-cognate substrates, including its natural *in vivo* substrate acetyl-coA synthetase, as well acetylated histone H4 peptide (target of e.g. ySIR2) and p53 peptide (human SIRT1 substrate) (Zhao et al., 2004).

The most well-studied role of protein acetylation is its participation in the definition of the histone code, *i.e.* epigenetic, post-translational modifications (typically of the N-terminal regions) of histones in the context of the nucleosome that are made in a position sensitive manner according to the distribution of a given nucleosome across the genome. The codes can be transient and their genome-wide patterns reflect and help determine the transcriptional requirements of a genome according to the environmental/developmental status of the cell/organism.
Acetylation of histone tails, carried out by histone acetyltransferases (HATs), is generally associated with relaxed chromatin structure (euchromatin) making it more accessible to the DNA replication and transcription machinery as well as other histone modifying proteins. The permissive chromatin state is reversed through the action of histone deacetylases (HDACs) ultimately rendering chromatin compact and silent (heterochromatin). Histone deacetylation is performed by the majority of SIR2 proteins and is to date the most studied enzymatic activity of the sirtuin family. HDACs are conventionally divided into four classes, and the sirtuin family falls into class III deacetylases. Significant distinction of sirtuins from the other three classes of HDACs is their NAD^+ dependency and their unique insensitivity to the action of the general HDAC inhibitor trichostatin A (TSA).

In common with all HDACs sirtuins were shown to be active beyond the nucleus and deacetylate not only histones but also other (cytoplasmic/mitochondrial) proteins thereby regulating their activity and localisation. The deacetylase activity of sirtuins have so far been shown to regulate actions of at least 20 proteins including such diverse targets as histones, p53 (tumour suppressor gene), tubulin, Werner

syndrome protein (WRN), FOXO3, PGC-1α, acetyl-CoA synthetase 1, NF-κB, MEF2 to name a few (for recent reviews see Michan and Sinclair, 2007; Wang et al., 2008;). An illustrative example of non-histone sirtuin-mediated regulation is its putative role in DNA repair processes in damaged cells. p53 and WRN proteins are both DNA damage response proteins implicated in cancer: acetylated active p53 induces cell cycle arrest and apoptosis. Mammalian SIRT1 (the closest ySIR2 homologue) was found to deacetylate the p53 protein (which decreases its transcriptional activity) preventing apoptotic signalling whilst simultaneously deacetylating WRN thereby increasing its helicase and exonuclease enzymatic activity. WRN activation facilitates DNA repair during temporary inactivation of p53 – both events resulting from SIRT1 deacetylation action. The recent appreciation that the spectrum of protein acetylation is vastly expanded (Choudhary et al, 2009) will probably also result in a much wider spectrum of sirtuin target proteins; although these targets are yet to be discovered their identification will strengthen the already established links to various cellular pathways as well as uncovering new areas of sirtuin influence.

I.6.4.2 SIR2 proteins as ADP-ribosyltransferases

Bacterial sirtuins first demonstrated ADPRT activity involved in cobalamine biosynthesis (Tsang AW et al., 1998) a finding subsequently broadened to eukaryotic forms Frye, 1999; Tanny et al 1999) This latter study also showed that the ADPRT activity of SIR2 is essential for gene silencing in yeast. Subsequently, the N-terminal domains of histones H3 and H4 were found to be ADP-ribosylated by yeast and mouse SIR2 proteins, though only when already acetylated (Imai et al., 2000). The requirement for acetylated histone substrate is not absolute, in a recent report by Fahie and collegues (2009) one of *Trypanosoma brucei* sirtuins TbSIR2RP1 was shown to perform ADP-ribosylation reaction both in the presence and absence of an acetylated substrate, however in the latter case the ADPR moiety modifies arginine (and not lysine) residues. Furthermore, cysteine-specific mitochondrial ADP-ribosylation has been reported for hSIRT4, which regulates glutamate dehydrogenase (GDH) activity (Herrero-Yraola et al., 2001; Haigis et al., 2006). It is however important to note that ADP-ribosylation reaction usually occurs orders of magnitude more slowly than deacetylation (Kowieski et al., 2008; Du et al., 2009 and references within). For instance for yeast SIR2 deacetylation is 1000 fold faster than ADP-ribosylation (Tanner et al., 2000). However, least two of the mammalian sirtuins, namely SIRT6 and SIRT4 are predominantly ADP-ribosyl transferases having negligible deacetylase activity (Liszt et al., 2005; Haigis et al., 2006; Ahuja et al., 2007). Currently, the role of mono ADP-ribosylation of proteins in cellular processes and the interplay between ADP-ribosylation and other modifications remains to be fully uncovered. However, the capacity of sirtuins to perform two different post-translational modifications extends still further the complexity of process regulation and the role(s) of sirtuins therein.

I.6.5 Function-dependent localisation

In keeping with the extensive range of proteins that can be acetylated and/or ADP-ribosylated the physical locations of modified proteins are widespread, in some cases dynamic and have been found in cell nucleus, cytoplasm and mitochondria, and probably other cellular organelles (Fig. 17 top panel). Reflecting the sub-cellular distribution of these post-translational modifications, e.g. mouse and human four of the seven sirtuins (SIRT1, 2, 6 & 7) are localised either to or in some cases shuttling between the nucleus, nucleolus or cytoplasm (Fig. 18, represented in red). In fact, one of most important sites of action of many SIR2-like proteins are telomeres (Fig. 18, bottom panel), where they participate in the TPE process (described in a previous section “Telomere Position Effect”.

SIRT3 - 5 are predominantly if not exclusively mitochondrial (Fig. 18 green sirtuins), however, our knowledge on the function and exact localisation of these mitochondrial sirtuins is limited (Michishita et al., 2005; Schwer et al., 2002; Cooper and Spelbrink, 2008). On the other hand SIRT1 for instance is not only able to shuttle between the nucleus and cytoplasm but under certain physiological conditions also relative distribution between these two sites varies depending on tissue type (Tanno et al., 2007; Michishita et al., 2005).SIR2 also associates with and forms complexes with a variety of proteins the precise nature of which determine the localisation and process in which SIR2 participates and its regulation. For instance mouse SIRT1 (mSIRT1) was found to be a member of the MRN complex, which is responsible for DNA damage responses (Yuan and Seto, 2007). Through deacetylation of one of the complex members NBS1 SIRT1 controls cell cycle checkpoints ensuring genomic stability. Furthermore, in neural progenitor cells (NPCs) mSIRT1 directs neurogenesis by associating with HES1 under oxidising conditions (Prozorovski et al., 2008)The HES1-SIRT1 complex binds to the transcriptional repressor *Mash1* promoter blocking its transcription and expression, which in turn leads to NPC-to-astrocyte differentiation.

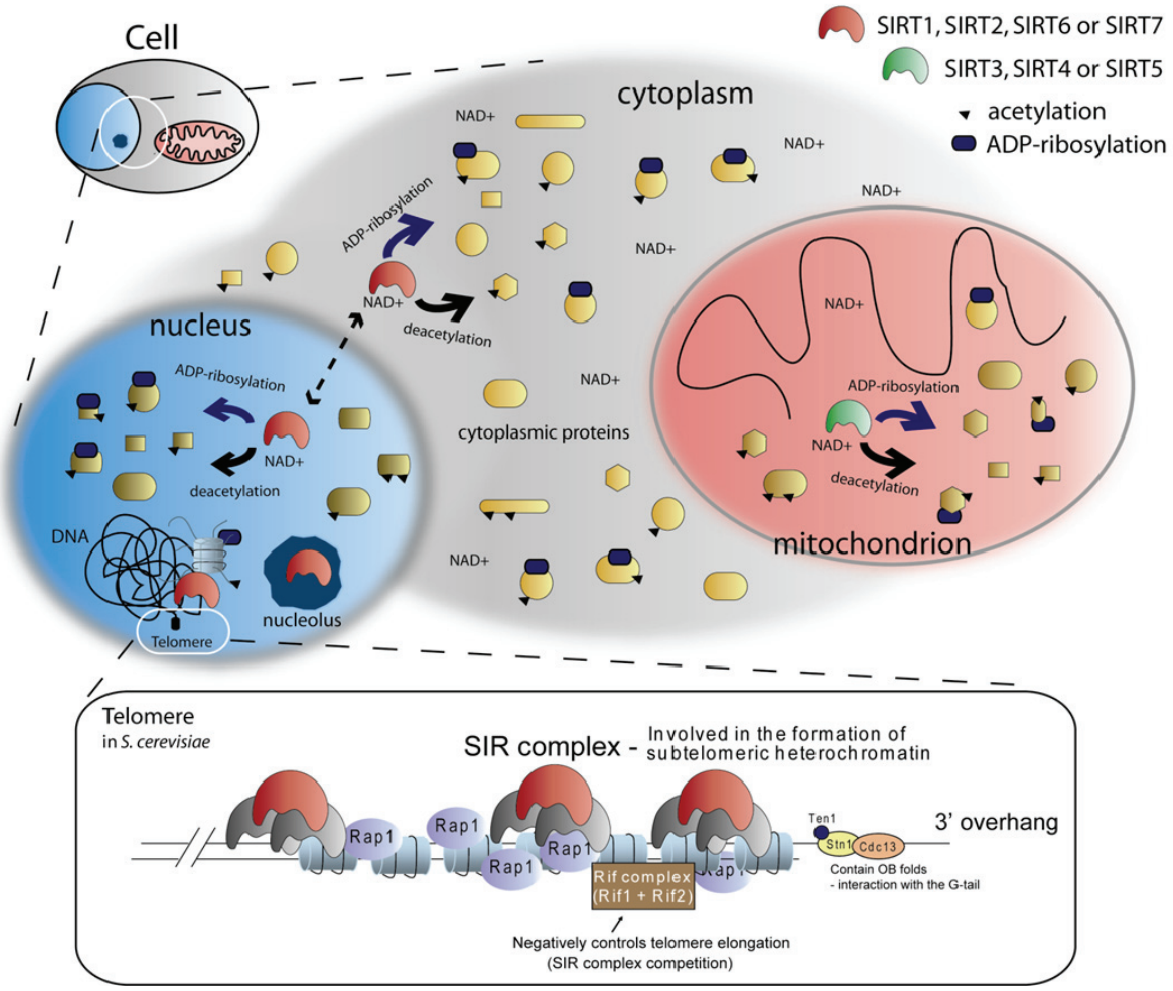

Fig. 18 General function and localisation of sirtuins. Sirtuins function as NAD^+-dependent deacetylases and/or ADP-ribosyltransferases affecting a variety of cellular proteins and processes. Commonly in cells of higher mammals (top panel) the seven sirtuins (SIRT1-SIRT7) localize to the nucleus and nucleolus (light blue and dark blue structures), cytoplasm (grey) and mitochondrion (red). A number of proteins (yellow shapes), which can be acetylated (black triangle) are sirtuin targets of deacetylation or ADP-ribosylation (indicated by dark blue elipse). Depending on the sirtuin type, tissue/cell type and current cellular state different sirtuin family members localise to various cellular compartments, with possible shuttling e.g. between the nucleus and cytoplasm as indicated by the dashed arrow. The nuclear sirtuins are involved in heterochromatin formation at several genomic locations, including telomeres. In *S. cerevisiae* SIR2, SIR3 and SIR4 form a silencing complex at subtelomeric region. Heterochromatin formation is initiated by other proteins such as dsDNA- binding protein Rap1. Rif1-Rif2 compete for binding with the SIR complex. One of many other proteins at telomeres is Cdc13, here depicted interacting with Stn1- Ten1 proteins. This complex, binding to the G-rich 3' overhang through OB domains, serves a protective function but also negatively regulates telomere elongation.

I.6.6 Biological roles of SIR2s – from calorie uptake through gene regulation to aging

SIR2 was found to be linked to life-span regulation in a number of organisms. Over-expression leads to increased survival period as shown for instance in yeast, worms and flies (Tissenbaum and Guarente, 2001; Rogina and Helfand, 2004); whereas deletion causes accelerated cell senescence and death. A number of studies since the discovery of ySIR2 have tried to pinpoint the exact function of SIR2 in the aging process. To date it is evident and in keeping with their varied intracellular distribution that SIR2 family members exert their aging-related effects through participation in several important cellular processes. First of all, ySIR2 for instance was shown to increase genome stability

through suppression of double-stranded breaks (Mieczkowski et al., 2007) and decrease rates of homologous recombination most likely by direct association with the break points (Gottlieb and Esposito, 1989). Secondly and as noted earlier, residence of SIR2 at specific genomic loci, especially at telomeres, delays transcription of a set of genes believed to be linked to the onset of senescence. Telomeres shorten with age in human somatic cells, therefore, TPE/PEV could be a mechanism to gradually alter phenotype with cellular age (Wright and Shay, 1992). Another mechanism through which sirtuins might increase cellular life-span is through "sensing" the intracellular levels of NAD+ which is greatly affected by calorie uptake. Since SIR2-like proteins are NAD+ -dependent histone deacetylases they are good candidates to effect and relay the status of external environmental nutrients from the cytoplasm to the intracellular organelles, including mitochondria and nucleus, where sirtuins family members most frequently reside. Thus sirtuins can affect both gene transcription (in the nucleus) and the activity of many cellular processes *e.g.* energy metabolism (for instance through mitochondria). Increased SIR2 activity resulting from high NAD+ levels will not only lead to decreased gene transcription at targeted loci (e.g. telomere-proximal "aging" genes suppression), but also protect the genome from free electrons or ROSs and protect telomeres from unnecessary recombination; all of which leads to enhanced genome and cellular stability. Furthermore, 2'-O-acetyl-ADPR, which is almost exclusively produced by sirtuins, as shown and quantified in yeast (Lee et al., 2008) is a potential second messenger itself. The functions of 2'-O-acetyl-ADPR are currently obscure, however data from *in vitro* studies suggests that the molecule binds to several targets such as histone H2A.1.1 (Kustatscher et al., 2005), cation channel TRPM2 (Grubisha et al., 2006) and SIR2 complexes themselves (Liou et al., 2005). Further studies are needed to elucidate the effects sirtuins exert through the unique *O*AADPr reaction product (see Fig. 16). A number of studies have provided a link between transcription levels and the availability of nutrients (see a review by Vaquero and Reinberg, 2009). Long term research in mice and recently monkeys showed that calorie restriction increases life-span in a seemingly SIRT1-dependent manner (Cohen et al., 2009; Colman et al., 2009) .The cellular effects of calorie restriction are yet to be studied in humans and the area remains controversial.

I.6.7 Two SIR2 proteins in *Plasmodium*

Two *sir2*-like genes were bioinformatically identified in the universal *Plasmodium* HDAC/HAT cohort based on sirtuin domain homology. SIR2A is best described as an orphan sirtuin placed close to but outside the class III sirtuin clade (Tonkin et al., 2009). *Plasmodium* SIR2A proteins consist of little more than the PFAM SIR2 domain sharing a protein sequence identity between 74 and 97% (CLUSTALW scores). SIR2B contains possibly a sirtuin Class IV domain with overall protein homology of 38 - 91 %, and sirtuin domain homology ranging between 53 – 90%.

I.6.7.1 *Plasmodium* SIR2A

1) Structure and function

PfSIR2A (or PfSIR2-13 encoded by PF13_0152; www.plasmodb.org) was identified through homology to the conserved core domain characteristic of the SIR2 proteins (Freitas-Junior et al., 2005) and is the better characterised of the two SIR2 proteins in *P. falciparum*. Two research groups have independently shown that PfSIR2A is a mediator of transcriptional silencing at the subtelomeric regions (Freitas-Junior et al., 2005; Duraisingh et al., 2005). SIR2A-mediated modifications spread more than 50 kb into subtelomeric regions of *P. falciparum* chromosomes (Freitas-Junior et al., 2005), significantly further than the estimated 3 kb in yeast. Interestingly telomere restriction fragment (TRF) analysis showed that PfSIR2A deletion causes an increase in average telomere from approximately 1.5 kb to 3 kb (Tonkin et al., 2009) although this had no obvious effect on parasite growth over 145 generations (Merrick et al., 2010)

PFSIR2A foci co-localise with the telomeric clusters at the nuclear periphery (Freitas-Junior et al., 2005), as was previously observed in *S. cerevisiae* (Gotta et al., 1996b)., This distribution results from PfSIR2A binding to the subtelomeric rep20 element (TARE 6) that is implicated in *Plasmodium* chromosome clustering (Freitas-Junior et al., 2005; Mancio-Silva et al., 2008). The resulting alignment of chromosome ends might facilitate ectopic recombination thereby contributing to *var* multigene family diversification. An inverse correlation between PfSIR2A presence and histone acetylation at *var* loci was observed, supporting the function of PfSIR2A as a major *var*-associated histone deacetylase. Upon activation of a specific telomere-associated *var* gene (*var2csa*), SIR2 is removed from the promoter region initiating transition to transcriptionally active chromatin through histone hyperacetylation (Freitas-Junior et al., 2005; see scheme in Fig. 19).

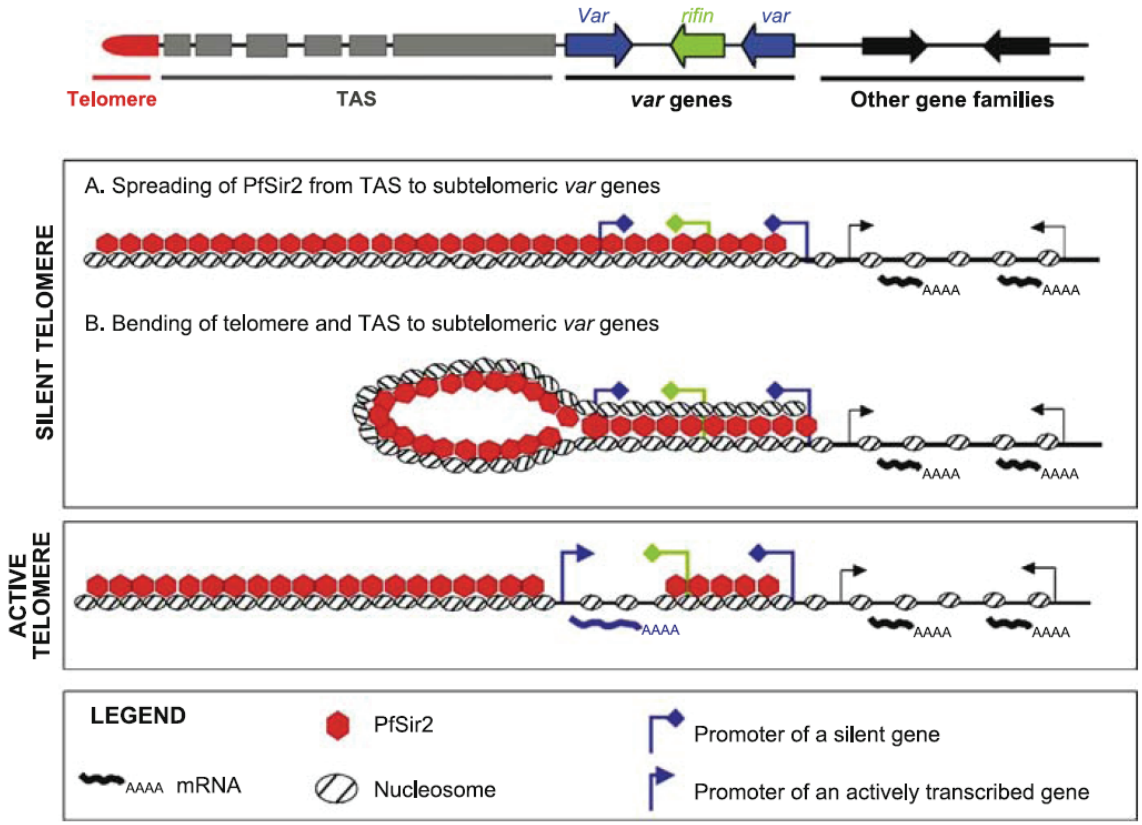

Fig. 19 A proposed model for SIR2-mediated silencing of *var* genes at subtelomeric regions. At a silent telomere-proximal region (TAS) and further towards centromere PfSIR2 presence prevents *var* gene transcription. Silencing occurs either by direct PfSIR2 binding to the region where *var* gene family is located, or by interactions from PfSIR2-covered TAS (by bending of the chromosome end towards centromere). Upon activation of a specific *var* gene PfSIR2 is removed from the promoter region by a yet unknown mechanism, enabling transcription of a specific *var* gene. Figure from Figueiredo and Scherf, 2005.

Interestingly PfSIR2A deletion disrupts H3K9me3 mark only at specific locations within the genome, including 5' UTRs of *vars* and the *rifin* multigene family (Lopez-Rubio et al., 2009). Microarray analysis of global gene transcription in *ΔPfsir2a* parasites showed upregulation of transcription of many *var* genes compared to the wild type parasites (Duraisingh et al., 2005). The most significantly affected *var* genes were those controlled by *upsA*, *upsE* (subtelomerically located transcribed towards the telomere) and *upsC* promoters (chromosome-internal). A number of *rifin* multigene family members generally located in close proximity to the upregulated *upsA*- and *upsE*-type *var* genes was also found to be upregulated. Subsequent analysis of 4 independent parasite clones of *P. falciparum Δsir2a* confirmed differential expression (~2-3 fold up-regulated) of 8-10 *var* genes/clone on average and broader in spectrum including *upsBA*- *upsBC* sub-type, with at least one product, VAR2CSA (*upsE*), present on the iRBC surface (Merrick et al., 2010). Interestingly several "silent" *var* members (*upsB* type) were further down-regulated in the *sir2a*-deletion clones. Similar *var* sets were expressed by 4 different *Δsir2a* clones (derived from *Δsir2a* population). However no DNA motifs common to the

upregulated *vars* were found implying epigenetic regulation although switching of *var* gene transcription was slightly affected in the *sir2a*-deficient line when compared to the wild type. Although the overall surface expression of pfEMP1 (VAR2CSA) was higher for *ΔPfsir2a* parasites than for the WT but lower than for the CS2 control line expressing large amounts of VAR2CSA, RNA transcripts levels for VAR2CSA were similar in the *Δsir2a* knockout and CS2, which might indicate surface "saturation" or additional post-transcriptional mechanisms of var transcript control as mentioned above.

The function of SIR2A in *Plasmodium* was to date solely studied at blood stages of *P. falciparum in vitro*. Analysis of PfSIR2A at insect stages might bring new insights to the parasite-specific protein functions.

2) Biochemistry

Recombinant PfSIR2A possesses the canonical function of a nicotinamide sensitive, protein deacetylase, more specifically a NAD^+-dependent histone deacetylase (Chakrabarty et al., 2008; Merrick and Duraisingh, 2007). PfSIR2A is able to partially substitute for the *sir2* gene absence in *S. pombe* proving that the *P. falciparum* sirtuin exhibits some fractional functional and structural conservation (Merrick and Duraisingh, 2007). PfSIR2A performs protein deacetylation *in vitro* at a slow rate with k_{cat} values at an order of 10^{-4} s^{-1} (Chakrabarty et al., 2008; French et al., 2008) compared with a typical sirtuin deacetylation rate of 0.1-0.01 s^{-1}. PfSIR2A can specifically deacetylate histone H3 lysine 9 and 14, as well as histone H4 at lysine 16 (French et al., 2008). Curiously, in this study PfSIR2A exhibited preference for a human p300 (an auto-acetylating acetyltransferase regulated by hSIRT1 and hSIRT2 by deacetylation) over highly conserved histone peptide targets, indicating a possible involvement of other molecular and/or spatial factors contributing to PfSIR2A activity *in vivo*. The *P. falciparum* SIR2A protein was also found to possess a mono-ADP-ribosyltransferase activity on a variety of acetylated substrates including histones, BSA and itself *in vitro* (Merrick and Duraisingh, 2007). The ADP-ribosyltransferase activity seems to be significantly higher than that of simultaneously tested yeast Hst2, as shown in a qualitative experiment. Uniquely PfSIR2A is an acetyllysine-independent, NAD^+ glycohydrolase (French et al., 2008) and nicotinamide insensitive although all the identified PfSIR2A functions are suspected to be catalysed by the same active site within the enzyme (French et al., 2008). On the basis of two recent studies PfSIR2A has been reported to undergo multimerisation via C-terminal interactions, though unlike its trimeric yeast counterpart the complex was shown to disassemble to SIR2 monomers upon NAD^+ binding (Chakrabarty et al., 2008). These observations are supported by a crystal structure of PfSIR2A, which has been recently solved at a resolution of 2.65 Å (PDB ID: 3JWP; Wernimont et al., unpublished). The structure when aligned in PyMOL is similar to that of hSIRT5 (PDB ID: 2B4Y), which is a class III sirtuin (Fig. 20 below).

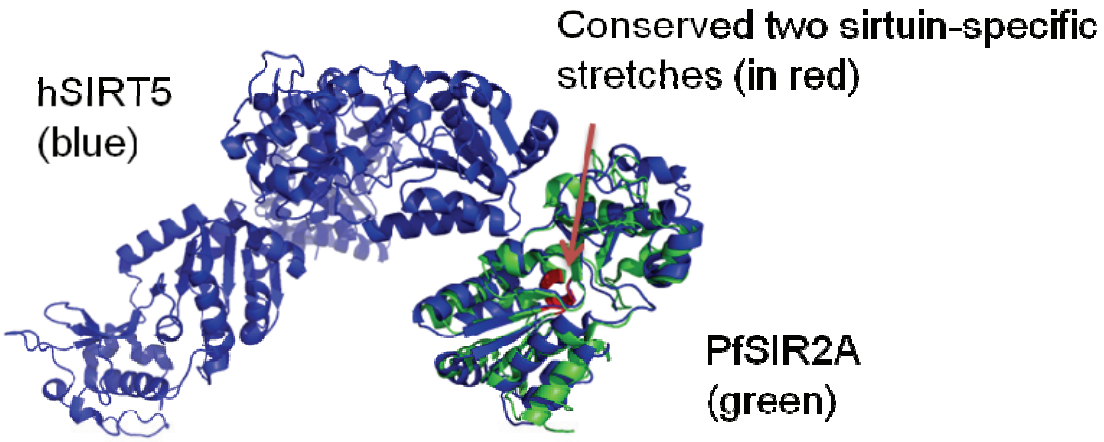

Fig. 20 PfSIR2A has a conserved structure of a sirtuin. The crystalised part of PfSIR2A molecule aligns very well (RMS value: 2.088 Å) with the canonical sirtuin domain of human SIRT5. The residues highlighted in red indicate the perfectly conserved GXG residues of a sirtuin domain.

Given the role of PfSIR2A in *var* gene transcriptional regulation it is not surprising to find PFSIR2A localises to the parasite nucleus and more specifically, predominantly to the nucleolus (Freitas-Junior et al., 2005). Interestingly PFSIR2A shuttles to the cytoplasm as well, which is thought be a result of known PfSIR2A sumoylation (Issar et al., 2008) although PfSIR2A possesses 3 theoretical sumoylation sites the precise site of such modification has not been determined. Sumoylation is known to occur at Lys 734 in hSIRT1 and which enhances its deacetylase activity (Yang et al., 2007). It is currently unknown if PfSIR2A undergoes the extensive (at least 13 generally conserved sites) phosphorylation undertaken by the cyclinB/CDK1 complex as does hSIRT1 (Sasaki et al., 2008) and what the effects of such modification might be.

I.6.7.2 *Plasmodium* SIR2B

Plasmodium SIR2B (PF14_0489) is a distant homologue of SIR2A and at 1304aa predicted to be almost five times larger than PfSIR2A (Tonkin et al., 2009). SIR2B is present and organisationally conserved in all *Plasmodium* spp. Predicted *Plasmodium* SIR2Bs are large (>1000 aa) with a recognised SIR2 superfamily domain (of approx. 384 - 512 aa) at the N-terminus of the predicted protein. *Plasmodium* SIR2B domain is plausibly phylogenetically placed in the class IV sirtuins (Tonkin et al., 2009) and thus most closely resembles the SIRT7 sub-type conserved domain which includes human sirtuin SIRT6, SIRT7 and several bacterial homologues. The mammalian SIRT6 protein was shown to exhibit predominantly ADP-ribosyltransferase activity (Bell et al., 2002) and SIRT6$^{-/-}$ mice show a premature aging phenotype caused by a defect in the Base Excision Repair pathway (Mostoslavsky et al., 2006). Interestingly, SIRT7 is the only mammalian sirtuin that preferentially localises into nucleoli (Michishita et al., 2005) and it has been recently shown to be an

activator of RNA polymerase I transcription of rRNA genes (rDNA) by interactions with RNA polymerase I and histones (Ford et al., 2006). The sub-cellular distribution of PfSIR2B has not yet been reported. Despite being paralogous, *Plasmodium* SIR2A and SIR2B are highly divergent, indicating distinct functions. The NAD^+-binding sirtuin domain at the N terminus of both proteins is the only stretch of high amino acid homology, as presented in Fig. 21. Phylogenetic alignments and motif analysis by MEME (http://meme.sdsc.edu; data not shown) of all apicomplexa sirtuins demonstrates the localised very high conservation within the sirtuin domain (data not shown). Interestingly *Plasmodium* SIR2B domains cluster phylogenetically along with *Toxoplasma, Neospora, Theileria* and *Babesia* sirtuins and all contain several additional motifs, outwith the canonical sirtuin domain, which appear to be SIR2B specific but their functional significance awaits characterisation.

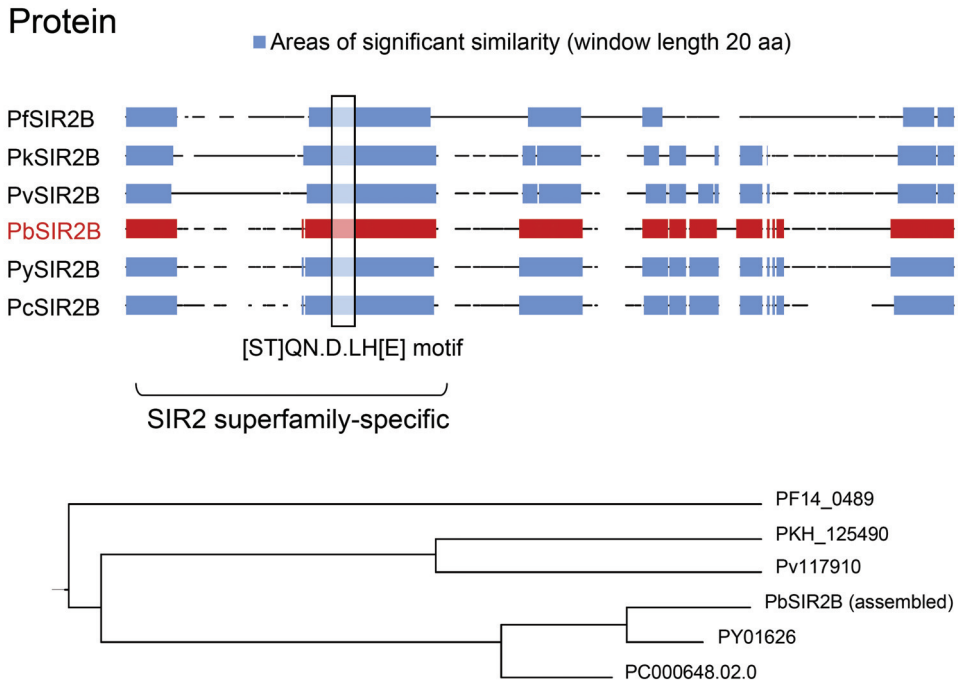

Fig. 21 Multi-way alignment of available, complete *Plasmodium* SIR2B protein sequences. SIR2B protein sequences from *P. falciparum, P. knowlesi, P. vivax, P. berghei, P. yoelii* and *P. chabaudi* (order of appearance) were aligned by pairwise alignment of all sequences and progressive assembly of alignments using Neighbour-Joining phylogeny. Schematic representation of the alignments is depicted on top. The longest protein sequence (of PfSIR2B) is 1304 amino acids long. All *Plasmodium* SIR2Bs contain signature motifs of SIR2 superfamily at their N termini. The region containing the conserved SIRT7-like motif (of SIR2 superfamily) is indicated. The high homology parts are indicated in blue (60% similarity in 20 aa window length). The black lines show sequence conservation between two species within the alignment. The white spaces symbolize no significant sequence homology. The distance tree of results (from the same alignment) is shown at the bottom. The three rodent malaria species (*P. berghei, P. yoelii*, and *P. chabaudi*) cluster together, whereas *P. falciparum* SIR2B appears to be the most distant from all other *Plasmodium* SIR2B proteins. The analysis was performed in Clone Manager 9 Professional Edition.

Fascinatingly, gene ablation studies implicate PfSIR2B in the transcriptional silencing of a complementary subset of *var* genes to SIR2A, acting predominantly at the centromerically located *vars*

of *upsB* types (Tonkin et al., 2009). In contrast to PfSIR2A, PfSIR2B deletion does not affect telomere length, as measured by TRF analysis, which might indicate that this protein is present at telomeres at relatively low concentrations, and/or that it might exert other yet unidentified effects in the parasite. No biochemical analysis of the sirtuin domain of *Plasmodium* SIR2B has yet been reported leaving open the possibility that SIR2B may exhibit different NAD^+-dependent deacetylation/ADP-ribosylation rates than SIR2A, as well as additional novel functions yet to be discovered.

I.7 The malaria parasite

Approximately 500 million people worldwide are affected by malaria, and between 1 and 1.5 million people die from it every year. Malaria is caused by protozoan parasites of the genus *Plasmodium*, which currently contains 74 classified and 283 unclassified *Plasmodium* species according to the NCBI Taxonomy browser website (http://www.ncbi.nlm.nih.gov/Taxonomy/taxonomyhome.html/). Of those classified four of them are thought to exclusively infect humans: *P. falciparum*, *P. vivax*, *P. ovale* and *P. malariae*. *Plasmodium vivax* is the prevalent malaria species in humans, excluding sub-Saharan Africa, where *P. falciparum* causes the most severe form of malaria, accounting for approximately 85 – 90% of malaria fatalities. A primate malaria *Plasmodium knowlesi* is also capable of causing lethal infection in humans and qualifies as the fifth human infectious malaria. The malaria parasite life cycle involves two hosts – female mosquitoes of the genera *Anopheles*, and possibly *Culex*, *Ciliceta*, *Mansonia* and *Aedes* and the target host being human and other primates, rodents, a few other species of reptiles, and birds. The *P. falciparum* life cycle is depicted in Fig. 22 below.

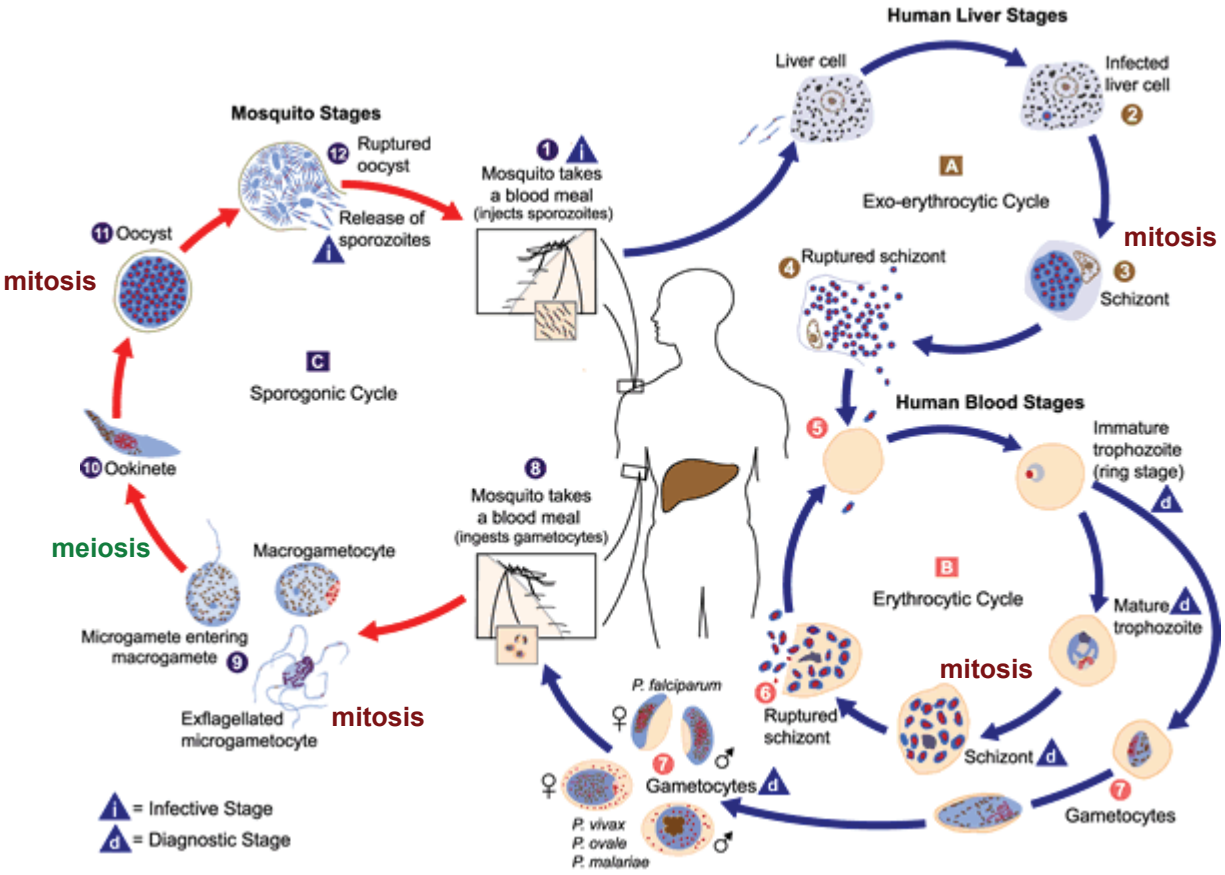

Fig. 22 The malaria parasite life cycle (see text for details). The image was downloaded from Centres for Disease Control & Prevention website (http://www.dpd.cdc.gov/dpdx). The points in the life cycle where mitosis and meiosis take place are indicated.

The *Plasmodium* life cycle starts with an invasion of the host liver cells by vector-borne haploid sporozoites injected into the blood stream upon mosquito blood meal (Fig. 22, number 1). Within the hepatocyte the sporozoite develops into the trophozoite stage, and approximately 24 hours after invasion nuclear division starts and the trophozoite matures into the liver schizont, containing between 1500 and 8000 merozoites (Fig. 22, number 3). In *P. vivax* and *P. ovale* infecting man, hypnozoites (a dormant stage) can persist in the liver for even years, causing delayed disease symptoms. Following schizont maturation, the merozoites are released into the blood stream by rupture of the liver cell (Fig. 22, 4 and 5). After completion of the exo-erythrocytic cycle (~ 48 hrs for *P. falciparum*, 22 – 24 hrs for *P. berghei*) the merozoites invade mature erythrocytes or reticulocytes (for instance *P. vivax*, *P. berghei*). Following maturation into the trophozoite the parasite undergoes mitotic DNA replication and nuclear divisions giving rise to 16 – 32 merozoites in *P. falciparum* and 8 – 18 merozoites in *P. berghei*. The rupture of the mature schizonts (6) results in merozoites release into the bloodstream. This erythrocytic cycle (Fig. 22 marked as B) can be repeated multiple times. In *P. berghei* each

asexual cycle a small portion of the parasites differentiate into sexually defined cells termed gametocytes (7). In *P. falciparum* cycles of asexual development alternate with gametocyte production. The male and female gametocytes are ingested by an *Anopheles* mosquito during a blood meal (8). After leaving the red blood cell the female gametocytes differentiates into a single macrogamete, whereas the male gametocyte undergoes mitosis and gives rise to 8 motile microgametes (Fig. 22, 9). Fertilisation occurs when the male gamete enters the female gamete (both haploid), resulting in zygote formation (diploid). Following fusion of the nuclei, meiosis takes place and the tetraploid ookinete develops within 24 hours and (10) traverses the mosquito midgut by invasion of epithelial cells. When the ookinete reaches the basal lamina, it develops into an oocyst which undergoes multiple mitotic divisions (formation of sporozoites). The haploid sporozoites, released upon the oocyst rupture (Fig. 22, number 12) travel in haemocoele to the salivary gland, from where they are injected into the blood stream of the vertebrate bitten by the mosquito. The complete cycle is then repeated.

Plasmodium berghei

P. berghei is one of the four parasite species that infect African murine rodents. It is naturally transmitted by the mosquito *Anopheles dureni* although *Anopheles stephensi* is compatible (YOELI et al., 1965; BRAY, 1954) and commonly used for rodent laboratory infections. *P. berghei* experimental malaria is characterised by acute infection in laboratory mice, with symptoms resembling those of *P. falciparum* infection in humans. The erythrocytic stages of the parasite frequently cause anaemia and failure of essential organs such as lungs, liver and spleen. The infection can also affect the brain, which leads to cerebral complications (known as experimental cerebral malaria, ECM). A less studied animal model for *P. berghei* malaria is the Brown Norway (BN) strain of the laboratory rat (*Rattus Norvegicus*). In these rats the infection persists at low density over long period of time (chronic infection), though it is unclear whether the parasite clearance occurs, as seen in chronic infections of *P. chabaudi* and *P. yoelii*. The *Plasmodium berghei* genome shares high gene content and organisational homology with those of human malaria parasites manifest in high levels of synteny (Kooij et al., 2005). In contrast to the other rodent malaria species *P. berghei* is relatively easy to manipulate genetically owing to the recently developed highly efficient transfection system (Janse et al., 2006b; Janse et al., 2006a). The *P. berghei* model has enabled valuable contributions to be made furthering the understanding of the developmental biology of *Plasmodium*, parasite-host interactions, vaccine development and drug testing.

Factors in host-parasite interactions

I.7.1 Anti-parasite response in mouse and Brown Norway (BN) rat models

Studies on mice revealed that to control and clear *Plasmodium* infection both humoral and cellular responses are required. Among others, CD4+ (e.g. Meding and Langhorne, 1991) and CD8+ T cells (Doolan and Hoffman, 1999), as well as B cells play the most prominent role in development of immunity against murine malaria. Furthermore, several reports point to natural killer T (NKT) cells acting in the early phase of infection allowing the host to mount an effective antibody response leading to parasite clearance (Su and Stevenson, 2002). Unlike the *P. chabaudi* and some *P. yoelii* infections, a *P. berghei* infection in laboratory mice is eventually lethal. In contrast BN rats are able to effectively control the *P. berghei* parasitaemia throughout the course of disease. However data available on the BN rat model is limited and not much is known about the malaria course of infection or the host factors participating in the immune response in these animals. The *P. berghei* chronic infection BN rat model could greatly contribute to our current knowledge on the host immune responses to *Plasmodium* infection, and facilitate studies on host-parasite interactions.

To date research on malaria infections in BN rats has been focused mainly on the liver stage infection. From data gathered, Kupffer cells – specialised phagocytic liver cells, were shown to inhibit development of *P. berghei* exoerythrocytic forms (EEFs) (Vreden et al., 1993). In addition, liver schizont development was reported to be negatively regulated by a cytokine Interleukin-6 (IL-6; (Vreden et al., 1992). Some studies have indicated age as an important factor in peak parasitaemia and mortality in rats infected with *P. berghei* (ZUCKERMAN and YOELI, 1954). A recent investigation by Adam et al. (2003) revealed that young rats are more sensitive to infection than older ones (around 8 weeks of age), in which the infection was eventually eliminated. However, the divergent disease outcomes are not dependent on differences in reticulocyte production in respect to age (Smalley, 1975).

I.7.2 Anti-parasite response in *Anopheles* spp.

Anopheles mosquito infection represents a major bottleneck to *Plasmodium* development and propagation. A mature banana-shaped ookinete invades the mosquito midgut epithelium between 18-30 hours post feeding. It is at this stage that most of the parasites are compromised by the *Anopheles* defence mechanisms. One of the best characterised players in the mosquito immune response is a member of the component system thioester-containing protein TEP1 (Blandin et al., 2004; Fraiture et al., 2009). TEP1 is found in the mosquito haemolymph but upon *Plasmodium* infection it is transported to the mosquito tissues by an as yet unknown mechanism, and binds to the surface of midgut-invading ookinetes. Importantly when over-expressed, TEP1 completely blocks *P. berghei* ookinete development (Frolet et al., 2006). Other recently characterised immunity factors are two leucine-rich repeat (LRR) haemolymph-localised proteins, namely Leucine-Rich IMmune protein 1 (LIRM1) and

Leucine-rich repeat protein 1 (APL1) (Osta et al., 2004; Riehle et al., 2006). LIRM1 and APL1 are found in a complex circulating in the mosquito haemolymph, and were shown to interact with TEP1. Single and double RNAi knockdown of LIRM1 and APL1 increases *Plasmodium* survival in the vector plausibly through affecting TEP1 binding (Fraiture et al., 2009; Povelones et al., 2009). The exact mechanism of TEP1-mediated parasite killing is yet to be characterised. In contrast to the complement function, several proteins were found to positively affect *Plasmodium* survival. Parasite melanisation is induced in *Anopheles* susceptible strain upon RNAi-mediated silencing of two C-type lectins CTLMA and CTL4 (Osta et al., 2004), as well as a serine protease inhibitor SRPN2 (Michel et al., 2005) and clip-domain serine proteases (Volz et al., 2005; Volz et al., 2006)

Interestingly mosquito midgut epithelium penetration does not seem to be the major site of anti-parasitic response since this step is very rarely observed microscopically and therefore thought to occur very rapidly. Instead it appears that most of ookinetes are only killed at the basal side of the epithelium, beneath the basal lamina, and that this process occurs mainly through TEP1-induced ookinete lysis (Shiao et al., 2006).

To date little is known about both the anti-oocyst and anti-sporozoite response in the mosquito. *Plasmodium* oocysts were shown to be marked by TEP1 proteins though with no effect (E. Levashina, unpublished data). In contrast ~ 80 – 90% of sporozoites, released into the haemolymph, are actively attacked and phagocytosed by haemocytes while travelling to the SGs (Hillyer et al., 2003; Hillyer et al., 2007). The anti-sporozoite immune response molecular components and the mechanism of their activation remains to be studied.

I.7.3 Parasite invasion of the mosquito vector

While the *Anopheles* host raises an effective immune response against the parasite, killing approximately 80-90% of ookinetes and same number of sporozoites, *Plasmodium* has developed multiple survival strategies, starting from mosquito midgut epithelium penetration through to successful invasion of the mosquito salivary glands (SGs). *Plasmodium* ookinetes secrete a number of proteins to the extracellular space. These proteins, implicated in the processes of attachment, invasion and motility are stored and released from mostly apically-localised organelles called micronemes. *Plasmodium* micronemal protein chitinase has been implicated in overcoming the first obstacle to the ookinete, which is a chitinaceous peritrophic matrix. Deletion or inhibition of chitinase in several *Plasmodium* species significantly impairs or completely abolishes ookinete invasion of the midgut epithelium (Dessens et al., 2001; Shahabuddin et al., 1993; Tsai et al., 2001). Ookinete motility is certainly another factor in the early stage of epithelium invasion. A calcium-dependent kinase 3 (CDPK3) was shown to participate in efficient ookinete movement, which is essential for ookinete traversal and further oocyst development (Ishino et al., 2006; Siden-Kiamos et al., 2006). Gliding motility has recently been shown to also involve cyclic nucleotide 3', 5'-cyclic monophosphate (cGMP) signal transduction pathways (Hirai et al., 2006; Moon et al., 2009). For instance, deletion of a guanylyl

cyclase β (GCβ), a cGMP producing enzyme, leads to deficiencies in ookinete motility and therefore blockage in parasite transmission (Hirai et al., 2006). A genetic knockout of another member of the pathway, namely a phopshodiesterase δ (*pdeδ*), which normally functions in degrading cGMP, results in the molecule accumulation in the mature gametocytes (Taylor et al., 2008a) causing morphological changes during *P. berghei* zygote development. In the study by Moon et al. (2009) the resulting misshapen ookinetes were physically greatly hampered in reaching the mosquito midgut epithelium (>94% reduction in oocyst numbers). Interestingly PDEδ function is limited to the ookinete stage since bypassing the midgut barrier by injection of mutant ookinetes into *Anopheles* haemocoels restored wild type-like oocyst production and the pde*δ*¯ parasites were subsequently able to successfully infect mice. One additional player in cGMP signalling is a cGMP-dependent protein kinases (PKG), which transfers the γ-phosphate of ATP to a variety of substrate proteins. PKG is essential for asexual blood stages development and when selectively inhibited blocks gliding motility of *P. berghei* ookinetes (Moon et al., 2009).

A number of microneme-derived ookinete surface proteins mediate the attachment/invasion/traversal process. Circumsporozoite- and TRAP-related protein (CTRP), which bind to *Anopheles* laminin, was shown to be essential in midgut invasion as well as parasite motility (Dessens et al., 1999; Mahairaki et al., 2005; Yuda et al., 1999). Other micronemal proteins important for midgut barrier passage is a membrane attack protein (MAOP) (Kadota et al., 2004), secreted ookinete adhesive (SOAP) (Dessens et al., 2003), as well as two surface proteins P25 and P28 (Siden-Kiamos et al., 2000; Tomas et al., 2001; Vlachou et al., 2001). P25 and P28 are two proteins of partially redundant function(s), and were shown to affect *Plasmodium* both at levels of ookinete development and midgut traversal. Of these proteins SOAP, P25 and P28 all bind laminin *in vitro*. In addition, a recently identified Plasmepsin 4 (IV) (PM4), as the first member of a family of aspartic proteases, has been shown to play a major role in ookinete infectivity to mosquitoes (Li et al., 2010). Interestingly, CelTOS is a universal invasive stage micronemal protein, important for both ookinete and sporozoite epithelium cells traversal (Kariu et al., 2006). To date only few sporozoite proteins participating in either sporozoite development or salivary gland invasion have been identified. The circumsporozoite protein (CSP) is the major surface protein of both oocyst and sporozoite stages and in its absence sporozoite development within an oocyst is completely abolished (Menard et al., 1997). Other proteins essential for oocyst/sporozoite development include (LCCL)-lectin adhesive-like protens (LAPs) (Claudianos et al., 2002; Dessens et al., 2004; Trueman et al., 2004), Falcipain-1 cysteine protease (Eksi et al., 2004), Plasmepsin VI aspartic protease (Ecker et al., 2008), and Egress Cysteine Protease 1 (ECP1) belonging to the serine repeat antigen (SERA) family of proteases (Aly and Matuschewski, 2005). Following development within an oocyst sporozoites are released and travel through haemolymph towards salivary glands. A protein required for the salivary gland invasion is the first identified member of the TRAP family, simply called TRAP (Muller et al., 1993; Sultan et al., 1997). TRAP is necessary for sporozoite gliding motility as it is a part of the anticipated universally conserved gliding machinery. Other components of the motility complex include Myo-A, MTIP, aldolase and actin filaments, all thought to be highly conserved across all motile/invasive stages of *Plasmodium* (for a recent review see Morahan et al., 2009).

II. MATERIALS AND METHODS

II.1 *P. berghei* transfection.

Genetic transformation of *Plasmodium berghei* has been recently improved (reaching transfection efficiency of 10^{-3} – 10^{-4}), owing to utilisation of the nonviral Nucleofector technology for schizonts electroporation. The following protocol is thoroughly described in Nature protocols (Janse et al., 2006b). Shortly, blood from previously infected mice was collected when parasitaemia was in the range of 5 – 15%. Between 4 and 16 µl of tail blood was mixed with 0.4 ml of PBS and split in two halves. Two mice were infected, each with 0.2 mL of the solution. After approximately four days blood was collected by cardiac puncture under anaesthesia (at the parasitaemia 1 – 3%) and resuspended in 5 ml complete RPMI1640 medium with heparin. Following centrifugation the erythrocytes were resuspended in 50 ml of the medium, split in two and transferred into two 250-ml flasks, with additional 25 ml of the culture medium. CO_2 gas mixture was added to the flasks, and the infected erythrocytes were then incubated overnight at 37°C. The next day the infected erythrocytes with mature schizonts were collected by 5s centrifugation, and the suspension was distributed into three 50-ml falcon tubes. Ten ml of 50% Nycodenz solution was then under-laid to each tube to obtain two phases. The tubes were subsequently centrifuged for 20 min. at 450*g* at RT. Approximately 20 – 25 ml of the interphase solution was collected, culture medium was added, and the schizonts were collected by 8 min. centrifugation. After discarding the supernatant the cells were resuspended in 10 ml medium in total. For transfection the solution was transferred into Eppendorf tubes (1 ml in each). The tubes were then shortly spun, the supernatant was discarded and 100 µl of Nucleofector solution containing between 5 and 10 µg DNA for transfection was added. Following resuspension, the solution was transferred into an electroporation cuvette and the electroporation was performed in the Amaxa Nucleofector device and 50 µl of medium was added immediately after electroporation. The total of 150 µl of the transfection solution was injected into a mouse (tail vein).

II.1.1 Selection of transformed parasites

One day after injection of transfection solution mice are treated with an appropriate drug, depending on the selectable marker used in the DNA construct. The two most commonly used: *Tgdhfr-ts* and human *dhfr* confer resistance to pyrimethamine (the *T. gondii* gene), or to pyrimethamine and WR99210 (the human gene). Pyrimethamine is administered orally to mice (with water), whereas WR99210 is injected subcutaneously. In the performed transfections pyrimethamine drug was used for positive selection of the transfected parasites. Between 10^{th} and 15^{th} day after transfection, when parasitaemia was 2 – 5% blood was collected by cardiac puncture under anaesthesia. Heparin was added (stock solution 200 I.U./ml in RPMI1640 medium, pH = 7.2); 0.2 mL was mixed with glycerol-PBS solution and stored in liquid N_2. To the remaining suspension cold erythrocyte lysis buffer (10x

stock-solution: 1.5M NH_4Cl, 0.1M $KHCO_3$, 0.01M EDTA) was added, and the tube was placed on ice for 3 to 5 min. After complete lysis, the parasites were collected by centrifugation for 8 min. The parasite pellet was stored at -20 °C for further analysis.

II.1.2 Cryopreservation of blood stage parasites

Plasmodium blood stage parasite lines/clones are stored in liquid N_2.
Approximately 1 ml of infected blood was collected by cardiac-puncture from a mouse or rat with parasitaemia of 1-10%. The blood was mixed with 1 ml of a glycerol/PBS solution (30% glycerol; v/v), containing 0.05 ml of Heparin stock solution. The suspension was split into 4 cryotubes (Nunc), 0.5 ml per tube. The vials were then placed into the liquid N_2 tank. A mouse intraperitoneally injected with 0.1 ml of the suspension usually developed a parasitaemia of 1-10% within 3-5 days.

II.2 Cloning of the transfected parasites by limiting dilution

The transfected parasites are normally a population consisting of both the transfected and the wild type parasites. Therefore cloning procedure is necessary for further analysis of a homogenous line. Usually 10 mice are infected for obtaining cloned parasite lines. According to the calculations 2 parasites are injected intravenously (i.v.) into each mouse, resulting in an infection rate of 20-50% of the mice (probably due to a statistical error not every mouse receives a parasite). On day 0 two mice were injected intraperitoneally with 0.01 ml of a blood-suspension from cryo-preserved transfected parasites. On day 3 or 4 parasitaemia was checked (usually parasitaemia ranged between 0.3 and 1%) and 5 µl of tail blood was collected in a heparin-treated capillary tube. The blood was diluted in 1 ml of complete culture medium and 20 µl was used for red blood cell counting using a Bürker cell counter. The number of uninfected and infected erythrocytes per µl of the cell suspension was calculated and the sample was diluted to a final concentration of 2 parasites/0.2 ml culture medium. 0.2 ml of the suspension was injected per mouse intravenously (in total 10 mice were used/cloning). At day 8 after infection the parasitaemia was determined. Usually 20 – 50% of mice become positive with a parasitaemia of 0.3 – 1%. Blood was collected and 5 ml of complete RPMI1640 medium was added. Following centrifugation cold erythrocyte lysis buffer was added (10 – 50 ml, depending on the blood volume) in order to lyse the red blood cells, leaving the parasites, leukocytes and platelets intact. After the lysis was completed (3 – 5 min. on ice) the parasite pellet was obtained by 8 min. centrifugation at 2000 rpm.

- erythrocyte lysis buffer: 10x stock-solution: 1.5M NH_4Cl, 0.1M $KHCO_3$, 0.01M EDTA
- Heparin stock solution: 200 I.U./ml in RPMI1640 medium, pH = 7.2

II.3 Negative selection (5-Fluorocytosine treatment)

Removal of the *hdhfr/yfcu* cassette is necessary for further genetic manipulation of the same parasite line. 1079 *sir2b* knockout population was negatively selected using the following protocol. On day 0 mice were injected intraperitoneally with 0.01 ml of a blood-suspension from cryo-preserved transfected parasites (for uncloned population at this stage mice were pyrimethamine treated). On day 6 three mice were infected. Three days later (at parasitaemia 0.01-0.1%) the treatment with 10 mg of 5-fluorocytosine injected i.p. started (10 mg/ml ancotil). When growth inhibition was observed (around day 13-14 post infection), blood was collected and the parasite pellet was stored for gDNA extraction and analysis by Southern blotting.

II.4 Field Inversion Gel Electrophoresis (FIGE)

FIGE is an electrophoresis-based technique for chromosome separation according to the molecular sizes. With the FIGE Chromopulse Apparatus intact chromosomes up to 3.5 Mbp can be separated. This electrophoresis technique is based on full inversion of the orientation of the electric field. A constant voltage is applied, and to improve the resolution of the bands, the duration of pulses is increased progressively during a run. Net forward migration is achieved by increasing the ratio of forward to reverse electrical current. A higher forward electrical current results in less resistance, which in turn leads to a faster forward migration. With each reorientation of the electric field relative to the gel, smaller sized DNA molecules move more quickly in the new direction than larger DNA molecules. Thus, the larger the size of the DNA molecule the slower it re-orientates, providing a size-based separation. For FIGE analysis the parasite agarose blocks were prepared from 0.3 ml of proteinase K-treated mouse blood at 2 – 3% parasitaemia. The blocks were fixed on a glass plate with additional 1% agarose solution. Following solidification, the gel was run for at least 24 hours in a cooling chamber. The next day the standard blotting procedure was employed (see Southern/Northern blotting).

II.5 Removal of leucocytes from infected blood.

When high purity of parasite preparations are required leukocytes can be removed from the infected blood by using commercially available leukocyte filters (Plasmodipur filters, Euro-Diagnostica). The following procedure was utilised in the parasite RNA and protein material preparation. The Plasmodipur filter was pre-washed with 10 ml of RPMI1640 culture medium or PBS. The infected blood suspension (diluted 1:1 in either RPMI1640 or PBS) was passed through the filter using a 20ml syringe. The filter was washed with additional 15-20 ml of culture medium or PBS to collect all the material. The infected erythrocytes were pelleted by centrifugation (8 min. at 1500 rpm) and the

supernatant was discarded. The live parasites were then further processed for either *in vitro* culture or DNA/RNA/protein collection.

II.6 Purification of gametocytes.

P. berghei gametocytes obtained for RNA sequencing were collected from synchronised infections in rats. Shortly, purified schizonts were intraveneously injected into a rat (=0 hpi). At 48 hpi blood was collected and leucocytes removed as described in the previous point. Ten ml of the Nycodenz solution was added at the bottom of the 35 ml of diluted filtered blood (in a 50 ml falcon tube). The tube was then centrifuged for 20-25 min. at 1500 rpm in a swing out rotor at room temperature (without brake). The brown/grey-coloured layer containing gametocytes (and if present schizonts) at the interface between the two suspensions was collected to a fresh 50 ml tube. The parasites were pelleted by centrifugation at 1500 rpm for 8 min. and the supernatant discarded. The pellet was resuspended in 1 ml of TRIzol and stored at -80˚C until further processing.

II.7 *In vitro* fertilisation/zygote development assay

Standard *in vitro* assay for ookinete development of *P. berghei* was used to analyse gamete formation fertilisation and development of zygotes into ookinetes (as described by Janse and Waters, 1995). Shortly, 2 mice were treated with phenylhydrazine the day before parasite injection. After several days the blood was collected and gametocyte purified. For complete maturation, the purified gametocytes were incubated for 6 h under standard culture conditions (NB the standard culture conditions are: RPMI1640 medium, pH 8.0, without NaHCO,10% foetal calf serum; 1% cell suspension). In these cultures usually 30-90% of the female gametocytes are fertilised and develop into ookinetes. Male gamete production was analysed by counting exflagellating male gametocytes in a cell counter. Unfertilised female gametes, zygotes and ookinetes were counted in Giemsa-stained thin blood films of the culture material (Janse et al., 2006b).

II.8 Ookinete culture *in vitro*

P. berghei ookinetes for protein/RNA extraction or immunofluorescence assays were obtained either from gametocytes from asynchronous infections in mice treated with phenylhydrazine and subsequently with sulfadiazine or from animals treated with sulfadiazine only. Sulfadiazine is an antimalarial drug killing asexual blood stages but not gametocytes. Following injection of animals with glycerol-stored parasites (see previous sections), sulfadiazine was administered in drinking water on day 3-4 post-infection in case of phenylhydrazine-treated mice, and on approx. day 4-6 post-infection in case of animals not injected with phz. Two days after the sulfadiazine treatment heart blood was

collected under isofluorane-anaesthesia using an 1 ml syringe containing 0.05 ml heparin-stock solution. The blood was diluted in 5 ml of ookinete culture medium (see the components below) at 21°C, pH 8.0. Leucocytes were removed using a Plasmodipur leucocyte filter and the ookinete medium as a collection and elution medium (see "Removal of leucocytes from infected blood" in this chapter). The cells were diluted in a total volume of 70-80 ml of ookinete culture medium in a 100 ml culture bottle. The ookinetes were cultured for 16-30 hours at 21˚C. Ookinete production (ookinete conversion) rates, defined as the percentage of female gametes that develop into mature ookinetes, were determined by Giemsa-stained smears analysis.

- Ookinete culture medium: RPMI1640 pH 8.0 (filtered)
  - RPMI1640 containing 25 mM HEPES and 2mM L-glutamine (Sigma)
  - 10 mM sodium bicarbonate (0.85g/L)
  - 5U/ml penicillin, 5 µg/ml streptomycin
  - 50 mg/l hypoxanthine
  - 50 µM xanthurenic acid (0.01g/l)
  - 10% foetal calf serum (v/v)

Note: for the chitinase assay (described below) instead of 10% foetal calf serum, glucose was added at 10mM final concentration.

II.9 Preparation of DNA constructs for transfection.

The DNA constructs were prepared according to the standard molecular biology techniques. The homology arms for all generated constructs were obtained by PCR on wt gDNA with the following programme: 94°C for 5 min. for 1 cycle, followed by 26 cycles of 94°C for 20 sec., (T_m) of the primer pairs for 30 sec., 68°C for up to 4 min., and the last cycle with the final step of 72 °C for 7 min. The obtained PCR products were subcloned directly into the target plasmids, or into the pCR 2.1-*TOPO*® *plasmid* (Invitrogen). For direct subcloning, each PCR product was digested with appropriate restriction enzymes for 1 hour at 37°C and purified with High pure PCR product purification kit (Roche diagnostics). The target plasmid was digested with appropriate enzymes (double digestion) and purified. The concentration of both the insert and the vector was determined by 1% agarose gel stained with ethidium bromide. The insert and the vector were mixed in a molar ratio 3:1 and the ligation reaction was performed for 10 min. at RT using Rapid DNA ligation kit (Roche diagnostics). After that the ligation mix was added to the PMC103 competent *E.coli* cells, and the sample was placed on ice for 10 min. Heat-shock transformation was performed at 42°C for 45 seconds. The sample was placed immediately on ice for 10 min. The transformed bacteria were spread on pre-warmed LB agar plate with 100 µg/ml ampicilin and incubated overnight at 37°C. The next day bacterial colonies were inoculated in 4 ml LB medium with ampicilin (100 µg/ml). After overnight incubation, the cultures were spun down and plasmid was extracted using the GenElute plasmid mini-prep kit (Sigma) or by the following protocol. Three hundred µl of cold P1 solution (50 mM Tris-Cl pH 8.0, 10 mM EDTA pH 8.0) was added to resuspend the cell pellet by vortexing. After that 300 µl of

room temperature P2 solution (200 mM NaOH, 1% (v/v) SDS) were added, the tubes were inverted several times and incubated for 5 min. at RT. Another 300 µl of cold P3 solution (5 M Kac, 11.5% (v/v) Acetic acid) were added and the cells were spun for 10 min. at maximum speed. The supernatant was transferred into a clean Eppendorf tube and 300 µl of chloroform/isoamyl alcohol solution was added. Following centrifugation for 10 min. the supernatant was transferred into a new tube, 1 volume of isopropanol was added and the sample was centrifuged for 10 min. The DNA pellet was washed with 70% ethanol, centrifuged at 4°C, air-dried and resuspended in 30 µl of demineralised water with RNase A (final concentration 50 µg/ml). The obtained plasmids were analysed by restriction enzyme digestion and sequencing. The final plasmids with correctly introduced homology arms were digested with the following one or two restriction enzymes: ApaI/XbaI (pl1009 *sir2a* k.o. plasmid), EcoRI/HindIII (pL1325 *sir2b* k.o. plasmid), SfuI (F85 *sir2a::gfp* plasmid), XhoI (psd141 *sir2b::myc*), Asp718I/XbaI (pL1324 TERT k.o. plasmid), in order to obtain the linearised constructs. Five µg of each replacement fragment was used for *P. berghei* transfection. The *tert* replacement DNA fragment was additionally gel-purified (without ethidium bromide addition to the agarose gel).

II.10 Genomic DNA extraction

In order to analyse the genotype of the transfected or cloned parasites genomic DNA had to be extracted. The parasite pellet was resuspended in 350 µl of the lysis buffer (10 mM Tris pH 8.0, 5 mM EDTA pH 8.0, 100 mM NaCl), transferred to an Eppendorf tube and the following supplements were added: 100 µg RNase (10 µl of a 10 mg/ml solution), 1% (v/v) SDS (50 µl of a 10% solution) and 90 µl of demineralised water. The sample was incubated for 10 minutes at 37ºC. Following addition of 100 µg Proteinase K (10 µl of a 10 mg/ml solution) the tube was incubated for 1 hour at 37ºC. After that 500 µl of buffered phenol:chloroform:isoamylalcohol (25:24:1) was added and the sample was centrifuged at maximum speed for 5 min. The aqueous phase was transferred into a new Eppendorf tube and 500 µl of chloroform:isoamylalcohol (24:1) was added and the sample was spun again. The aqueous phase was transferred into a new 2 ml tube. 0.1 volume of 3 M NaAc, pH 5.2, and 2 volumes of 96% ethanol were added and the DNA was precipitated at -80 °C for 30 min. Following 20 min. centrifugation at 4°C the DNA pellet was washed with 500 µl of 70% ethanol and centrifuged for 10 min. at maximum speed at 4ºC. The supernatant was discarded and the DNA pellet was air-dried. The DNA was resuspended in 50 - 100 µl of demineralised water (depending on the pellet size).

II.11 Plasmid rescue from gDNA

E. coli PMC103 competent cells (200 µl) were thawed on ice. Approximately 0.5 µg of parasite gDNA from 1065 clone 1, 2 and 3 (1065: *tert* k.o. transfected line) was added to the cells, incubated 10 min. on ice and transferred into a water bath at 42 °C for 45 seconds (the heat shock step). The cells were immediately transferred back to ice for approximately 10 min. All cells were plated onto LB-agar plates

supplemented with 100µg/ml ampicilin and incubated overnight at 37˚C. The next day plates were checked for bacterial colonies presence. Twenty colonies from one positive transformation (1065 cl.2) were picked and cultured in 4 ml of LB medium with 100 µg/ml ampicilin for several hours at 37°C with 250 rpm agitation. Plasmid DNA was isolated according to the mini-prep protocol described before. The obtained samples were analysed by restriction enzyme digestion.

II.12 Total RNA extraction

High quality total RNA is usually obtained from "fresh" parasite pellets obtained directly from the animal or from overnight *in vitro* culture. The following procedure for parasite RNA extraction was modified from TRIzol manufacturer's instructions (Invitrogen). In short, the parasite pellet was resuspended in 1 ml of TRIzol reagent and vigorously vortexed until a homogenous solution was obtained. Two hundred µl of chloroform was added and the sample was vortexed for 30 seconds. Following 10 minutes incubation at room temperature the sample was centrifuged at maximum speed at 4ºC in order to obtain phases separation. The upper aqueous phase was transferred to a fresh Eppendorf tube and 500 µl of isopropanol was added. Precipitation was performed at -20^{o}C for 1 h or overnight. On occasions 20 µg of glycogen as was added as a co-precipitant in order to enhance precipitation. The RNA was pelleted by centrifugation at maximum speed for 15 min at 4ºC, and supernatant decanted. The pellet was washed with 1 ml of 70% ethanol and spun again for 10 minutes at maximum speed at 4ºC. The supernatant was removed and the pellet dried for up to 10 min. at RT. The dry pellet was then resuspended in 30 - 50 µl RNase-free demineralised water (depending on the pellet size). The RNA concentration was measured using the NanoDrop 2000 (Thermo Scientific). The RNA sample was stored at –80ºC.

II.13 Southern/Northern analysis

Southern and Northern blotting are routinely used techniques for analysis of DNA or RNA sequence, respectively. The DNA/RNA sample is first run on a 0.8 – 1% agarose gel for size separation of the molecules and then transferred to a membrane for probe hybridisation. The protocol used was the following. After running the DNA or RNA sample on an agarose gel overnight at 20V, the gel was rinsed with demineralised water and then incubated with shaking with 0.25 M HCl for 5 minutes at room temperature (for FIGE gel, 2x 15 minutes). The gel was then rinsed with demineralised water and incubated with denaturing buffer (0.5 M NaOH, 1.5 M NaCl) for 25 min. The neutralisation step was done by incubation in 20x SSC for 30 min. A glass plate was assembled on a container with 10x SSC. The gel was placed upside down on the glass plate with two Whatman 3 MM pieces soaked in 10x SSC. A nylon membrane (Hybond-N+ nylon transfer membrane, GE healthcare) soaked in 2x SSC was placed on top and covered by three pieces of Whatman paper. A stack of paper towels was added on top and pressed with a weight to ensure the capillary transfer of the buffer. Blotting was

performed for 16 hours. The structure was then disassembled, and the membrane with the transferred DNA or RNA molecules was rinsed with 2x SSC and baked for 1 hour at 80°C. A double stranded probe specific to the analysed sequence was α-^{32}P dATP labelled and added to the membrane. After overnight hybridisation at 60°C the blot was washed three times with 3x SSC/0.5% (v/v) SDS and once with 1x SSC/0.5% (v/v) SDS at 60°C (each washing step for 15 min.). The signal was detected using a storage phosphor screen (Molecular Dynamics).

II.14 Telomere Restriction Fragment (TRF) analysis

Telomere Restriction Fragment analysis is a technique to measure the average telomere length. It relies on the fact the telomeric does not contain any restriction enzyme cutting site. Upon digestion of genomic DNA (gDNA) with frequently cutting restriction enzymes, telomere sequences are released intact.

In the TRF experiments approximately 700 ng of gDNA was incubated overnight at 37°C with four frequently cutting enzymes: AluI, MboII, RsaI and Sau3AI (5 units each). The samples were run on 1% agarose gel overnight and blotted by capillary transfer for 16 hours onto a positively charged nitrocellulose membrane (Hybond-N$^+$ membrane, GE Healthcare). The membrane was washed shortly in 2X SSC and pre-hybridised for at least 1 hour at 65 °C. The hybridisation buffer was replaced and the membrane was probed with α-^{32}P dATP labelled double stranded telomere-specific probe from pTB4.1 plasmid (Ponzi et al., 1990). After 6 hours hybridisation at 60°C the blot was washed three times with 3x SSC/0.5% (v/v) SDS and once with 1x SSC/0.5% (v/v) SDS at 60°C (each washing step for 15 min.).

II.15 Western analysis

For Western analysis fresh parasite pellets obtained either from a rodent host or overnight *in vitro* culture were resuspended in 2x SDS gel-loading buffer (100 mM Tris-HCl pH 6.8; 200 mM dithiothreitol; 4% SDS; 0.2% bromophenol blue; 20% glycerol) with prior addition of 1 µl of PMSF (C_i = 100mM, C_f = 1mM). The samples were then run on a SDS-PAGE gel and transferred to a polyvinylidene fluoride (PVDF) membrane, which was subsequently probed with a primary antibody of choice and a compatible HRP-labelled secondary antibody detectable by an Enhanced Chemiluminescence (ECL) detection system (see below for more detailed protocol).

II.15.1 Sodium dodecyl sulphate polyacrylamide gel electrophoresis (SDS-PAGE)

The Mini-PROTEAN® cell system (Bio-Rad) was used for both protein gel preparation and running. The protocol utilised for protein gel pouring, running and blotting was as follows. A short-plate and a spacer-plate were cleaned with alcohol and placed into the casting frame. The resolving gel (12%) for standard protein analysis was prepared (see Table 3 below) and casted. The top of the gel was cover with 2 ml of isopropanol and allowed to polymerise for approximately 40 minutes. The stacking gel was prepared (according to Table 3) and following the isopropanol draining immediately poured. Following rapid comb insertion the gel was allowed to polymerise for 20 minutes.

	Resolving gel (12%)	**Stacking gel**
Deminerlised H_2O	3.8 ml	2.03 ml
40% Acrylamide/Bis	3.0 ml	0.38 ml
Tris buffer	2.5 ml (1.5 M, pH 8.8)	0.38 ml (0.5 M, pH 6.8)
10% SDS	0.1 ml	0.03 ml
10% Ammonium persulphate (APS)	0.1 ml	0.03 ml
Glycerol	0.5 ml	0.15 ml
TEMED	4.0 µl	3.0 µl

Table 3. SDS-PAGE resolving and stacking gel preparation; volume sufficient for casting 2 gels. Acrylamide/Bis solution is mixed 29:1 (Bio-rad).

Following gel polymerisation the gel cassette was removed from the casting frame and placed into the electrode assembly with the short plate facing inward and placed into the mini tank. The inner chamber was filled with ~125 ml of running buffer. Approximately 200 ml of running buffer was added to the mini tank (lower buffer chamber). Following the comb removal and loading well washing the protein samples were load into the wells. The gel was run at 100V for 1.5 – 2 hours at 4˚C.

II.15.2 Protein transfer onto a membrane

The Trans-Blot® electrophoretic transfer cell system (Bio-Rad) was used for protein gel blotting onto a polyvinylidene fluoride (PVDF) membrane. The following steps were followed:

1. Place the transfer buffer (Tris 2.8g, Glycine 2.9 g, Methanol 200 ml, H_2O until 1 L) on ice 1 hour before blotting.
2. Place the blot-cell on ice.
3. Cut 4 pieces of Whatman 3MM filter paper (9 x 7 cm) and soak together with fibre pads in transfer buffer.
4. Cut a piece of Hybond™-P PVDF membrane (Amersham Biosciences, GE Healthcare) in size of the protein gel.

5. Hydrate the PVDF membrane in methanol for 10 seconds, wash in distilled water for 5 min. and in transfer buffer for 10 min. (with rocking).
6. Remove the gel from the electrophoresis apparatus.
7. Place the gel in transfer buffer for 10 min. (with rocking).
8. Assemble the transfer cassette as follows (black side down): fibre pad, 2 layers of Whatman filter paper, gel (upside down and without bubbles), PVDF membrane (without bubbles), 2 layers of Whatman filter paper, and fibre pad.
9. Place the cassette in the transfer cell (black on black), insert the ice element, and add transfer buffer.
10. Connect the transfer cell to the power source and run it on constant current of 200mA for 2 hours.

II.15.3 Immuno-detection

Following membrane transfer an immobilised antigen of interest was detected by the antigen specific primary monoclonal or polyclonal antibody, which was then recognised by a secondary anti-IgG antibody conjugated to horseradish peroxidise (HRP). The complex was visualised using the ECL Plus™ Western blotting detection reagents (Amersham Biosciences), which utilises a technology based on the enzymatic generation of acridinium ester intermediates. These intermediates react with peroxide under slight alkaline conditions to produce a sustained, high intensity chemiluminescence.
The PVDF membrane was first blocked in 3% non-fat dried milk/0.1% Tween in PBS for 1 hour at RT or 4˚C overnight in order to block non-specific binding sites. The primary antibody was diluted in 3% non-fat dried milk/ 0.1% Tween in PBS (diluted 1:100 up to 1:5000 depending on the antibody; determined empirically). Following 1 hour (RT) to overnight (4˚C) incubation with rocking the membrane was briefly rinsed in 0.1% Tween in PBS, and washed 3x for 15 minutes in the same buffer at room temperature. The secondary HRP labelled antibody (Dako) was diluted either 1:10000 or 1:5000 in 3% non-fat dried milk/0.1% Tween in PBS. The membrane was incubated for 1 hour at RT (with rocking). The membrane was again rinsed in 0.1% Tween in PBS and washed 3x for 15 minutes at RT. The detection solution (Amersham Biosciences) was prepared by mixing solutions A and B in a ratio of 40:1. The washed PVDF membrane was placed on a sheet of Saran Wrap and the detection solution was pippeted onto the membrane. Following 1 minute incubation the excess detection reagent was drained and the membrane wrapped in Saran Wrap. Finally the membrane was placed in an X-ray film cassette. Chemiluminescence detection was carried out in a dark room using an X-ray film. Exposure times varied according to the signal strength.

II.16 Immunofluorescence assay (IFA)

IFAs were performed on both asexual and sexual *Plasmodium* stages. The primary antibody dilutions were determined empirically and varied, ranging from 1:100 (e.g. Plasmepsin 4) up to 1:5000 (P28). Freshly made parasite smears were preferred though when necessary stored slides were also utilised. The protocol used was as follows. Smears were fixed with 4% formaldehyde (in PBS) for 10 min. at RT. Fixed cells were washed twice in PBS and permeabilised with 0.1% Triton X-100/PBS for 10 min. at RT Following washing in PBS, slides were blocked in 3% BSA/PBS for 1 hour at room temperature or overnight at 4˚C. The primary antibody was diluted to a desired concentration in 3% BSA in PBS and applied to the slides. Incubation was carried out for 2 hours at RT or overnight at 4 ˚C. Cells were washed three times in PBS for 10 min. each to remove excess primary antibody. Secondary antibody was added at 1:2000 dilution (in 3% BSA/PBS) and allowed to bind for 1 hour at RT. Cells were washed three times for 10 min. in PBS. Following a quick dip in distilled water, the slides were mounted in Vectashield® mounting medium with DAPI (Vector labs), and sealed with nail varnish to prevent drying. Fluorescence was analysed and images acquired using either a Leica microscope (DMRA; ColourProc software, developed by H. Tanke's lab, LUMC, The Netherlands) or Zeiss Axioplan II microscope (Volocity software, Improvision).

II.17 Fluorescent in situ hybridization (FISH)$^{DNA\text{-}DNA}$

The following protocol was used for telomeric DNA detection in *P. berghei* blood stage parasites. Adapted from Ersfeld, K. & Gull, K., 1997; by Liliana Mancio-Silva, Lucio Freitas-Junior and Artur Scherf, Institute Pasteur, Paris

Specialised materials and reagents

- 3-well microscope slides (Cell-Line) and coverslips
- In situ frame for 25 µL (AbGene, Thermo Scientific)
- Hybridization solution (HS): (unfiltered, stored at 4˚C)
    - 50% formamide (Roche Applied Science)
    - 10% dextran sulfate (Sigma)
    - 2x SSPE (Sigma)
    - 250 µg/mL Herring sperm DNA (Sigma)

- 10% paraformaldehyde (Electron Microscopy Sciences)
- Vectashield® mounting medium with DAPI (Vector Laboratories)
- Nail varnish

Probes: The telomere-specific fluorescein labelled DNA probe was prepared using the "Fluorescein High-Prime kit" (Roche Applied Science) according to manufacturer's instructions.

Procedure

Parasite fixation:

- The parasites (10% parasitaemia) were washed twice in PBS and centrifuged at 5000 rpm 1 min.
- Following resuspension in paraformaldehyde 4% (in PBS) for 10-15 min. on ice, the parasites were washed once with cold PBS (centrifuge 5000 rpm 1 min.).
- The parasites were then resuspended in ~400 µl cold PBS (fixed parasites can be stored at 4˚C at this step for around 2 months).
- A monolayer of parasites was deposited on each well of the microscope slide (by pipetting up and down several times), and the slides were air-dried for 30 min. at room temperature (prepare the probe in the meantime).

In situ hybridization:

- The plastic frame (Thermo Scientific) was fixed around the wells containing the parasites
- The slides were washed once in PBS for 5 min. at room temperature (wash/aspirate cycles for several times, ~50 µl/wash).
- The HS solution with the labeled probe (denatured at 95˚C for 5 min.) was applied to each well – 25 µl + 1 or 2 or 3 µl of the labeled probe (quantity of the probe determined empirically).
- The well was covered with In situ Frame coverslip and the slides were denatured in for 30 min. at 80˚C followed by hybridization at 37˚C overnight.

Washing:

- Following removal of the In situ Frame coverslip and the HS solution (by vacuum aspiration), the slides were washed in 2x SSC/50% Formamide for 30 min. at 37˚C, followed by 1x SSC for 10 min. at 50˚C, 2x SSC for 10 min. at 50˚C, and 4x SSC for 10 min. at 50˚C (washing stringency dependent on the probe).
- The cells were equilibrated in PBS/0.5% Tween for 5 min. at RT in a humid chamber protected from light and the slides were washed three times in PBS/0.5% Tween solution – 5-10 min at RT, with agitation.
- The slides were air-dried, mounted using Vectashield® mounting medium with DAPI (Vector labs) – 8 – 10 µl, sealed with nail varnish and analysed by fluorescence microscopy.

Comments : Probe size – 1.5 – 3 kb

II.18 Matrigel™ ookinete motility assay.

The ookinete motility assay protocol was adapted from Robert Moon (O. Billker's laboratory, WTSI, Cambridge, UK). The ookinete motility assay uses *in vitro* cultured *P berghei* ookinetes set in the commercially available basement membrane preparation Matrigel™ (BD Biosciences), combined with time-lapse microscopy to determine the motility of individual ookinetes. The protocol was modified from manufacturer's instructions. Overnight in vitro cultured mature ookinetes (starting from 22 hours post-fertilisation) were collected and centrifuged in a table top centrifuge at max. speed. The supernatant was discarded and the parasite pellet resuspended in 20 – 50 µl of ookinete medium. Twenty µl of cold Matrigel™ was gently but thoroughly mixed with an equal volume of the parasite suspension. Six µl of the mix was spotted onto a glass slide, covered with a coverslip rimmed with Vaseline, sealed with nail varnish and left to set for 30 min. at room temperature. Ookinete motility was recorded using a Leica fluorescence steromicroscope integrated system M205 FA. Images were taken every 5 seconds for 10 – 20 minutes at 40x or 63x magnification and analysed using ImageJ (http://rsbweb.nih.gov/ij/).

II.19 Mosquito haemocoel injections of mature ookinetes.

An ookinete microinjected into the *Anopheles* haemocoel is able to develop into a mature fully functional infective oocyst at any site within the haemocoel. In order to analyse the ability of mutant ookinetes to generate oocysts female mosquitoes were thorax microinjected with ~800 *in vitro* cultured ookinetes (Nanoject II hand-held microinjector, Drummond; see Results chapter for information on parasite lines). Mosquito midguts were dissected at day 10 and 21 post-injection and oocyst numbers were determined using a Leica fluorescence steromicroscope (Leica M205 FA), taking advantage of the constitutive GFP expression of the analysed parasite lines.

II.20 Mosquito midguts dissections

Adult female *A.stephensi* mosquitoes (approximately 50/cage) were starved for 1-2 days prior to blood feeding. Following the starvation period mosquitoes were allowed to feed for approximately 1-2 hours on *P. berghei*-infected mice with gametocytaemia of ~0.5%. Unfed mosquitoes were removed from the cage and the remaining mosquitoes were maintained on glucose at 21˚C. For ookinete traversal determination mosquito midgut were dissected at day 1 and day 2 post-feeding. Oocyst numbers were determined at day 11-18 post-feeding.

II.21 Preparation of midguts for electron microscopy and paraffin embedding.

Following dissections *A. stephensi* midguts were directly places into a falcon tube containing 1% paraformaldehyde/2.5% glutaraldehyde. Following overnight incubation at 4˚C the fixation solution was exchanged with 1x PBS. For epoxy-resin embedding the midguts were stored in the first PBS solution until further processing (performed externally by L. Tetley and M. Mullin, Universtiy of Glasgow). For paraffin embedding the midguts were incubated for 1 hour in the first PBS buffer change (4˚C). Following a short PBS wash the solution was replaced with subsequently 20%, 50% and 70% ethanol (1 hour incubation for each dehydration step). The prepared midguts were then further processed externally using an automated standard embedding protocol (Pathology unit facility, LUMC, the Netherlands).

II.22 Toluidine blue-staining of midgut sections.

Thick (5-10 µm; paraffin) and semi-thin (0.35-1 µm; epoxy-resin) sections were cut using an ultramicrotome. The sections were mounted on a glass slide, dried on a hot plate at either 65˚C or 95˚C for paraffin and epoxy resin sections, respectively. Paraffin sections were de-waxed in Xylene (2x 3 min.), rehydrated in a series of 100%, 90%, 70% EtOH (3 min. each), stained with 0.1% Toluidine blue for 2 min. and rinsed with water. The slides were then washed in 95% and 100% EtOH (10 dips), cleared with Xylene (10 dips) and mounted. The epoxy resin sections were stained with 0.1% Toluidine blue for 1 – 2 min. and rinsed with tap water.

II.23 Chitinase assay

The protocol used was modified from Vinetz et al. (2000). Twenty four to 30 h cultures of ookinetes were centrifuged, and supernanatants transferred into a fresh eppendorf tubes. The parasite pellet was resuspended in 500 – 1000 µl of cold 0.1% Triton X-100/PBS and centrifuged for 20 min. at maximum speed at 4˚C. The assay was performed in a black 96-well plate (Nunc). For each well 50 µl of ookinete medium or ookinete extract or negative ookinete medium (control) was added to 120 µl of 20 mM Tris, pH 8.0, and 30 µl of the 4-methylumbelliferyl-*N,N*',*N*''-β-D-triacetylchitotrioside (4-MU Glc-NAc3) substrate. Enzyme reactions were incubated at 21°C for 4 hours or overnight. The fluorescence was read in a microplate fluorimeter (PerkinElmer Envision; filters, excitation 365 nm and emission 450 nm). A value for each well is a mean of two subsequent measurements and is expressed in relative fluorescence units (RFUs).

III. RESULTS

PART 1 – SIR2

III.1 Generation of the *sir2a*, *sir2b* single and *sir2a/b* double deletion cloned parasite lines.

III.1.1 Silent Information Regulator 2 b (Sir2b) knockout.

To study the SIR2B function, the *Pbsir2b* gene (PBANKA_131510) was disrupted using the positive/negative selectable marker system. This approach was chosen to enable subsequent generation of a *sir2a*/*sir2b* double knockout parasite line in *P. berghei* (described later in detail). The *sir2b* construct was designed in the positive/negative selection marker plasmid pL0035 (Braks et al., 2006). The plasmid has two multiple cloning sites, enabling the generation of both single and double cross-over constructs. For DXO *Pbsir2b* construct two homology arms were generated by amplifying fragments of the wt *Pbsir2b* locus by PCR using primer pairs 3368 x 3369 and 3370 x 3371, for the first and second flanks respectively (Fig. 23). The first flank included 620bp upstream of *Pbsir2b* gene, whereas the second flank of 726 bp was obtained from the middle portion of the gene. The two flanks were subsequently cloned into the pL0035 vector.

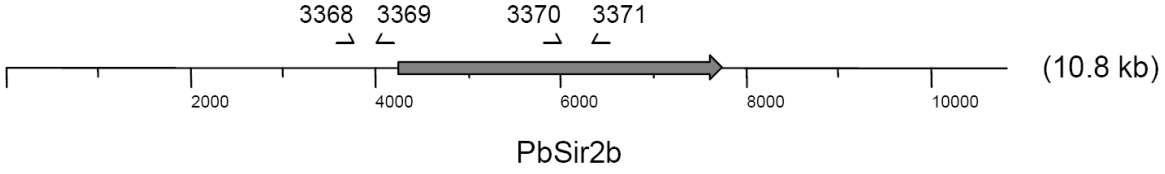

Primers	3368 x 3369	3370 x 3371
Products	**620 bp**	**726 bp**

Fig. 23 *Pbsir2b* homology arms of 620 bp and 726 bp were amplified by PCR from wt gDNA with 3368 x 3369 and 3370 x 3371 primer pairs, respectively.

The pL0035 is a plasmid used for construct delivery, selection of the transfected parasites and subsequent selectable marker recycling, allowing for introduction of a second construct using a standard vector (e.g. pL001 previously described). This strategy allows for generation of double knockout single parasite line, or alternatively multiple knockouts if pL0035 is used multiple times.
The pl0035 plasmid, shown in Fig. 24, contains the positive/negative selection cassette under the *P. berghei* elongation factor 1 α promoter, which ensures constitutive expression throughout all the cycle

stages. The two selectable marker genes – *hdhfr* and *yfcu* are flanked 5' and 3' by 3' *Pbdhfr-ts* UTRs. Additionally, the pL0035 vector contains *Amp*^{R} gene for bacterial selection. The two homology arms for *Pbsir2b* construct generation were subcloned into HindIII/NotI and XhoI/EcoRI sites in the pL0035 plasmid, creating pL1325 *sir2b* k.o. vector (Fig. 24 on the right). For transfection the plasmid was linearised using the EcoRI and HindIII restriction enzymes.

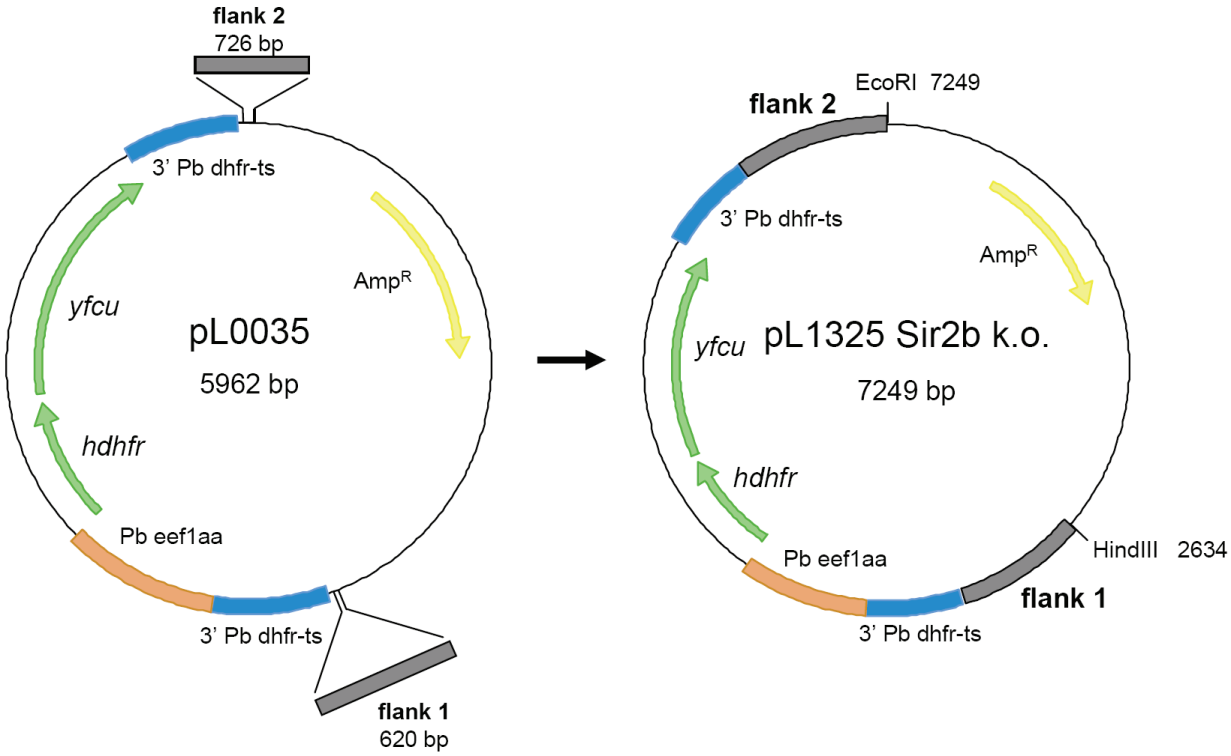

Fig. 24 The pL0035 plasmid was used for generation of the pL1325 *sir2b* knockout construct. The pL0035 (on the left) contains the positive/negative selection cassette, with selectable marker which is a combination of the human *dhfr* gene and a fusion of the yeast gene cytosine deaminase and uridyl phosphoribosyl transferase (UPRT) (*yfcu*). The *hdhfr* and *yfcu* are placed under the strong *P. berghei* elongation factor 1 α promoter, which provides constitutive expression of the positive-negative selectable marker throughout the complete life cycle. The two flanks for the *Pbsir2b* DXO knockout were subcloned into HindIII/NotI and XhoI/EcoRI sites in pL0035 plasmid, giving rise to the pL1325 *sir2b* k.o. vector.

The linearised *Pbsir2b* construct (4.6 kb in size) was transfected into *P. berghei* schizonts using the procedure described in the section Materials and Methods. Schematic representation of the construct integration into the target site, and the resulting double cross-over locus is shown in Fig. 25 below.

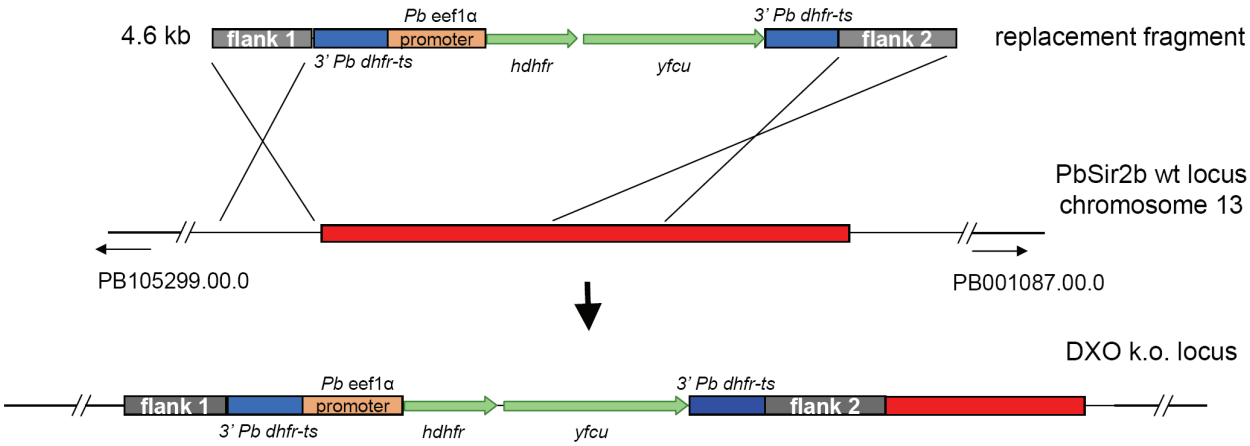

Fig. 25 Schematic representation of the recombination event leading to the deletion of the *Pbsir2b* gene. The replacement fragment (4.6 kb in size), obtained from double digestion of the pL1325 *sir2b* k.o. plasmid, is integrated in the *Pbsir2b* wt locus by double cross-over recombination between the homology regions. The resulting DXO k.o. locus should contain the whole replacement construct, including the *hdhfr/yfcu* selectable cassette, as well as the end portion of the *sir2b* gene. The two 3' *Pbdhfr-ts* UTR regions provide homology regions for recombination within the locus, and removal of the selectable marker cassette, see text for details.

The positive/negative selection system is based on expression of both the positive selectable marker, namely human *dhfr* and the negative selectable marker – fusion of yeast cytosine deaminase and uridyl phosphoribosyl transferase (*yfcu*). yFCU bifunctional protein converts the pro-drug 5-fluorocytosine (5-FC) into a toxic 5-fluorouracil interfering with DNA synthesis. The selection procedure involves first treatment on pyrimethamine or WR99210. At that time the parasites express both human DHFR as well as the yFCU protein. Subsequent *in vivo* treatment with 5-fluorocytosine selects those parasites that have eliminated the *yfcu* gene and therefore avoid the toxic effect caused by the yFCU protein. The excision is accomplished through homologous recombination between the two 3' *Pbdhfr-ts* UTRs present in the transfected construct (Fig. 26). The disrupted locus remains disrupted but the parasite line, once cloned, is available for further genetic manipulations.

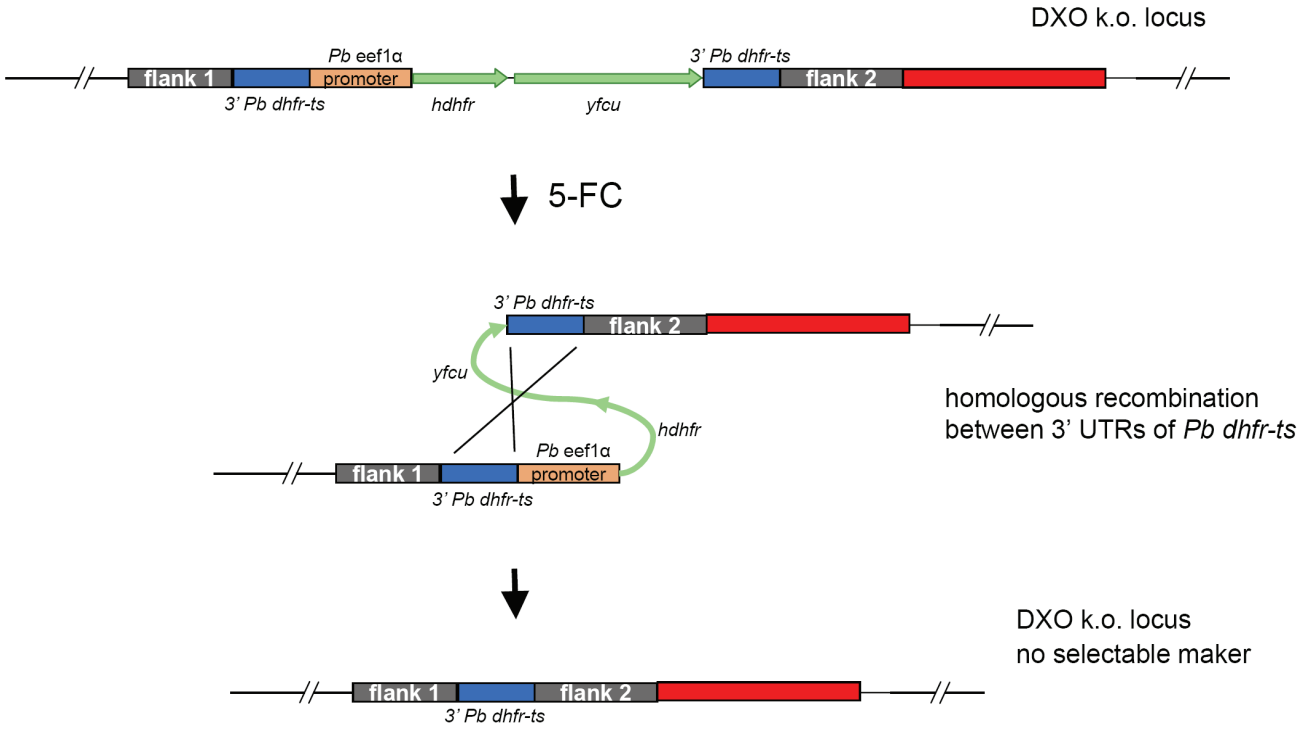

Fig. 26 Positive/negative selection cassette removal. Following the construct integration and positive selection with pyrimethamine, the parasites are treated with 5-fluorocytosine (5-FC), which is lethal to the parasites which express the *yfcu* gene product. Drug application selects for the parasites which removed the negative/positive cassette by homologous recombination between the two 3' UTRs of the *Pbdhfr-ts* UTRs. The resulting locus is still a knockout locus, but contains no selectable marker, allowing for further genetic manipulation of the same parasite line.

III.1.1.1 Analysis of the *Pbsir2b* knockout transfection population

Following genomic DNA extraction from the *Pbsir2b* transfection population (1079), the line was analysed for construct integration by PCR and FIGE (Fig. 27). The 5' and 3' integration PCRs were performed with 3542 x 3071 and 2128 x 3543 primer pairs, respectively. The presence of the selection cassette was confirmed by amplification with L307C x L1511 primers. The *sir2b* internal fragment amplification (primers 3544 x 3545, lane 3) resulted in a very faint band, in comparison to the wild type control. Thus it seemed that a high percentage of the parasites contained the disrupted *sir2b* locus. Probing the FIGE blot with the 3' *Pbdhfr-ts* UTR resulted in the strong signal at chromosome 13/14 (integration should occur at chromosome 13) confirming the positive result from the PCR experiment (Fig. 27B). Apart from wt 3' UTR location (chromosome 7) the probe bound to chromosome 2/3 as well. This is due to the fact that for the *sir2b* k.o. construct transfection the parasite line with stably integrated *gfp* was used (507 cl1; *P. berghei* ANKA HP GFP_{con}; Franke-Fayard et al., 2004).

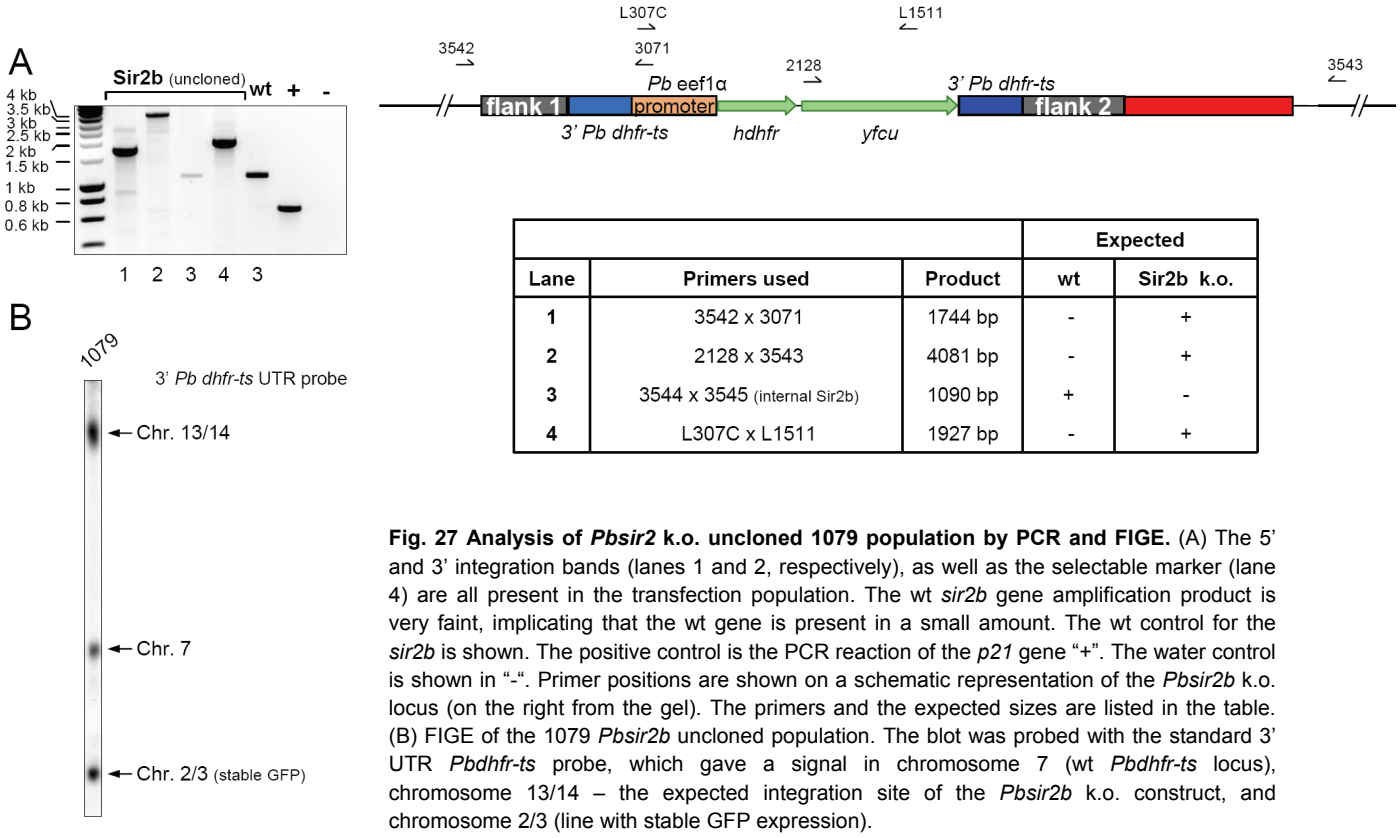

			Expected	
Lane	**Primers used**	**Product**	**wt**	**Sir2b k.o.**
1	3542 x 3071	1744 bp	-	+
2	2128 x 3543	4081 bp	-	+
3	3544 x 3545 (internal Sir2b)	1090 bp	+	-
4	L307C x L1511	1927 bp	-	+

Fig. 27 Analysis of *Pbsir2* k.o. uncloned 1079 population by PCR and FIGE. (A) The 5' and 3' integration bands (lanes 1 and 2, respectively), as well as the selectable marker (lane 4) are all present in the transfection population. The wt *sir2b* gene amplification product is very faint, implicating that the wt gene is present in a small amount. The wt control for the *sir2b* is shown. The positive control is the PCR reaction of the *p21* gene "+". The water control is shown in "-". Primer positions are shown on a schematic representation of the *Pbsir2b* k.o. locus (on the right from the gel). The primers and the expected sizes are listed in the table. (B) FIGE of the 1079 *Pbsir2b* uncloned population. The blot was probed with the standard 3' UTR *Pbdhfr-ts* probe, which gave a signal in chromosome 7 (wt *Pbdhfr-ts* locus), chromosome 13/14 – the expected integration site of the *Pbsir2b* k.o. construct, and chromosome 2/3 (line with stable GFP expression).

III.1.1.2 Negative selection of the 5-FC treated *sir2b* knockout parasites

Since the transfected 1079 population showed a high ratio of chromosome 13/14 to chromosome 7 and 2/3 signal, the cloning step was omitted and the population was directly used for the 5-fluorocytosine treatment (to select for the parasites with removed positive/negative selection marker cassette). On day 0 one mouse was injected with the 1079 transfection population. Pyrimethamine treatment was started on day 1. Six days later blood was collected by cardiac puncture under anaesthesia and three mice were subsequently infected with the diluted blood sample (see cloning by limiting dilution procedure in Materials and Methods). These three animals were not treated with pyrimethamine, so that the removal of the positive/negative selection cassette could occur. Approximately four days later (at low parasitaemia) the three mice were intraperitoneally injected with 1 mL of 5-fluorocytosine solution (for details see Materials and Methods). When growth inhibition was observed the surviving parasites were collected and genomic DNA was extracted from the three parasite pellets. Genomic DNA was analysed for positive/negative cassette presence by Southern blotting. Approximately 1.5 µg of DNA was digested overnight with BamHI and SnaBI restriction enzymes (10 units each). The samples were run on a 0.8% agarose gel and blotted onto a nylon membrane. The blot was probed with a probe specific to flank 1. As seen in Fig. 28 (on the right, and the table) double digestion results in three fragments of different sizes depending on the locus status.

The wt *Pbsir2b* locus digestion should yield a 3.55 kb band. The integration of the *Pbsir2b* replacement construct introduces an additional BamHI site, causing a decrease in the size of the fragment to 2.8 kb (the untreated parasites). The loss of the positive/negative selection cassette should result in a fragment of 2.4 kb. In the wild type parasites only the original locus is present indicated by the band at 3.55 kb (Fig. 28, top left, lane 5). In the case of the untreated parasite population only the 2.8 kb band is detected implying that all the transfected parasites integrated the *Pbsir2b* k.o. construct. However, this is contradicted by the results from the 5-FC treated populations (Fig. 28, blot lanes 1 – 3). After the 5-FC treatment the majority were the wild type parasites, deducing from the high signal ratio of the 3.55 kb to 2.4 kb and 2.8 kb bands. This could be because the transfection population contained a percentage of the wild type parasites, which retained the circular plasmid throughout the pyrimethamine (positive) selection, allowing them to survive. Releasing the pyrimethamine pressure before the 5-FC treatment (~3-4 days in mice) allowed the parasites to discard the plasmid before the 5-FC treatment. The efficiency of plasmid loss, occurring regularly in *Plasmodium* transfection (in *P. berghei* with each erythrocytic cycle approximately 40% of the parasites will not retain the plasmid), is much greater than the rate of homologous recombination: in estimated 95% of the parasites with the integrated positive/negative selection construct marker recycling will not occur. Therefore the wild type parasites, even if initially present in a low number, having the advantage of rapid plasmid loss, will outgrow the originally dominant mutant population. The absence of the wt 3.55 kb band in the untreated 1079 sample (Fig. 28, lane 4) can be explained by low sensitivity of the FIGE and Southern blotting method (even as high as 10% of the transfected parasites containing the plasmid can be still undetectable). The presence of the 2.8 kb band indicates that some parasites with the positive/negative cassette persisted despite the 5-FC treatment.

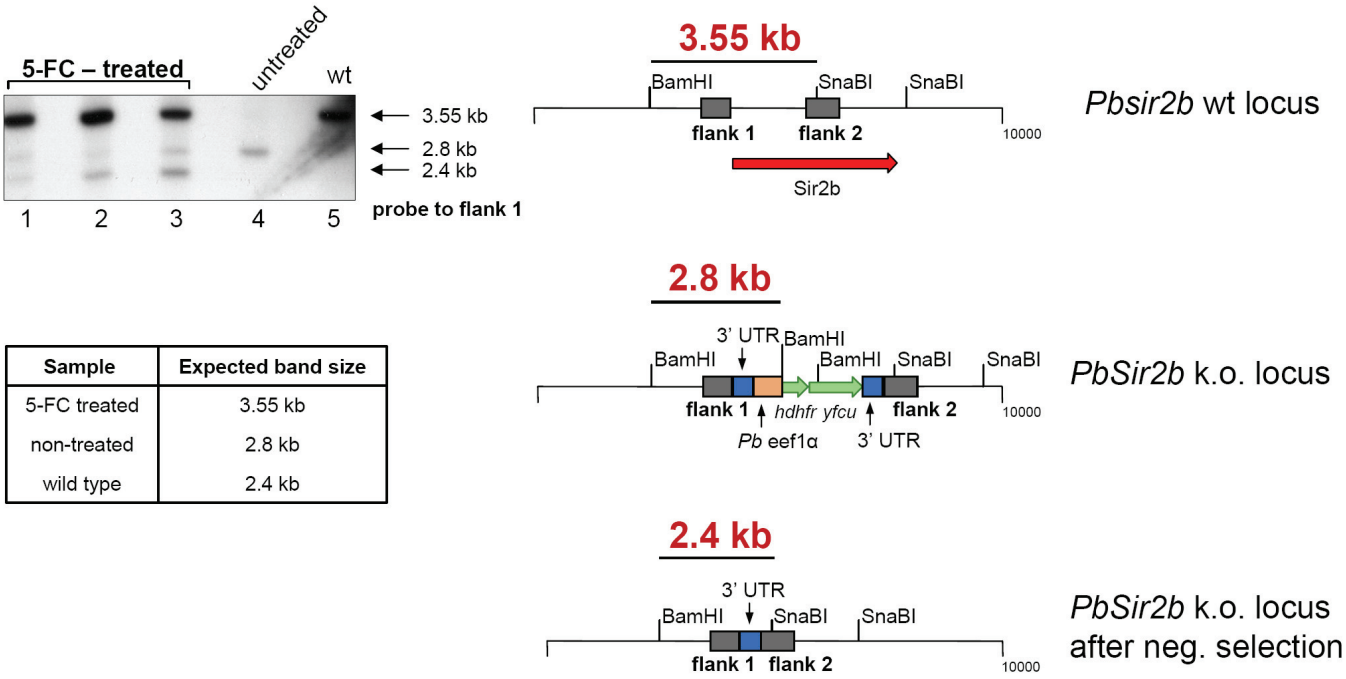

Sample	Expected band size
5-FC treated	3.55 kb
non-treated	2.8 kb
wild type	2.4 kb

Fig. 28 Analysis of the negatively selected parasites by Southern blotting. Genomic DNA (1.5 µg) from the three 5-FC treated parasite populations was digested with BamHI and SnaBI restriction enzymes. As a control untreated and the wild type gDNA was used. The DNA samples were run on a 0.8% agarose gel overnight and blotted onto a nylon membrane. The blot was probed with flank 1-specific sequence amplified by PCR. The image of the radioactive labelled bound probe is shown on the top left. The wild type control exhibits the predicted 3.55 kb (scheme on the right). The untreated sample shows only the band specific for the *Pbsir2b* knockout locus. The three 5-FC parasite genomes (lane 1 – 3) contain the strong wild type band (3.55 kb) and both the 2.8 kb and 2.4 kb bands. High signal ratio of the wild type to knockout and negatively-selected knockout bands indicates that the majority of the population are the wt parasites with no construct integration. The absence of the wt band in the untreated parasites indicated that less than 10% of the wild type parasites were present in the transfection population. These wild type parasites must have retained the plasmid used for transfection to survive the positive selection (by pyrimethamine) and excluded the plasmid before the negative selection (with 5-FC) began. The presence of the 2.8 kb fragment shows that some parasites may have found a way to survive the negative treatment, even with the positive/negative selection cassette still present.

III.1.1.3 Cloning of the *Pbsir2b* knockout parasites

Due to inefficient negative selection of the 1079 uncloned population, first a homogenous parasite line with stably integrated construct should be obtained, to later proceed to the negative selection. The cloning was preformed following the procedure previously described (also see Materials and Methods for details). Genomic DNA was extracted from the four stored parasite pellets (7/10 mice became positive). Clones 1079 1 – 4 were analysed for construct integration and the wild type *Pbsir2b* gene presence by PCR (Fig. 29). The set of primers used for the 5' and 3' integration-specific PCRs were 3542 x 3071 and 1662 x 3543, respectively. 1079 clones 1, 2 and 3 showed specific amplification products of the expected sizes in lanes 1 and 2 (5' and 3' integration), whereas 1079 clone 4 did not. The wild type *Pbsir2b* gene fragment (lane 3) is present in the wild type sample, as well as 1079 cl.4.

The presence of the selectable cassette fragment (lane 4) in 1079 clones 1 – 3, together with the result from lanes 1 – 3 PCR reactions indicates that all the three clones have successfully integrated the *PbSir2b* construct into their genomes. In the case of clone 4 the selectable cassette band is present (lane 4) indicating that this clone is the wild type with retained pL1325 *sir2b* k.o. vector. 1079 clone 1 was chosen for proceeding with the negative selection, in order to select for the *Pbsir2b*-deficient parasites with removed positive/negative selection cassette.

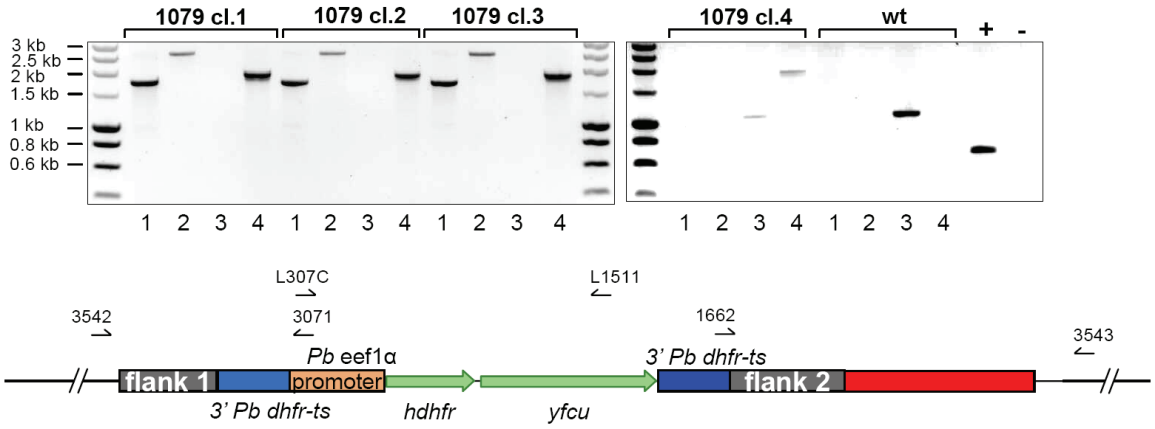

			Expected	
Lane	**Primers used**	**Product**	**wt**	**Sir2b k.o.**
1	3542 x 3071	1744 bp	-	+
2	1662 x 3543	2616 bp	-	+
3	3544 x 3545 (internal Sir2b)	1090 bp	+	-
4	L307C x L1511	1927 bp	-	+

Fig. 29 *Pbsir2b* knockout clones analysis by PCR. Genomic DNA from the four 1079 1 – 4 clones was used in PCR reactions for 5' and 3' construct integration, wt *Pbsir2b* gene and positive/negative selectable marker presence. Schematic representation of the *PbSir2b* DXO k.o. locus with indicated primers used for the PCR reactions is shown below the gel. 1079 clones 1 – 3 show all the expected bands of the correct sizes (listed in the table). In the wild type control only the wt *Pbsir2b* gene band is observed. In the case of clone 4 both the wild type *sir2b* gene, as well as the *hdhfr/yfcu* bands are observed, indicating that clone 4 is the wild type parasite line with retained pL1325 *sir2b* k.o. plasmid used for transfection.

III.1.1.4 Second negative selection and cloning of the *Pbsir2b* mutant line.

The attempt to directly select from the transfected 1079 population by 5-fluorocytosine (5-FC) treatment for parasites that have lost the positive/negative selection marker cassette (omitting the parasite cloning step before the 5-FC treatment) was unsuccessful. Therefore the 1079 population was first cloned (generating 4 clones as described before) and 4 mice infected with 1079 clone 1 for subsequent treatment with 5-FC. When growth inhibition of the infections was observed during

continuous exposure to 5-FC the 4 populations of surviving parasites were collected, genomic DNA was extracted, digested with SnaBI/BamHI and analysed by Southern blotting (Fig. 30). As seen in Fig. 30, right scheme, double digestion resulted in three fragments of different sizes depending on the locus status (described previously; also see Fig. legend for description). The presence of the 2.8 kb band in lanes 1-4 (the 5-FC treated parasites from the 4 mice) indicates that some parasites with the positive/negative cassette persisted despite the 5-FC treatment.

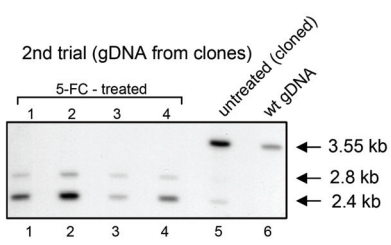

Sample	Expected band size
5-FC treated	2.4 kb
non-treated	2.8 kb
wild type	3.55 kb

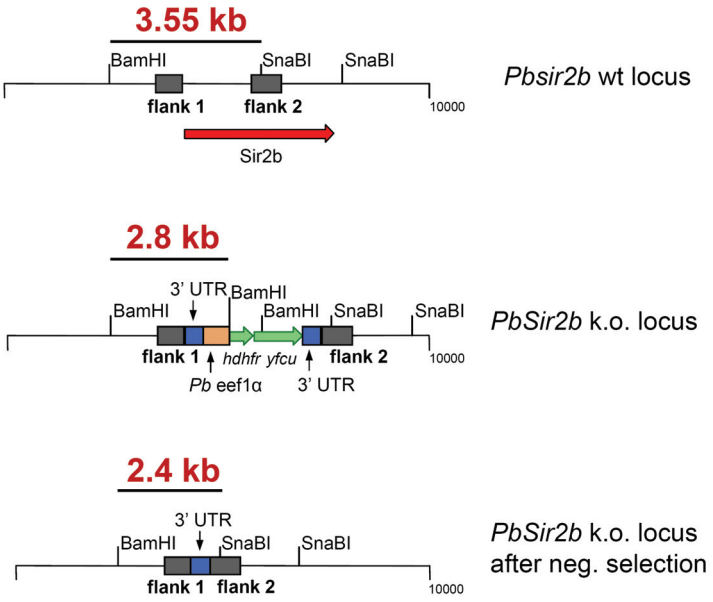

Southern after the 2nd negative selection, ON exposure					
Lane	**Sample**	**Band 2.4 kb**	**Band 2.8 kb**	**Band 3.55 kb**	**2.4 kb/ 2.8 kb ratio**
1	5-FC treated mouse 1	189.47	59.84	-	3.17
2	5-FC treated mouse 2	255	86	-	2.97
3	5-FC treated mouse 3	67.42	41.26	-	1.63
4	5-FC treated mouse 4	141.58	39.05		3.63
5	1079 cl.2 untreated	38.42	very faint	254.58	
6	wt gDNA	-	-	108.84	

Fig. 30 Analysis of the 5-FC 1079 clones by Southern blotting. Four mice injected with 1079 cl1 parasites were treated with 5-fluorocytosine (5-FC), which is toxic to the parasites expressing the *yfcu* gene product. Parasite genomic DNA extracted from blood of the four mice was digested with SnaBI/BamHI restriction enzymes. Following Southern blotting, the membrane was probed with ^{32}P-labeled probe specific to flank 1 (top left panel) of the introduced *Pbsir2b* knockout construct. The expected band sizes for the wt locus, *Pbsir2b* k.o. with the positive/negative selection cassette, and *Pbsir2b* k.o. with removed selection cassette are shown on the scheme on top right. The peak intensities for each band are summarized in the table. The 2.4 to 2.8 kb ratios for each sample are shown in the rightmost column. The row marked in red indicates the sample with the highest 2.4/2.8 kb ratio. This sample (1079 cl1 m4) was used for isolation of the cloned *Pbsir2a/Pbsir2b* double deletion parasites.

Due to the incomplete removal of the positive/negative selection cassette cloning of the 1079 line had to be repeated. The 5-FC selected parasites of 1079 clone 1 mouse 4 were chosen for further cloning due to the highest 2.4 kb to 2.8 kb band ratio (see Fig. 30, bottom table, highlighted in red). Two mice were infected with the 1079 cl1 m4 parasites and treated with 5-FC for 4 days. Subsequently 10 mice were injected with approximately 2 parasites/mouse (see cloning by limiting dilution, Materials and Methods). Four mice developed detectable parasitaemia and were considered clonally infected. Blood was collected by cardiac puncture under anaesthesia. Genomic DNA was extracted from the obtained parasite pellets and analysed for the positive/negative cassette presence by PCR and Southern blotting (Fig. 31).

A

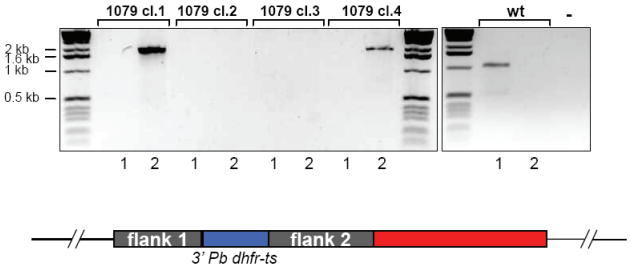

			Expected	
Lane	Primers used	Product	wt	Sir2b k.o.
1	3544 x 3545 (internal *sir2b*)	1090 bp	+	-
2	L307C x L1511 (*yfcu*)	1927 bp	-	-

B

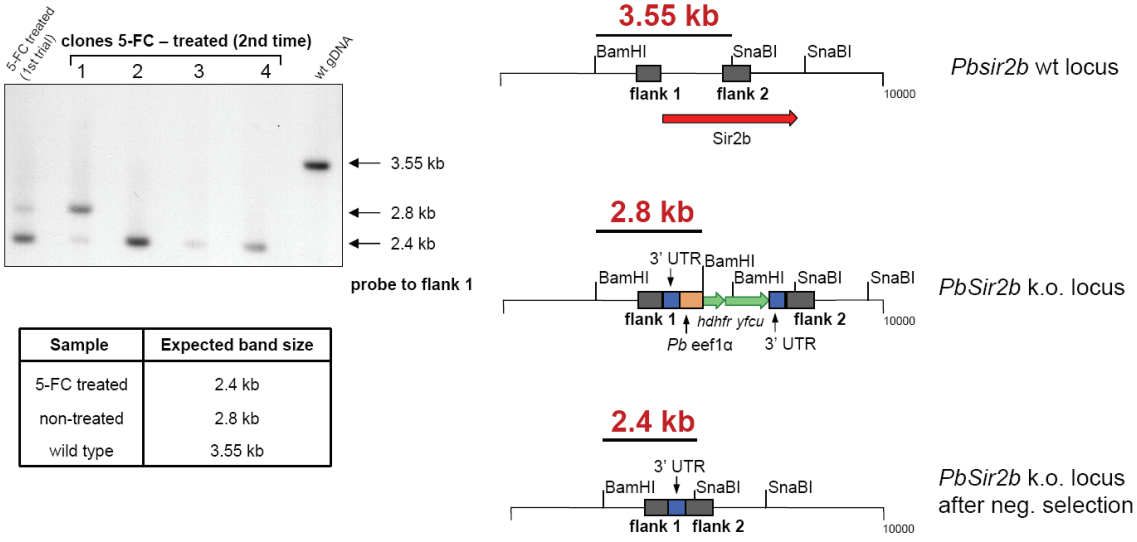

Sample	Expected band size
5-FC treated	2.4 kb
non-treated	2.8 kb
wild type	3.55 kb

Fig. 31 1079 clones analysis. Four clones of 1079 (*Pbsir2b* k.o. with the positive/negative selection marker) were analysed for *sir2b* and the *yfcu* marker presence by PCR **(A)**. Clones 2 and 3 are negative for *sir2b*- and *yfcu*-specific amplification (lanes 1 and 2, respectively) indicating the *sir2b* gene absence and removal of the positive/negative selection cassette. The wild type shows the *sir2b* gene band, and no *yfcu* marker, as expected. The *Pbsir2b* knockout locus and the primers used in the PCR reactions are shown below the gel. **(B)** Southern analysis of 1079 cl. 1-4 genomic DNA digested with SnaBI/BamHI restriction enzymes showed that clones 2, 3 and 4 contain no pos/neg selection cassette. The scheme on the right shows the possible band sizes in the Southern analysis when probed with flank 1-specific probe.

Out of four generated clones (experiment 1079 cl1 m4) PCR analysis of clones 2 and 3 indicated the removal of the positive/negative selection cassette as analysed by PCR (Fig. 31A) with primers amplifying the *Pbsir2b* gene (3544 x 3545) and the *yfcu* selectable marker (primers L307C x L1511). For Southern analysis (Fig. 31B) approximately 1.5 µg of gDNA was digested overnight with BamHI and SnaBI restriction enzymes (10 units each). The samples were run on a 0.8% agarose gel and blotted onto a nylon membrane (Amersham). The blot was hybridised with a probe specific to flank 1. In the 5-FC treated parasites 1079 clones 2, 3 and 4 (2^{nd} treatment, 2^{nd} cloning) only the 2.4 kb band is detected implying that all parasites had removed the positive/negative selection cassette. The Southern analysis results of 1079 clone 4 are inconsistent with the PCR results. The 2.8 kb band indicative of the positive/negative selection cassette presence was not observed in the 1079 clone 4 lane. This can be explained by relatively low sensitivity of Southern blotting. In order to generate the *Pbsir2a/b* double knockout parasites 1079 cl1 m4 cl2 was selected as a background for deletion of the *Pbsir2a* gene. The *Pbsir2a* knockout plasmid used was the same as the one utilised to obtain the *Pbsir2a*-deficient parasites (see below).

III.2 Generation of the *Pbsir2a*$^{-}$ line.

The *Pbsir2a* deletion construct (pl1009) was generated by Joke de Jong (Leiden Malaria group, unpublished data). The integration locus of the deletion construct is that of the *P.berghei sir2a* gene locus (see scheme Fig. 32A). The knockout construct designed contains two homology arms for double cross-over homologous integration into the target locus, and the *Tgdhft*-ts selectable marker cassette (homology arms primers: flank 1: 2160 x 2161; flank 2: 2162 x 2163). The integration fragment and the resulting DXO *sir2a* locus are shown. Parasite transfection was performed as described in previous sections. Cloning of the 1022 line resulted in 1 successful clone, 1022 cl2 (out of 4 positive clones obtained). No growth delay or morphology defects were observed during the cloning procedure and later re-growth of the clone in mice or rats. The 1022 cl2 PCR and Northern analysis are shown in Fig. 32B and C. The PCR amplification sites and the corresponding primers used are indicated in Fig. 32A, and the results shown in Fig. 32B. 5' and 3'-integration specific PCR as well as *Tgdhfr-ts* amplification were all positive (lanes 1,2 and 4). The unmodified *sir2a* locus was successfully amplified in the wild type but not in the *sir2a*-deletion clone. Since FIGE analysis for this parasite clone was not conclusive Northern was performed to confirm the *sir2a* transcript absence (Fig. 32C). Both for PCR and Northern analysis asexual HP and *Δsir2a* (1022 cl2) parasites were used in order to obtain DNA and RNA, respectively.

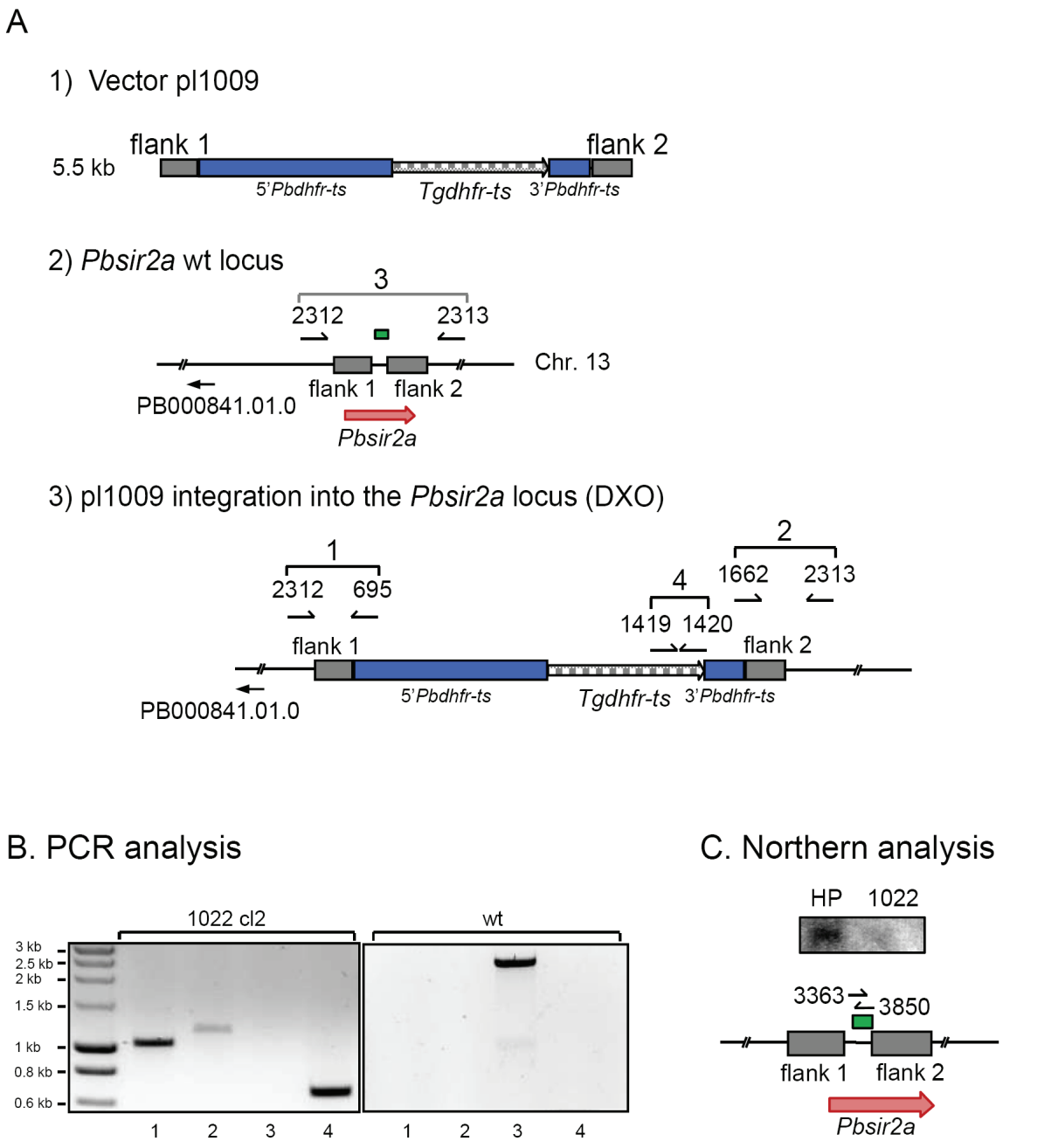

Fig. 32 *Δsir2a* generation. A. The digested 5.5 kb fragment from pl1009 was used for integration into the wild type *sir2a* locus (2) via double cross-over homologous recombination. The resulting deletion locus containing the *Tgdhfr-ts* selectable marker cassette is shown in (3). B. PCR analysis of the obtained 1022 cl2. The expected 5'-, 3'- and *Tgdhfr-ts*-specific bands (lane 1, 2 and 4, respectively) are all present in the 1022 cl2 and absent from the wild type. *Pbsir2a* locus (lane 3) was only amplified in the wild type. C. Northern analysis with a *sir2a*-specific probe (coloured in green on the schematic locus representation; 145 bp long).

III.2.1 Generation of the *Pbsir2a/sir2b* double knockout parasites.

Plasmodium berghei 1079 cl1 m4 cl2 schizonts from overnight culture were transfected with the linearised *Pbsir2a* deletion construct (experiment 1184). After approximately 10 days of parasite

growth in mice blood was collected by cardiac puncture. Genomic DNA extracted from the obtained parasite pellet was analysed for the construct integration. PCR analysis showed successful integration of the *Pbsir2a* knockout construct (Fig. 33A) for both mouse 1- and mouse 2-derived 1184 parasites. The 1184 m1 parasite population was cloned by limiting dilution and six clones were obtained. Genomic DNA from each clone was extracted and analysed by PCR (Fig. 33B) for the *Pbsir2a* deletion construct integration and the *Pbsir2b* gene presence.

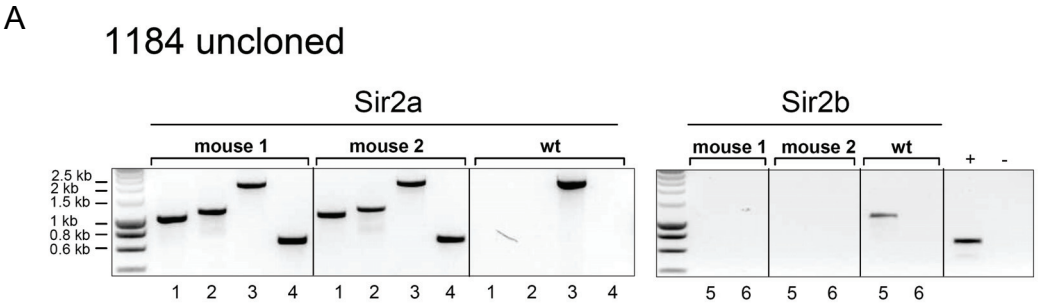

B. PCR analysis

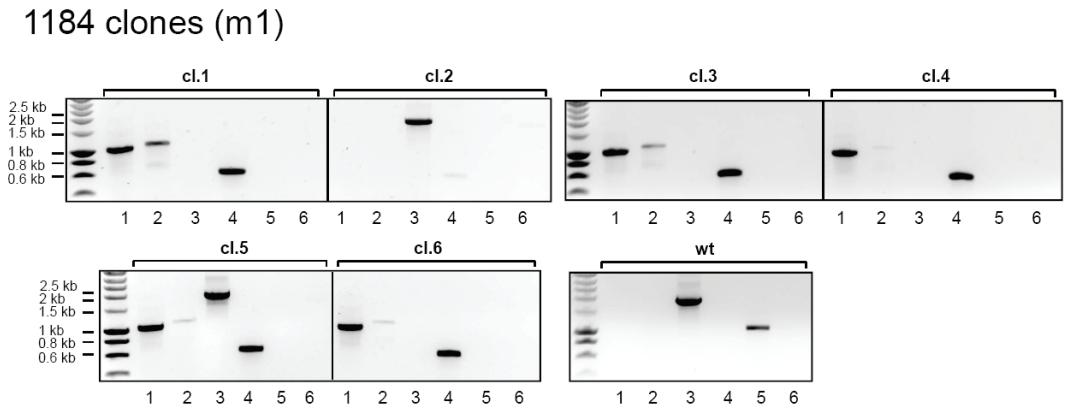

			Expected	
Lane	**Primers used**	**Product**	**wt**	**double k.o.**
1	2312 x 695 (5')	1034 bp	-	+
2	1662 x 3436 (3')	1172 bp	-	+
3	2312 x 2313 (internal *sir2a*)	1961 bp	+	-
4	1419 x 1420 (*Tg dhfr-ts*)	635 bp	-	+
5	3544 x 3545 (internal *sir2b*)	1090 bp	+	-
6	L307C x L1511 (*yfcu*)	1927 bp	-	-

C. Northern analysis

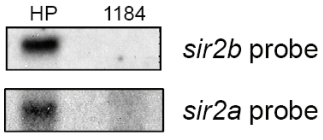

Fig. 33 *Δsir2a/b* analysis. (A) The uncloned 1184 mixed asexual parasite populations from mouse 1 and 2 were analysed by integration-specific PCR for both *sir2a* and *sir2b* presence (top panel, lanes 3 and 5). 5' and 3' integration of the *Pbsir2a* knockout construct was confirmed using 2312 x 695 and 1662 x 3436 primer pairs, respectively (lanes 1 and 2). The wt *sir2a* gene is present in the mixed transfection population. The presence of the *Tgdhfr-ts* selectable marker was also examined (lane 4). To confirm the absence of *Pbsir2b* in the 1184 m1 clones *sir2b*- and *yfcu*-specific PCRs were performed (as expected all clones were negative). In the wt control only the *Pbsira* and *Pbsir2b* gene fragments could be amplified. (B) Clones obtained from 1184 m1 parasites were analysed by integration-specific PCRs as described in (A). (C) Northern analysis with *sir2a*- and *sir2b*-specific probes showed the presence of both transcripts in the wild type asexual parasites but not in the 1184 m1cl1 parasites chosen for further studies.

1184 m1 clone 1 and 3 – 6 were all positive for *Pbsir2a* construct integration, since the expected PCR products were obtained for both 5' and 3' integration, as well as the *Tgdhfr-ts* selectable marker (see Fig. 20B lanes 1, 2 and 4). All clones were additionally analysed for the *Pbsir2b* gene and *yfcu* negative selectable marker presence (lanes 5 and 6, respectively). As expected both gene-specific PCRs were negative in all 1184 m1 clones. Northern analysis was performed to confirm the absence of both *sir2a* and *sir2b* transcripts in the 1184 m1cl1 PCR-positive line (C).

III.3 Generation of parasite lines expressing tagged PbSIR2A and PbSIR2B

Plasmodium falciparum SIR2A appears to be a central component in the *var* multigene family regulatory mechanism. Several recent studies report identification of proteins other than SIR2A binding to subtelomeric regions of *P. falciparum* chromosomes, including PfORC1 (Mancio-Silva et al., 2008). However direct PfSIR2A interaction partners have not been determined. The knowledge of *P. berghei* SIR2A interactome may provide insights into a more general SIR2A-mediated silencing mechanism, and point to *P. falciparum* SIR2 interactome orthologies. Furthermore, since SIR2B has not been extensively studied in either *P. berghei or P. falciparum*, the SIR2B interaction partners may provide preliminary indications concerning the function of the protein, and allow direct comparison of SIR2A- and SIR2B-interacting proteins. Furthermore, expression of the two SIR2 proteins can be analysed at time points of the life cycle other than asexual blood stages, e.g. ookinetes, using commercially available antibodies against the tags used. For these purposes PbSIR2A and PbSIR2B were each tagged with *gfp* and *myc* tag, creating four transgenic lines, of which two were analysed (Fig. 34 and Fig. 35 and 36).

III.3.1 SIR2A::GFP line

The modified *P. berghei* line expressing a C-terminal GFP-fusion of endogenous PbSIR2A was previously generated in the lab (experiment 503, Marta Tufet Bayona and Blandine Franke-Fayard, unpublished data). The integration construct used for single cross-over (SXO) homologous integration and the resulting modified *sir2a* locus are shown in Fig. 34A. Following transfection cloning of the 503 parasite population was performed. Two out of 4 clones were positive for integration by PCR analysis. Line 503 cl1 was used for further studies. PCR analysis of genomic DNA from 503 cl1 was positive for 5' *gfp*-tagging construct integration and *hdhfr* marker presence (see Fig. 34B). FIGE analysis of the 503 clone confirmed the PCR results (Fig. 34C). The ratio of signal intensity of chromosome 13/14 (*Pbsir2a* locus) to chromosome 7 is higher than 1 indicating that more than one copy of the tagging construct integrated in chromosome 13/14.

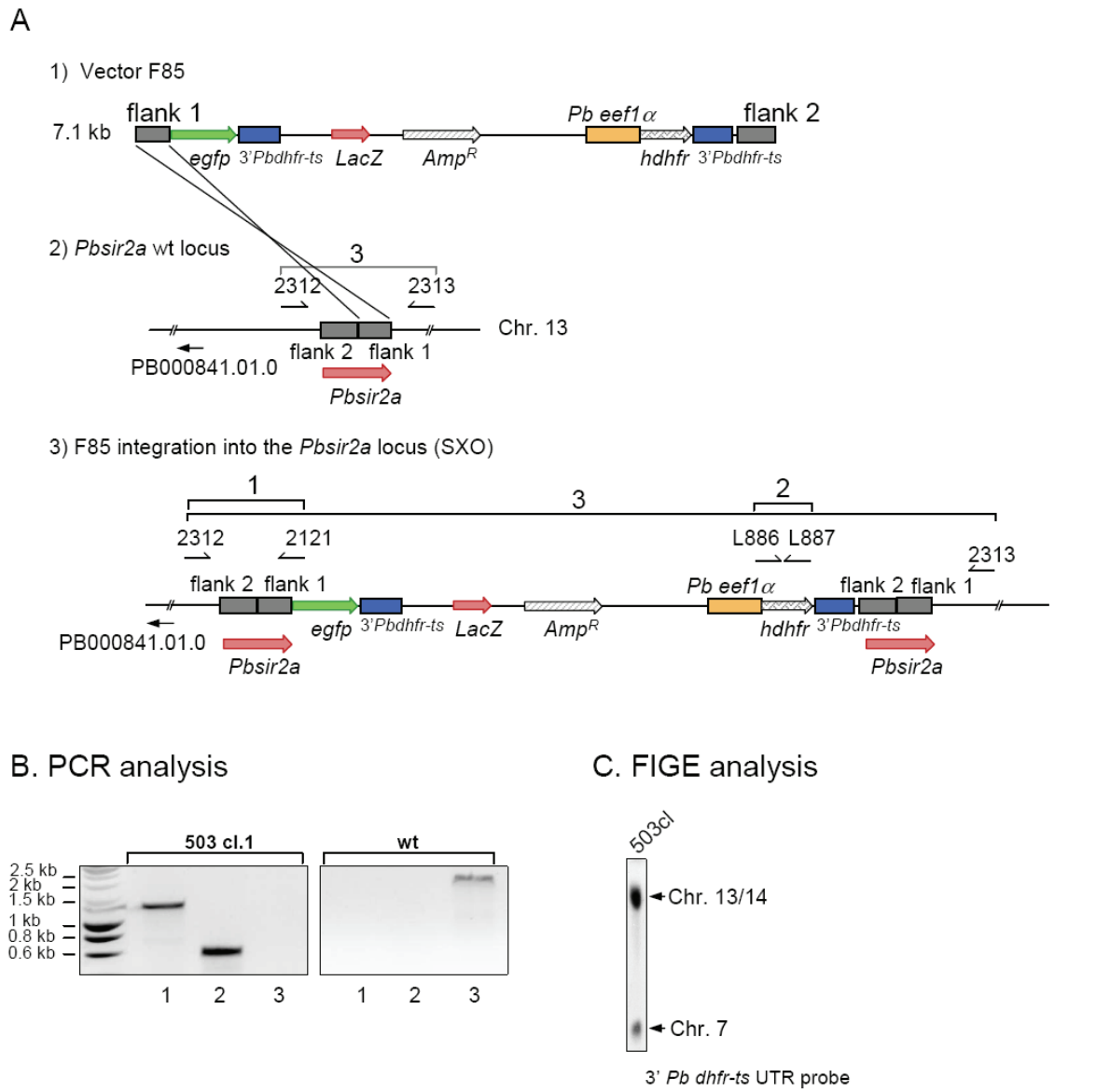

Fig. 34 Analysis of PbSIR2A::GFP expressing parasite line (experiment 503). (A) Linearised F85 construct targeting the wild type *sir2a* locus is shown in 1). The resulting transgenic locus, with C-terminal *egfp* fused with *Pbsir2a* is depicted in 3).
(B) 5' integration and *hdhfr* marker presence were determined by PCR using the primer pairs 2312 x 2121 and L886 x L887, respectively. Successful amplification products were obtained in 503 cl1. The wild type *Pbsir2a* locus amplified using 2312 x 2313 primers is present in the wild type but not in the 503 cl1 parasites, since the modified *sir2a*-egfp locus is too large to obtain under the chosen PCR conditions. (B) FIGE of 503 clone 1. A strong signal in chromosome 13/14 confirms the correct integration of the *gfp* tagging construct. Chromosome 7 (*Pbdhfr-ts* locus) signal intensity is lower than that of chr. 13/14 indicating multiple construct integrations at the *Pbsir2a* locus.

SIR2A::GFP parasites were analysed for protein expression and localisation by Western analysis and fluorescence microscopy (Fig. 35). Total protein extract of 503 cl1 (*sir2a::gfp*) and 1022 cl2 (*Δsir2a*) *in vitro* cultured mature ookinetes was run on a 12% SDS-polyacrylamide gel. Western analysis was performed with an anti-GFP mouse primary antibody (Roche) in 0.1% Tween in PBS/3% BSA (dilution 1:1000). Following the secondary anti-mouse HRP-conjugated antibody binding for 1hr at RT (dilution 1:10000) a weak but specific band was detected at ~ 56 kDa in the 503 cl1 lane (Fig. 35A). 1022 cl2 (*Δsir2a*) served as a positive control for GFP detection (strong band).

SIR2A::GFP localisation was analysed in live 503 cl1 parasites by fluorescence microscopy (Fig. 35B-D). In the asexual parasite stages (rings, trophozoites, schizonts) we could observe a stronger signal concentrated within the nuclei. In trophozoites additionally a cytoplasmic localisation of SIR2A::GFP was detected. These observations are consistent with SIR2A localisation in *P. falciparum* (Freitas-Junior et al., 2005; Mancio-Silva et al., 2008). SIR2A expression in the mosquito stages of *Plasmodium* has not been previously analysed. Localisation of C-terminally tagged SIR2A in zygotes at 6 hours, 9 hours and 24 hours of *in vitro* development is shown in Fig. 35C. SIR2A::GFP distributes evenly throughout 6 hours zygotes (retort form) . At 9 hours the localisation remains unspecific though on several occasions punctuate patterns were observed. The GFP localisation could in fact be auto fluorescence of parasite-specific structures, such as the scattered hemozoin pigment, noticeable especially upon longer image acquisition times. Interestingly fully mature ookinetes exhibit a very specific SIR2A::GFP localisation, concentrated in a vicinity of the parasite membrane, in a region proximal to the apical end. This localisation has been consistently observed and becomes evident only in mature ookinetes starting at 24-hours post fertilisation (arrowed). In addition, GFP signal is also prominent along the nuclear border of mature ookinetes. Fig. 35D depicts a sequence of still images recorded during a mature *sir2a::gfp* ookinete movement. MitoTracker™ (Invitrogen) was used to assess mitochondrial localisation. Several sirtuins have been shown to localise and/or affect cellular and protein functions within mitochondria. Despite MitoTracker™ staining (100 nM; red channel) appearing mostly distinct to the SIR2A::GFP localisation although intriguing, any possible partial co-localisation or connection of the two signals is beyond the resolution of light microscopy. The captivating SIR2A::GFP localisation has been confirmed by Immunofluorescence assay using an anti-GFP mouse antibody (mix of two monoclonal antibodies; Roche; see Fig. 35E). Expression of SIR2A in *P. berghei* was also analysed in oocysts and sporozoite. Oocysts observed on midguts at day 12 are intensively fluorescent (Fig. 35F). An interesting phenomenon has been witnessed during the oocyst *sir2a::gfp* expression analysis. In Fig. 35F the top panel represents an oocyst which was partially delocalised from the *Anopheles* mosquito midgut *ex vivo*. Both MitoTracker™ and Hoechst dyes appear to have penetrated the parasite. In contrast an oocyst fully embedded in the midgut is less accessible to the dyes (Fig. 35F, bottom panel). SIR2A::GFP is also expressed in mature *P. berghei* sporozoites (day 21 post-feeding; Fig. 35G). Intriguingly, in sporozoites the SiR2A signal concentrates into several foci, only partially overlapping with the nuclear Hoechst staining. The possible sites of SIR2A::GFP localisation at this parasite stage await characterisation.

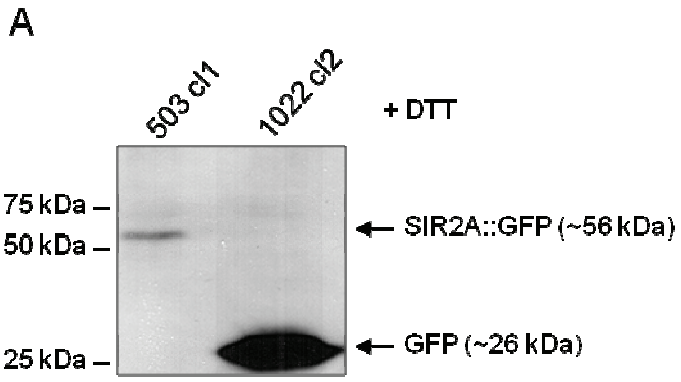
A
503 cl1
1022 cl2
+ DTT
75 kDa –
50 kDa –
25 kDa –
SIR2A::GFP (~56 kDa)
GFP (~26 kDa)

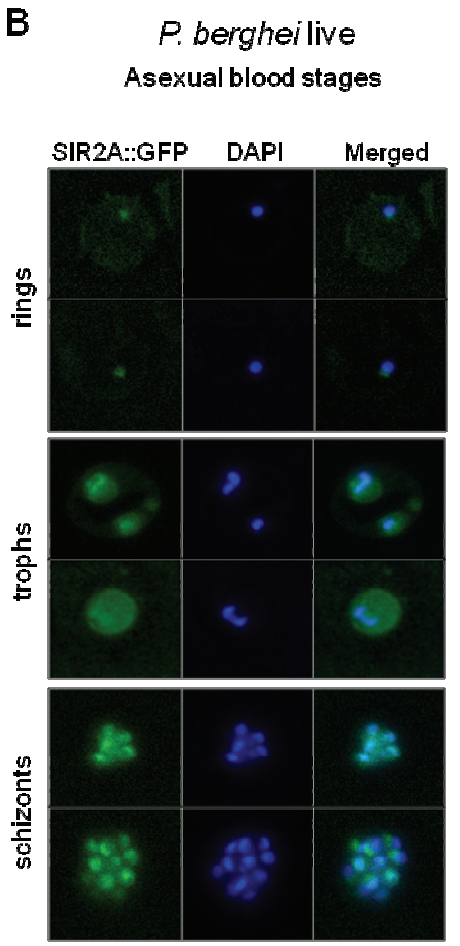
B
P. berghei live
Asexual blood stages
SIR2A::GFP
DAPI
Merged
rings
trophs
schizonts

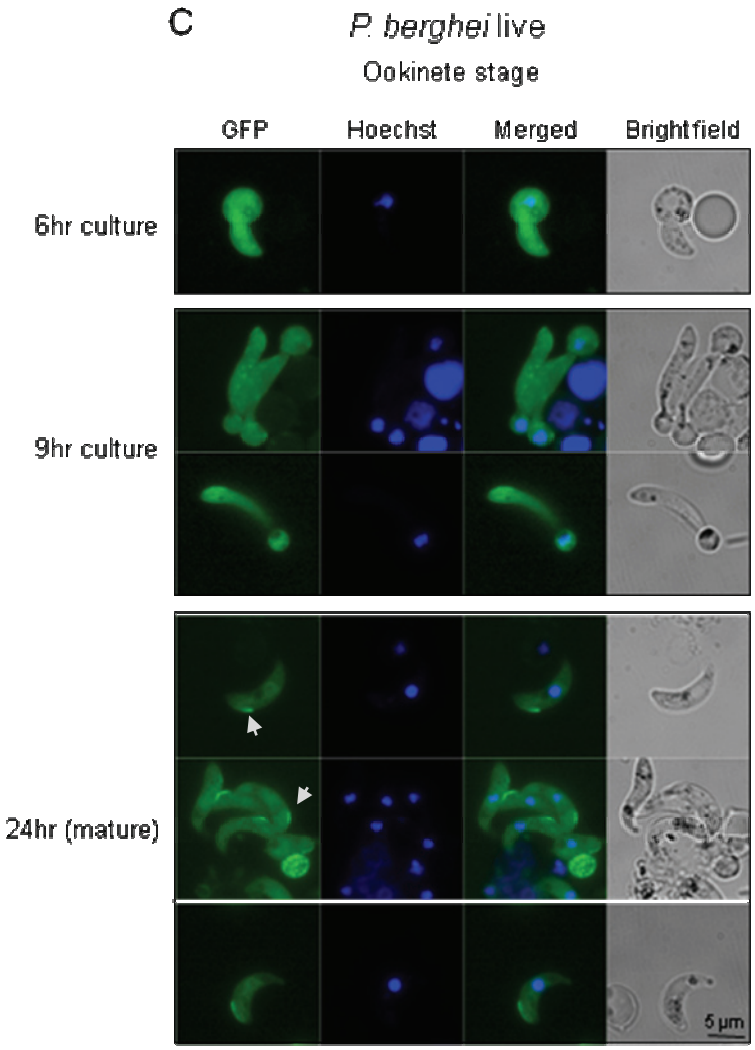
C
P. berghei live
Ookinete stage
GFP
Hoechst
Merged
Brightfield
6hr culture
9hr culture
24hr (mature)
5 µm

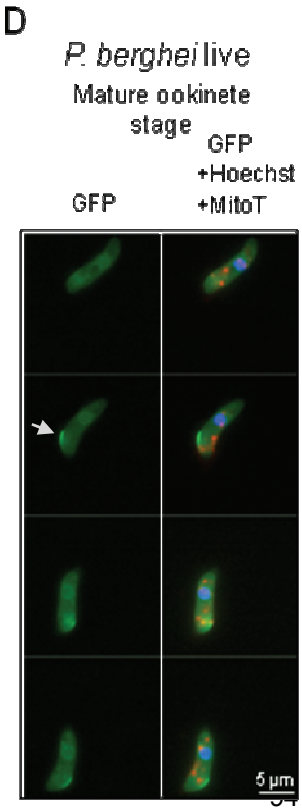
D
P. berghei live
Mature ookinete stage
GFP
GFP +Hoechst +MitoT
5 µm

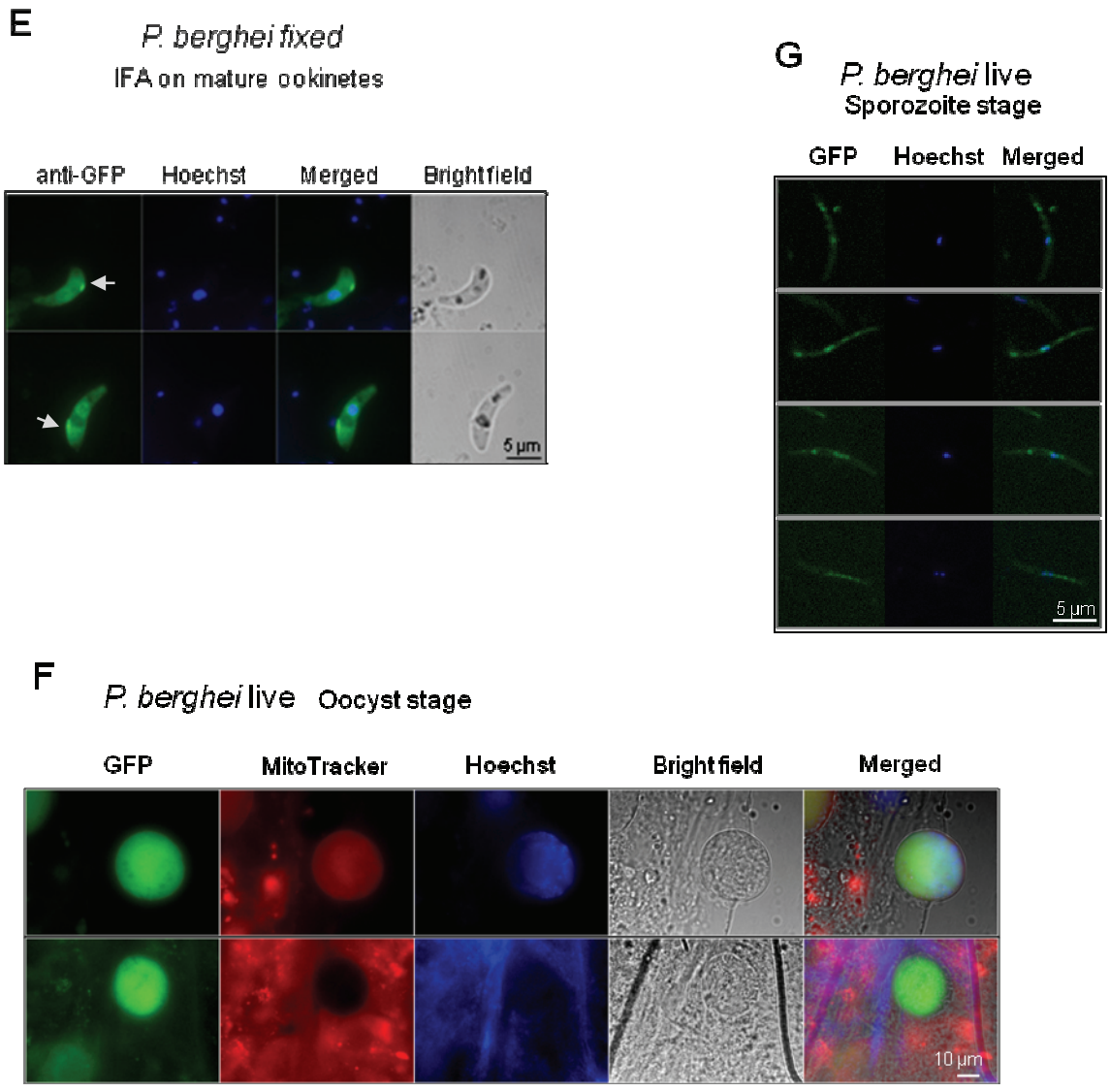

Fig. 35 SIR2A::GFP expression and localisation. (A) Western analysis of 503 cl1 expressing SIR2A::GFP. Under denaturing conditions SIR2A::GFP is detected in the 503 cl1 parasites at an expected size of ~ 56kDa. 1022 cl2 constitutively expressing GFP was used as a positive control (the expected GFP band at 25 kDa). (B)-(D), (F);, (G) Live parasites were analysed for *gfp* expression. Nuclei were stained with Hoechst dye. (B) In all asexual stages (rings, trophs, schizonts) SIR2A::GFP localises to the parasite nucleus. At the trophozoite stage a stronger signal is also observed in the cytoplasm. (C) Zygote stages after 6 (retort), 9 (mature retort/juvenile ookinete) and 24 hours (mature ookinete) culture *in vitro*; evenly distributed or slightly punctate signal is visible at 6 and 9 hours post-fertilisation. At 24 hours onwards SIR2A::GFP concentrates in one zone of the apical area (membrane proximal staining) and at the nuclear border. (D) Still images of an ookinete moving on a glass slide. On the left: GFP signal only. On the right: still images merged to facilitate structural recognition (in green: SIR2A::GFP; Hoechst: blue; MitoTracker™ for mitochondrial staining: red. (E) Fixed *P. berghei* ookinetes probed with anti-GFP antibody in order to confirm the SIR2A::GFP presence. (F) *P. berghei* live oocysts on dissected mosquito midguts. Top panel – an oocyst partially exposed out of the mosquito midgut is accessible to stains such as MitoTracker™ and Hoechst, whereas a more embedded oocyst is partially impenetrable to the mentioned dyes. It could also be that the background from the surrounding *Anopheles* tissue emits very strong fluorescence making the oocyst fluorescence signal appear as negative.

III.3.2 SIR2B::MYC line

The *Pbsir2b c-myc* tagging construct was generated using the psd141 plasmid (courtesy of Dr. O. Billker, WTSI UK), containing 2x *myc* tag, and *hdhfr* gene as a selectable marker. The plasmid was linearised with XhoI restriction enzyme and 5 µg was used for transfection of *P. berghei* schizonts cultured overnight at 37 ˚C. The tagging construct and the integration locus are represented in Figure 36 below.

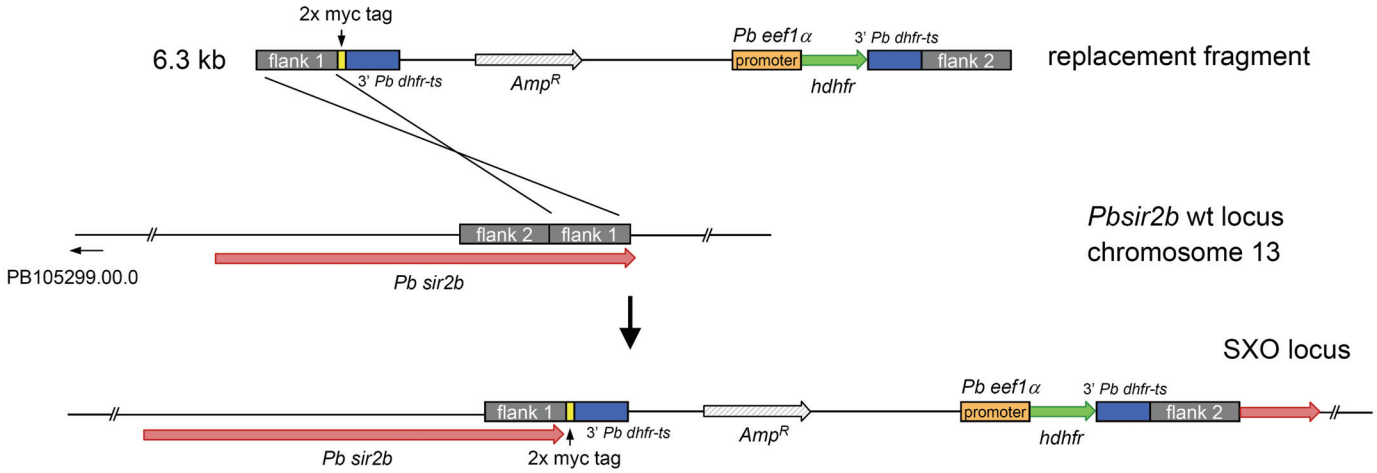

Fig. 36 *Pbsir2b::myc* tagging construct was generated using the psd141 plasmid (courtesy of Dr. O. Billker). Approximately 1.5 kb of the *Pbsir2b* end sequence was used for homology region, excluding the STOP codon. Homologous single cross-over integration at the *Pbsir2b* locus (on chromosome 13) introduced a 2x myc tag at the C terminus of the gene.

The transfected parasite population (experiment 1209) was selected with pyrimethamine. FIGE analysis of agarose-embedded parasites, followed by Southern blotting and probing with ^{32}P-labeled 3' *Pbdhfr-ts* UTR showed a signal specific to chromosome 13/14 as well as chromosome 7 (endogenous *Pbdhfr-ts* gene locus) (Fig. 37B). The 1209 parasite population was cloned by limiting dilution (see Materials and Methods) and three clones obtained. PCR analysis of genomic DNA from these clones revealed the expected, human *dhfr* product as well as the 5' and 3' integration-specific products (Fig. 37A) in all three 1209 clones.

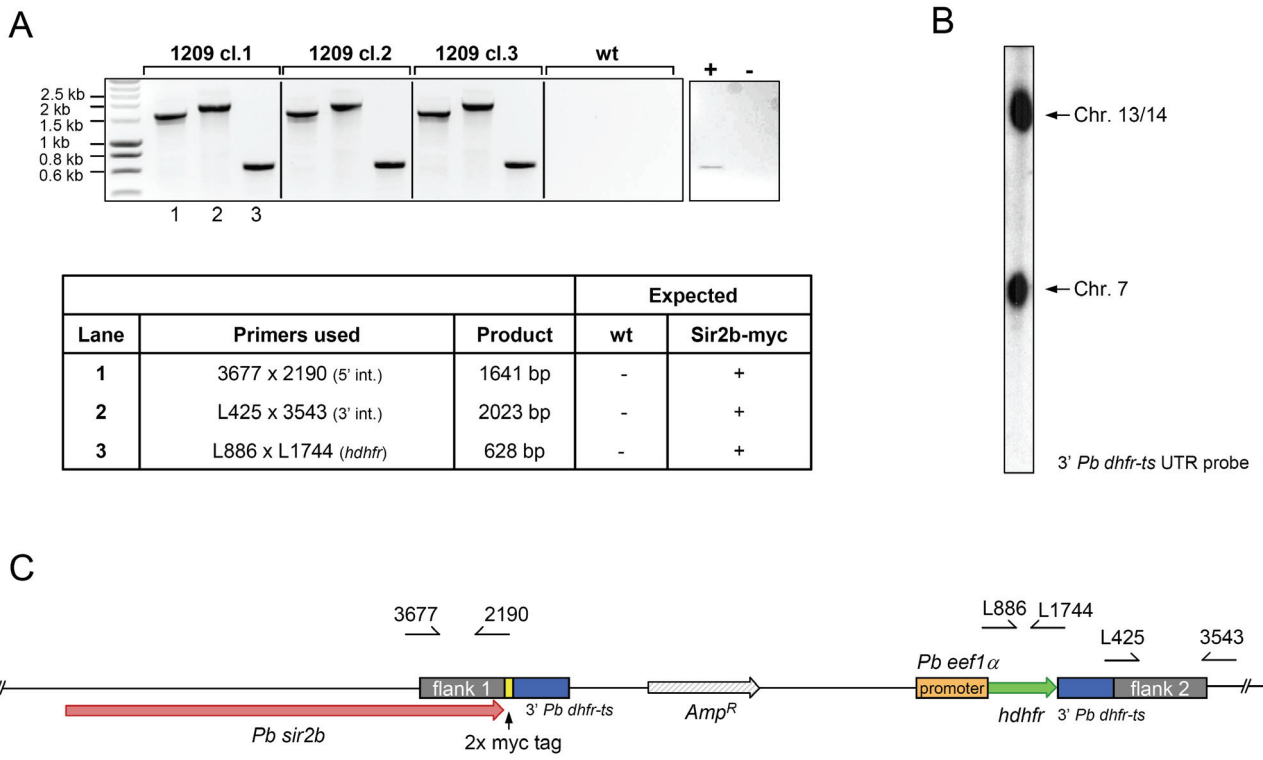

			Expected	
Lane	**Primers used**	**Product**	**wt**	**Sir2b-myc**
1	3677 x 2190 (5' int.)	1641 bp	-	+
2	L425 x 3543 (3' int.)	2023 bp	-	+
3	L886 x L1744 (*hdhfr*)	628 bp	-	+

Fig. 37 Analysis of the *Pbsir2b::myc* tagging construct integration. Genomic DNA extracted from three 1209 parasite clones was analysed by integration-specific PCR (A). The 5' and 3' integration was confirmed using 3677 x 2190 and L425 x 3545 primer pairs, respectively (lanes 1 and 2). The selectable marker presence (human *dhfr*) was verified using L886 x L1744 primers. All 1209 clones showed the correct integration of the targeting construct. (B) FIGE of 1209 uncloned population. Probing with 3' *Pbdhfr-ts* UTR probe resulted in a specific signal at chromosome 13/14, indicating the expected integration site of the *Pbsir2b-myc* tagging construct. Signal presence at chromosome 7 is due to endogenous *Pbdhfr-ts* gene. (C) Modified *Pbsir2b* locus. Primers used in the PCR analysis are indicated.

Since the correct integration of the tagging construct was confirmed, the next step was to verify the tagged PbSIR2B::MYC protein expression by Western analysis (Fig. 38).

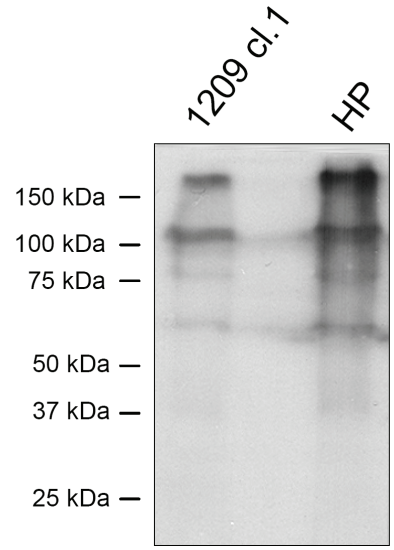

Fig. 38 Western analysis of the PbSIR2B::MYC (1209 cl1). Total protein extract of asynchronous blood stages 1209 cl1 and HP parasites was run on a 12% SDS-polyacrylamide gel. Following blotting the membrane was blocked in 3% milk in 0.1% PBS-Tween solution overnight. 1 hr incubation with a monoclonal rabbit anti c-MYC antibody (Sigma) at a dilution 1:1000 was followed by extensive washing in 0.1% PBS-Tween. The secondary anti-rabbit HRP-conjugated antibody was incubated for 2 hours (dilution 1:10000). The PbSIR2B-MYC protein band should appear at approximately 135 kDa.

Total parasite protein of asexual blood stages of 1209 cl1 and *P. berghei* ANKA strain (HP) were run on a 12% SDS-polyacrylamide gel. The samples were then transferred onto a Hybond-P membrane (Amersham). Following overnight blocking in 3 % milk in PBS-Tween (0.1%) the membrane was incubated with an anti-c-MYC primary antibody (Sigma) (1:1000 in PBS-Tween 0.1%). Following multiple washing in PBS-Tween, the secondary anti-rabbit HRP-conjugated antibody was added (1:10000). The PbSIR2B-MYC protein should be detected at approximately 135 kDa. Unfortunately no band of this size was observed. Instead an identical pattern of multiple bands were detected in both 1209 cl1 lane and HP control sample. The possible reason for unsuccessful detection could be lack of PbSIR2B-MYC expression. However multiple bands detected in the control sample indicate the need for experimental procedure optimisation. It could be that both 1209 cl1 and HP samples are degraded due to multiple freezing/thawing steps, since both samples were used in a previous experiment. An additional control, namely a protein sample containing another MYC-tagged protein (verified expression) could have been used as a positive control in the Western analysis.

III.4 Assessment of *PbSir2a/b* double knockout parasites survival in Brown Norway rats compared to a wild type GFP-LUC expressing line

The Brown Norway rats were shown to efficiently control rodent malaria parasite infection (see Introduction). This animal model was used to analyse the course of infection and concomitant immune response to the 1184 parasites and the 676 reference line (Franke-Fayard et al., 2004). The 676 line expressing the bioluminescent report protein luciferase (under *ama-1* promoter) has been generated to further studies on sequestration patterns of the schizont stage and its role in pathology in live animals. The GFP-LUC expressing (676) parasites could be visualised in the live Brown Norway rats by intraperitoneally injecting a substrate luciferin (at a final concentration of 120 mg/kg of body weight, Synchem OHG) that is oxidised by the luciferase enzyme expressed in the genetically engineered parasites. This oxidation reaction produces light emission which is detected by a specialised IVIS *in vivo*-visualisation system (Xenogen), and allows for locating the parasites within the animal body as well as assessment of parasite numbers.

A group of four Brown Norway rats was injected per line (676 and 1184 *Pbsir2a/Pbsir2b*$^{-/-}$, asynchronous blood stage parasites). One rat injected with 1184 m1 cl1 to date has not developed parasitaemia. Throughout the experiment the parasite levels in both lines have been monitored by light microscopy of Giemsa-stained blood smears (approximately every 2 days) and starting from day 19 by bioluminescence measurements of 676-infected rats (see Fig. 39). Initially parasites could be detected in all BN rats (with the exception of the one negative 1184-infected rat). Bioluminescence measurements of 676-infected animals initially indicated the parasite presence only in two BN rats (rat 1 cage 1 and rat 1 cage 2) (Fig. 39A). Following the period of undetectable parasitaemia, the previously bioluminescence-negative rat 0 (cage 1) has developed detectable parasitaemia persistent until the next measurement 2 days after; whereas the other 676-infected rats remained negative. This ambiguous observation might be due to technical detection limit of the *in vivo*-imaging system or

plausibly parasite re-emergence following an apparent successful escape from clearance by the host immune system.

Throughout the course of the experiment (2.5 months) parasite presence was verified by weekly injections of naïve mice with BN rat blood. All mice were developing patent parasitaemia, with the exception of the last batch (week 10), where all 676-infected mice remained negative. Interestingly, the *Δpbsir2a/b* 1184-injected mice developed detectable parasitaemia. The genotypes of the collected 1184 m1 cl1 parasites were confirmed by PCR analysis. Notably, investigation of microscopy slides in search of eventual abnormalities revealed occasional schizonts in the case of 1184 smears (observed for the 676 clone though more sporadically and in lower numbers). This observation could be an artefact of high parasitaemia or alternatively a result of the 1184 *Pbsir2a/Pbsir2b* double mutant phenotype characteristics which are yet to be investigated.

A

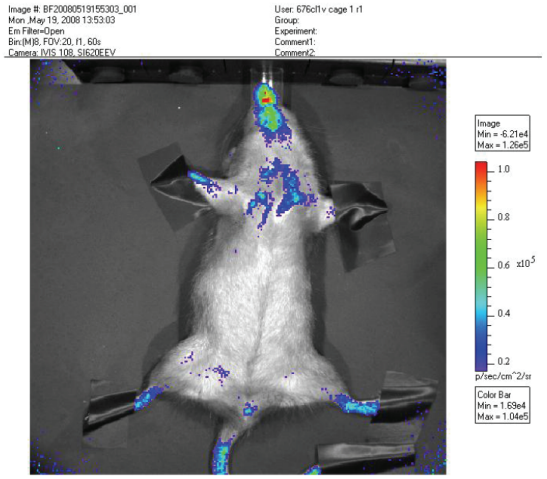

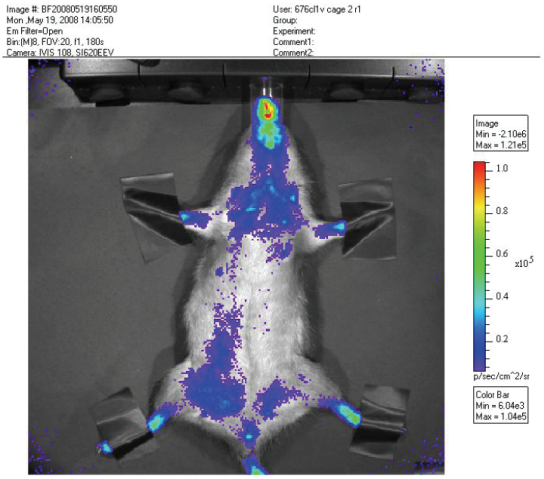

B

C

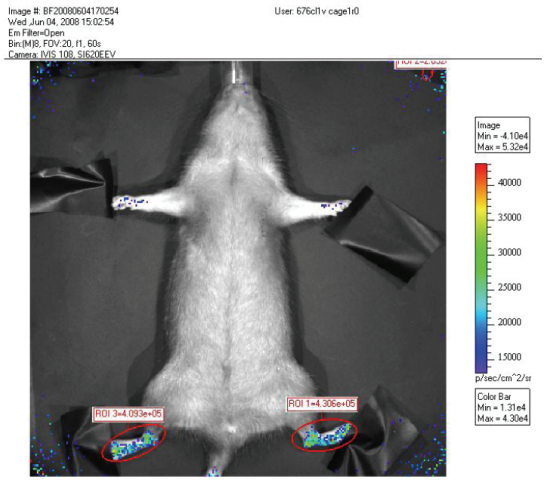

676 m1 cl1 (*gfp-luc*)

	Cage 1		Cage 2	
	rat 0	rat 1	rat 0	rat 1
2008-05-19	neg	pos	neg	pos
2008-05-21	neg	neg	neg	neg
2008-05-23	neg	neg	neg	neg
2008-05-26	neg	neg	neg	neg
2008-05-30	neg	neg	neg	neg
2008-06-02	pos	neg	neg	neg
2008-06-04	pos	neg	neg	neg
2008-06-06	neg	neg	neg	neg
2008-06-09	neg	neg	neg	neg
2008-06-19	neg	neg	neg	neg

Fig. 39 Bioluminescence measurements of 676-infected BN rats using an *in vivo*-imaging IVIS system (Xenogen). The measurements were performed on the dates indicated in the table. Four rats were controlled on each indicated day. The animals which showed parasite presence are shown in A, B and C, according to the table (bioluminescence-positive measurements are indicated in red). As seen in A the BN rat 1 (cage 1) and rat 1 (cage 2) were clearly positive for GFP-LUC expressing parasites. Approximately 1 month later the parasites were hardly detectable (B and C). Interestingly, the two positive BN rats were not the same ones measured in A.

III.4.1 Average telomere length measurement in 1184 *Pbsir2a/Pbsir2b*$^{-/-}$ parasites

The absence of SIR2 deacetylases is suspected to induce a more open chromatin structure at generally inaccessible subtelomeric regions, as a result of persisting histone acetylation. One can imagine that in this chromatin state telomeres are more available to the telomerase complex (TERT subunit). Therefore with increased TERT activity at chromosome ends the average telomere length in the SIR2-deletion mutant parasites might increase with time. To determine the average telomere length in the 1184 parasite clone Telomere Restriction Fragment (TRF) analysis was performed (Fig. 40) of 1184 and 676 parasites that were obtained from mice that have been infected with parasites taken from ongoing infections of Brown Norway rats was extracted and digested in parallel with four frequently cutting enzymes. Following Southern blotting the membrane was probed with a ^{32}P-labelled telomere-specific probe. The observed smear is characteristic of telomeres as they are heterogeneous in size. The lane signal intensity analysis showed that the average telomere length in the double knockout parasites (Fig. 40, lanes 1-5) was increased by approximately 0.3 – 0.36 kb (or up to ~45%) comparing to that of the wild type measured in this experiment (approximately 0.8 kb). The wild type average telomere length is shorter than previously measured using the same technique (~0.95 kb). This might be due to the resolution around the 1 kb band size, since the previous gel was run for a shorter time, causing a more “compact” signal at the telomere smear. The 676 sample (lane 6) from the parasites grown in Brown Norway rats, in parallel with the 1184 parasites shows a very faint signal at around 0.8 kb. Interestingly, two major intensity signals can be observed in 1184 parasites (particularly visible in the case of 1184 12/06 m0 sample). The lower intensity peak is of the same size as the observed in the wild type (around 0.8 kb). It is probable that telomere elongation does not occur at the same rate in all parasites, and possibly not even on different telomeres within one parasite. However the sharpness of the 0.8 kb peak appearing as a high intensity band on the probed membrane (Fig. 40 right panel, lane 2, indicated by an arrow) is quite puzzling and remains to be clarified. To ensure the conclusions drawn from this experiment the TRF measurement will be repeated including additional 676 samples.

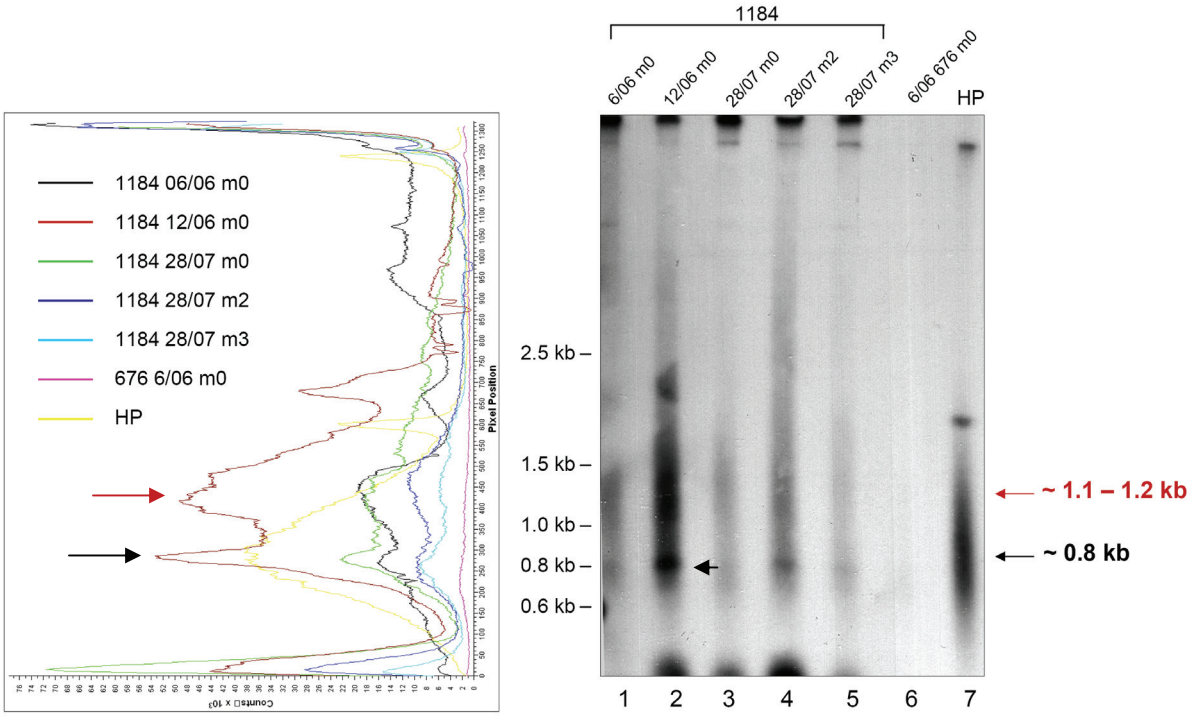

Fig. 40 Average telomere length measurement of the 1184 samples. Genomic DNA was extracted from the parasites grown since 1/05/2008 in Brown Norway rats and at several dates transferred to mice for approximately one week (until blood collection). Right panel: TRF measurement – 700 ng of parasite genomic DNA was digested in parallel with AluI, RsaI, MboII and Sau3AI overnight. Following Southern blotting the membrane was probed with a ^{32}P-labelled telomere-specific probe. The lanes are labelled according the parasite line and the date of parasites collection from mice. The 1184 samples show higher average telomere length - approximately 1.1-1.2 kb (indicated by the red arrow) than the HP *P. berghei* ANKA strain sample (lane 7, 0.8 kb indicated by the black arrow). Interestingly a high intensity band of around 0.8 kb can be observed in all 1184 samples (most prominent in lane 2, black arrow). Left panel: plotted signal intensities along each lane of the blot shown on the right. The black arrow indicates the peak at 0.8 kb (wild type population, and 1184 high intensity band), whereas the red arrow the 1.1-1.2 kb peak (the "shifted" 1184 population).

III.5 Global transcriptome analysis of *Pbsir2a/b* double deletion line versus wild type line

III.5.1 Microarray analysis of 4 asexual parasite stages

In yeast *Saccharomyces cerevisiae* SIR2 histone deacetylase has been shown to repress transcription by regulating local chromatin structure predominantly at the silent mating type HML and HMR loci as well as the subtelomeric regions (Rine et al., 1979; for a review see Lustig, 1998). *P. falciparum* SIR2A affects predominantly transcriptional states of mainly subtelomeric upsA- and upsE-controlled *var* genes, proximal *rifin* genes, as well as several other genes in the parasite genome (Duraisingh et al., 2005). We hypothesised that *P. berghei* SIR2 might exert an effect on transcription of several *P. berghei* multigene families and other types of genes regulated by SIR2 activity. Therefore to study the effects of the SIR2A and SIR2B absence on the level of transcription some pilot microarray experiments comparing the wild type to the *Pbsir2a/sir2b* double knockout parasites (1184 m1 cl1) were performed.

1) RNA preparation, quality assessment and array hybridisation of the 1184 and HP samples

In *P. falciparum* SIR2A controls the expression of *var* that encode PFEMP1 adhesins associated with parasite sequestration in the deep vasculature of various tissues (Ho and White, 1999; Sherman et al., 2003). The schizont forms of *P. berghei* also sequester in lungs and adipose tissue in a CD36-dependent manner (Hearn et al., 2000). Therefore, four time points of 5 (rings), 10 (late ring/early trophozoite), 16 (late trophozoite/early schizont stage) and 22 (mature schizonts) hours post invasion were collected from synchronized *P. berghei* HP ANKA strain and 1184 (*Pbsir2a/b* double deletion mutant) parasites. In this section the initial analysis of the 10 and 16 hpi samples is described. The four time points microarray results are shortly described toward the end of this section.

Biological replicates of both HP and 1184 samples per each time point were collected from separate mice (in total 16 samples). RNA extraction was performed using TRIzol reagent (Invitrogen) following the supplier's protocol (see RNA extraction in Materials and Methods). Parasite pellets from each mouse were split into two prior to extraction. Total RNA from the two time points was extracted on two different days. RNA concentration was determined using the NanoDrop 1000 (Thermo Scientific). RNA integrity of 10 and 16 hpi was assessed on a RNA formaldehyde gel (Fig. 41). Following blotting the membrane was probed with the L87R probe specific for the LSU regions of the four rRNA units (A/B/C/D) of *P. berghei.* Due to the limited quantity of total RNA in several preparations only 6 out of 9 samples were analysed (3 of 10 hpi and 3 of 16 hpi time point). An estimated 2 µg/lane of total RNA was loaded for each sample. In the case of the 10 hpi samples (Fig. 41, lanes 1-3) the measured RNA concentration (Table 4) is in disagreement with the quantity visible on the RNA gel. This could be due to an elevated absorbance around 230 nm in all 10 hpi samples. The 10 hours HP m1 sample appears to be degraded. This sample was substituted with a previously extracted parasite RNA of the same time point. The OD measurements of the 16 hpi samples correlate well with quantities visible on the gel (lanes 4-6). Nevertheless all eight RNA preparations were additionally column-purified using RNeasy Mini Kit (Qiagen).

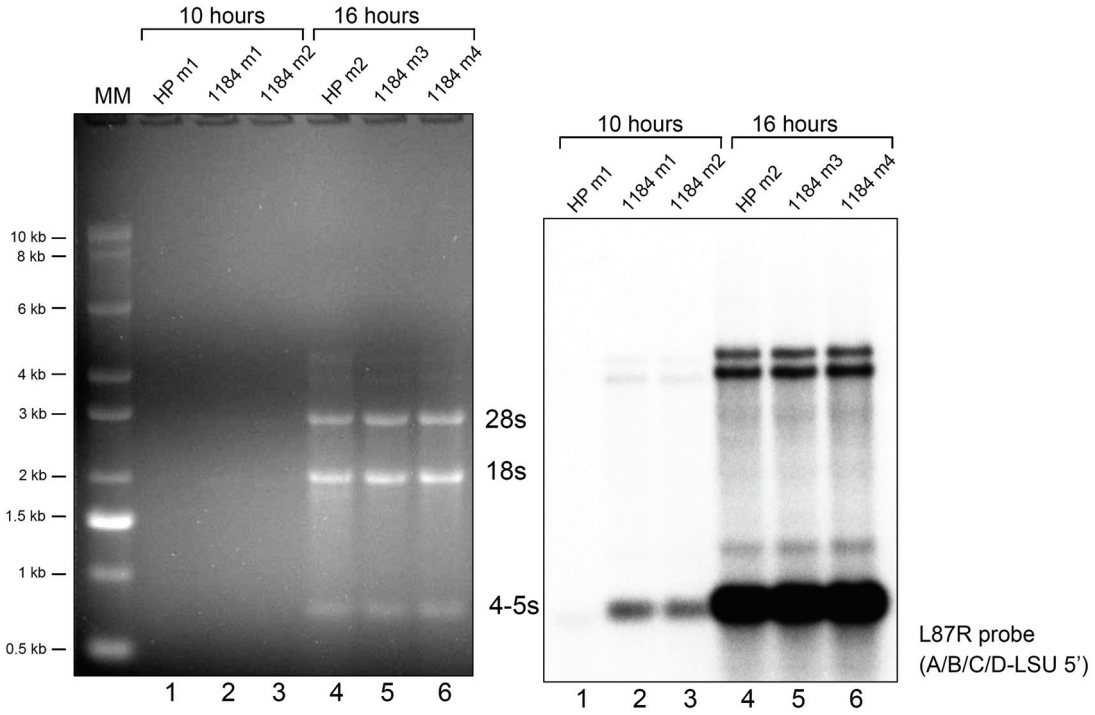

Fig. 41 RNA samples analysis. Three samples of each time point (10 hpi and 16 hpi) were analysed on a formaldehyde RNA gel (left panel). The three 10 h samples (lanes 1-3) could not be clearly seen on the gel. The remaining three samples of the 16 h time point exhibit good RNA integrity with clear 4-5s, 18s and 28s ribosomal bands. Following Northern blotting the membrane was probed with L87R ^{32}P-labeled oligonucleotide specific to 5' LSU regions of the A/B/C/D rRNA units (right panel). Ribosomal bands were detected in lanes 2 and 3 indicating good RNA integrity though of lower concentration than that expected from the prior RNA measurements.

Despite inconsistencies in measured and observed RNA concentrations the 10 hours 1184 m1 and 1184 m2 samples (Fig. 41), right panel, lanes 2 and 3) appear of good quality, as indicated by the presence of higher ribosomal bands. All samples apart from HP m1 10 hpi were used in the microarray experiment.

Sample	Mouse	A260/280	Estimated total quantity (µg)
HP	m0	1.95	5.5
	m1	2.29	16.0
1184	m0	1.89	12.0
	m1	2.22	6.5

10 hpi

Sample	Mouse	A260/280	Estimated total quantity (µg)
HP	m2	1.96	11.0
	m3	1.97	10.5
1184	m3	2.02	10.0
	m4	2.04	10.0

16 hpi

Table 4 ***P. berghei*** **ANKA HP and P. berghei** ***Δpbsir2a/b*** **RNA samples** used for the pilot microarray experiment (10 and 16 hour time points). Here HP m1 is a previously isolated parasite RNA sample.

The microarrays and data pre-processing was performed at The Wellcome Trust Sanger Institute on the basis of collaboration (A. Ivens & C. Carret). Approximately 5.5 micrograms of total RNA from each sample was used for cDNA synthesis. *P. berghei* samples were hybridised on a single colour RMSANGER (Rodent Malaria Sanger) Affymetrix array (15µg of cRNA per chip). cDNA synthesis, cRNA labeling, hybridisation, washing/staining/scanning were carried out according to Affymetrix protocol (Euk_450_v5). Pre-processing and data mining was performed by Dr. Celine Carret using R/Bioconductor software (Carey et al., 2005).

RMSANGER Affymetrix chip characteristics.

The Affymetrix RMSANGER array consists of approximately 6.5 million 25-mer oligonucleotides immobilised on a silicon chip at a 5µm resolution.
The chip definition file (CDF) used for the final expression analysis comprises 21776 probe sets specific for *Plasmodium berghei* designed using the 3x coverage of *P. berghei* genome (~12000 coding sequences predictions). The probes on the array are represented by sense and antisense probe sets (21776) that can be divided into the following categories:

(1) genes predicted within the central region of a contig (assumption: complete gene sequence present). Approximately 4690 coding sequences (CDS) (PlasmoDB data) or 4855 (GeneDB data) on the array belong to this category (PB000000.00.0 to PB001669.02.0), of which 4383 CDS have an orthologoue in other *Plasmodium* species.

(2) genes predicted at contig boundaries (assumption: gene incomplete or part of a larger transcript). Approximately 6000 CDS on the array (PB100000.00.0 to PB406162.00.0).

(3) PB500000.00.0 to PB500059.00.0 annotated as *bir* genes. 42 CDS (PlasmoDB) / 62 (GeneDB) (overlapping genes). Note: currently 264 genes are annotated as *bir* (PlasmoDB and Gene DB)

The second category most probably contains additional unannotated *bir* genes. At least 3040 probe sets have less than 6 probes mapping the CDS, making these probe sets unsuitable for statistical analysis.

2) Quality control, data pre-processing and normalisation.

The first step in every microarray experiment is the quality assessment of the data obtained. Non-biological variability can be introduced through array printing, labelling, hybridisation and washing steps and may lead to incorrect interpretation of the data and improper final conclusions. Therefore, it is crucial to discard low quality data in the early phases of a microarray experiment.

All steps described here required for obtaining interpretable data were performed by Dr. Celine Carret, The Wellcome Trust Sanger Institute, Cambridge, United Kingdom. The quality control steps involved RNA degradation assessment (Bioconductor software analysis) and Principal Component Analysis (PCA). The RNA degradation plot (Fig. 19) represents each of the eight arrays as a separate line. The curves follow approximately the same trend indicating that the arrays are comparable and all eight can be used for further data normalisation and analysis.

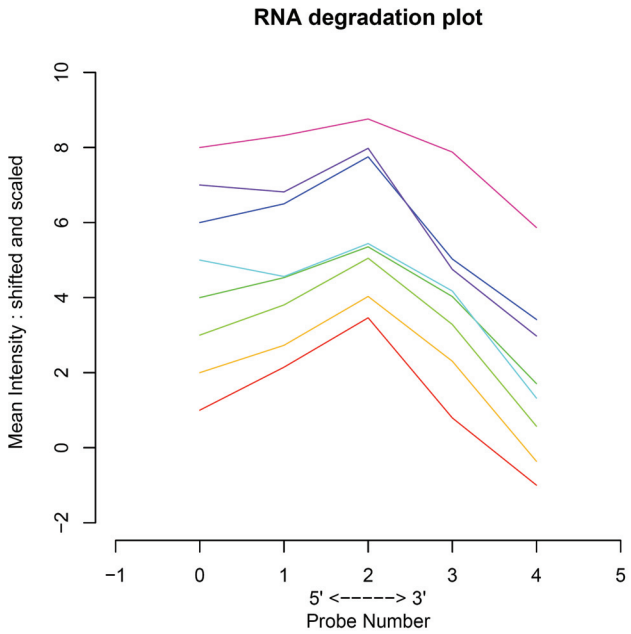

Fig. 42 RNA degradation plot of the HP and *Δsir2a/b* (1184) samples based on the signal intensities of each array. The curves follow approximately the same trend, a criterion that should be fulfilled to obtain meaningful sample comparisons.

The raw data obtained from each array image capture cannot be directly interpreted due to variations in signal intensities among the chips. In order to make intensity data comparable among the arrays signal intensities are standardised (or normalised). Normalisation of the eight chips was performed using RMA software (robust multi-array averaging). Each probe is background adjusted, quantile normalised across the whole set of chips, then the probes are grouped per probe sets (here a probe set = annotated CDS) and their signal intensities averaged and given as log2. Following normalisation Principal Components Analysis (PCA) was performed. PCA is a statistical technique for determining the key variables in a multidimensional data set. Briefly, PCA allows simplified rapid initial comparison of obtained data sets to expose the most prominent differences between samples and eventually identify outlier signals. In Fig. 42 a global principal component plot is shown, indicating differences between the two parasite lines (HP and 1184) with regards to the 10 and 16 hpi time points. In the case of the HP 10h and 16h no grouping is evident. The 1184 16h and one sample of the 10h time point do group together, though one replicate of 1184 10h seems quite distant (red triangle in the top right part of the plot). Since no obvious grouping is observed for the HP samples all were used for further analysis. The 1184 10h replicate was not discarded since its presence did not cause major changes in the final differentially regulated genes list.

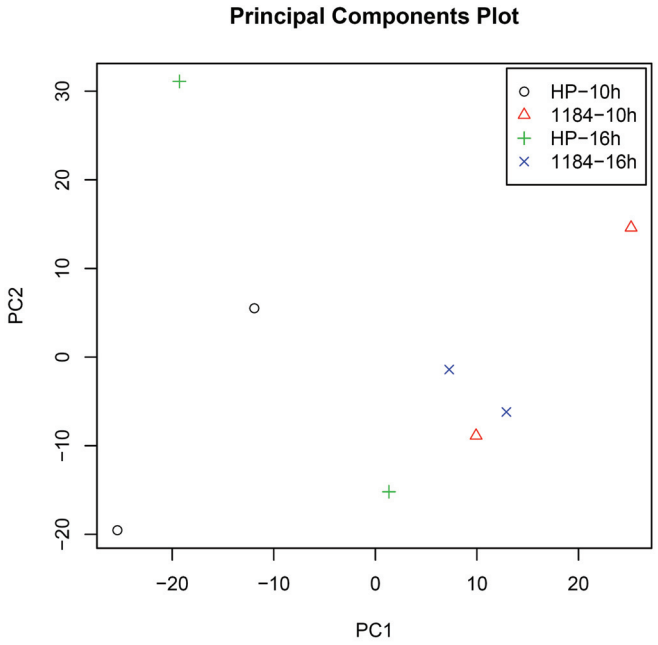

Fig. 42 PCA plot of the *Δsir2a/b* 1184 and HP 10 and 16 hpi samples. 1184 samples group together with the exception of one replicate of 1184 10 hpi. The wild type (HP) samples do not group. Due to the disperse appearance of the samples no outliers were identified and all were used for further analysis.

3) Data analysis – differentially expressed genes in the 1184 compared to the wild type.

Differential expression (DE) between all the analysed samples of HP and 1184 *Pbsir2a/Pbsir2b* double mutant was assessed using a limma library within the Bioconductor software. The initial analysis of the data yielded 1814 differentially expressed genes between the HP and 1184. Following filtering of the obtained data by false positive value < 0.05, and taking the genes of which expression change value was higher than that of 75% of genes in the set (top 25th percentile) the data set decreased to 188 most up- and down-regulated genes (see Table 6 and Fig. 43). In both 10 and 16 hour time points exactly the same set of genes was most differentially expressed. The differences were more prominent in the 10 h gene list (late ring/early trophozoite), with 16 and 19 genes at least 2 fold up- and down-regulated, respectively. Less pronounced changes were observed in the late ring/early troph stage (16 hpi) with less genes most differentially expressed (n=11 for up- and n=6 for down-regulated). The log2 values were generally smaller in the case of 16 hpi sample. Please refer to Table 5 below.

Gene list	Range of log2 values (up-regulated)	Range of log2 values (down-regulated)	No. max up-regulated genes, in log2 (fold)	No. max down-regulated genes, in log2 (fold)	Overlapping highly up-regulated genes (log2 ≥ 1) / all up-regulated overlapping	Overlapping highly down-regulated genes (log2 ≥ 1) / all down-regulated overlapping
10 h	3.2 - 0.006	5.7 - 0.005	16	19	6 / 10	3 / 15
16 h	3.6 - 0.00003	1.9 - 0.002	11	6		

Table 5. Comparison of an extent of up- and down-regulation in 10 versus 16 hpi. Overlapping (or common) genes are the genes found in both 10 h and 16 h data sets.

Nearly 70% of the genes are located at the end of the available contigs, meaning the majority of the gene models is probably incomplete (the *P. berghei* genome is not finished). Assigning available annotations (GeneDB) revealed that most of the genes are hypothetical (71%) which is more than the proportion of such genes in the whole annotated genome (55%). Out of the 188 genes 11 are annotated as *Pb-fam* or *bir* genes, though it is noteworthy that in the unfiltered DE gene list (1814 genes) there are 35 and 38 annotated *bir* and *Pb-fam* genes, respectively. Approximately one third of the genes contain either a predicted transmembrane domain (TM), signal peptide (SP) or a PEXEL motif, based on *P. falciparum* orthologoues data on PlasmoDB. This is consistent with the representation of genes with the same features within the whole genome (~30%). However, it is important to note that the *P. berghei* subtelomeric regions are underrepresented on the RMSANGER microarray. Therefore it is highly probable that the number of genes with SP, TM or PEXEL – features characteristic of multigene families' antigens, is in fact greater than that obtained from this analysis and the proportion of the total number of similar genes therefore, increased. For a list of DE genes please refer to the table below (only the 10 hpi list is shown).

Upregulated genes (10 hours post infection)

P. berghei	Annotation (PlasmoDB)	*P. falciparum* orthologues
PB102175.00.0	hypothetical protein	MAL13P1.119
PB300398.00.0	hypothetical protein	PFL1620w
PB102883.00.0	hypothetical protein	#N/A
PB301516.00.0	Pb-fam-2 protein	#N/A
PB403124.00.0	Pb-fam-1 protein	#N/A
PB102109.00.0	hypothetical protein	#N/A
PB106629.00.0	hypothetical protein	#N/A
PB300917.00.0	Pb-fam-2 protein	#N/A
PB106656.00.0	hypothetical protein	#N/A
PB400242.00.0	hypothetical protein	#N/A
PB401981.00.0	hypothetical protein	#N/A
PB000546.00.0	conserved hypothetical protein	PFE0425w
PB103192.00.0	hypothetical protein	PFNF54_MIT0002
PB107954.00.0	hypothetical protein	#N/A
PB301055.00.0	hypothetical protein	#N/A
PB301082.00.0	hypothetical protein	#N/A
PB402667.00.0	hypothetical protein	PFE0465c
PB404919.00.0	hypothetical protein	#N/A
PB402195.00.0	hypothetical protein	#N/A
PB402574.00.0	hypothetical protein	#N/A
PB301411.00.0	hypothetical protein	PFC0570c
PB300277.00.0	hypothetical protein	#N/A
PB401936.00.0	hypothetical protein	#N/A
PB404513.00.0	hypothetical protein	#N/A
PB001176.01.0	conserved hypothetical protein	MAL6P1.229
PB000196.00.0	hypothetical protein	#N/A
PB200019.00.0	BIR protein, pseudogene, putative	#N/A
PB102832.00.0	hypothetical protein	#N/A
PB102891.00.0	hypothetical protein	#N/A
PB001087.02.0	40S ribosomal protein S15, putative	MAL13P1.92
PB405193.00.0	hypothetical protein	#N/A
PB000756.01.0	ribosomal protein S28e, putative	PF14_0585
PB404935.00.0	hypothetical protein	#N/A
PB000465.03.0	eukaryotic initiation factor 5a, putative	PFL0210c
PB106844.00.0	hypothetical protein	#N/A
PB102237.00.0	hypothetical protein	#N/A
PB101395.00.0	hypothetical protein	#N/A
PB000169.03.0	60S ribosomal subunit protein L18, putative	PF13_0224
PB402440.00.0	hypothetical protein	#N/A
PB104758.00.0	hypothetical protein	#N/A
PB104184.00.0	BIR	#N/A
PB401263.00.0	hypothetical protein	#N/A
PB001001.03.0	ribosomal protein L21e, putative	PF14_0240
PB001110.01.0	60S ribosomal protein L12, putative	PFE0850c
PB106580.00.0	hypothetical protein	#N/A
PB300961.00.0	hypothetical protein	#N/A
PB000915.02.0	40S ribosomal protein S5, putative	PF07_0088
PB001107.01.0	60S ribosomal subunit protein L8, putative	PFE0845c
PB000099.01.0	small nuclear ribonucleoprotein, putative	PFB0865w
PB000338.03.0	hypothetical protein	#N/A
PB001643.02.0	40S ribosomal protein S3A, putative	PFC1020c
PB108171.00.0	hypothetical protein	#N/A
PB108194.00.0	hypothetical protein	#N/A
PB107945.00.0	hypothetical protein	#N/A
PB000391.01.0	ribosomal phosphoprotein P0, putative	PF11_0313
PB000862.03.0	RNA binding protein, putative	PF13_0315
PB001303.00.0	hypoxanthine phosphoribosyltransferase, putative	PF10_0121
PB000822.02.0	ribosomal protein S3, putative	PF14_0627
PB000761.03.0	ribosomal protein L10, putative	PF14_0141
PB001195.02.0	ribosomal protein L6 homologue, putative	PF13_0129
PB000967.01.0	60S ribosomal protein L27a, putative	MAL6P1.244
PB000913.01.0	histamine-releasing factor, putative	PFE0545c
PB000840.00.0	conserved hypothetical protein	MAL8P1.95
PB108030.00.0	conserved hypothetical protein	#N/A
PB000733.01.0	10 kd chaperonin, putative	#N/A
PB402485.00.0	hypothetical protein	#N/A
PB000730.02.0	conserved hypothetical protein	PF14_0344
PB105278.00.0	BIR	#N/A
PB105908.00.0	hypothetical protein	#N/A
PB406027.00.0	hypothetical protein	#N/A
PB000360.03.0	ribosomal protein L13, putative	PF10_0043
PB403330.00.0	hypothetical protein	#N/A
PB105079.00.0	hypothetical protein	#N/A
PB000817.02.0	heat shock 70 kDa protein, putative	PF08_0054
PB103091.00.0	hypothetical protein	#N/A
PB108762.00.0	conserved hypothetical protein	PFE1190c

Downregulated genes (10 hours post infection)

P. berghei	Annotation (PlasmoDB)	*P. falciparum* orthologues
PB000626.02.0	ubiquinol-cytochrome c reductase hinge protein, putative	PF14_0248
PB001603.02.0	conserved hypothetical protein	PF08_0057
PB300904.00.0	hypothetical protein	#N/A
PB500031.00.0	BIR protein, putative	#N/A
PB403064.00.0	Pb-fam-1 protein	#N/A
PB001603.02.0	conserved hypothetical protein	PF08_0057
PB107675.00.0	hypothetical protein	#N/A
PB403217.00.0	hypothetical protein	#N/A
PB000056.02.0	conserved hypothetical protein	#N/A
PB404871.00.0	hypothetical protein	#N/A
PB405136.00.0	hypothetical protein	#N/A
PB000910.00.0	50S ribosomal subunit protein L14, putative	PFE0960w
PB000164.02.0	tubulin beta chain, putative	PF10_0084
PB000593.02.0	mitochondrial import inner membrane translocase subunit tim17, putative	PF14_0328
PB300700.00.0	flavoprotein subunit of succinate dehydrogenase, putative	#N/A
PB300235.00.0	ubiquitin--protein ligase, putative	PFC0845c
PB106367.00.0	conserved hypothetical protein	#N/A
PB000776.02.0	conserved hypothetical protein	PF14_0375
PB108445.00.1	conserved hypothetical protein	#N/A
PB106399.00.0	hypothetical protein	#N/A
PB401324.00.0	hypothetical protein	#N/A
PB401804.00.0	hypothetical protein	#N/A
PB301058.00.0	hypothetical protein	#N/A
PB402607.00.0	hypothetical protein	#N/A
PB001136.00.0	ATP synthase gamma chain, mitochondrial precursor, putative	PF13_0061
PB000896.02.0	ATP synthase beta chain, mitochondrial precursor, putative	MAL12P1.343
PB402011.00.0	hypothetical protein	#N/A
PB405136.00.0	hypothetical protein	#N/A
PB300252.00.0	hypothetical protein	#N/A
PB300299.00.0	hypothetical protein	#N/A
PB400070.00.0	hypothetical protein	#N/A
PB102740.00.0	hypothetical protein	#N/A
PB104012.00.0	hypothetical protein	#N/A
PB108423.00.0	hypothetical protein	#N/A
PB301075.00.0	hypothetical protein	PFL0545w?
PB301228.00.0	hypothetical protein	#N/A
PB000605.01.0	hypothetical protein	PFF0860c
PB405813.00.0	hypothetical protein	#N/A
PB105110.00.0	hypothetical protein	#N/A
PB103133.00.0	hypothetical protein	#N/A
PB103170.00.0	hypothetical protein	#N/A
PB300291.00.0	hypothetical protein	#N/A
PB106763.00.0	hypothetical protein	#N/A
PB301528.00.0	hypothetical protein	PFL0385c
PB103118.00.0	hypothetical protein	PFI0180w
PB300694.00.0	hypothetical protein	#N/A
PB107905.00.0	hypothetical protein	#N/A
PB301347.00.0	hypothetical protein	#N/A
PB301140.00.0	hypothetical protein	#N/A
PB000609.00.0	hypothetical protein	PFD1050w
PB105837.00.0	hypothetical protein	#N/A
PB400059.00.0	hypothetical protein	#N/A
PB200050.00.0	BIR protein, putative	#N/A
PB107616.00.0	hypothetical protein	PF13_0196
PB301063.00.0	hypothetical protein	#N/A
PB301219.00.0	actin, putative	PFL2215w?
PB402163.00.0	hypothetical protein	#N/A
PB105315.00.0	Pb-fam-1 protein	#N/A
PB000918.03.0	conserved hypothetical protein	MAL13P1.228
PB300735.00.0	hypothetical protein	#N/A
PB108816.00.0	Pb-fam-3 protein	#N/A
PB405908.00.0	hypothetical protein	#N/A
PB000633.00.0	conserved hypothetical protein	PF14_0522
PB105992.00.0	hypothetical protein	#N/A
PB102632.00.0	hypothetical protein	#N/A
PB301219.00.0	actin, putative	#N/A

Legend

- upregulated at least 2 fold
- downregulated at least 2 fold
- manual orthologue (BLAST)

PB401398.00.0	hypothetical protein	#N/A
PB402289.00.0	hypothetical protein	#N/A
PB105055.00.0	hypothetical protein	#N/A
PB300506.00.0	hypothetical protein	#N/A
PB000541.02.0	60S ribosomal subunit protein L4/L1, putative	PFE0350c
PB001110.01.0	60S ribosomal protein L12, putative	PFE0850c
PB301308.00.0	hypothetical protein	#N/A
PB000194.03.0	60S ribosomal protein L24, putative	PF13_0049
PB001284.02.0	Nucleosome assembly protein, putative	PFI0930c
PB104051.00.0	hypothetical protein	#N/A
PB401968.00.0	hypothetical protein	#N/A
PB000920.03.0	ribosomal protein S4, putative	PF11_0065
PB000242.02.0	guanine nucleotide-binding protein, putative	PF08_0019
PB106784.00.0	hypothetical protein	#N/A
PB000856.03.0	conserved hypothetical protein	PF11_0174
PB102502.00.0	hypothetical protein	#N/A
PB102747.00.0	hypothetical protein	#N/A
PB001195.02.0	ribosomal protein L6 homologue, putative	PF13_0129
PB001532.02.0	hypothetical protein	PF07_0029
PB107784.00.0	hypothetical protein	#N/A
PB102416.00.0	hypothetical protein	#N/A
PB100934.00.0	hypothetical protein	#N/A
PB001129.00.0	conserved hypothetical protein	PF08_0115
PB000893.01.0	fibrillarin, putative	PF14_0068
PB300193.00.0	hypothetical protein	#N/A
PB104533.00.0	hypothetical protein	#N/A
PB102177.00.0	hypothetical protein	#N/A
PB404817.00.0	hypothetical protein	#N/A
PB001312.02.0	conserved hypothetical protein	PF14_0510
PB000178.02.0	40S ribosomal subunit protein S14, putative	PFE0810c
PB000767.01.0	conserved hypothetical protein	PF11_0502
PB104593.00.0	hypothetical protein	#N/A
PB000652.02.0	hsp70 interacting protein, putative	PFE1370w
PB404868.00.0	hypothetical protein	#N/A
PB100173.00.0	hypothetical protein	#N/A
PB104409.00.0	hypothetical protein	#N/A
PB000275.02.0	60S Ribosomal protein L36, putative	PF11_0106
PB000748.02.0	conserved hypothetical protein	PFC0262c
PB108471.00.0	hypothetical protein	#N/A
PB401903.00.0	hypothetical protein	#N/A
PB102420.00.0	hypothetical protein	#N/A
PB000829.01.0	conserved hypothetical protein	PF11_0494
PB401830.00.0	hypothetical protein	#N/A
PB001100.02.0	structure specific recognition protein, putative	PF14_0393
PB301270.00.0	hypothetical protein	#N/A
PB001018.00.0	histone h3, putative	PF13_0185

Table 6. Differentially expressed genes in the 1184 *Pbsir2a/Pbsir2b*$^{-/-}$ at 10 hours post infection. On the left the up-regulated genes are listed, whereas on the right the down-regulated. The most up- and down-regulated genes are highlighted in red and blue, respectively. The *P. falciparum* orthologues were found automatically through GeneDB, or some were assigned manually (highlighted in yellow) using BLAST algorithm.

Unexpectedly the list comprises a number of ribosomal proteins (n=24), majority of which are up-regulated (n=22) and the remaining ones only slightly down-regulated. In yeast *Saccharomyces cerevisiae* SIR2 silences ribosomal DNA genes, but not ribosomal proteins (Smith and Boeke, 1997; for a review see Blander and Guarente, 2004). Furthermore the differentially regulated genes include some (n=4) with a predicted mitochondrion-targeting sequence, which is an over-representation of these genes (~3%) compared with the whole genome (0.8%).

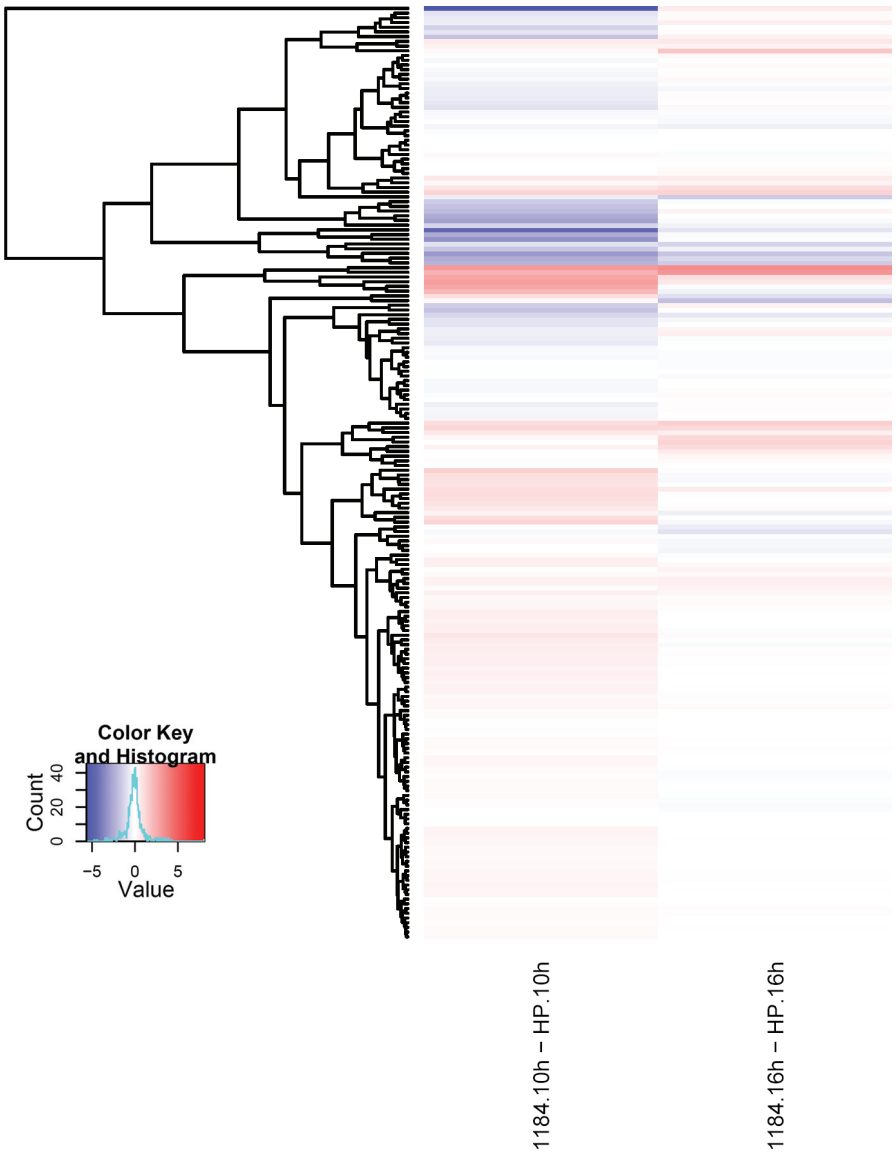

Fig. 43 The heatmap representation of 188 differentially expressed genes, based on Euclidean distance clustering. As it is a KO-WT (1184-HP) comparison, red colour indicates genes that are over-expressed in the 1184 parasites, whereas blue shows down-regulated genes. Each raw represents one gene, and each column one time point (10 hpi and 16 hpi).

A tentative analysis of the obtained gene list showed that the unannotated genes that are most highly up- and down-regulated appear either rodent-specific or show some similarity to various antigen genes annotated in other *Plasmodium* species, including *clag, Pv-fam-g,* an orthologue to *P. yoelii* latency associated antigen-related (at the current stage of analysis at least 15%). As already mentioned, the analysis of the *P. berghei* genes is hampered by the incomplete *P. berghei* genome data, and therefore both limited and time-consuming.

In order to confirm these data and to obtain a complete view of the expression changes in the 1184 m1 cl1 mutants versus the wild type parasites in the asexual blood stages further collection of the time points was performed. The RNA samples regarded to be relevant for the phenotype analysis were obtained from parasites pellets collected at four consecutive time points in four replicates per time

point per parasite line/clone – wild type high producer (HP) ANKA strain and 1184 *Pbsir2a/Pbsir2b* double mutant parasites. The summary of the samples is shown in the table below.

Sample type	No. of replicates	Time point
1184 HP	4 4	5 hpi (ring)
1184 HP	4 4	10 hpi (late ring/early troph)
1184 HP	4 4	16 hpi (late troph)
1184 HP	4 4	22 hpi (schizont)

Table 7. Samples collected for an extended second microarray analysis.

The microarrays were performed at WTSI (Dr. Celine Carret, Dr. Arnab Pain) and Nanyang Technological University (Dr. Peter Preiser, Dr. Zbynek Bozdech) on a collaborative basis. Importantly, the collaborators operate different microarray systems since the NTU arrays consist of glass slides upon which are mounted long oligonucleotides (50-70nt; described below) compared with the shorter oligonucleotide (25-mer) format of Affymetrix arrays available at WTSI. The consistency of the data from the two systems was monitored.

4) The long oligo DNA microarray

The long oligonucleotide DNA microarrays are designed using a different algorithm to the one utilised for the RMSANGER array, taking advantage of similarities between the *P. berghei*, *P. chabaudi* and *P. yoelii* genomes enabling for "complementation" of the missing genes in a particular rodent genome analysed from the remaining genomes (at the same time excluding false-positives). The array probes were designed based on PlasmoDB v4.4 (released in 2005) and despite the usage of the three genomes low coverage is still problematic. An overview of all the genes affected either in one or more asexual parasite stages is shown in Fig. 44.

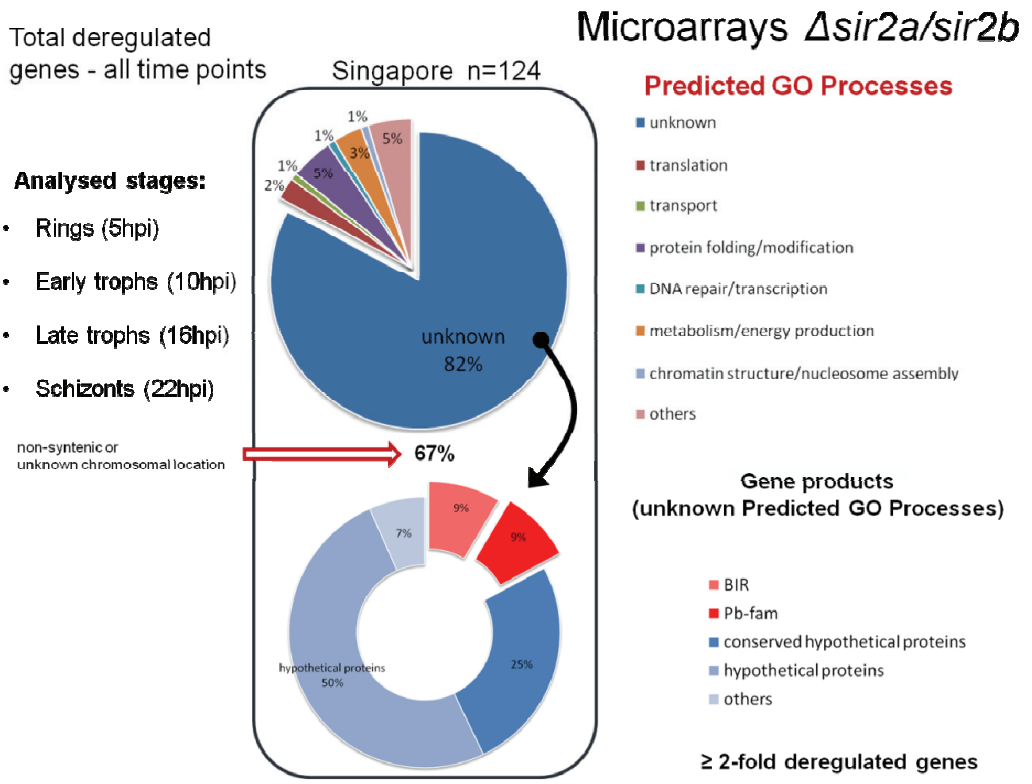

Fig. 44 Total number of 124 genes deregulated solely in the long oligo DNA array (Singapore) in either one or more asexual parasite stages. Of the genes assigned to the "unknown GO process" category almost 20% is contributed by *bir* and *Pb-fam* multigene family members; the remaining 80% are mostly hypothetical genes. Small percentages of the 124 genes belong to translation/transcription, protein folding or metabolism-related GO processes.

5) Summary of the differentially expressed genes – Sanger vs. Singapore

To our disappointment the 2FC gene sets deregulated in the *Pb Δsir2a/Δsir2b* vs. wild-type obtained from the Sanger and Singapore microarray analysis differ substantially. Of the Sanger 2FC set (n=624) and Singapore 2FC set (n=124) there are only 10 genes common to both sets.

Classification of genes into Predicted GO Process showed that most of the genes in both data sets are not assigned to any process (94% for Sanger; 82% Singapore); of these genes 96% and 67% are non-syntenic or of unknown chromosomal location for Sanger and Singapore arrays respectively. Within the unknown Predicted GO Process genes most gene products are described as hypothetical or conserved hypothetical. Interestingly BIR and Pb-fam gene products are present in both sets, with more members represented in the Singapore array analysis than that of Sanger. Rodent species share high similarity between the *pir* family member (*P.yoelii yirs, P. chabaudi cirs, P. berghei birs*). One reason for greater representation of multigene family members on the Singapore chip might be a difference in the analysis of the array hybridisation results (based on all three rodent genomes in case), and might indeed indicate true changes in gene expression that would otherwise be overlooked using the Sanger array only. The global difference in the results might also stem from the differences in material preparation, such as reverse transcription and amplification procedure, chip hybridisation conditions and detection limits.

Number of genes at least 2 fold deregulated

	5h	10h	16h	22h	Total (with common entries)	Common	Total unique genes affected
Sanger	601	46	2	0	649	25	624
Singapore	96	63	65	16	240	116	124

Sanger	5h	10h	16h	22h
Max upregulation (fold change)	29.5	3.8	2.7	-
Min upregulation (fold change)	18.2	13.8	-	1.8

Singapore	5h	10h	16h	22h
Max upregulation (fold change)	5.1	2.8	4.2	3.1
Min upregulation (fold change)	7.4	8.1	7.6	6.8

Table 8. A summary of genes at least 2 fold deregulated in the Sanger and Singapore data sets. In total 649 and 240 genes are changed at least 2 fold according to Sanger and Singapore microarray sets, respectively. A 2FC genes shown here can be deregulated at any given time point (either 5h, 10h, 16h or 22h, or more than 1 time point). The biggest changes from both Sanger and Singapore microarrays are observed in rings, whereas least transcriptional changes occur at 22 hpi (schizonts) in both data sets. The "Common" column refers to the number of genes deregulated in one type of array which were also significantly deregulated in the other array (so e.g. only 25/649 DE genes on the Sanger array were found also deregulated in the Singapore array). The biggest up- and down-regulation for all time points found in both Sanger and Singapore arrays are shown in the 2 smaller tables.

III.6 Analysis of the effect of absence of PBSIR2A and PBSIR2B in sexual stages of *Plasmodium berghei*.

III.6.1 Mosquito passage of the *Pbsir2* mutants.

The effects of SIR2 protein absence has to date been extensively studied only in erythrocytic stages of *P. falciparum* (Freitas et al., 2005; Duraisingh et al., 2005; Tonkin et al., 2009) and *P. berghei* (this thesis). However, the two SIR2 genes are transcribed in all asexual blood stages, gametocytes, and sporozoites, according to *P. falciparum* expression data from PlasmoDB (see Fig. 45) and PbSIR2A::GFP expression analysis confirms this.

The ability of the different *Δsir2* parasite lines to undergo sexual development in the mosquito and complete the life cycle was assessed by passage of the parasites through *Anopheles* mosquito host and subsequent establishment of blood stage infection in naïve mice through mosquito bites.

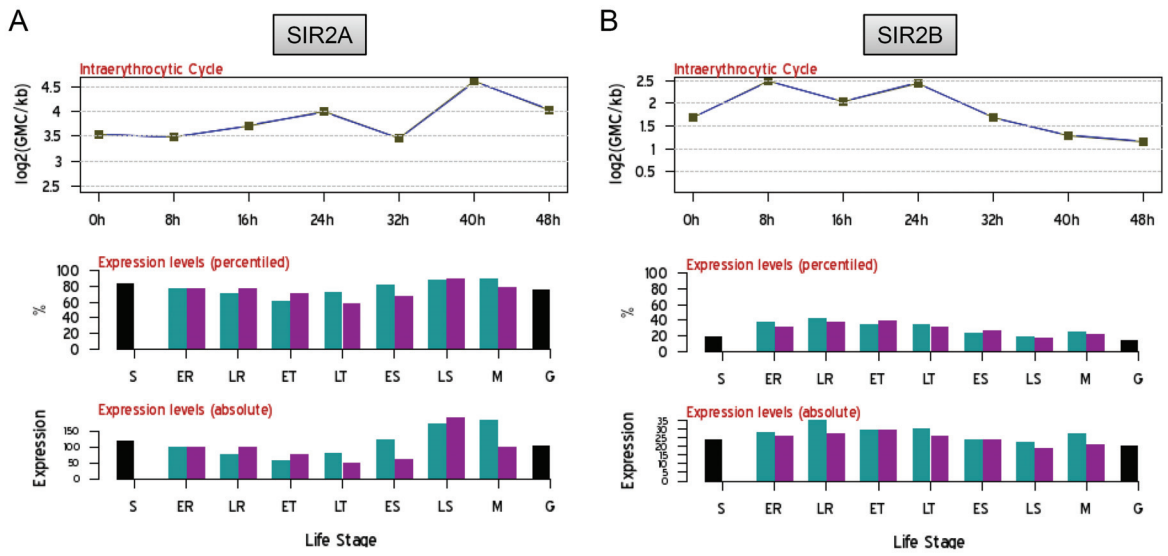

Fig.45 ***P. falciparum*** **expression data deposited on PlasmoDB** (www.plasmodb.org). A, B top graph represents *P.falciparum* RNA sequence profiles at intraerythrocytic cycle, GMC/kb = geometric mean of coverage / kb of unique sequence. A, B bottom graphs show expression levels (percentiled and absolute) at S = sporozoites, ER = early rings, LR = Late Rings, ET = Early Trophs, LT = Late Trophs, ES = Early Schizonts, LS = Late Schizonts, M = Merozoites, G = Gametocytes. Colour codes: teal = sorbitol schynchronisation, purple – temperature synchronisation. Please note different scales of absolute expression levels for SIR2A and SIR2B profiles. PlasmoDB IDs for SIR2A: PF13_0152; SIR2B: PF14_0489.

The HP and *sir2b*-deficient parasites (1079 cl1m4cl1) have successfully completed the life cycle establishing a blood stage infection in naïve mice, with patent parasitaemia at day 4-5, whereas *sir2a* single and double mutants (1022 cl2 and 1184 m1cl1, respectively) failed to produce asexual parasites (monitored at microscopy-detectable levels in Giemsa-stained blood smears). The transmission experiments were repeated three times (C. Janse's laboratory, Leiden University Medical Centre; R. Sauerwein's laboratory, Nijmegen Center for Molecular Life Sciences; O. Billker's laboratory, The Wellcome Trust Sanger Institute) with the same result. These findings triggered us to perform a more detailed analysis of the *sir2a*-deficient lines during sporogonic development.

III.6.2 *sir2a*$^{-}$ and *sir2a/b*$^{-/-}$ ookinetes arrest at an ookinete-to-oocyst stage.

The unexpected transmission blockage of the *sir2a*$^{-}$ and *sir2a/b*$^{-/-}$ clones prompted us to pinpoint the arrest stage of these parasites. We first decided to analyse ookinete production *in vitro* by an established method of *in vitro* culture of *P. berghei* ookinetes (Janse et al.,1985). In short, infected mouse blood was added to the exflagellation/ookinete medium (pH = 8.0, temp. 20-21˚C) and incubated overnight at 20-21˚C (see Materials and Methods for detailed protocol). Four lines were analysed simultaneously – two *Δsir2a* deficient clones (1022 cl2 and 1184 m1cl1), *sir2a::gfp* (503 cl1) and HP (wild-type) (Fig. 46, top left graph). Ookinete conversion rates of all four lines were similar to that of a typical wild type, which is normally between 50 and 90%.

Having confirmed normal ookinete production rates for the *sir2a*-deficient parasites oocyst development was assessed *in vivo*. Mosquito infections were repeated for the following parasites lines:

- two *Δsir2a* deficient clones (1022 cl2 and 1184 m1cl1)
- *sir2a::gfp* (503 cl1)
- HP (wild-type)
- *Δsir2b* (containing the positive/negative selectable marker cassette *Tgdhfr-ts::fcu*)
- *Δsir2b* (positive/negative selectable marker removed)

The *sir2b*-deficient lines were included in the analysis firstly to determine any non-critical changes, which could be occurring at sexual stages of parasite development in the absence of SIR2B. A single *P. berghei* oocyst produces on average 8000 sporozoites (*Anopheles stepensi* infection, Sinden 1997), a number sufficient for successful mosquito salivary gland invasion and subsequent establishment of an infection in a mammalian host. Hence major deficiencies could be overlooked at this parasite stage if transmission is analysed in a qualitative manner. Furthermore, parasite manipulation such as a selection procedure for selectable marker cassette removal could be a reason for undefined genetic and/or phenotypic changes. These changes could in turn possibly result in the observed failure of *sir2a/b*$^{-/-}$ deficient parasites to be transmitted.

In vivo oocyst counts for the 6 analysed lines are shown in Fig 46 (top right panel). For each line 15 – 20 mosquito midguts were dissected and oocysts were counted using light microscopy and/or fluorescence microscopy. The experiment was performed twice. *Δsir2b*, *sir2a::gfp* and wild-type parasites produced standard oocyst numbers (typical count for HP line ranges between ~100 – 350 oocysts). Oocyst production was completely abolished in *Δsir2a* and *Δsir2a/b* lines (1022 cl2 and 1184 m1cl1). The deficiency appeared to occur at an ookinete-to-oocyst stage since no young oocysts were observed in the two *sir2a* k.o. lines.

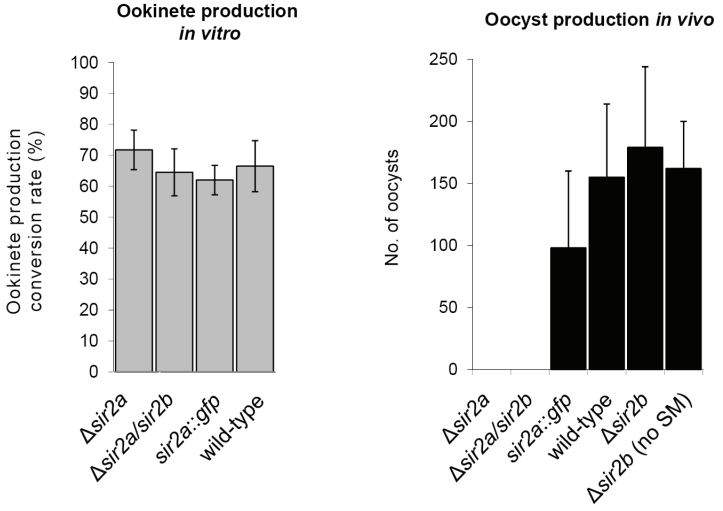

Fig. 46 Ookinete and oocyst production in *sir2*-modified lines. Ookinete conversion rate *in vitro* (graph on the left), expressed as a percentage of female gametes which develop into ookinetes, was determined for *Δsir2a*, *Δsir2a/b*, *sir2a::gfp* and wild type (*P. berghei* ANKA strain HP GFP_{con}). Ookinete production was in the typical wild type range (50-90%) for all analysed lines. Oocyst production *in vivo* (graph on the right) was unaffected in the *sir2a::gfp*, wild-type, *Δsir2b* and *Δsir2b* (selectable marker cassette removed) but was completely abolished in the *sir2a* single- and double- deletion mutants.

III.6.3 *sir2a*$^{-}$ and *sir2a/b*$^{-/-}$ ookinetes are not able to cross the mosquito midgut epithelium

In order to analyse the ability of *sir2a*-deficient parasites to penetrate the mosquito midgut epithelium *Anopheles* mosquitoes (approx. 50 per cage) were fed on mice infected with the following three parasite lines:

- wild type GFP_{con} (507 cl1)
- *sir2a*/*b* double k.o. (1184 m1cl1)
- *sir2a* single k.o.(1022 cl2)

Since all three parasite lines express GFP constitutively the presence of ookinetes in the midguts was assessed using fluorescence stereomicroscope (Leica), following whole midgut dissection at day 1 and 2 post-feeding (between 10 and 15 midguts/line). We observed a number of ookinetes in the blood meal of mosquitoes fed on all three lines-infected mice (see Fig. 47, 507 cl1 (C) and 1184 m1cl1 & 1022 cl2 (B)). At day 1 post-feeding several parasites were visible on top of dissected midguts of 507 cl1-fed mosquitoes. At day 2 we could observe a number of parasites, which had passed the midgut epithelium barrier, some of which started developing into young oocysts (507 cl1 (A & B)). No ookinetes could be detected on the midguts of 1022 cl2 and 1184 m1cl1-infected mosquitoes at day 1 and 2 post-feeding (1184 m1cl1 (A) & images 1-4; 1022 cl2 (A)). Interestingly, we could visualise parasites inside the same midguts thereby confirming the presence of live parasite forms in the blood meal (concluded to be ookinetes on morphological considerations; indicated by arrows on 1184 m1cl1 (A)).

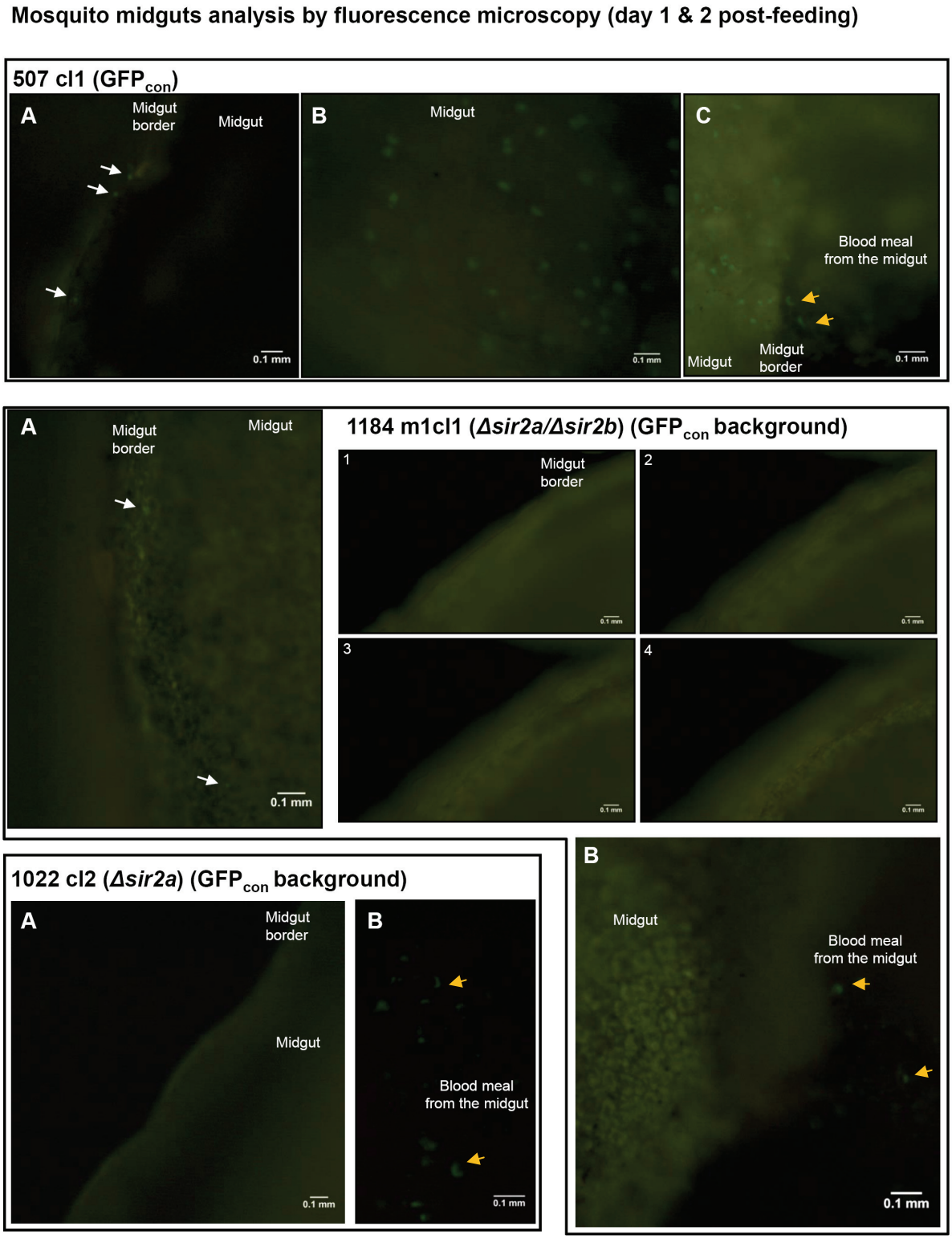

Fig. 47 Mosquito midgut analysis by fluorescence stereomicroscopy. Mosquito midguts infected with 507 cl1 (GFP_{con}), 1184 m1cl1 (*Δsir2a/b*) and 1022 cl2 (*Δsir2a*) were dissected at day 1 and 2 post-feeding and analysed for presence of developing parasites. 507 cl1: (A). A midgut side-view. Arrows indicate ookinete/young oocysts, which crossed the midgut epithelium and are seemingly located under the basal lamina. (B) top-view of the midgut; multiple green forms present. (C) blood meal from the midgut containing a number of green-fluorescent parasites (ookinetes and round forms). 1184 m1cl1: (A) side-view on a midgut. (1-4) consequent focal planes, no parasites were detected under the basal lamina. (B) blood meal from the same midgut, containing a number of ookinetes and round forms. 1022 cl2: (A) side-view of a midgut indicating that no parasites have crossed the midgut epithelium. (B) blood meal from the same midgut with parasites visible. Mosquito structures autofluoresce.

The observations from fluorescence stereomicroscopy were confirmed by determining the ratios of blood meal zygotes/ookinetes and epithelium ookinetes/oocyts in mosquitoes that were allowed to feed on infected mice. 48- and 72-hours after direct feeds on mice infected with wild type (GFP_{con}) and SIR2A-null parasites mosquito midguts were dissected and the blood meal washed away. Blood meal zygotes and ookinetes were counted in a haemocytomer following staining with an anti-Pbs25-cy3-conjugated antibody. Epithelium ookinete and oocyst numbers were detected using the same Pbs25 antibody (red) and green-fluorescence of GFP_{con} parasites. Blood meal zygote and ookinete numbers were comparable between the wild type and *Δsir2a* line, at an average of 2200 and 2580 ookinetes/midgut for wild type and the mutant, respectively (Fig. 48A). However epithelium-associated ookinetes and oocyst numbers were drastically reduced in the *sir2a* k.o. compared to wild type at day 2 (8.7/0.8 and 49/247.5 ookinetes/occysts per midgut for *Δsir2a* and WT, respectively). At day 3 oocysts were microscopically undetectable in the *sir2a*$^-$ line (1.7/0 and 17/409 ookinetes/oocysts for *sir2a*$^-$ and WT) (Fig 48B). It is important to point out that oocysts were counted as round forms emitting light in the expected emission wavelength range (GFP filter). However, at detection threshold levels one cannot be certain that the round forms are indeed oocysts associated with epithelium and not structures intrinsic to the mosquito epithelium itself. Furthermore, despite extensive washing of the midguts residual blood meal parasites might have been observed and mistakenly counted as epithelium-derived. Nevertheless, the differences between wt and mutant parasites seem clear.

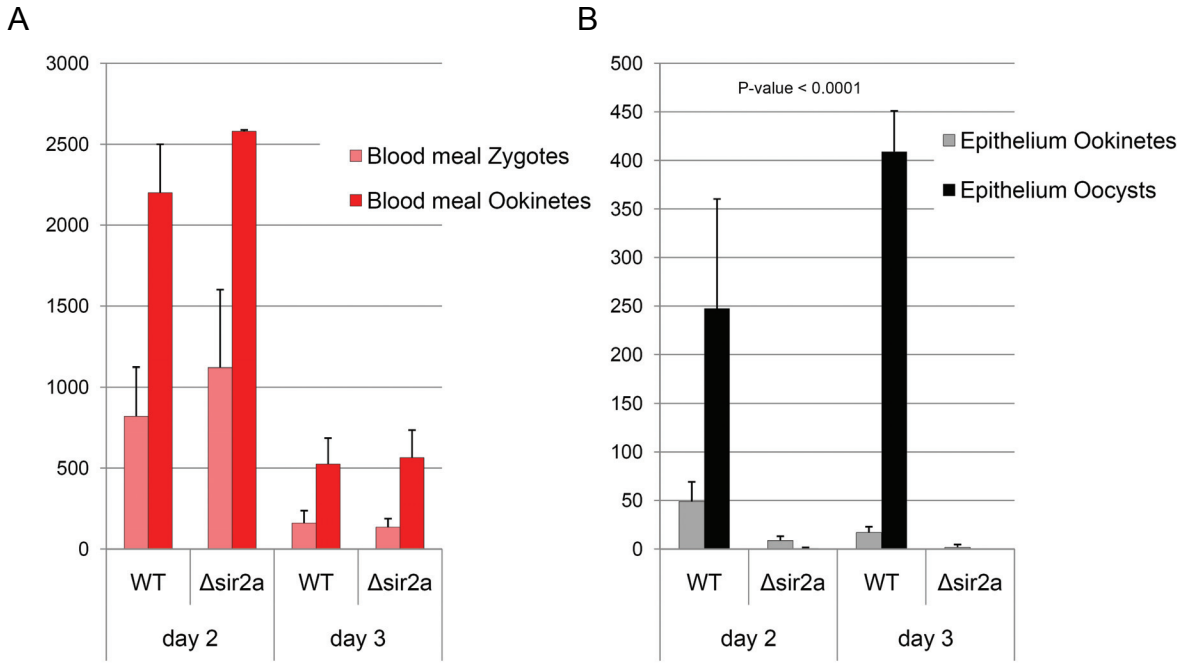

Fig.48 Blood meal and epithelium wild type and *Δsir2a* parasite numbers in *Anopheles* midguts. Mosquitoes fed on wt and *Δsir2a*-infected mice were dissected at day 2 and day 3 post-feeding. A. Blood meal of the dissected midguts was extracted and zygotes and ookinetes quantified using fluorescence detection of anti-Pbs25-cy3 antibody. Similar parasite numbers were obtained for both lines. B. Following blood meal removal and wash midgut epithelium ookinetes and oocysts were detected taking advantage of green fluorescence of the parasites. At day 2 oocysts could already be identified on wt-infected epithelium and possible several oocysts were observed in *Δsir2a*. At day 3 no oocysts were found associated with epithelium, whereas on average 400 oocysts were counted for the wild type line. Both graphs represent an average number of parasites/midgut with standard deviation as error bars.

III.6.3.1 *Δsir2a* parasites cannot penetrate the peritrophic membrane

In order to further define the defect of the *sir2a* mutants the ability of HP::GFP, *Δsir2a and Δsir2a/b* mutants ookinetes to invade mosquito midgut epithelium cells was tested. Mosquito midguts were dissected and processed for toluidine blue staining, which has been routinely used to assess the ability of *Plasmodium* ookinetes to invade and/or traverse mosquito midgut epithelium cells (e.g. Gupta et al., 2005; Shahabuddin and Pimenta, 1998). Damaged (invaded cells) stain heterogeneously light blue whereas intact cells stain relatively uniformly dark blue upon 1-2 minute incubation with the dye. Two methods were used to preserve the whole *Anopheles* midguts: paraffin preservation with prior fixation in 1% paraformaldehyde/2.5 % glutaraldehyde and subsequent dehydration in 20%, 50% and 70% ethanol (see Materials and methods for detailed procedures), as well as epoxy resin embedding as if for standard transmission electron microscopy. The prepared samples were sectioned using a microtome to the thickness of 5-10 μm (paraffin sections) or 0.35 to 1 μm (epoxy-embedded midguts). For the paraffin method 12 mosquito midguts were prepared for each of the three parasite lines at day 1 post-feeding on infected mice (see Fig. 49A below). Unfortunately the obtained section thickness was too high for proper assessment of the state of midgut epithelium in the prepared midguts. Nevertheless several ookinetes were observed in the midgut epithelium of HP GFP_{con} (507 cl1; orange arrows). No parasites were encountered in the epithelium of either *Δsir2a* or *Δsir2a/b* mutants (1022 cl2 and 1184 m1cl1, respectively). However, ookinetes were observed in the lumen of mosquito midguts infected with all three lines (orange arrows). Mosquito infections and midgut collection was repeated (n=20 for each line) and the collected midguts were fixed, dehydrated and processed for epoxy-resin embedding suitable for analysis by toluidine blue staining (see Fig. 49B). The resulting sectionresolution is greater than from the paraffin sections. Epithelium could be clearly discerned from the peritrophic matrix. Several objects of a size and morphology of a possible ookinete were found in the epithelium of the wild type-infected midguts but not in the *Δsir2a*-infected midguts (orange arrows on Fig. 49B). Despite improved resolution the localisation of the mutant ookinetes within the whole dissected midguts could not be determined, due to the epithelium-proximal concentrated blood meal presence. This thick layer was inefficiently penetrated by the epoxy resin used, and so a possible solution would be to remove the blood meal from the midguts by microdissection before proceeding with the embedding protocol.

Mosquito immune responses against *Plasmodium* ookinetes are deployed only after the ookinete passage through the epithelium, in the space between the epithelium cells and the basal lamina (see Introduction for details). Therefore the fact that SIR2A-deficient ookinetes were never observed in the midgut epithelium layer in either paraffin or epoxy resin-embedded midgut sections suggests they are unable to attach and/or initiate invasion of the epithelium layer of the mosquito midgut.

Another method to detect possible penetration of the midgut epithelium by wt or mutant ookinetes would be examination of an immune response which had been invoked by parasite-infected blood meals for instance by analysing TEP1 activation.

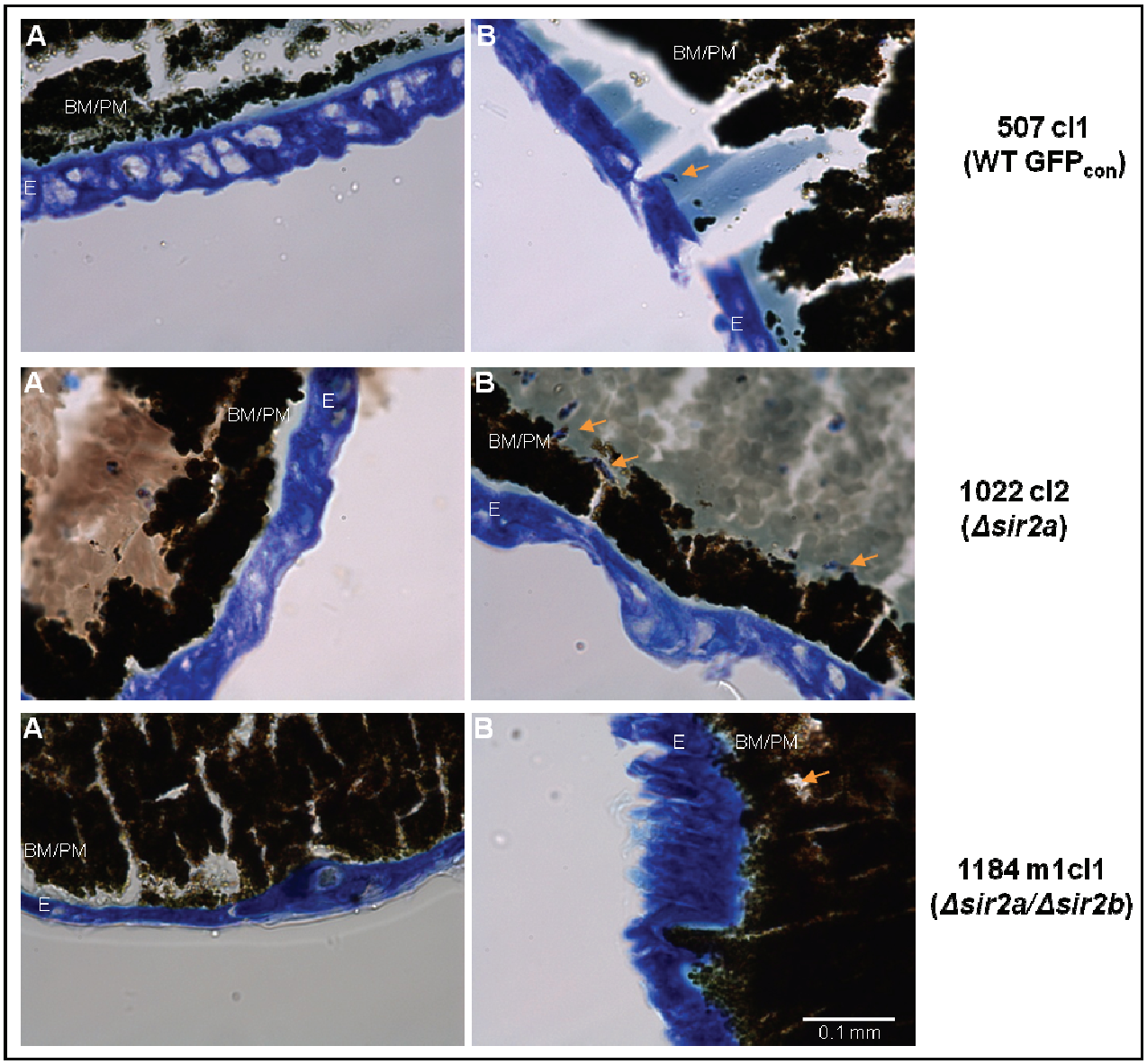

Fig. 49 Assessment of *A. stephensi* mosquito midgut invasion ability of wild type, *Δsir2a* and *Δsir2a/b* ookinetes. 507 cl1- (wt), 1022 cl2- (*sir2a*$^{-}$) and 1184 m1cl1-(*sir2a/b*$^{-/-}$)-infected paraffin (A) or epoxy resin (B) -embedded midguts, dissected at day 1 post-feeding were analysed by toludine blue staining of thick (A) and semi-thin (B) sections. **A.Top panel**: paraffin sections. A general damage to the epithelium was observed in the wild type-infected midguts in contrast to both *sir2a*- mutants-infected organs. A number of ookinetes were identified in the lumen of all parasite-infected midguts (orange arrows). However ookinetes crossing the midgut epithelium were spotted only in the wild type infections and not the mutants. Unfortunately the section thickness did not allow for single epithelium layer differentiation leaving the results suggestive but not conclusive. Scale bar indicates 0.1 mm for all images. **B.Bottom panel (below)**: epoxy resin sections showed improved resolution comparing to the paraffin sections. Indicated by orange arrows are possibly ookinetes (judging by size and morphology) crossing the epithelium layer. Damaged epithelium cells are visible in 507 cl1 (A, C). The *Δsir2a* epithelium appears relatively intact. E: epithelium, BM/PM: blood meal/peritrophic matrix. Scale bars are shown on each image.

B. Mosquito midguts – epoxy resin sections (day 1 post-feeding)

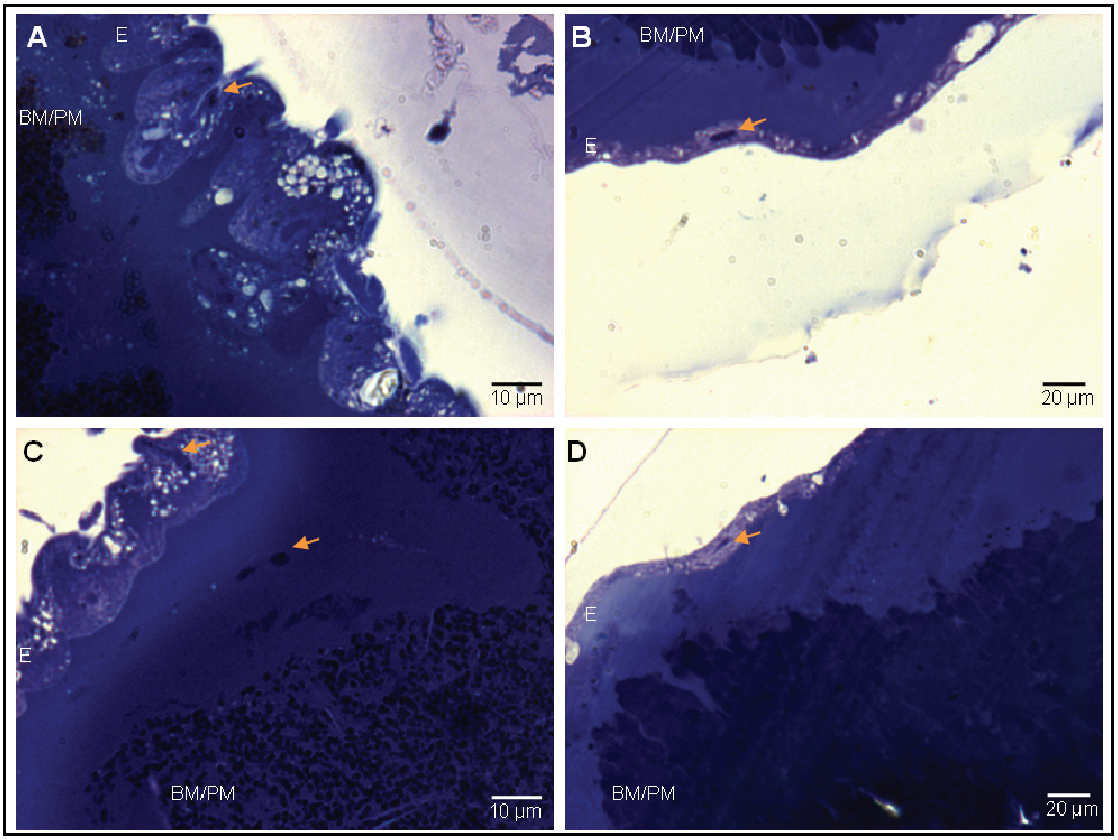

507 cl1 (WT GFP$_{con}$)

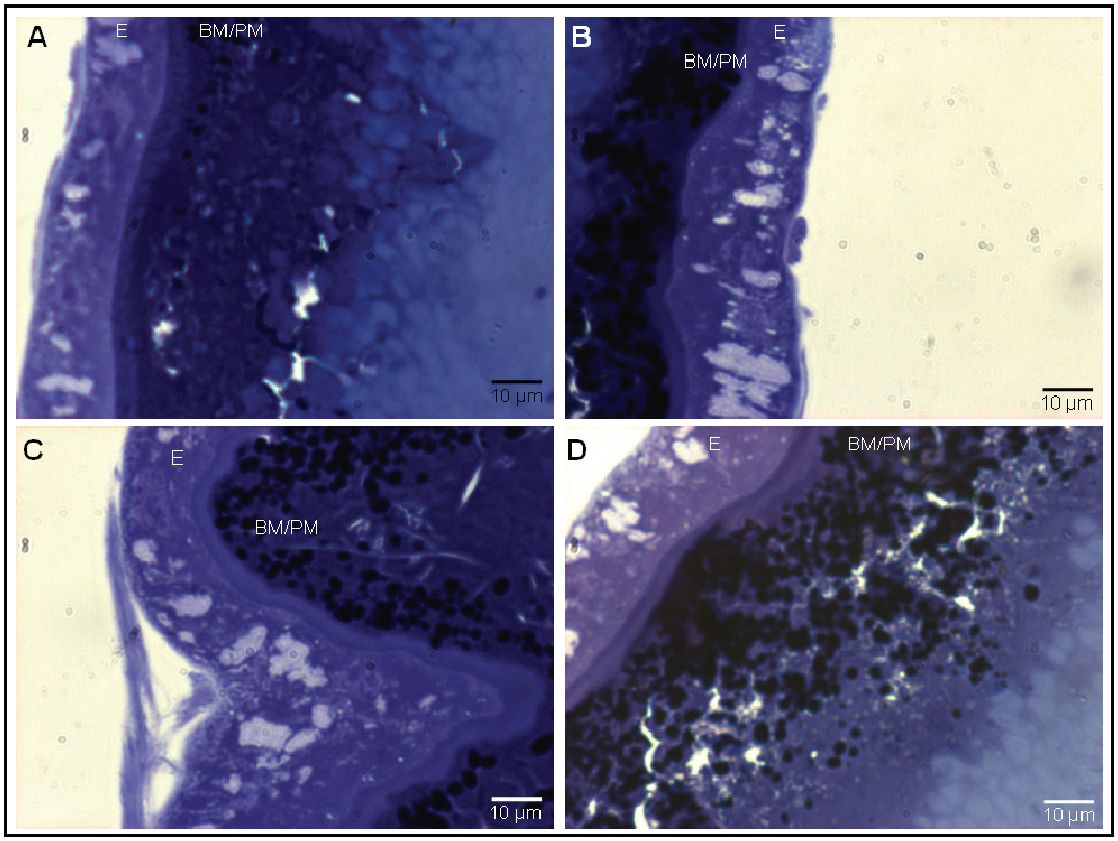

1022 cl2 (*Δsir2a*)

III.6.1 *sir2a*-deficient ookinete stage morphology

All mutant lines generated in our laboratory are standardly analysed for any morphological abnormalities by Giemsa staining of blood smears of *in vitro* cultured ookinetes. All generated *sir2s*-deletion mutant parasites exhibited wild type-like appearance with the exception of *in vitro*-cultured ookinetes of two SIR2A-deficient clones *Δsir2a* and *Δsir2a/b* respectively (1022 cl2 and 1184 m1cl1, respectively). Giemsa staining is used to differentiate nuclear and cytoplasmic morphology of parasites as it exhibits pH-dependent staining patterns. Blue/grey staining indicates alkaline pH, whereas acidic environment is designated by pink to red staining. Both *sir2a*$^{-}$ and *sir2a/b*$^{-/-}$ ookinetes showed a very consistent pale pink staining at their anterior end (Fig. 50), creating an impression of an "empty" apical end region (indicated by arrows). In comparison *sir2a::gfp* (503 cl1) ookinetes showed only a small area of pink colour at the apical end, which is typically observed in Pb ANKA HP ookinetes (Fig. 50 bottom panel). This aberrantly-stained appearance has been observed in all mutant ookinetes (note: approximately 15% of wild type ookinetes can have a morphologically similar appearance to that of the *Δsir2a* mutants).

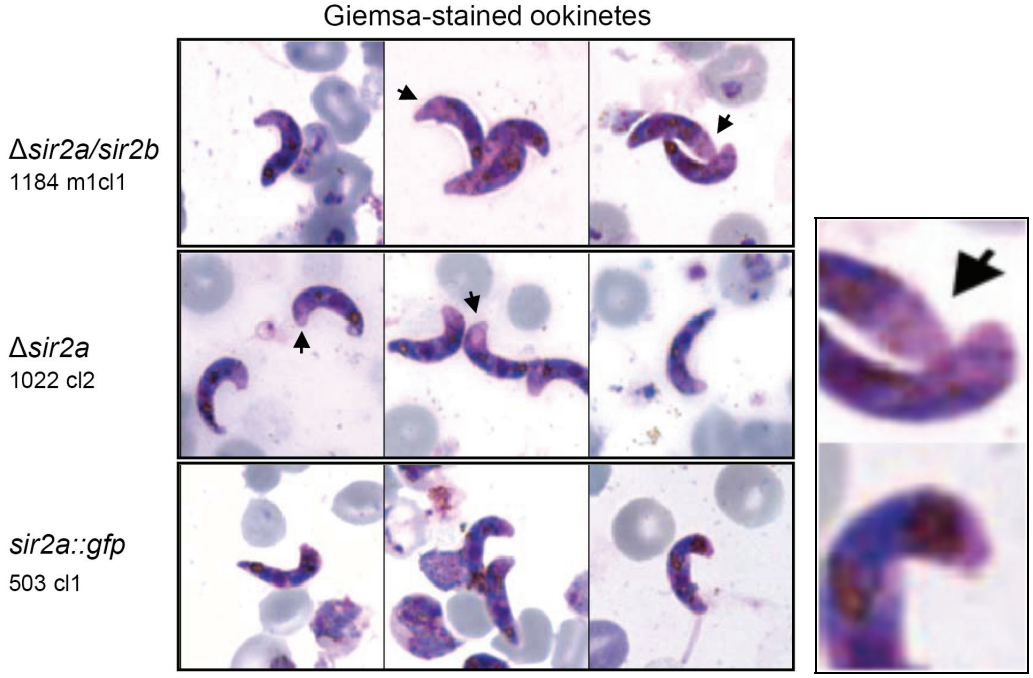

Fig.50 Giemsa-stained *in vitro* ookinetes of *Δsir2a/b*, *Δsir2a* and *sir2a::gfp* clones. Both mutants (top and middle panel) exhibit the "empty" apical end appearance (arrows), whereas *sir2a::gfp* appear morphologically indiscernible from wild type.

The intriguing apical end appearance of the SIR2A-deficient ookinetes was further analysed by transmission electron microscopy (TEM; in collaboration with Laurence Tetley, Glasgow University). *In vitro* ookinete cultures of *sir2a*$^{-}$ line (1022 cl2) and wild type were prepared by standard epoxy resin embedding procedure. Thin sections of the obtained resin blocks were counter stained and analysed with an electron microscope (Zeiss). No general gross and consistent phenotypic changes were observed in the *sir2a*-decificient mutants, which contain an apical complex and a number of

micronemes appearing morphologically indistinguishable from published images of wild type (Fig. 51; wild type images from Aikawa et al., 1984).

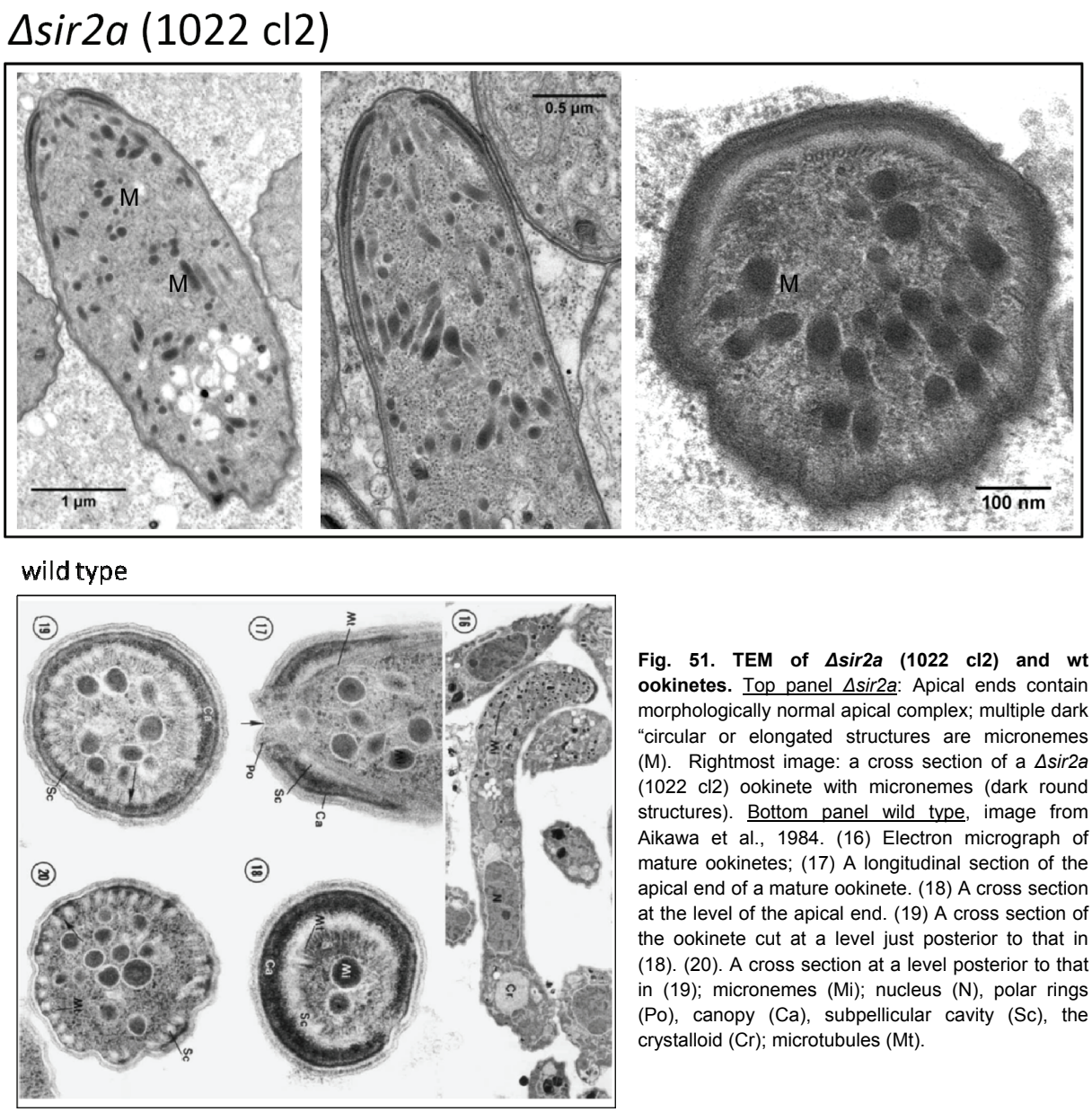

Fig. 51. TEM of *Δsir2a* (1022 cl2) and wt ookinetes. Top panel *Δsir2a*: Apical ends contain morphologically normal apical complex; multiple dark "circular or elongated structures are micronemes (M). Rightmost image: a cross section of a *Δsir2a* (1022 cl2) ookinete with micronemes (dark round structures). Bottom panel wild type, image from Aikawa et al., 1984. (16) Electron micrograph of mature ookinetes; (17) A longitudinal section of the apical end of a mature ookinete. (18) A cross section at the level of the apical end. (19) A cross section of the ookinete cut at a level just posterior to that in (18). (20). A cross section at a level posterior to that in (19); micronemes (Mi); nucleus (N), polar rings (Po), canopy (Ca), subpellicular cavity (Sc), the crystalloid (Cr); microtubules (Mt).

III.6.2 SIR2A is not essential for oocyst formation.

The preceding experiments led us to a conclusion that SIR2A is required for mosquito midgut traversal. The observations of possible very young oocysts motivated us to investigate this *Δsir2a* developmental stage in more detail. A valid assumption was that *sir2a*-deficient oocyst growth is in fact wild type-like if a physical barrier of mosquito midgut epithelium is circumvented. One method to analyse *in vivo* oocyst development potential is microinjection of mature ookinetes into *Anopheles*

haemocoel (first performed in *Plasmodium* by Weathersby, 1952). *Plasmodium* ookinetes can develop into functional oocysts bearing infectious sporozoites anywhere in a mosquito body.

Injections with 800 ookinetes per haemocoel were performed for 507 cl1 (Pb ANKA HP GFP_{con}), 1022 cl2 (*Δsir2a*) and 1184 m1cl1 (*Δsir2a/b*). At day 10 fluorescent round forms considered to be oocysts were detected on wild type-injected midguts and remaining parts of haemocoels. Interestingly, oocysts were also observed in both SIR2A mutants. Due to technical problems with tissue homogenisation we could not quantitatively assess the relative numbers of oocysts in the three analysed lines. Therefore at day 21 post-injection sporozoites were quantified following tissue homogenisation, which in contrast to oocysts did not affect sporozoite integrity. For each parasite line approximately 20 salivary glands (SGs) were dissected and homogenised. The average number of sporozoites for the wild type line injections was 1736/SG (see Table 9A). No sporozoites were detected in the SGs of *Δsir2a*- and *Δsir2a/b*-injected mosquitoes. Repeating the experiment with wild type and *Δsir2a* line confirmed our previous observations. At day 10 oocysts could be detected in mosquitoes injected with ookinetes of both lines. Curiously, at day 27 post-injection sporozoites could also be detected in mosquitoes infected with the mutant ookinetes (Table 9B). Due to time limits the experiment has not been repeated. It is possible that SIR2A-deficient sporozoites exhibit defects in salivary gland invasion, which could be one explanation for the observed delay. At this point it is not certain if SIR2A-deficient sporozoites do penetrate the SG epithelium.

Mosquito haemocoel micro-injections

Table 1A. Sporozoite numbers in salivary glands at day 21 post-injection (2 independent experiments)

	Sporozoites	No. of SGs	Infected	Average per SG	SD
WT	15120	11			
	19600	9	20/20	1736	316.78
Δsir2a	0	10			
	0	9	**0/19**	**0**	**0**
Δsir2a/sir2b	0	11			
	0	12	**0/23**	**0**	**0**

Table 1B. Oocyst production, sporozoite numbers at day 21 and 27 p.i.

Stage	Parasite line	day 10 p.i.	day 21 p.i.	day 27 p.i.
oocysts*	**wt**	some	yes	yes
	Δsir2a	some	yes	yes
SG sporozoites	**wt**	-	~3000	yes
	Δsir2a	-	0	**yes!**

Table 9 Mosquito haemocoel micro-injections.

A. Sporozoite numbers in salivary glands (SGs). At day 21 post-injection (p.i.) on average 1736 sporozoites were counted per SG for wild type-injected mosquitoes. No sporozoites were detected in SGs of mosquitoes injected with *Δsir2a* and *Δsir2a/b* ookinetes. SD = standard deviation.

B. Oocyst production and sporozoite detection at day 21 and 27 p.i. At day 10 post-injection oocysts were detected in haemocoels of both wild type and *Δsir2a*-injected mosquitoes. In case of *sir2a*-injected mosquitoes no sporozoites were present in SGs at day 21 but at day 27 p.i. sporozoites could be detected, either attached or in the lumen of the SGs.

III.6.3 Analysis of possible causes of *Δpbsir2* ookinete deficiencies.

III.6.3.1 SIR2A contributes to ookinete motility

One possible *sir2a*-deficient ookinete deficiency that results in failure to cross the midgut epithelium could be a defect in ookinete motility. We analysed ookinete motility *in vitro* in a commercially available murine basement membrane-like gel preparation Matrigel™ (BD Biosciences; protocol by R. Moon, O. Billker's laboratory cite ref). In short, equal volumes of *in vitro* cultured *P. berghei* ookinetes and Matrigel™ (stored at 4˚C) were mixed, spotted onto a glass slide and covered with a vaseline-rimmed coverslip. The gel was left to set at RT for 30 min. Ookinete motility was recorded every 30 seconds for 10-20 minutes (Leica stereomicroscope) and the analysis of distance travelled was performed (associated Leica software). Initially a slight decrease in motility of both *sir2* mutant ookinetes was observed. An in-depth analysis of the recorded sequences showed that the movement ability of 1022 cl2 and 1184 m1cl1 ookinetes was impaired when compared to the wild-type ookinetes (Fig. 52). *sir2a*$^{-}$ ookinetes did translocate in a characteristic corkscrew-like fashion but the speed (distance travelled over time) was decreased approximately 2 fold for *Δsir2a* and 2.5 fold for *Δsir2a/b* in comparison to wild type.

Our results indicate that the average speed of wild type ookinete is lower than previously observed (e.g. Moon et al., 2009). *Plasmodium* ookinetes exhibits a corkscrew-like motion with abrupt changes in the direction of movement, which makes the true analysis on the extent of the motility challenging. The results represent the analysis with the software available at the time of the experiment. Tracking strategies evolve rapidly and new algorithms are being developed and implemented in the analysis software. It is highly like that the results, if anything, are an underestimation of both the average wild type ookinete speed and the differences between the mutant and wild type ookinetes. In addition the reported average of ookinete movement differs, depending on the gliding substrate used as well as experimental conditions implemented.

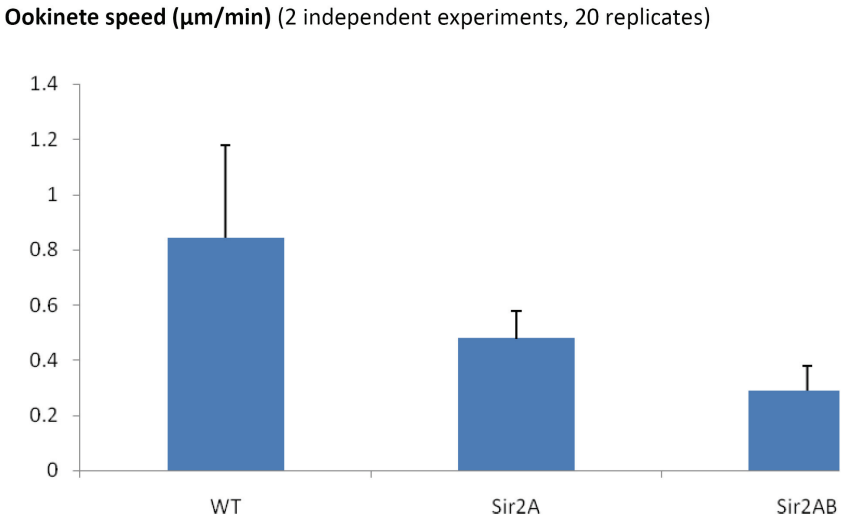

Fig. 52 Ookinete motility assay in Matrigel™. Motility of *sir2a* k.o. *sir2a/b* double k.o. and wild type GFP-positive ookinetes was recorded every 30 seconds for 20-30 minutes at RT using a green-fluorescence channel (Leica stereomicroscope). Twenty measurements were taken for each parasite line.

This data points to ookinete motility as a possible contributing factor to the observed ookinete deficiency in midgut barrier traversal, through physical movement impairment. The degree of the ookinete speed decrease cannot be the sole explanation for the transmission blockage phenotype since a percentage of ookinetes should access the luminal side of the midgut epithelium and initiate epithelium invasion and traversal (see also Discussion and Future perspectives chapter).

III.6.3.2 Investigation of microneme proteins.

1) Chitinase

Chitinase secreted by *Plasmodium* ookinetes is instrumental for parasite crossing of the *Anopheles* mosquito midgut border (Shahabuddin et al., 1993; Tsai et al., 2001; Dessens et al., 2001). The chitinous layer, called peritrophic matrix (PM) surrounding the blood meal is digested by a chitin lytic (chitinase) activity of parasite origin which allows the ookinete to penetrate the PM layer and proceed through the midgut epithelium until it reaches basal lamina, where oocyst development occurs. Therefore, one hypothesis for the observed defect of *sir2a*-deficient ookinetes to cross the midgut barrier could be inability to traverse the PM resulting from abnormal chitinase enzyme production, activity or secretion. To test this hypothesis an *in vitro* chitinase assay was set up (modified from Vinetz et al., 2000). Chitinase activity can be quantitatively measured by analysing the enzyme's ability to cleave an established, fluorescent chitinase substrate 4-methylumbelliferyl-*N,N*',*N*''-β-D-triacetylchitotrioside (4MU-GlcNaC3, Fluka). This substrate when digested by chitinase or certain lysozymes emits fluorescence peaking at 450 nm (excitation at around 365 nm).

Serum-free ookinete medium (50 µl) or ookinete culture cell extract (50 µl of 0.1% Triton-X/PBS lysate) from overnight *in vitro* ookinete culture of HP GFP_{con} (507 cl1), *sir2a* k.o. (1022 cl2) and *sir2a/b* k.o. (1184 m1cl1) was measured for chitinase activity at pH=8.0 (see Materials and Methods for details protocol). The test was performed in a black 96-well plate (Nunc) and fluorescence measured in relative fluorescence units (RFUs) in a microplate reader (PerkinElmer Envision). Preliminary tests showed that 4-hour and longer incubation time at room temperature was optimal for proper detection of chitin lytic activity at low concentrations of chitinase i.e. in ookinete media. In general, the highest chitinase activity was detected in cell lysates (Fig. 53 below; left graph red bars). The 4MU substrate breakdown was slightly higher in the parasite lysate from the Δ*sir2a* mutant when compared to the wild type (507 cl1), and significantly smaller in the SIR2A/B double deletion parasite extract. Chitinase activity in ookinete media was low presumably due to enzyme dilution in large volume of ookinete medium used for ookinete cultures. However ookinete medium fluorescence detected in all samples was higher than the background fluorescence measured for parasite-free serum-free ookinete medium. Ookinete media from the two knockouts showed lower RFU values than the wild type medium (Fig.53, graph on the left, blue bars).

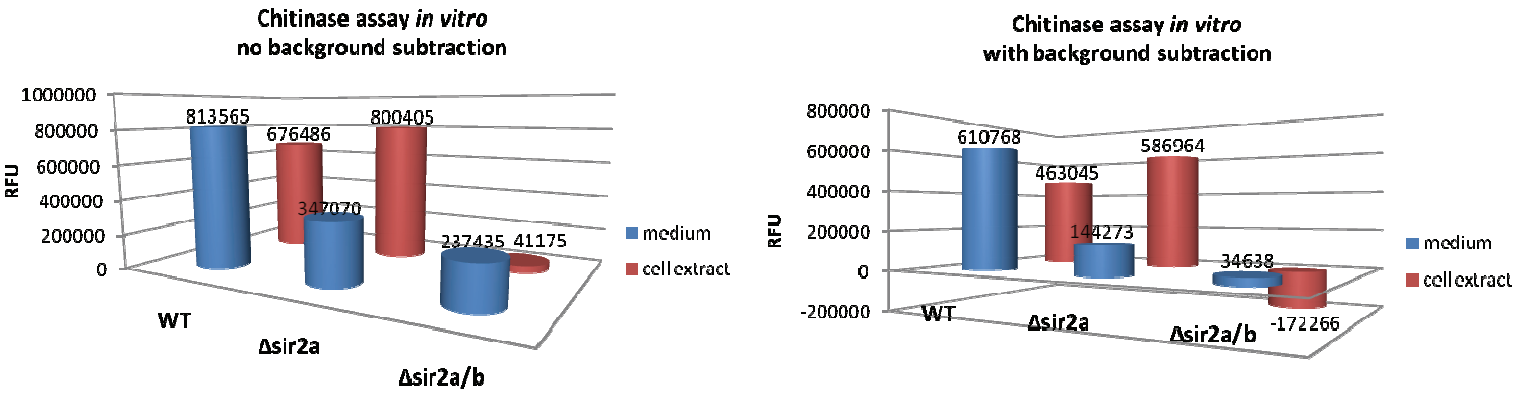

Fig. 53 Chitinase assay results *in vitro*. The assay has been performed once on *in vitro* cultured ookinetes of wild type (507 cl1), *Δsir2a* and *Δsir2a/b*, in a serum-free M199 medium. The breakdown of the substrate 4MU added to the ookinete medium (blue bars) or cell extracts (red bars) was measured as RFU (emission peak at approx. 450 nm). Left: raw RFU numbers obtained from the assay. Right: RFUs obtained after subtraction of the relative background samples (ookinete-free serum-free medium for medium samples; 0.1% Triton-X in PBS for cell extracts).

Interestingly, upon background subtraction of serum-free ookinete-free medium (for medium measurements) and 0.1% Triton-X in PBS (for cell extracts measurements) the value for the fluorescence emitted by the *Δsir2a/b* (1184 m1cl1) cell extract became negative. This result could due to near- or below-threshold value in the fluorescence measurement, or due to fluorescence quenching in the 1184 m1cl1 extracts, dependent on the sample contents. It is important to note that the number of ookinetes in the 1184 m1cl1 (*sir2a/b*-deficient) culture appeared to be generally lower than in the remaining two *in vitro* cultures, with ookinetes developing comparably worse than the wild type and *Δsir2a* parasites. At this point it is not clear whether the low RLU numbers result from generally low parasite numbers or an additional deficiency resulting from SIR2B absence, compared to the *sir2a* single mutant.

The assay has been performed once and should be repeated. Quantification of ookinetes in the total ookinete medium was attempted by Western analysis of equal amounts of the chitinase assay cell extracts analysed for P28 protein presence (anti-P28 antibody, mouse; data not shown). P28 is expressed in ookinetes but also in both fertilised and unfertilised female gametocytes. Therefore the resulting band intensity from the Western analysis does not directly correspond to the quantity of mature ookinetes in the *in vitro* cultures. Despite this fact the P28 total quantification showed that 507 cl1 and 1184 m1cl1 (*sir2a/b*$^{-/-}$) P28 band intensity is similar (relative ratio of 1 to ~0.8, respectively), whereas for the *Δsir2a* ookinete extract the P28 band appears ~ 2-3 times stronger. These results, though preliminary, strongly suggest that chitinase is synthesised and active at least in the *Δsir2a* parasite line (1022 cl2) but that it is not efficiently secreted to the surrounding medium. Therefore the proposed chitinase mislocalisation would subvert the ability of the parasite to digest the peritrophic matrix thereby impeding the ookinete traversal of the midgut barrier. Unfortunately antibodies that recognise chitinase from *P. berghei are* not in existence and further investigation of under-production/mislocalisation awaits their production.

2) CTRP, P25 & P28

Circumsporozoite- and TRAP-related protein (CTRP; PBANKA_041290) is another microneme protein expressed at late ookinete stage essential for ookinete infectivity where it plays the role of a surface ligand used by the gliding motility apparatus of the ookinete (e.g. Yuda et al., 1999; Dessens et al., 1999; see the Introduction chapter). The presence and localisation of the CTRP protein was detected using a polyclonal anti-PbCTRP antibody (courtesy of Prof. Yuda, Mie University). Western analysis of the *sir2a::gfp* (503 cl1), *sir2a*$^{-}$ and *sir2a/b*$^{-/-}$ (1022 cl2 and 1184 m1cl1) lines resulted in a detection of a single band at an expected size of approx. 250 kDa (Fig. 54). The intensity of the band is almost 5 fold higher in the *Δsir2a*-deficient lines compared to the *sir2a::gfp* line.
Equal quantities of prepared protein extracts were used in the Western analysis. Unfortunately the protein content in the samples is difficult to normalise since one cannot be sure of changes at protein level occurring in the modified parasites.

P28 (PBANKA_051490) and P25 (PBANKA_051500) which are the two major ookinete surface proteins, and are both highly expressed following female gamete fertilisation (Vermeulen et al., 1985)These two abundant proteins, having partially redundant activities, play an important role in ookinete survival in the *Anopheles* host and in ookinete midgut epithelium traversal (Tomas et al., 2001). *p28* and *p25* are known to be translationally repressed (Mair et al., 2006) and interestingly *p28* and *p25* are also the two most abundant transcripts in gametocytes (see later in this chapter). In the *Δsir2a/b* gametocytes the levels of these two transcripts are entirely unaffected compared to wild type. P28 protein presence and correct localisation in ookinetes was confirmed by immunofluorescence, and appears similar to that of wild type (see Fig. 55, bottom panel P28). Therefore the P28 protein could be considered as a loading control for CTRP protein level analysis. Taking this assumption into consideration CTRP levels in the two *sir2a* mutant lines appear approximately 2 times higher than in the *sir2a::gfp* lines (used as a wild type positive control).

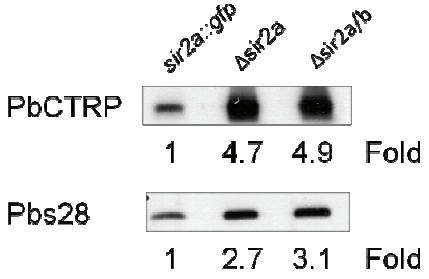

Fig. 54 Western analysis of three parasite lines for CTRP and P28 expression. Equal volumes of total ookinete extracts were run on a 12% SDS-PAGE gel. Following membrane blotting, the anti-CTRP antibody (10 ng/µl; rabbit) and anti-P28 antibody (1:10000) was hybridised in 0.1%Tween in PBS/3% milk for 2 hours at RT. The secondary anti-mouse and anti-rabbit HRP conjugates were used in a 1:10000 dilution. If P28 is considered a loading control ~ 2 times more CTRP is present in both *sir2a*-deletion mutants when compared to the *sir2a::gfp* line (503 cl1), here serving as a wild type control.

Despite apparent upregulation of CTRP expression in the SIR2A-null ookinete, CTRP protein levels and/or distribution differed in the fixed *sir2a*$^{-}$ and *sir2a/b*$^{-/-}$ mature ookinetes when compared to the wild type (507 cl1) (Fig. 55 below, red channel). A significant portion of CTRP localised to the apical end of mature wild type ookinetes. CTRP was also partially distributed in the cytoplasm appearing as a punctate staining, which could indicate localisation into vesicular structures such as micronemes or pre-micronemal particles. Interestingly in both SIR2A mutants CTRP appeared to be relatively evenly distributed throughout ookinetes. In both *Δsir2a and Δsir2a/b* mutants ookinetes the "empty" apical end was observed (Fig. 55 1022 e.g. panel 1 & 2; 1184 panel 1 & 2) reminiscent of the observed "empty" appearance of this region in the Giemsa-stained *sir2a* knockouts (see Fig. 50). The GFP channel (green) provides an indication of the background fluorescence (resulting from phenylhydrazine treatment of animals), as well as residual post-fixation parasite fluorescence, since all analysed lines constitutively express GFP throughout the life cycle.

P28 IFA is shown in Fig. 55 (bottom panel). The characteristic surface staining is visible in the wild type and both mutant lines (red channel) and does not appear to be significantly different. The residual GFP (green) is shown.

CTRP

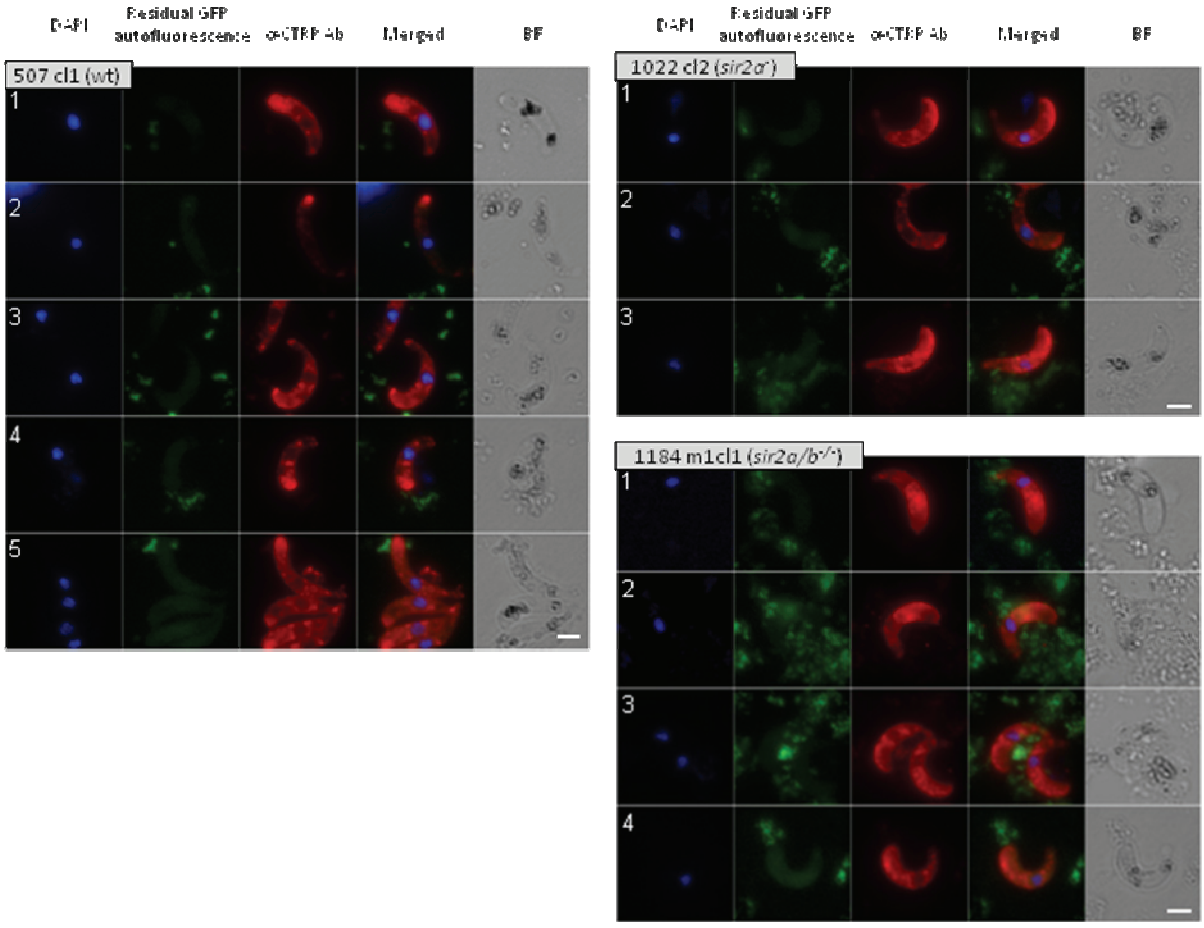

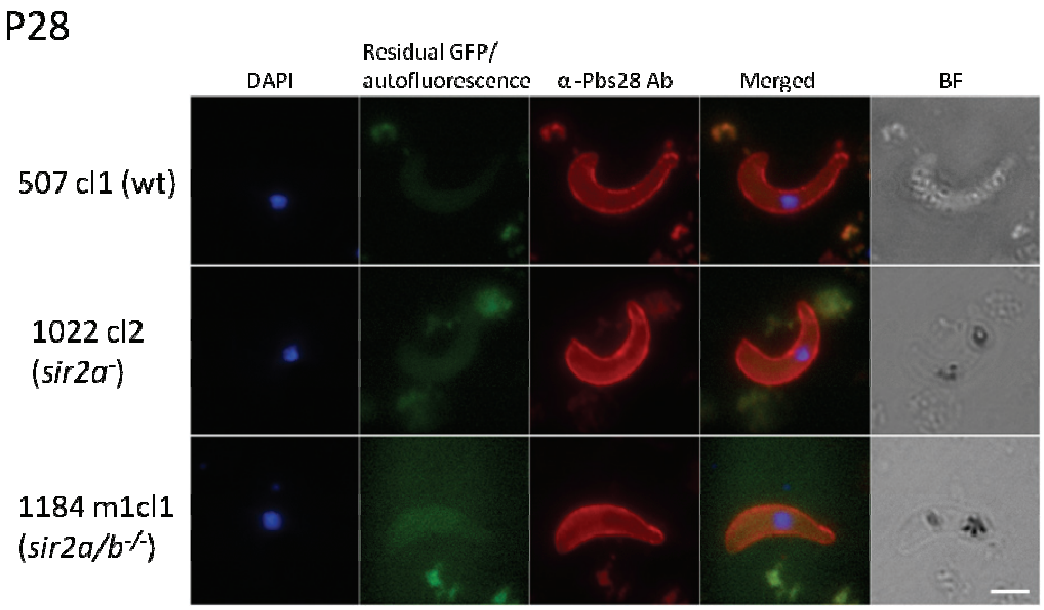

Fig. 55 CTRP and P28 IFA on mature wild type, *sir2a*- and *sir2a/b*$^{-/-}$ ookinetes. Both anti-CTRP and anti-P28 antibodies were detected with Alexa Fluor-594 secondary antibody (red channel). The green channel serves as a background reference for both non-parasite-derived auto-fluorescence and parasite residual fluorescence since all lines were generated in the GFP_{con} background (507 cl1). CTRP: A mostly apical staining is prominent in the wild type ookinetes (top left montage). The CTRP distribution is different in both Δsir2a mutants, with frequently recognisable "empty" apical end (e.g. panels 1 & 2 for both 1022 and 1184). P28 IFA yielded a typical surface staining in all three lines (see red channel). Scale bars indicate 5 µm in both CTRP and P28 images.

3) Plasmepsin 4

Plasmepsin 4 (PBANKA_103440) is a member of a family of aspartic proteases, which have previously shown to function in the digestive vacuole of asexual parasite stages (Banerjee et al., 2002; Dame et al., 2003). Plasmepsin 4 (PM4) as the first member of the family has recently been shown to play a major role in ookinete infectivity to mosquitoes (Li et al., 2010). Immunodetection demonstrated its localisation into *P. gallinaceum* ookinete micronemes, from where is it is secreted into the surrounding medium. These findings prompted us to analyse PM4 expression and localisation in the SIR2A-null parasites. Immunofluorescence analysis with α-PgPM4 antibody (courtesy of J. Dame, University of South Florida, USA) showed a speckled PM4 localisation throughout the analysed wild type, 1022 and 1184 ookinetes (Fig. 56, red channel) similar to that of CTRP and consistent with the presence of the PM4 in micronemes and their precursors. Strikingly a very concentrated signal, appearing as a dot at the tip of the apical end of all ookinetes was consistently observed in all ookinetes. The green channel served the purpose of background recognition (autofluorescence and residual GFP of GFP_{con} fixed ookinetes). No major differences in both localisation and intensity were observed between the wild type and the two *sir2a* mutant parasite lines. Western analysis, which is needed to quantitatively determine the protein levels in the mutant ookinetes compared to wild type has not been performed to date.

It is important to note that *plasmepsin 4* steady state transcripts like *ctrp* and *p28* transcripts remained unchanged (1.1 up-regulated) in the 1184 (double deletion) mutant in gametocytes (gametocyte RNA-seq data).

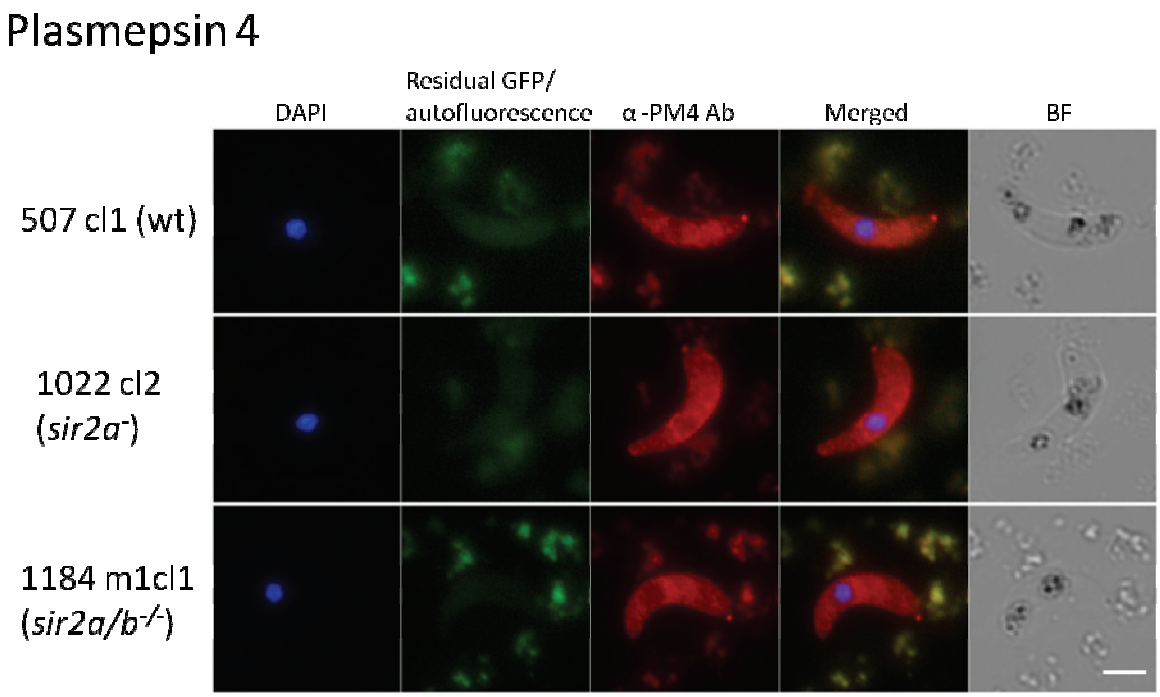

Fig. 56 Plasmepsin 4 IFA on mature wild type, *sir2a*$^{-}$ and *sir2a/b*$^{-/-}$ ookinetes. Primary anti-*P. gallinaceum* PM4 antibody was used at 1:100 dilution. Secondary antibody (anti-rabbit Alexa Fluor 596 conjugate) was applied to detect the PM4 localisation (red channel). A highly characteristic concentrated apical tip staining is visible in the ookinetes of all analysed lines. The additional signal in the red channel comes from phenylhydrazine- and sulfadiazine-induced background.

III.6.3.3 Acetylation level analysis

SIR2 proteins are principally histone deacetylases that affect the acetylation status of histone proteins and other proteins in the cell. Hence deletion of SIR2A and SIR2B should plausibly result in a general increase of acetylation levels in the nucleus of the mutant parasites. Acetylation levels were analysed by IFA using a commercial anti-acetyllysine (AcK) antibody (mouse mAb, Cell signaling, cat. no. 9681s) at a dilution 1:500. A relatively weak nuclear signal was obtained for wild type parasites (507 cl1; see Fig. 57, top panel). Interestingly upon longer exposure a weak speckled staining was observed outside the nucleus, both towards the apical and the rear end of ookinetes (top panel, marked “overexposed”). A slight increase in the nuclear signal was observed for both the single *sir2a* and double *sir2a/b* mutants. Although the observation might be background and/or software settings dependent the exposure time was the same for all observations. Upon overexposure (either 3x the initial exposure, or using ImageJ software) the same speckled localisation of the anti-AcK antibody, specific to the red channel was revealed in both mutants (middle and bottom panel). Analysis of the

acetylated protein pools in the *sir2* mutant parasites extracts vs. the wild type either by Western analysis or Mass Spectrometry is necessary to draw more conclusions about the effects of *sir2* deletion on the global acetylation status of proteins in the 1022 and 1184 parasites.

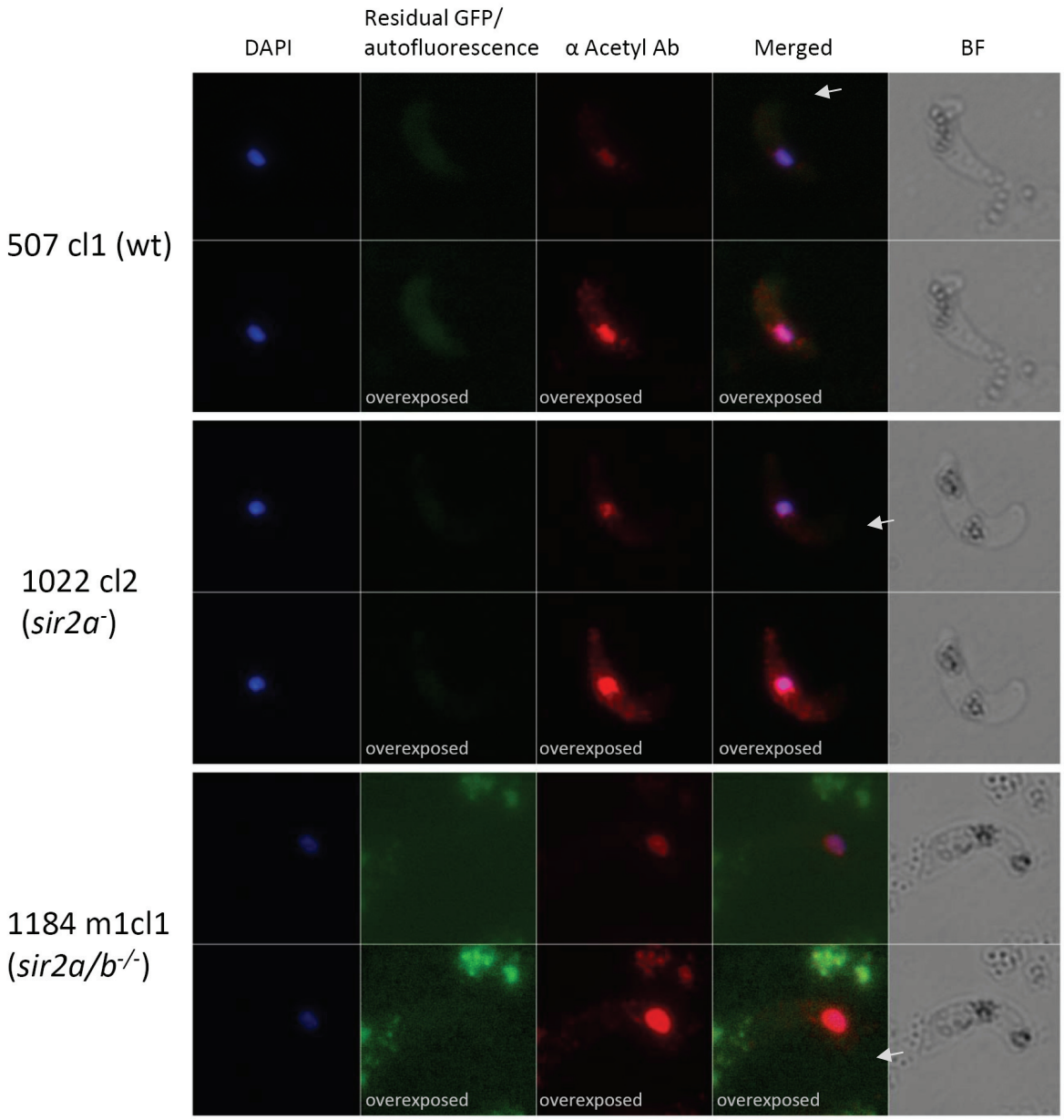

Fig. 57 Immunofluorescence assay using anti-acetylation antibody on 507 cl1 (HP GFPcon); 1022 cl2 (*sir2a*$^{-}$) and 1884 m1cl1 (*sir2a/b*$^{-/-}$) *in vitro* cultured mature ookinetes. Acetylation patterns were detected with anti-acK polyclonal rabbit antibody (Cell signalling; dilution 1:500) and goat anti-rabbit Alexa Fluor 594-conjugated 2˚ antibody (1:2000). All parasites are in the GFP_{con} background (hence the residual GFP fluorescence). Host cells exhibit strong autofluorescence due to phenylhydrazine and sulfadiazine treatment of animals prior to overnight *in vitro* incubation of ookinete cultures. The anti-acK antibody is mostly specific to the red channel. Arrows indicate the apical end.

III.6.3.4 Gametocyte transcriptome analysis of sir2a/b double deletion parasites by RNA-sequencing

Advantages of RNA sequencing technology

RNA-sequencing (in short RNA-seq) is a recently developed technique for obtaining high-precision, wide-scale and in-depth transcriptome profiles. Existing hybridisation-based methods are relatively inexpensive but have several limitations including cross-hybridisation, signal saturation and detection equipment sensitivity (Wang et al., 2009). Furthermore microarray data comparison is challenging first due to the quality of the data itself (resulting from e.g. variable chip hybridisation conditions) as well as use of a variety of normalisation methods. In contrast to microarrays, RNA-seq allows for direct determination of the cDNA sequence in a quantitative manner (without upper limit for quantification other than available data storage space) and presents an accurate in-depth picture of all mRNA transcripts in a particular sample. Therefore the collected data is relatively independent of a current genome coverage and assembly and is relatively straight-forward to analyse and, in the case of incomplete genomes, can be retrospectively analysed.

In case of *P. berghei* transcriptome studies, there are additional limitations besides those imposed by the microarray technology itself. *P. berghei* microarray analysis is biased due to the data processing procedure which is based on the far from complete *P. berghei* genome assemblies (3x or 8x coverage) available at the time of the different microarray designs. Therefore the obvious advantages of RNA-seq prompted us to continue the analysis of the generated *P. berghei* mutants using this technology. RNA-seq presented an opportunity to obtain comprehensive sequence data on both the *P. berghei* wild type and SIR2A/B k.o. parasite transcriptomes. An added benefit here is that the *P. berghei* HP transcriptome can further be utilised by the scientific community in any other studies requiring single- or genome-wide transcription profiles analysis. Lastly a more recent assembly and gene prediction of the *P. berghei* HP genome became available (January 2010) during this study from which this analysis was able to benefit.

RNA-seq analysis

Solexa RNA sequencing was performed in collaboration with Henk Stunnenberg and Wieteke Hoeijmakers from Nijmegen Center for Molecular Life Sciences, The Netherlands. Three parasite stages of both HP (wild type) and the *sir2a*/*b* double deletion mutant were processed and prepared for analysis:

- rings (5 hpi)
- gametocytes
- ookinetes

The parasite ring stage has previously been analysed using microarrays. In addition to obtaining a more complete view of transcriptional changes, this sample can serve as a comparison platform between the two methods utilised for total transcriptome analysis.

Of the sexual *Plasmodium* stages, both gametocyte and ookinete stages of the *sir2a/b*-deficient parasites were collected for analysis since the effects observed in ookinetes could originate at an earlier gametocyte stage, as a result of a process called translational repression (TR). TR is utilized by *Plasmodium* female gametocytes (Hall et al., 2005; Paton et al., 1993; Thompson and Sinden, 1994; Vervenne et al., 1994). Specialised protein complexes, dispersed throughout the female gametocyte cytoplasm and organised into so called P-granules, function as "storage and stabilisation" sites for transcribed mRNA molecules and are physically distinct from ribosomes. These mRNAs are therefore translationally repressed but are released from the complexes and translated at a later parasite stage, beginning in the zygote. The first characterised protein member of the TR complexes in *Plasmodium* is a DEAD-box helicase DOZI (Development of Zygote Inhibited; Mair et al., 2006). DOZI-null mutants show impaired P-granule function followed by defects in zygote development and failure to produce ookinetes. Further analysis by affinity purification of GFP-tagged P-granules permitted identification of 18 different protein components that include widely conserved proteins integral to P-granule function of metazoans such as homologues of Trailer-hitch (CITH), poly-(A) binding protein and the mRNA modified cap binding protein eIF4E and an eIF4E binding protein (Mair et al., 2010). In addition, the P-granules include ALBA proteins (Acetylation Lowers Binding Affinity) (Mair et al 2010) which, are ancient nucleic acid-binding proteins known to undergo deacetylation by SIR2 proteins which in their acetylated form have a much reduced binding affinity for nucleic acids, including RNA (Bell et al., 2002).

The implication of this information for P-granule function is that in the absence of SIR2 activity ALBA proteins become hyper-acetylated and lose their affinity for nucleic acids thereby compromising P-granule stability. In this scenario the mRNA associated with P-granules might become destabilised as it does in the absence of DOZI or CITH (Mair et al 2006, 2010). Therefore RNA sequencing of purified SIR2A/B knockout gametocytes was undertaken (in collaboration with Henk Stunnenberg; performed by Wieteke Hoeijmakers at the University of Nijmegen, The Netherlands) in order to assess if one role of SIR2 in *Plasmodium* is to assist in the stabilisation of stored mRNA in female gametocytes.

Unfortunately due to time limitations this is an incomplete study, and the ring and ookinete parasite stages will be analysed by RNA-seq at a later date. The results of gametocyte stage RNA sequencing are described in the following sections.

1) Gametocytes

(a) Material collection and preparation

Gametocyte stage purification from asynchronous infections has been previously described (Beetsma et al., 1998). Replicating asexual parasite stages are killed and removed from the circulation by the spleen upon *in vivo* application of the drug sulfadiazine which inhibits DNA synthesis, leaving mature circulating gametocytes unaffected. In short, phenylhydrazine-treated rats were infected with either HP or 1184 m1cl1 line (*Δsir2a/b*) from a previously infected mouse (day 2 of the procedure). At day 5 (parasitaemia approx. 10-15%) treatment with sulfadiazine was started. At day 7 whole blood was collected by cardiac puncture into enriched-PBS at 37˚C to prevent gametocyte activation. In order to obtain the purest possible gametocyte population the collected blood was passed twice through a Plasmodipur filter to eliminate host white blood cells. Following addition of 49% Nycodenz/PBS-solution (v/v) to the PBS-diluted blood the samples were centrifuged at 1500 rpm for 15-20 min. The brown layer containing mature gametocytes (and if present late trophozoites and schizonts) was collected and centrifuged to obtain a parasite pellet, which was washed in PBS. The resulting parasite pellets were immediately resuspended in the TRIzol reagent (Invitrogen) and stored at -80˚C until further processing.

The following protocol was used for processing of the RNA samples and obtaining the raw RNA sequence data. Half of each total RNA sample was chloroform-extracted and cleaned with Qiagen RNeasy kit (with DNase treatment on column). Following Poly-A selection (Qiagen Oligotex mRNA mini kit) mRNA was fragmented by hydrolysis. Double-stranded cDNA synthesis was performed in 2 steps using a linear amplification protocol based on *Plasmodium* Solexa protocol optimised by the Stunnenberg lab. For first strand cDNA synthesis AT-corrected random N9 primers were used. qPCR amplification reactions of the reverse transcriptase- control mRNA samples with several primer pairs were negative for genomic DNA presence (see Appendix Table A3 for primers information). Second strand cDNA synthesis primed on mRNA. The resulting cDNA was analysed by Solexa/Illumina sequencing (Illumina Genome Analyzer GAIIx) generating ostensibly 76bp reads.

(b) Data processing

The obtained cDNA sequence reads were analysed for host contamination by mapping the reads against the mouse genome. The remaining sequence data was normalised such that the wild type and *Δsir2a/b* (1184 m1cl1) samples contained equal amounts of total mapped reads, in order to allow a direct comparison. Individual cDNA sequence tags were mapped onto the latest *P. berghei* genome assembly (as of January 2010) available from ftp://ftp.sanger.ac.uk/pub/pathogens/P_berghei) and compiled into .gff file format, which can be viewed using SignalMap (v 1.8, NimbleGen Systems).

The original 76-bp sequences were utilized for *P. berghei* genome mapping. Longer reads were initially chosen as in theory this should increase the unique mapping potential of each read, a feature particularly favourable in case of genes and genomes with high sequence redundancy (i.e. an AT rich genome with large and diverse multigene families). Mapping of the 76-bp reads showed disappointingly low coverage of the genome (51% and 23% for wild type and *Δsir2a/b*, respectively). One reason for the low coverage could be a high number of so called junction reads in the total reads pool. Junction reads can span two or more exons excluding introns, since all reads are derived from mRNA molecules. Hence the alignment score of these reads to a genome is naturally lower than for pure exon reads (containing only exon sequence). An in-depth analysis of the reads showed that the highest error rates occured in the first ~10 bases and approximately 20 last bases of the 76-bp reads. Following several optimisation trials the tags were reduced *in silico* to a length of 45 bp, by systematic deletion of first 10 and last 21 base pairs in all analysed reads. This modification greatly increased the mapping accuracy of the sequences and general coverage of the genome sequence to approximately 85% for both samples (see Table 10 below).

Sample	Number of raw tags	Tag length	% uniquely mapped tags
Gametocytes			
wild type	1.84E+07	76bp	50.86%
		45bp	84.29%
		57bp	82.02%
sir2a/b double k.o. (1184 m1cl1)	1.06E+07	76bp	23.05%*
		45bp	85.46%
		57bp	81.64%
		53bp	82.75%

* increased error rate (up to 20%)

Table 10. Optimisation of tag length and respective changes in the percentage of uniquely mapped tags.

Transcriptional changes were compiled into separate data batches (.gff files) containing 2 different types of tags:

- Uniquely mapped – tags with maximum 4 mismatches allowed (out of 45 bp), which map to a unique position within the *P. berghei* genome

- Repeat or non-unique – tags mapping to multiple positions within the genome (multigene families are most likely found in this category)

The non-unique data set was found to show an increased coverage of subtelomeric regions since sequence similarity between multigene families members such as *birs* and *Pb-fams* is generally high. For this reason the *bir*- and *Pb-fam*-like tags and tags to other multi-gene families mapped to multiple sites in the *P. berghei* genome. The same phenomenon was observed for *var* genes (a 60 member

multi-gene family) in *P. falciparum* transcriptome profiling experiments (W. Hoeijmakers, personal communication).

The data set containing both unique and non-unique sequence tags was used for further analysis of differences in transcription profiles between the *sir2a/b*-null (1184 m1cl1) parasites and wild type. The differential log2 values were calculated by the formula: log(number of tags/gene in *Δsir2a/b*)/log2 – log(number of tags/gene in wild type)/log2. The differential track of *sir2a/b* k.o. signal / wt signal was constructed by plotting the differential log2 values onto the *P. berghei* genome.

(c) Determination of a degree of contamination with host RNA and other parasite stages

Despite the fact that the material was obtained from sulfadiazine-treated animals and gametocytes were Nycodenz-purified contamination with other stages was still a possibility. Given the previous phenotyping of the SIR2A/B null mutants had not revealed any defects in gametocyte production, a valid assumption is that the degree of contamination with asexual stages should be the same in both HP and *Δsir2a/b* (1184 m1cl1) gametocyte preparations. Therefore in order to determine the degree of contamination several merozoite/schizont-specific genes were analysed for changes in transcription. The list of revised genes is shown in Table 11 below. Differences in transcriptional levels in SIR2A/B k.o. vs. wild-type were negligible; at no more than 1.35 fold change (fold change of 1 means no change).

Merozoite-specific genes

Gene ID	Previous ID	Gene description	wt number of tags/transcript	*Δsir2a/b* number of tags/transcript	log2 change (*Δsir2a/b* over wt)	Fold change
PBANKA_091500	PB000821.01.0	AMA1 apical membrane antigen 1 7100338:7102008 reverse	170	172	0.0169	1.01
PBANKA_083100	PB000172.01.0	MSP1 merozoite surface protein 1 6297074:6302449 forward	1202	889	-0.4352	-1.35
PBANKA_134910	PB000442.03.0	MSP7 merozoite surface protein 7 15103831:15104838 reverse	246	264	0.1019	1.07
PBANKA_110140	PB301475.00.0	RAP2/3 rhoptry-associated protein 2/3 9778679:9779845 reverse	1098	1284	0.2258	1.17
PBANKA_090130	PB000798.02.0	MAEBL merozoite adhesive erythrocytic binding protein 6555568:6561509 reverse	1097	1168	0.0905	1.06
PBANKA_111350	PB000503.03.0	Rab1a, putative 10218922:10219542 reverse	1303	1345	0.0458	1.03
PBANKA_083630	PB000048.01.0	clag9 cytoadherence linked asexual protein 9 6455909:6460810 reverse	1204	1481	0.2987	1.23
PBANKA_143360	PB001080.02.0	TRAMP thrombospondin-related apical membrane protein 16927516:16928562 forward	90	98	0.1229	1.09
PBANKA_141830	PB000489.00.0	PRP2 rhoptry protein 2, putative 16405830:16409648 forward	431	468	0.1188	1.09

Table. 11 Merozoite-specific gene transcription levels. Merozoite genes were assessed for transcriptional changes to determine the degree of gametocyte samples contamination. All analysed genes showed a fold change of close to 1, apart from merozoite surface protein 1 (MSP1), which is slightly down-regulated in the *sir2a/b* mutant (-1.35 fold change).

(d) Deregulated genes in the *Δsir2a/b* line

A differential track of log2 changes (*Δsir2a/b* over wt) on all 14 *P. berghei* chromosomes is shown in Fig. 58 below. Each data point represents a log(number of *sir2a/b* over wild type tags/gene)/log2 over 100-bp window. In general it appears, that no dramatic changes occur in the *sir2a/b* mutant parasites at the transcriptional level. The most highly deregulated genes are 13 and 8 fold down- and up-regulated respectively, which are a *Pb-fam* (PBANKA_094390) and *bir* (PBANKA_001030),

respectively. However these genes are transcribed at very low levels, with less than 15 sequence tags detectable in both parasite lines and so are statistically unreliable. Notably, the next gene in the top deregulated genes list is a *Plasmodium* exported protein (PBANKA_072260), which is approximately 9 fold down-regulated. The gene, previously annotated as Pb-fam-3, is expressed at a level of 325 sequence tags (per gene coding region) in the wild type sample, whereas only 35 sequence tags were counted in the *sir2a/b*$^{-/-}$.Importantly, 14 tags is the lowest detectable number of transcripts per gene for which peptides could be detected in the gametocyte proteome of Khan et al. (2005).

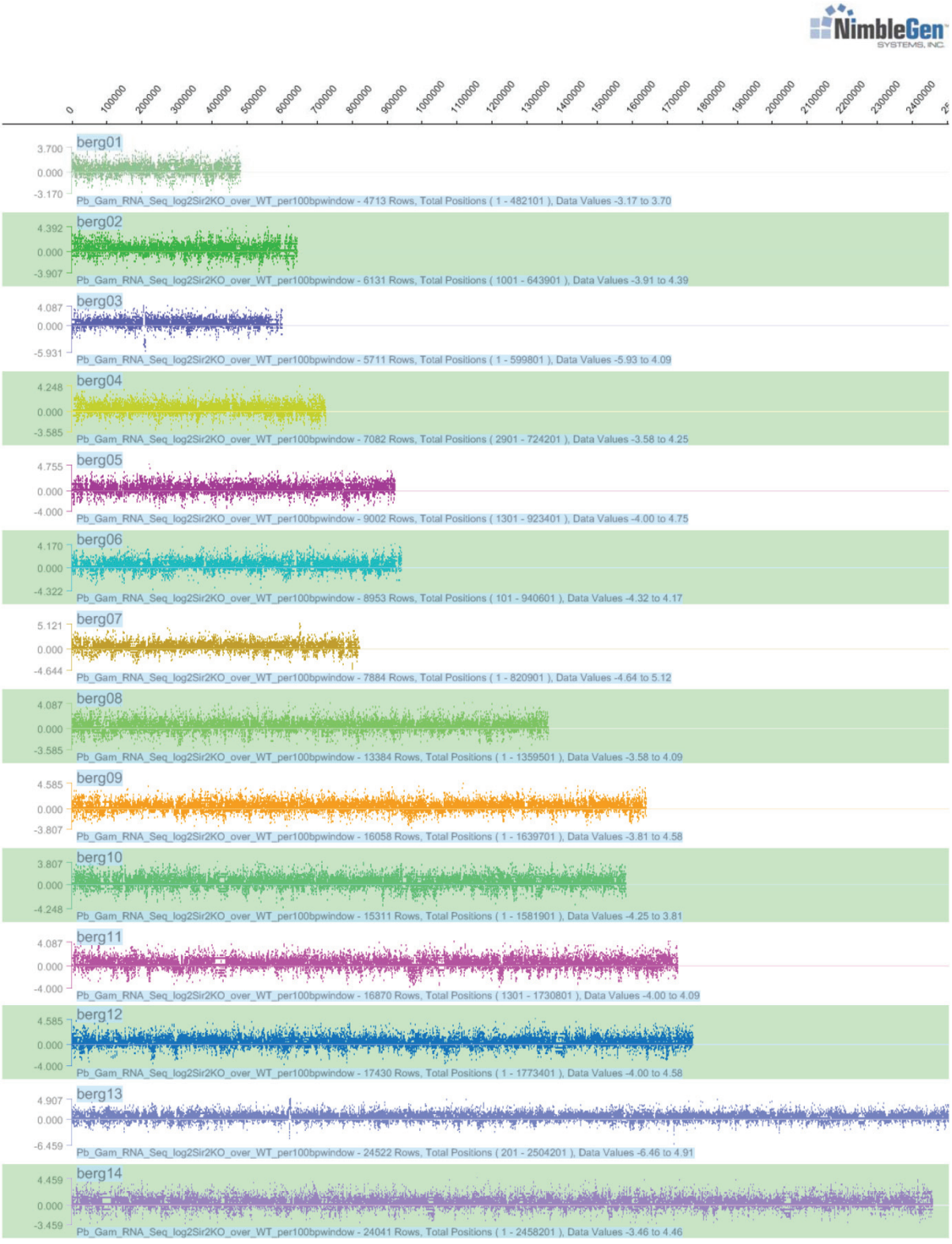

Fig. 58. A general overview of transcriptional changes at 14 chromosomes in the *P. berghei sir2a/b* double deletion mutant vs. wild type purified gametocytes. The y-scale at each chromosome indicates log(number of tags/gene in *Δsir2a/b* over wild type)/log2.

There are 364 genes at least 1.5 fold up-regulated and 111 genes at least 1.5 fold down-regulated in the *sir2a/b* double knockout in comparison to wild type; and of these 76 up- and 42 down-regulated

genes respectively belong to the top 50% of all *P. berghei* transcribed predicted genes (at ≥ 377 tags per gene in wild type gametocytes; see Appendix Fig. A1 for wild type transcript numbers/gene distribution). *birs* and *Pb-fams* multigene family members contribute 31 to 364 up-regulated genes and 22 to 111 down-regulated genes, of which only 1, Pb-fam-1 PBANKA_130030, is found in the top 50% higher-transcribed genes.

Figure 59 depicts different gene categories represented in the top 50 most highly up- and down-regulated gene lists. In both sets genes annotated as "of unknown function" contribute a significant part (16/50 in up- and 25/50 in down-regulated list). Other genes abundantly represented are multi-gene family members such as *birs* and *Pb-fams* located predominantly in the subtelomeric regions of *P. berghei* chromosomes (14 in both sets). Interestingly, ribosomal proteins, which according to microarray data are deregulated in asexual *Δsir2a/b* parasites, are also found up-regulated in gametocytes. Other genes in both data sets are listed in the tables on the left from the pie charts.

New ID	Prev systematic ID	log2 change (*Δsir2a/b* over wt)	Fold change	Description
PBANKA_131510	PB000549.02.0	1.44508	2.72	Sir2b transcriptional regulatory protein sir2b 13843507:13846992 forward
PBANKA_123700	PB300071.00.0	1.42623	2.69	S-adenosylmethionine-dependent methyltransferase, putative 12826039:12828107 reverse
PBANKA_101700	PB300290.00.0	1.25634	2.39	CorA-like Mg2+ transporter protein, putative 8817265:8818701 reverse
PBANKA_030600	PB000214.00.0	1.25572	2.39	transmission-blocking target antigen, putative 1329389:1336252 forward
PBANKA_130120	PB000767.03.0	1.22239	2.33	mediator complex subunit 31, putative 13287069:13287473 reverse
PBANKA_146410	PB102669.00.0	1.20163	2.30	coronin, putative 18096683:18098555 forward
PBANKA_071140	PB000100.01.0	1.16439	2.24	PPLP4 perforin like protein 4 4718221:4720269 reverse
PBANKA_123530	#N/A	1.12707	2.18	BIS(5'-nucleosyl)-tetraphosphatase (diadenosine tetraphosphatase), putative 12771232:12772384 reverse
PBANKA_132570	PB001018.01.0	1.0346	2.05	thioredoxin-like protein, putative 14218840:14219205 reverse
PBANKA_130580	PB000215.03.0	1.02857	2.04	transcription factor TFIIH complex subunit Tfb5, putative 13490720:13490923 forward
PBANKA_000510	PB001659.02.0	1	2.00	reticulocyte binding protein, putative, fragment 18385897:18388411 forward
PBANKA_080740	PB001065.01.0	1	2.00	proteasome regulatory protein, putative 5480940:5481614 forward
PBANKA_142260	#N/A	0.991067	1.99	Sel3 selenoprotein, putative 16561925:16562944 forward
PBANKA_121640	PB301249.00.0	0.982722	1.98	RNA triphosphatase, putative 12039988:12041907 forward
PBANKA_082050	PB000160.03.0	0.965235	1.95	dolichyl-diphosphooligosaccharide--protein- glycosyltransferase, putative 5938099:5939655 forward
PBANKA_136190	PB102634.00.0	0.965235	1.95	nucleoside diphosphate hydrolase, putative 15577867:15578773 reverse

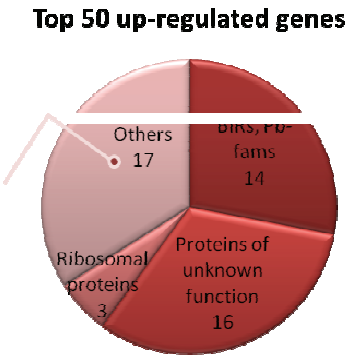

New ID	Prev systematic ID	log2 change	Fold change	Description
PBANKA_113310	PB100542.00.0	-1.21186	-2.32	serine/threonine protein kinase, putative 10936819:10947846 forward
PBANKA_000280	PB000487.00.0	-1.11548	-2.17	reticulocyte binding protein, putative, fragment 18284314:18286360 forward
PBANKA_011050	PB105848.00.0	-0.997881	-2.00	leucine-rich repeat protein 5, putative 398038:404879 reverse
PBANKA_090190	PB000497.00.0	-0.892722	-1.86	tubulin-tyrosine ligase, putative 6578032:6586572 reverse
PBANKA_000220	#N/A	-0.847997	-1.80	reticulocyte binding protein, putative, fragment 18250694:18253770 reverse
PBANKA_040940	PB105688.00.0	-0.83251	-1.78	protein kinase, putative 2082184:2090447 forward
PBANKA_060950	PB000464.00.0	-0.812124	-1.76	kinesin-related protein, putative 3751234:3756331 forward
PBANKA_135340	PB000652.03.0	-0.786293	-1.72	PSOP7 secreted ookinete protein, putative 15241844:15244282 reverse
PBANKA_082010	PB000018.00.0	-0.780069	-1.72	PPPDE peptidase, putative 5927549:5928409 reverse
PBANKA_052130	PB000684.01.0	-0.772399	-1.71	zinc finger protein, putative 3234218:3242626 reverse

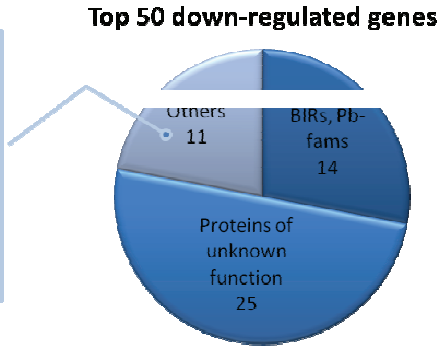

Fig. 59 Top 50 up- and down-regulated genes categorised according to the GeneDB newest release annotation (January 2010). Red pie chart depicts the top 50 up-regulated genes, whereas the blue chart down-regulated genes. Genes belonging to "Others" category are listed in the tables to the left of both charts.

The top 50 deregulated genes were analysed in terms of GO annotation, available GeneDB annotation and PlasmoDB annotation (based on previous systematic IDs) as well as recently published functional gene clusters (Zhou et al., 2008). The analysed total of 100 genes were categorised according to gene annotation, predicted or observed function and/or gene product localisation (Fig. 60). Additionally to multigene family products (BIRs, Pb-fams) motility-associated

genes are significantly over-represented in the down-regulated gene set. This observation is consistent with the observed decrease in ookinete motility in Matrigel™ (see point “SIR2A contributes to ookinete motility”). Of the top 50 up-regulated gene products 8 were annotated as membrane- or apicoplast-targeted. Furthermore, several transcription, chromatin remodelling and nucleotide (purine/pyrimidine) genes (n=7) as well as translation and metabolism-related genes were observed (4 and 5, respectively). Proteins of unknown function, predicted GO process or localisation routinely contribute a high percentage of analysed genes (18/50 top down-regulated genes and 12/50 top up-regulated genes).

Fig. 60 Top 100 deregulated genes assorted according to GO ontology, predicted gene function clusters, GeneDB and PlasmoDB annotation. The top 50 down-regulated in the absence of SIR2 genes (blue-bar chart) were divided into 4 categories, including birs/Pb-fams and motility-related group of 7 gene products. The top 50 up-regulated in the absence of SIR2 bar chart (red) shows 6 types of associations such as birs/Pb-fams, apicoplast/membrane-targeted predicted gene products, and transcriptional regulation-related genes. Unknown products contribute a significant percentage of analysed genes in both sets.

One important point to consider when analysing subtelomeric multigene families transcription patterns is clonal variation within a parasite line, as well as transcriptional changes occurring due to environmental cues (e.g. immune responses) in the animal host. Therefore the subtelomeric transcriptional differences observed between the *sir2a/b*-null and wt parasites might vary between biological replicates. Furthermore universally low transcription levels and sequence redundancy of multigene family members (*birs, Pb-fams*) makes the judgment of true observations relatively difficult. The observed changes therefore can be neither discarded or considered true unless several biological replicates are analysed and data confirmed by additional analyses such as qRT-PCR.

Nevertheless, a higher confidence of a true event can be assigned to genes deregulated in the mutant line and expressed in the wild type parasites, than to those genes which are silent in the wild type and

are deregulated in the mutant. Unfortunately this approach also means that one must partially disregard the possibility of SIR2 proteins functioning as transcriptional regulators.
As expected, *bir* and *Pb-fam* genes are among those of the lowest number of tags per gene. As little as 1 tag (*birs*, *Pb-fams*, *Pbs36p*) and as many as ~158000 tags (P28) have been observed per gene in both wild type and *Δsir2a/b* gametocyte samples. Top 100 deregulated genes and the respective number of sequence tags/gene observed for wild type and the mutant line are listed in the Appendix (Table A1, A2).

The SIR2-deregulated gene lists were cross-analysed with several other available databases. Interestingly 9 out of 50 top down-regulated genes are also significantly deregulated in the DOZI-null mutant gametocytes (Table 12). These include a serine/threonine protein kinase, kinesin-related protein, leucine-rich repeat protein 5 and tubulin-tyrosine ligase. The remaining 5 genes are annotated as conserved *Plasmodium* proteins. The kinesin-related protein (PBANKA_060950) and tubulin-tyrosine ligase are predicted to participate in ookinete motility. All of the listed genes are represented by high numbers of sequence tags per gene, with 12273 tags in case of wild type transcription of PBANKA_060950 being the most abundant transcript among the top 50 down-regulated genes. Importantly, DOZI (PBANKA_121770) transcript abundance and those encoding the other P-granule protein components remains unchanged in the SIR2A/B-deficient gametocytes implying that the absence of SIR2 does not generally affect the production of the components of the P-granule in the female gametocyte.

New ID	Prev systematic ID	Log2 fold change	Fold change	WT tags/gene	*Δ sir2a/b* tags/gene	Description
PBANKA_113310	PB100542.00.0	-1.21186	-2.32	1501	648	PBANKA_113310 serine/threonine protein kinase, putative 10936819:10947846 forward
PBANKA_011050	PB105848.00.0	-0.997881	-2.00	2041	1022	PBANKA_011050 leucine-rich repeat protein 5, putative 398038:404879 reverse
PBANKA_110850	PB000033.03.0	-0.971356	-1.96	2643	1348	PBANKA_110850 conserved Plasmodium protein, unknown function 10020941:10028587 forward
PBANKA_090190	PB000497.00.0	-0.892722	-1.86	4547	2449	PBANKA_090190 tubulin-tyrosine ligase, putative 6578032:6586572 reverse
PBANKA_050330	PB000784.01.0	-0.873976	-1.83	4875	2660	PBANKA_050330 conserved Plasmodium protein, unknown function 2582865:2587271 reverse
PBANKA_060950	PB000464.00.0	-0.812124	-1.76	12273	6990	PBANKA_060950 kinesin-related protein, putative 3751234:3756331 forward
PBANKA_141720	PB000157.01.0	-0.78236	-1.72	8383	4874	PBANKA_141720 conserved Plasmodium protein, unknown function 16357783:16360203 reverse
PBANKA_070560	PB000662.02.0	-0.776925	-1.71	5430	3169	PBANKA_070560 conserved Plasmodium protein, unknown function 4526219:4531004 reverse
PBANKA_134250	PB401942.00.0	-0.765595	-1.70	12011	7065	PBANKA_134250 conserved Plasmodium protein, unknown function 14883564:14888129 forward

Table 12 Down-regulated genes common to SIR2A/B- and DOZI-null gametocytes. Five out of the 9 listed genes are conserved *Plasmodium* genes, whereas the remaining 4 are 2 kinesin-like proteins, a tubulin-tyrosine ligase and a leucine-rich repeat protein 5. Transcript abundancy of the down-regulated genes is indicated by data bars (orange), which represent a quantity of tage/gene, relative to all top 50 down-regulated genes.

An interesting observation was made at the *sir2* genes loci themselves. Both *sir2a* and *sir2b* loci showed a significant up-regulation in the number of tags in the 5' and 3' regions adjacent to the

deleted gene sequence, which reassuringly was significantly down-regulated in the *sir2a/b* mutant (see Fig. 61A). The reason for the observed high transcription in the modified *sir2a* and *sir2b* loci could be the presence of the *sir2a* promoter upstream the selectable marker cassette possibly enhancing the *Tgdhfr-ts* gene transcription at the *sir2a* locus (see below for further explanation).

On several occasions an increased number of transcript tags at intergenic regions were also observed, such as in the case depicted in Fig. 61B. It appears that the upregulated regions on chromosome 7 are the 5' and 3' regions flanking the *P.berghei dhfr-ts* gene (PBANKA_071930). In the *P. berghei* transfection procedure *T. gondii dhfr-ts* is introduced in the genome as a selectable marker using the the original 5' and 3' flanking regions of *Pbdhfr-ts* to drive expression of the *Tgdhfr-ts* open reading frame (ORF). Curiously, neither the *Pbdhfr-ts* ORFor the two surrounding genes PBANKA_071920 (orthologue of *P.falciparum* PUF2) and PBANKA_071940 (LETM1-like protein) are significantly deregulated in the *sir2a/b* mutant (1.3 fold change for *Pbdhfr-ts* and *puf2* and 1 fold change for *letm1-like* genes). One possible explanation for the apparent regional up-regulation could be due to a "double effect" of the intact *sir2a* promoter and *Pbdhfr-ts* 5' UTR causing high transcription of the introduced *Tgdhfr-ts* selectable marker cassette at the *sir2a* locus. Sequence tags of 5' and 3' UTR regions derived from the *Tgdhfr-ts* cassette are bound to align perfectly with the endogenous 5' and 3' UTR sequences at the *Pbdhfr-ts* locus on chromosome 7. The tag assignment programme simply assigns tags to the first perfect hit in the anlaysis which is a random process. Therefore in much the same way that tags to multi-gene families are potentially mis-assigned, the homologous genetic elements that are duplicated in the genome as a result of being used to drive transgene expression may give rise to apparent up-regulation of transcription elsewhere in the genome

A

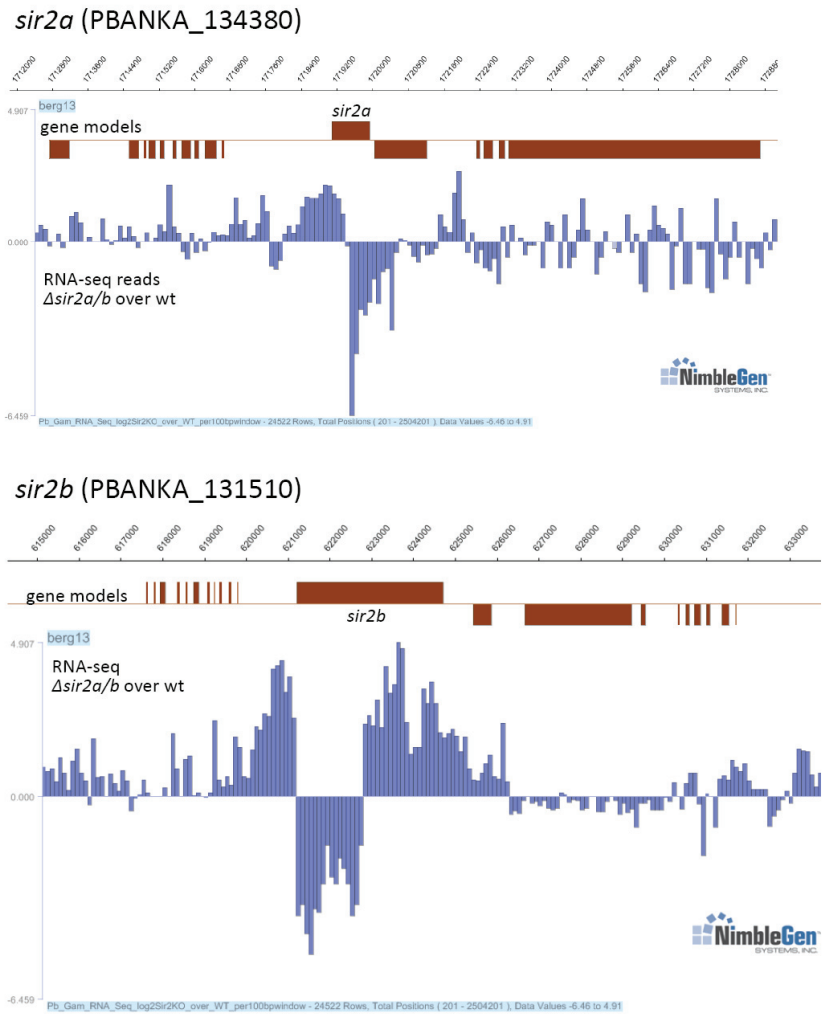

Fig. 61 A. Sequence reads levels at *sir2a* and *sir2b* loci. The upstream and downstream regions of the deleted gene parts show significant up-regulation, possibly due to an "enhancement effect" of the *sir2a* promoter preceding the introduced *Tgdhfr-ts* selectable marker cassette at the *sir2a* locus. B. The intergenic region surrounding the PBANKA_071930 (*Pb hdhfr-ts*) gene shows significant up-regulation in the 1184 m1cl1 parasites (*Δsir2a/b*). This observation might be an artefact of sequence reads alignment (see text for details).

B

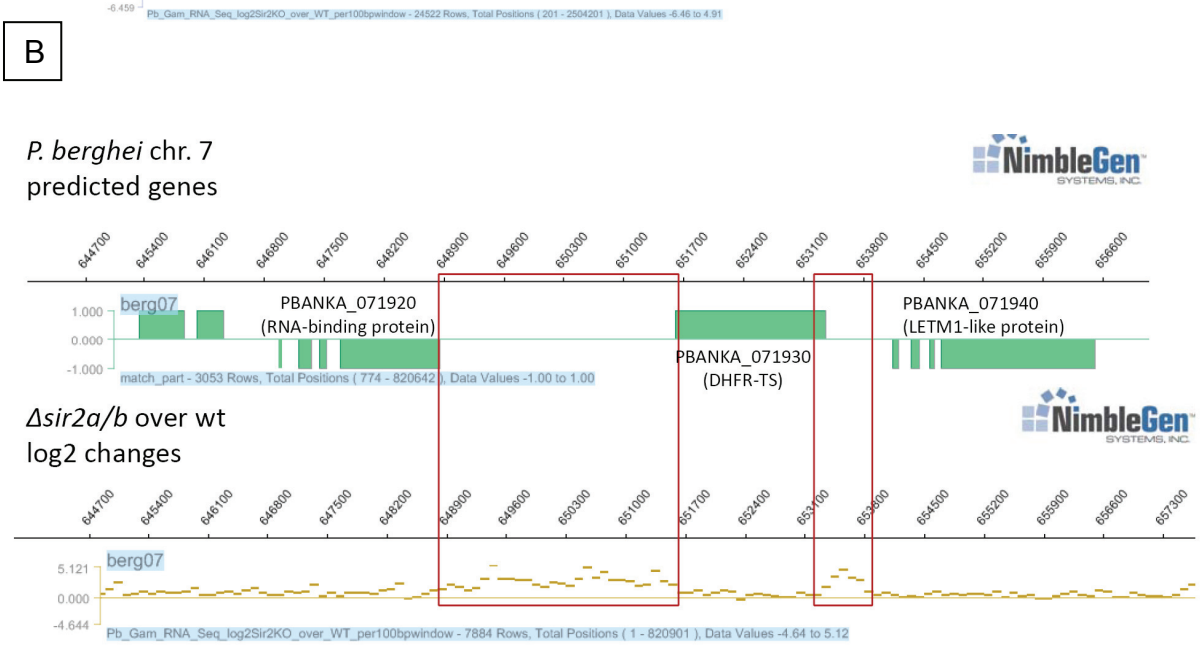

PART 2 - TELOMERASE

III.7 The average telomere length measurement

For the studies of telomerase and telomere related events it is essential to know the average telomere length in *P. berghei*, primarily to deduce if the planned telomerase knockout is possible to generate and analyse. The average telomere length analysis will allow for prediction of the possible effects of the TERT absence such as the global telomere shortening rate, and hence the number of cycles the *tert*-deficient parasites can survive in comparison to the wild type population. The average telomere length can be measured using telomere restriction fragment (TRF) analysis, developed by de Lange et al. in 1990. The TRF technique relies on the fact that there are no restriction sites in the telomeric repeat sequence. Therefore upon digestion of genomic DNA with frequently cutting restriction enzymes, complete telomeres are preserved. The DNA sample is then run on an agarose gel and the standard Southern blotting procedure is employed. Probing the membrane with telomere repeats-specific probe results in a “smeared” signal, where the highest intensity along the smear indicates the average telomere length. To date the mean telomere length has been analysed in five *Plasmodium* species: *P. yoelii*, *P. chabaudi*, *P. cynomolgi*, *P. vivax* and *P. falciparum* (several strains) (Figueiredo et al., 2002). The average telomere length for the rodent malaria species *P. yoelii* and *P. chabaudi* was found to be quite different at approximately 2080 bp and 960 bp, respectively. Therefore, as the first step in the project, the TRF method was used to determine the average telomere length in *P. berghei*. Approximately 700 ng of *P. berghei* wt gDNA was digested overnight with four frequently cutting restriction enzymes: AluI, Sau3AI, MboII and RsaI (5 units each), run on 1% agarose gel and blotted onto a membrane. The blot was probed with the previously described *Plasmodium* telomere-specific probe (Ponzi et al., 1990) (Fig. 62). A *P. yoelii* sample was used as a size control. Additional controls included a Field Inversion Gel Electrophoresis (FIGE) blot (described in Materials and Methods, and later in the text) of separated chromosomes from *P. berghei, P. chabaudi, P. vivax and P. yoelii* (Fig. 14 on the left). As can be seen on the FIGE blot, the probe recognized all *Plasmodium* chromosomes, whereas on the TRF-Southern blot a characteristic smear can be observed. The reason for this appearance is the length heterogeneity among all *Plasmodium* telomeres. The graph on the right depicts the signal intensity variations along the lane. The molecular marker intensities provide a size reference (grey line). The *P. yoelii* highest intensity peak almost coincides with the 2.5 kb peak of the marker, meaning that the average telomere length for *P. yoelii* is approximately 2.5 kb. This value is slightly higher than that observed by Figueiredo et al. However the difference might be due to the fact that a different genomic DNA sample, possibly from a different strain, was used for this study. Telomere size polymorphisms within the same strains of different *Plasmodium* species have been observed both *in vivo* and *in vitro* (for instance Ponzi et al., 1990; P. Alano, personal communication). As for the *P. berghei* lane (red line on the graph) the peak in the highest intensity region is a widened area positioned between molecular marker peaks for 0.8 kb and 1 kb, with a slight

shift towards 1 kb, indicating that the average telomere length for *P. berghei* is approximately 950 bp, closer to the value obtained for *P. chabaudi*.

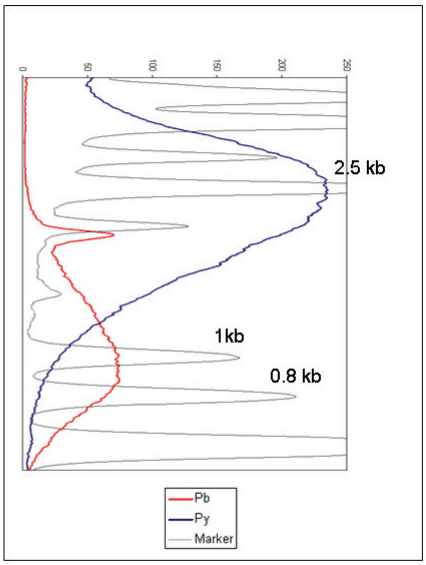

digestion control (5' dssu probe)

Fig. 62 Telomere length measurement by Telomere Restriction Fragment analysis. On the left: FIGE blot of *P. berghei*, *P. chabaudi*, *P. vinckei* and *P. yoelii* chromosomes was used as a control for the telomeric probe. All chromosomes were recognized. On the middle and right: Southern blot of digested *P. yoelii* (size control) and *P. berghei* gDNA probed with telomeric probe. The characteristic "smeared" pattern is visible in both the *P. yoelii* and *P. berghei* lanes. The average telomere length was measured as the highest peak of the signal intensity along the smear. Using the molecular marker (grey line on the graph) as a size reference, the mean telomere length was estimated to be approximately 2500 bp and 950 bp for *P. yoelii* (blue line) and *P. berghei* (red line), respectively. Complete digestion of gDNA was confirmed with a 5' *dssu* probe.

III.8 Fluorescence *in situ* hybridisation with telomere-specific probe

Fluorescence *in situ* hybridization (FISH) allows for detection of a desired DNA/RNA sequence within a cell using a fluorophore-conjugated sequence-specific probe. The FISH technique was adapted from A. Scherf et al. (see Materials and Methods for details). In order to confirm previously observed nuclear periphery-specific telomere clustering in *Plasmodium* species FISH was performed with a fluorescein-labelled (High-Primer Fluorescein kit, Roche Applied Science). A telomere sequence-specific probe (courtesy of Liliana Mancio-Silva, Institute Pasteur, Paris) (see Fig. 63) was hybridised to saponin-treated (lysis of RBC) and 4% paraformaldehyde-fixed parasites. Following overnight incubation at 80 ˚C the slides were extensively washed in PBS/0.5% Tween. Nuclei staining was performed with Hoechst nucleic acid binding dye (blue), the slides were then mounted and

fluorescence emission was analysed (Leica Fluorescence microscope). The probe gave a clear signal of several foci within the nucleus, putatively clustered at the nucleus border. The established and properly optimised FISH technique will allow for gene localisation studies within the nucleus and identification of a possible dependence between localisation, gene transcriptional status and *Plasmodium berghei* sirtuins gene regulation.

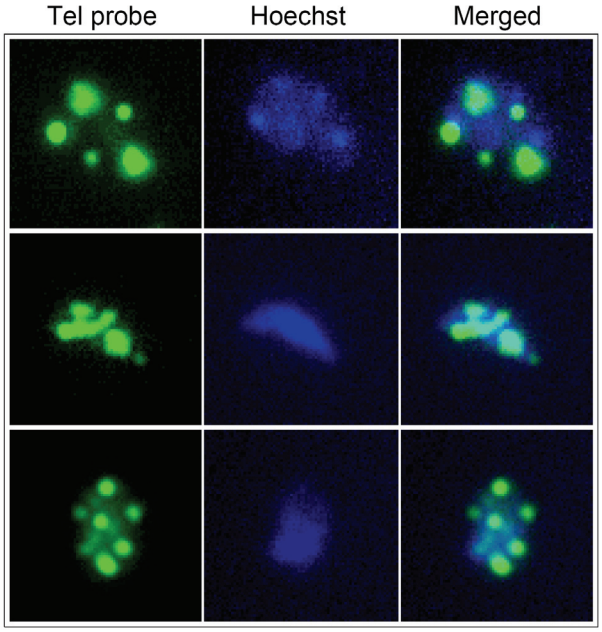

Fig. 63 Fluorescence in situ hybridization with a telomere-specific probe performed on fixed *P. berghei* ANKA strain parasites from overnight culture (mostly trophozoites and schizonts). Telomeric probe (1.5 kb in length, courtesy of A. Scherf and Liliana Mancio-Silva) was labeled with fluorescein. Hoechst dye was used for staning the nucleic acids. Telomeres are observed as foci within the parasites' nuclei.

III.9 Completing the *P. berghei* Telomerase Reverse Transcriptase gene structure.

The *P. falciparum tert* gene sequence was identified (Figueiredo et al., 2005) by searching the *P. falciparum* genome database (Gardner et al., 2002) with the conserved telomerase- and reverse transcriptase-specific motifs (T motif and the seven RT motifs). In the study by Figueiredo et al. searching the available genome sequences of other *Plasmodium* species with the resulting PfTERT protein sequence (PlasmoDB ID PF13_0080) revealed homologous proteins in one simian and two rodent malaria parasites, namely *P. knowlesi*, *P. yoelii* and *P. berghei* (partial sequence), respectively. Since the *Pbtert* sequence was incomplete, the first task of the project was to obtain to complete the *Pbtert* gene structure. The PlasmoDB synteny map provided three *P. berghei* genomic sequences that shared homology with the *P. falciparum* contig containing the *Pftert* gene (PlasmoDB ID MAL13): PB_PH3933, PB_RP3962 and PB_RP1629. Blasting these three *P. berghei* contigs against the other rodent malaria parasite genomes revealed the *P. chabaudi* homologous sequences (contig 1026) and allowed the identification of the *Pctert* gene. The previously identified *Pytert* and partial *Pbtert* were shown to share 78% identity in DNA sequence, suggesting close ancestry of the two rodent genes. The acquired *P. chabaudi* sequences showed even higher homology with the available *P. berghei*

contigs (88% in the global alignment). Therefore, the *P. chabaudi* contig (1026) was subsequently used as a reference for assembling the complete *PbTERT* gene (higher homology facilitated *P. berghei* alignments and sequence analysis). Based on *P. chabaudi* versus *P. berghei* alignments two gaps were identified in the *P. berghei* sequence (Fig. 64), 2.9 kb and 0.9 kb in size. The first gap included the predicted N-terminus of the putative PbTERT.

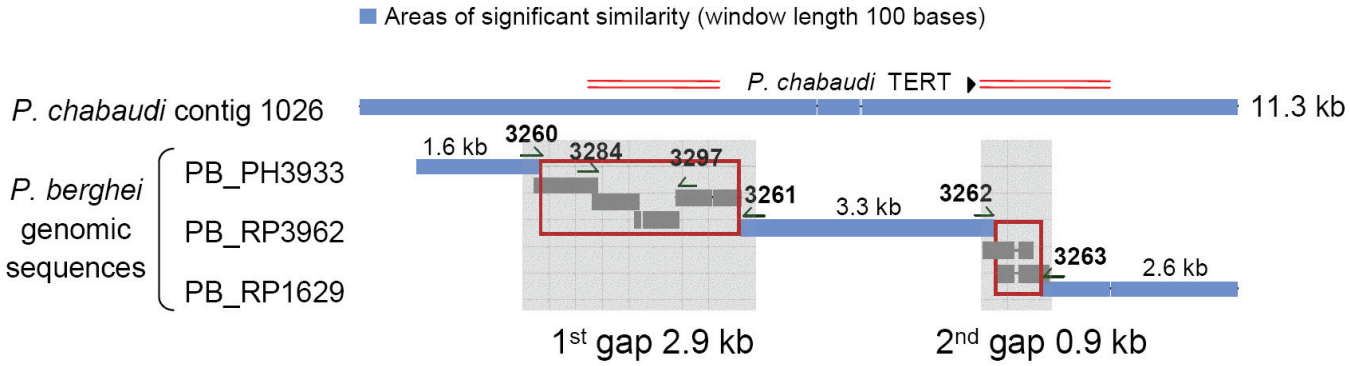

Fig. 64 The alignment of the P. chabaudi tert-containing 1026 contig and the P. berghei available genomic sequences revealed two gaps in this fragment of the *P. berghei* genome (red rectangles). The first gap (2.9 kb) included the conceptual N-terminus of the putative *Pbtert*. The second gap (0.9 kb in size) was located towards the end of the *Pbtert* sequence. The blue blocks indicate sequence similarity of 60 % or more, in windows of 100 bp. The grey boxes show the sequenced fragments using the primers indicated (for primer sequences see Materials and Methods). The alignment was performed in Clone Manager 9 Professional Edition.

Based on the previously identified *Plasmodium* TERTs, the predicted size of the *Pbtert* gene was approximately 7 kb, thus restricting direct sequencing. In order to complete the *Pbtert* sequence several primers were designed, specific to the available *P. berghei* genomic contigs. Using the data obtained from sequencing reactions of both forward and reverse designed primers, the first gap was closed in two subsequent steps, whereas the second gap required only one. The sequence assembly was performed in the Clone Manager 9 Professional Edition (Scientific & Education Software). The primer sequences are listed in the Materials and Methods section.

III.10 The *P.berghei* TERT knockout

The approach of first choice to investigate the Telomerase Reverse Transcriptase (TERT) function in *Plasmodium* species was loss-of-function studies. The *TERT* gene deletion was performed in *P. berghei*, using double cross-over (DXO) approach. Based on human cell studies, where telomerase knockout caused telomere shortening at a rate of 50 – 100 bp per population doubling (bp/pd) (Stoppler et al., 1997; Martin-Ruiz et al., 2004) one can calculate the approximate time that the *P. berghei tert*-deficient parasites can survive (regarding the erythrocytic cycle). Taking into account the number of merozoites (either in the mature erythrocytes or reticulocytes), the average number of nuclear divisions is between three and four per 24 hours. Assuming that four divisions occur in the

schizont stage, and that the complete telomere has to be lost in order for the parasite to die, then at a mean shortening rate of approximately 100 bp/cell division the parasite should survive the maximum of 2.5 blood stage cycles; the same, at a 50 bp shortening rate survival time would increase to approximately 6.5 cycles (assuming 3 divisions/schizont). The telomere shortening rate in *Plasmodium* is not known. However, taking into consideration the fact that human telomeres are much larger than the malaria parasite telomeres, one can speculate that the shortening rate is likewise smaller. Therefore the *P. berghei tert* knockout was considered possible to obtain.

III.10.1Vector design and *P. berghei* transfection

The two homology arms for designing the TERT DXO plasmid were amplified from wild type genomic DNA by PCR using primer pairs 3298 x 3299 (flank 1) and 3300 x 3301 (flank 2) (see Fig. 65). All primers carried a restriction enzyme recognition site at their 5' ends (for primer sequences see Materials and Methods) to enable subcloning into the pL001 plasmid (described below). The first homology arm contains mainly upstream sequence from the *Pbtert* gene and around 50 bp of the coding region, including the ATG start codon. The second flank includes the final portion of the gene and around 200 bp of the region 3' of *Pbtert*.

Fig. 65 The two homology arms for *Pbtert* DXO construct generation were amplified by PCR using 3298 x 3299 and 3300 x 3301 primer pairs. Most of the first flank contained the region upstream of *Pbtert*, and approximately 50 bp of the *Pbtert* gene (including the ATG codon). The second homology region contained the gene end and a small part from the region downstream *Pbtert*. The product sizes are listed in the table.

The two obtained flanks were subcloned into two multiple cloning sites using pL001 plasmid, which is one of the standard plasmids used for *P.berghei* transfection, containing the *Toxoplasma gondii* dihydrofolate reductase – thymidylate synthase gene (*dhfr-ts*; conferring resistance to pyrimethamine), flanked by the 5' and 3' untranslated regions (UTRs) of *P.berghei dhfr-ts* gene (van Dijk et al., 1995). The *T. gondii dhfr-ts* gene was shown to be constitutively expressed in all *P. berghei* life cycle stages, allowing for selection of the transfected parasites. Two multiple cloning sites in the pL001 vector are

placed upstream of the 5' UTR and downstream of the 3' UTR respectively (see Fig. 66). Additionally, the plasmid contains the *Amp*^{R} gene for bacterial selection. Two flanks of 743 bp and 930 bp in size were introduced into the pL001 plasmid by standard molecular cloning techniques and the ready pL001 TERT knockout vector (pL1324) was then amplified in bacterial cells. Since the *P. berghei* transfection is most efficient with linearized constructs (van Dijk et al., 1996), the obtained pL1324 was digested with Asp718I and XbaI restriction enzymes to obtain the linearized fragment containing the flank 1, the *Tg dhfr-ts* selectable cassette and flank 2. The fragment 6.3 kb in size was gel-purified and approximately 5 μg were used for *P.berghei* transfection to obtain the double cross-over *tert* knockout parasites.

Fig. 66 Design of the TERT double cross-over knockout plasmid. The pL001 standard plasmid contains the *Tgdhfr-ts* selectable marker, conferring resistance to pyrimethamine, flanked by the 5' and 3' untranslated regions (UTRs) from the *P. berghei dhfr-ts* gene. The pL001 vector was used for constructing the pL1324 TERT DXO plasmid (shown on the right). The two homology arms were subcloned into Asp718/HindIII sites and XbaI/EcoRI sites. The Asp718I and XbaI sites shown in the pL1324 were used for linearization.

The transfection was performed as follows. The blood stage *P. berghei* schizonts obtained from infected mouse blood were transfected with the *Pbtert* replacement construct (approximately 5 μg) by electroporation. The transfection solution was then injected intravenously into a mouse tail. One day after infection the drug treatment started (pyrimethamine in this case) and approximately 10 – 15 days later (parasitemia of 2 – 5%) blood was collected by cardiac puncture under anaesthesia. Erythrocytes were lysed in a cold erythrocyte buffer and the parasites were harvested by centrifugation. Genomic DNA was extracted and analysed for construct integration. The transfection was attempted three

times. No growth defects and no microscopically detectable abnormalities were observed during the parasite growth in mice. The schematic representation of the integration event is shown in Fig. 67.

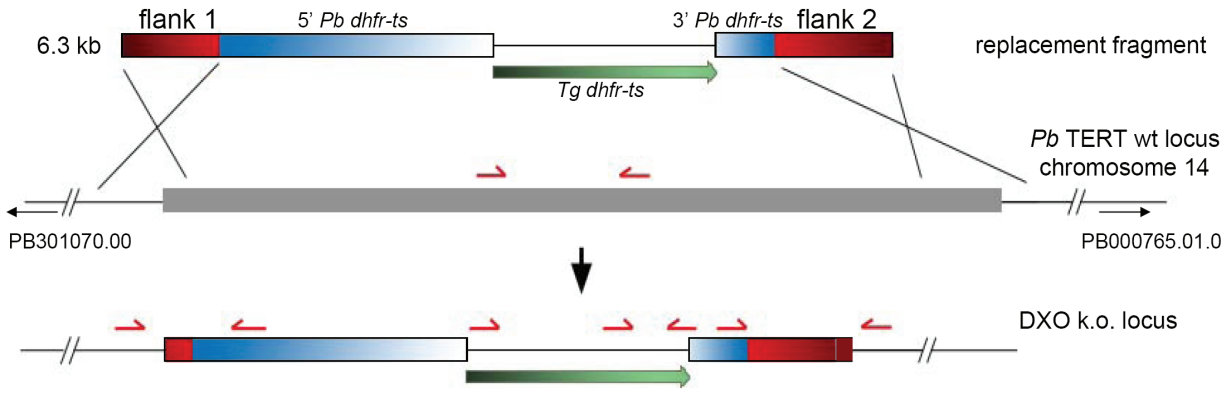

Fig. 67 Schematic representation of the tert knockout generation by homologous double cross-over integration. The replacement fragment, shown on the top, substituted the wild type *P. berghei tert* gene (located on chromosome 14), resulting in a modified locus, containing the *Tgdhfr-ts* selectable cassette conferring resistance to pyrimethamine. The red arrows indicate primers used for the integration-specific PCR reactions, described in detail below. The flanking genes IDs are shown.

III.10.2Diagnostic analysis of the TERT transfection population

Genomic DNA extracted from the transfected parasite population was analysed for the construct integration by Polymerase Chain Reaction (PCR) and Field Inversion Gel Electrophoresis (FIGE) (chromosome separation) (Fig. 68). Two PCR reactions were designed to check for 5' and 3' integration events. The primer pairs used: 3435 x 695, and 1662 x 3436 (see Fig. 68B), included one primer specific for the boundary between the wild type genomic DNA sequences (upstream and downstream respectively) and the integration locus, including several base pairs specific for the knockout construct. The other primer from the primer pair was specific exclusively for the knockout construct. The final primer pairs used were designed to confirm the *Tgdhfr-ts* gene presence (1419 x 1420 and 190D x 191D), and to analyse for the wild type *Pbtert* presence, the fragment that should not be detected in the positively transfected parasites (primers 3271 x 3272). The FIGE blot performed from the agarose-embedded parasite blocks was probed with the 3' *P. berghei dhfr-ts* UTR probe for determination of chromosomal integration. The probe binds both to the wild type 3' region of the *P. berghei dhfr-ts* gene located in chromosome 7 and to the integration site in the chromosomes of the positively transfected parasites. Three transfections of this *tert* knockout construct were performed, with the experiments number 1065, 1078 and 1138 (for detailed transfection procedure see Materials and Methods), and the analysis of genomic DNA by PCR was subsequently performed. Eight μL of each PCR reaction was run on a 1% agarose gel stained with ethidium bromide (final concentration 0.5 ug/mL). The expected products for successful site-specific integration of the construct into the *P. berghei* genome were obtained in all three transfection populations (see Fig. 68A and B). The 5' and 3'

integration PCRs (lanes 1 and 2 respectively) as well as the *Tgdhfr-ts* PCRs were all positive. In the analysis of the 1065 uncloned population two reactions were set up for the *Tgdhfr-ts* gene (lanes 4 and 5 in the first gel on the left in Fig. 68A). Since both set of primers were efficient in the reactions, subsequent analysis was performed with 1419 x 1420 primer pair only (lane 4). The presence of the band specific for the wild type *Pbtert* gene in the transfected population indicates the presence of the wt parasites (Fig. 68A lane 3) and that the population is mixed and parasite cloning is required.

The FIGE blots for 1065, 1078 and 1138 TERT transfections are shown in Fig. 68C. The positions of some of the *P. berghei* chromosomes are indicated. The *Pbtert* gene is located on chromosome 14. Therefore on a FIGE blot of a positive TERT transfection, probed with the 3' UTR *Pbdhfr-ts* probe, a signal in chromosome 13/14 should be visible (since the two chromosomes migrate together under standard conditions of separation), as well as in chromosome 7 (the 3' UTR of the wild type *Pbdhfr-ts* gene). From the performed transfections, only the 1065 experiment seems positive (left FIGE blot), where a clear signal in chromosome 14 and chromosome 7 can be observed. The ratio of the observed signals can provide additional information on the transfection/integration efficiency. In the case of 1065 population the signal ratio between chromosome 13/14 and chromosome 7 is relatively high. The probe has bound specifically to the two sites, and no plasmid signal is observed. The other two transfection experiments 1078 and 1138 seem negative, since there is no signal in chromosome 13/14, but the probe has bound to chromosome 7 (the middle and rightmost FIGE blots). In both cases the probe has also reacted with chromosome 2/3. This is because the TERT transfections 1078 and 1138 were performed in a parasite line stably expressing green fluorescent protein (GFP) throughout the complete life cycle (Franke-Fayard et al., 2004). The GFP was found to be integrated in chromosome 3, together with the 3' UTR from *Pbdhfr-ts*. The signals in other chromosomes of the 1078 and 1138 transfection populations are either the plasmid used for the transfections or random integrations, though random integrations of the *Pbtert* construct into chromosome 9, 10 and/or 11 only is very unlikely. Furthermore, a plasmid usually migrates at the sizes of chromosome 8 to 9/10/11. The strong signal observed in 1078 between chromosome 8 and co-migrating chromosomes 9-11 is most probably the TERT plasmid-derived signal. Another indication for plasmid presence is the signal ratio of the undefined band to the chromosome-specific bands, which is usually quite high (though in the case 0f 1138 all the signals are relatively strong). In the case of 1078 and 1138 transfection populations the inconsistency of the FIGE results with the PCR results is most probably due to the fact that the PCR method is a much more sensitive technique than FIGE.

Fig. 68 Analysis of the tert k.o. transfection populations by PCR and FIGE. Three transfections with the *tert* knockout construct were performed. (A) Analysis by PCR showed that all three transfections resulted in construct integration. The 5' and 3' integration products, as well as the *Tgdhfr-ts* gene fragment were obtained in 1065, 1078 and 1138 *tert* transfections. The wild type *tert* band, which is the only band visible in the wild type control (gel on the left), is also present in the transfection samples indicating the wild type gDNA presence. The primer pairs used are schematically depicted in (B), and the expected product sizes are listed in the table. (C) FIGE blots from the parasite blocks from each transfection were probed with the 3' *Pbdhfr-ts* UTR probe. The positions of some of the chromosomes are indicated. Only in the case of the 1065 transfection the signal is visible in chromosome 13/14, where integration should occur. In the 1078 and 1138 FIGEs the absence of the integration signal in chromosome 13/14 (marked by a star) is probably due to the low number of parasite chromosomes that contain the integrated construct. Chromosome 7 is the location of the *Pbdhfr-ts* gene, therefore the signal in that chromosome is due to the presence of the wild type 3' UTR. 1078 and 1138 transfections were performed in the reference GFP line, where the *gfp* gene together with the 3' *Pbdhfr-ts* UTR is present in chromosome 3. Signal in other chromosomes comes most probably from the plasmid used for transfection (see text for details). *p25*-specific primers were used as a positive PCR control, in the negative control "-" on gDNA was present.

III.10.3Cloning of the TERT knockout parasites.

In order to analyse the telomerase k.o. effects a homogenous parasite line should be obtained. Since the 1065 transfection population contained some wild type parasites cloning of the knockout parasites was performed. Even though all the three attempts to delete the *P. berghei* telomerase reverse transcriptase gene were positive by PCR, only the 1065 transfection population was chosen for further analysis. This was due to the fact that in the FIGE experiment transfection population 1078 and 1138 (Fig. 68C) showed no signal in chromosome 13/14, indicating that the percentage of the parasites with stably integrated *tert* replacement construct was very low, making the cloning procedure technically challenging. The 1065 transfection population exhibited high signal ratio of chromosome 13/14 to chromosome 7, with specific probe binding. Therefore the parasite cloning from the 1065 population should be highly efficient.

From the first successful transfection (1065) five clones were obtained by limiting dilution method (see Materials and Methods). Initially, according to the standard procedure, three out of five 1065 clones were analysed for *tert* replacement construct integration by PCR (Fig. 69 clones 1, 2 and 3). Eight μL of each PCR reaction was run on a 1 % agarose gel stained with ethidium bromide. The same set of primers like for the diagnostic PCR of gDNA from the transfection population (Fig. 68) was used. The 5' and the 3' integration-specific PCR reactions were run in lanes 1 and 2, respectively. Surprisingly, in none of the three clones PCR products from these reactions were obtained, and repeating the experiment gave the same results. Unexpectedly, both reactions for amplifying a fragment of the deleted *Pbtert* gene and the *Tgdhfr-ts* gene (lanes 3 and 4) gave the products of the correct sizes (see the table in Fig. 69). In the wild type control only the wild type *Pbtert* band is observed (the bottom right gel in Fig. 69). The uncloned 1065 population was used as an additional control in this experiment. Both the 5' and 3' integration bands are present, as well as the wt *Pbtert* gene fragment, and the *Tgdhfr-ts* gene fragment. Due to these unexpected results, the cloning of the 1065 parasite population was repeated with the liquid N_2-stored 1065 population. Out of ten infected mice, six had detectable parasitemia. Blood was collected from all six mice and all six parasite clones (1065 clones 4 – 9) were first analysed by integration-specific PCRs (see Fig. 69), as in the case of clones 1 – 3. Strikingly, the same results were observed like for the first three clones. The 5' and 3' integration bands were absent, whereas both the *Tgdhfr-ts* and the *Pbtert* gene fragments amplified.

Fig. 69 PCR analysis of 1065 clones 1 – 9. The 5' and the 3' integration PCRs (lanes 1 and 2 respectively) did not show any products, whereas surprisingly products of expected sizes were obtained from reactions for the presence of the wild type tert gene (lane 3) and *Tgdhfr-ts* gene (lane 4). The same set of primers like for the analysis of the uncloned populations was used. *p21*-specific primers were used as a positive control for the PCR reactions ("+"). The water control is marked as "-".

The first possible explanation of this unusual result was that the wrong parental parasite population had been used due to procedural errors during the initial storage of the parasites or during the cloning. Such an error would explain the presence of the wild type *tert* gene and the *Tgdhfr-ts* gene. Indeed, another line (1066) was cloned simultaneously with 1065 and the clones obtained from that line were positive, with successful target gene deletion. The integration PCRs specific for 1066 were performed on the putative 1065 clones 1, 2 and 3. In all three clones the 5' and 3' integration reactions did not show any products, whereas the deleted gene band was present, eliminating the possible line confusion.

Another way of explaining the results would be *Tgdhfr-ts* integration in an alternative locus in addition to the target site. To exclude the possibility of the *Tgdhfr-ts* gene integration in the wild type *Pbdhfr-ts* locus (chromosome 7), through recombination between this locus and the homologous 5' and/or 3' UTR regions of the selectable marker cassette, FIGE of 1065 clones 1, 2 and 4 – 9 was performed (Fig. 70). Probing the membrane with the commonly used 3' UTR probe resulted in two signals – one

in chromosome 13/14, where the integration event was expected to occur, and the second signal in chromosome 7, where the wild type 3' *Pbdhfr-ts* UTR is located. Following stripping, another probe specific to the *Tgdhfr-ts* complete gene was applied (blot on the right). The signal was only observed in chromosome 13/14 indicating that the *Tgdhfr-ts* gene is not present in chromosome 7, and that the integration occurred in chromosome 13 or chromosome 14. Increased exposure time did not reveal any additional signals.

Fig. 70 FIGE of 1065 clones 1, 2 and 4 – 9. The FIGE was first probed with 3' *Pbdhfr-ts* UTR-specific probe (blot on the left). Signals were detected in both chromosome 7 and chromosome 13/14. Then, the membrane was stripped, and re-probed with *Tgdhfr-ts* sequence. The signal was only visible in chromosome 13/14 indicating that *Tgdhfr-ts* gene did not integrate into the *Pbdhfr-ts* locus in chromosome 7.

To confirm the finding from the FIGE experiment for the presence of *Tgdhfr-ts* gene in chromosome 7, additionally a PCR was performed (for clones 1 – 3), implementing the same analysis scheme as for the diagnostic integration-specific PCRs of the transfection populations and the clones (Fig. 71). Two set of primers were used for the 5' and 3' integration reactions (primers 3580 x L391 and 1419 x 3581, respectively). The *tert* gene and *Tgdhfr-ts* gene presence was checked using primers amplifying the internal gene fragments (3271 x 3271 and 1419 x 1420, respectively). In lane 1 in Fig. 71 we can observe unspecific reaction products, with one particularly strong band, though not of the expected size. This is due to the GC-rich *T. gondii* gene-specific primer, which had to be used together with the *P. berghei* sequence-specific primer with significantly lower annealing temperature. Therefore the unspecific PCR products were caused by the *T. gondii* primer alone, what is shown in Fig. 71 on the lower gel (lane 1, 1a and 1b).

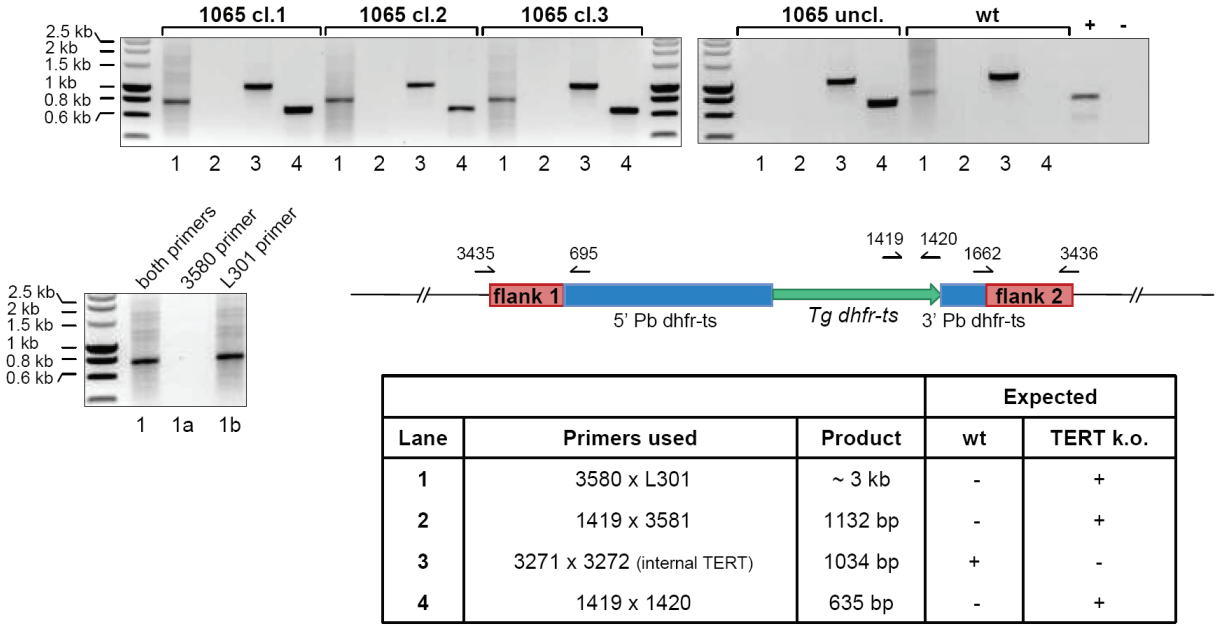

			Expected	
Lane	**Primers used**	**Product**	**wt**	**TERT k.o.**
1	3580 x L301	~ 3 kb	-	+
2	1419 x 3581	1132 bp	-	+
3	3271 x 3272 (internal TERT)	1034 bp	+	-
4	1419 x 1420	635 bp	-	+

.

Fig. 71 Determination of *Tgdhfr-ts* presence in chromosome 7 by PCR. The set of primers used included the 5' and 3' integration primers (lanes 1 and 2 in the table), internal *tert* and *Tgdhfr-ts* primers (lanes 3 and 4). Unspecific PCR products can be seen in lane 1. The unspecific amplification was caused by the GC-rich L301 primer used. This is proved by running a PCR reaction with both primers, and with each primer separately (3580 primer – lane 1a, L301 primer – lane 1b). No products were observed in lane 2, either in 1065 clones, or in the uncloned population. The *tert* band is present in the wt as well as in the uncloned population (lane 3). As previously described the *tert* PCR product is also seen in the 1065 clones. *Tgdhfr-ts* gene is present in all the clones and the uncloned sample (lane 4), it is absent in the wt. *p21*-specific primers were used as a positive control for the PCR reactions ("+"). The water control is marked as "-".

Yet another theory was that the plasmid, contrary to expectation and theory, was still present in the wild type parasites, enabling parasite survival under pyrimethamine pressure. The standard cloning procedure involves no drug selection and the parasites should therefore eliminate the plasmid. All the 9 clones were obtained from non-pyrimethamine treated mice. However one could not exclude that the copy of the *Tgdhfr-ts* gene in these parasites is carried on the pL1324 TERT plasmid. Using gDNA from 1065 clones 1, 2 and 3 PCR reactions were performed using the same principle as for the integration-specific PCRs, though this time the primers used for the 5' and 3' reactions were instead specific only to the plasmid used for transfection (Fig. 72, lanes 1 and 2 and the scheme below). The usual control PCRs for the wt *tert* and *Tgdhfr-ts* were also performed (lanes 3 and 4, respectively). No amplification was obtained in lanes 1 and 2 either for the clones or the 1065 uncloned. In the case of the pL1324 TERT plasmid used as a positive control, amplifications in lanes 1 and 2 (for the plasmid presence) were positive. The *Tgdhfr-ts gene* (lane 3) is present, because it is carried on the plasmid. Additionally, plasmid rescue was performed, which means that bacterial cells are transformed with the extracted parasite DNA. The method relies on the fact that if any plasmid with a gene conferring resistance to antibiotics (e.g. Amp^R gene) is present in the transfected sample, then the bacteria transformed with this plasmid would grow on antibiotic–containing agar. Since all plasmids used for *P. berghei* transfection contain the Amp^R gene, DNA from all the clones was transfected into bacteria. Only one agar plate contained bacterial colonies (1065 clone 2) – these colonies were picked and

amplified; plasmid was extracted and digested with restriction enzymes. No bands of the expected sizes were present, indicating the pL1324 TERT absence.

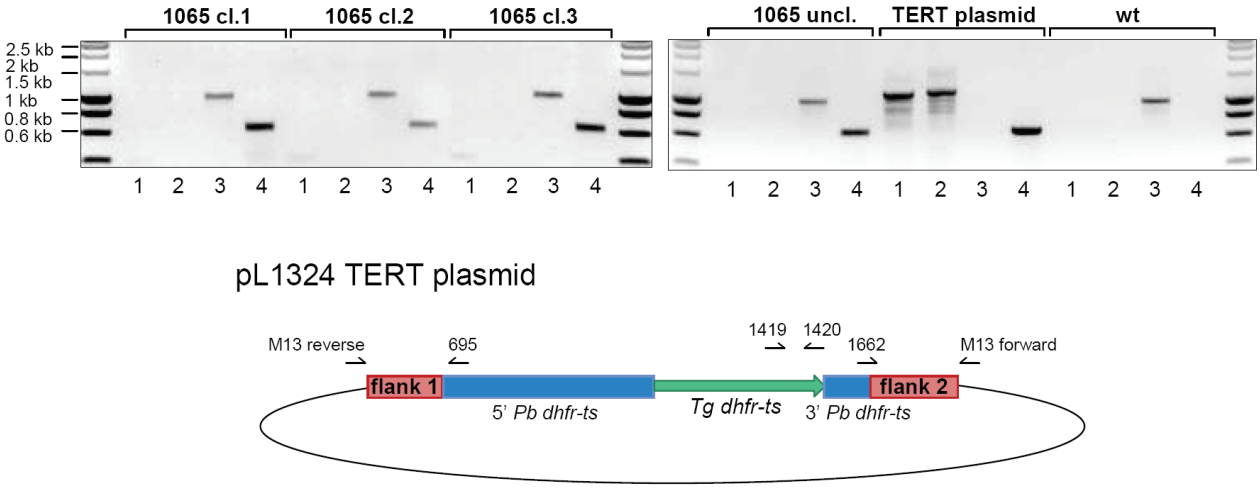

			Expected		
Lane	**Primers used**	**Product**	**wt**	**TERT k.o.**	**TERT plasmid**
1	M13 reverse x 695	1109 bp	-	-	+
2	M13 forward x 1662	1166 bp	-	-	+
3	3271 x 3272 (internal TERT)	1034 bp	+	-	-
4	1419 x 1420	635 bp	-	+	+

Fig. 72 Analysis for pL1324 TERT plasmid presence in 1065 clones 1- 3 and 1065 uncloned. Genomic DNA was used in PCR reactions with the primers listed in the table and indicated on the schematic plasmid representation. In lanes 1 and 2 products are present only in the TERT plasmid control, as expected. The *tert* and *Tgdhfr-ts* gene fragments (lanes 3 and 4, respectively) were amplified in all clones and the uncloned sample. The wt control shows only the TERT band (lane 3).

For each cloning procedure the transfected parasite population (stored in liquid N_2) has to first develop in mice for at least 11 days. The *Pbtert* k.o. parasite cloning was performed twice, each time the original transfection population was used. Therefore, three uncloned 1065 parasite populations were obtained: one from the transfection, second one from the first cloning procedure and the third one from the repeated cloning (1065 uncloned 1, 2 and 3, respectively). The populations were analysed for the 5' and 3' integration, *tert* gene presence and *Tgdhfr-ts* presence (Fig. 73). The 5' and 3' integration bands were present in the first two samples but absent in the sample collected before the second cloning procedure. However both the *tert* and *Tgdhfr-ts* genes were detected in all three uncloned 1065. Repeating the PCR for the 1065 uncloned 3 sample gave the same results. The 1065 uncloned 1 shows stronger 5' and 3' integration bands than the 1065 uncloned 2. According to these results the original transfection population (1065 uncloned 1) contains positively transfected parasites. The 1065 uncloned 2 and uncloned 3 populations were derived from the 1065 uncloned 1 population, therefore the 1065 uncloned 2 and 3 have undergone at least 12 additional erythrocytic cycles. Therefore the

transfected parasites in the latter two uncloned populations could be gradually disappearing (manifested by less prominent 5' and 3' integration bands in uncloned 2). The 1065 uncloned 2 and 3 persisted in mice for approximately same amount of time, since for each cloning procedure the parasites were taken from the initial liquid N_2-stored transfection population (1065 uncloned 1). Therefore it was surprising to see the absence of the integration bands in the 1065 uncloned 3 sample.

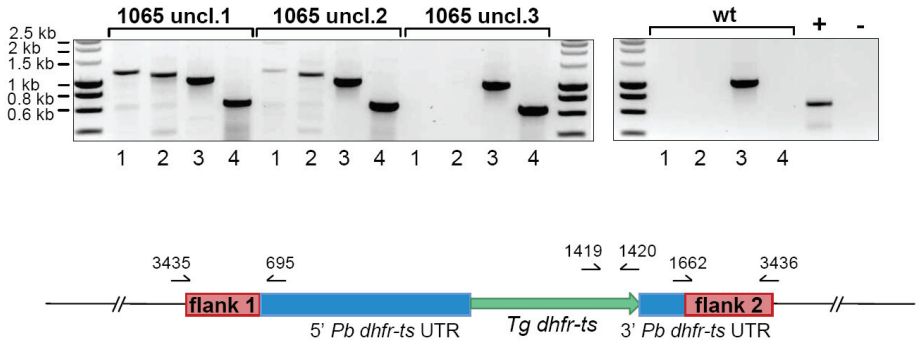

			Expected	
Lane	**Primers used**	**Product**	**wt**	**TERT k.o.**
1	3435 x 695	1208 bp	-	+
2	1662 x 3436	1132 bp	-	+
3	3271 x 3272 (internal TERT)	1034 bp	+	-
4	1419 x 1420	635 bp	-	+

Fig. 73 Analysis of the three uncloned populations collected after transfection (the original transfection population 1065 uncloned 1), before the first cloning procedure (1065 uncloned 2) and before the second cloning (1065 uncloned 3). The 5' and 3' integration-specific PCR products were run in lanes 1 and 2, respectively. In the case of 1065 uncloned 3 no products were obtained for the 5' and 3' integration check. The *Pbtert* gene band (lane 3), as well as the *Tgdhfr-ts* band (lane 4) are both present in all the uncloned samples (the same result obtained before). The wt control shows only the expected *tert* band. In the positive control for PCR primers for *p21* gene were used. The water control "-" without gDNA shows no products. Schematic representation of primer positions is depicted below the gel. The expected sizes are summarized in the table.

III.10.4Extensive cloning of the TERT mutant population.

The previous three attempts to delete the *tert* gene from the wt *P. berghei* genome were unsuccessful. The *tert* knockout construct was previously shown to be integrated in the expected locus (as shown for uncloned parasite populations). FIGE analysis of both the uncloned and cloned *tert*$^-$ parasites indicated correct integration of the targeting construct into chromosome 13/14 (wt *Pbtert* locus – chromosome 14). However the 5' and 3' integration-specific PCR products could not be obtained for the cloned parasites. Therefore yet two transfections were performed (experiments 1207 and 1217, Fig. 74A and B) with a positive outcome in both cases.

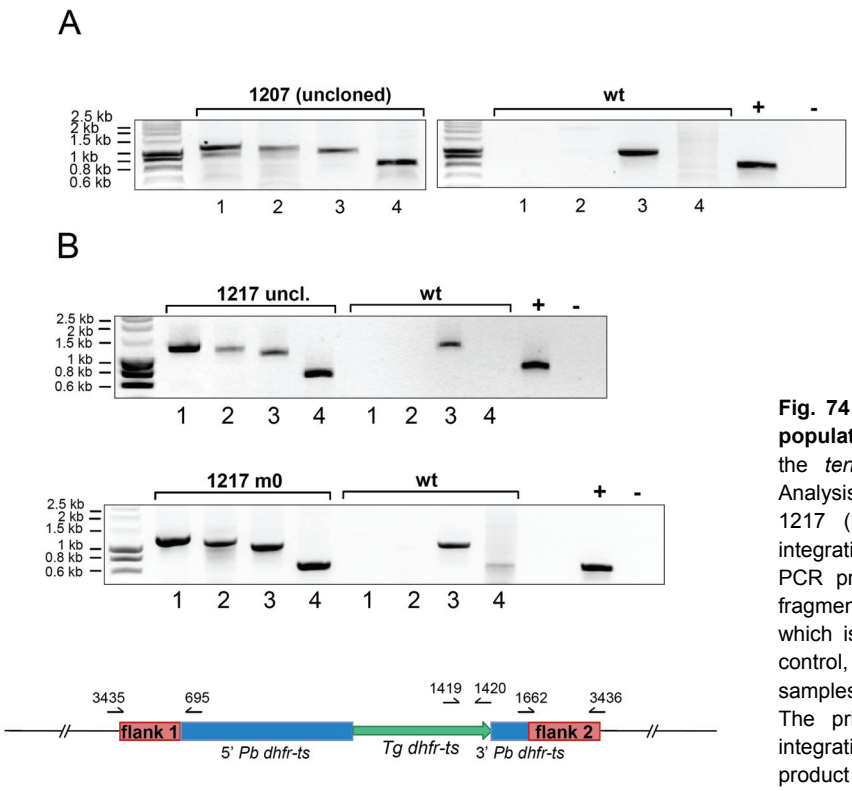

			Expected	
Lane	**Primers used**	**Product**	**wt**	**TERT k.o.**
1	3435 x 695	1208 bp	-	+
2	1662 x 3436	1132 bp	-	+
3	3271 x 3272 (internal TERT)	1034 bp	+	-
4	1419 x 1420	635 bp	-	+

Fig. 74 Analysis of the tert k.o. transfection populations. Two additional transfections with the *tert* knockout construct were performed. Analysis by PCR showed that both 1207 (A) and 1217 (B) transfections resulted in construct integration. The 5' and 3' integration-specific PCR products, as well as the *Tgdhfr-ts* gene fragment were obtained.The wild type *tert* band, which is the only band visible in the wild type control, is also present in the transfection samples indicating the wild type gDNA presence. The primer pairs used are depicted in the integration locus scheme, and the expected product sizes are listed in the table.

Since the previous cloning efforts failed to obtain cloned *tert*$^-$ parasites, a higher scale cloning procedure was employed, using the 1217 *tert* knockout population. The cloning procedure commonly involves ten mice of which usually between 1 and 5 become positive. In order to increase chances of obtaining *Pbtert*$^-$ cloned parasites the number of mice was doubled. Cloning was performed by limiting dilution, statistically resulting in 2 parasites per injection. Seven out of twenty mice developed patent parasitaemia. A tentative analysis of parasite clones' genomic DNA by integration-specific PCRs revealed no successful clones. Thorough analysis of the obtained clones has been performed, and did not result in a positive clone.

III.11 Telomerase RNA (TR) analysis

The telomerase-associated RNA molecule was analyzed for presence in several *P. berghei* stages by Northern blotting (Fig. 75). Probe specific to the sequence of the predicted telomerase RNA was used, and as a loading control 5' lsu-specifc probe was utilized. TR is found in all analysed samples, though

in much lower quantities in ring and early trophozoite stages than in mature trophozoite and schizonts, what is consistent with the PfTERT presence analysis by Figueiredo et al., where in immunofluorescence analyses of infected erythrocytes, signal from PfTERT was detectable beginning at a trophozoite stage, throughout schizogony, and until the release of merozoites. Here, one can see that TR is also readily detected in gametocytes.

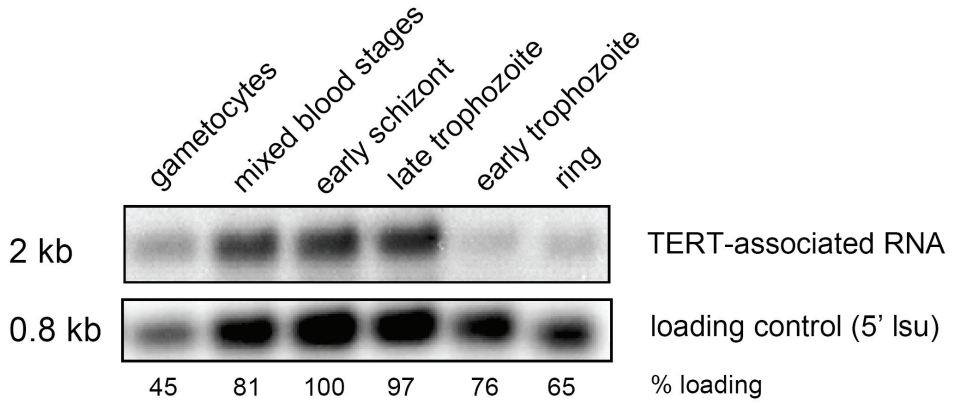

Fig. 75 Northern blot for the TR presence in several *P. berghei* life cycle stages. In the upper panel a probe to the putative TERT-associated RNA was used. In the lower panel a loading control is shown (probe to A/B/C/D-lsu 5').

III.12 Immunodetection of *P. berghei* TERT using PfTERT antibody.

PfTERT antibody specificity was assessed in Western analysis (Fig. 76). Total protein of *P. berghei* ANKA HP asexual blood stages in a reduced and non-reduced state was run on a 12% SDS-polyacrylamide gel. Following blotting and blocking overnight in 3 % milk (in 0.1% PBS-Tween) the protein membrane was probed with an anti-PfTERT antibody raised in rabbit (courtesy of Artur Scherf) at a 1:500 dilution in PBS-Tween. Subsequently the membrane was extensively washed (0.1% PBS-Tween), and the secondary antibody (anti-rabbit, HRP-conjugated) was applied at a 1:1000 dilution. Two specific bands (or alternatively 1 thicker band) were detected in the reduced HP sample. The expected molecular weight of the PbTERT protein is approximately 240 kDa (gene size of ~6.6 kb). The signal visible in the reduced HP lane appears to be of the correct size and is highly specific, indicating cross-reactivity of the PfTERT antibody to PbTERT protein.

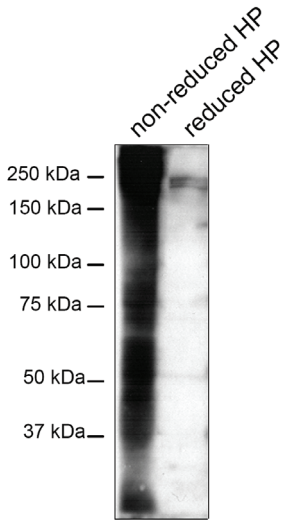

Fig. 76 Western analysis of PfTERT antibody. Total protein of *Pb* ANKA HP asexual blood stages was analysed on a 12% SDS-polyacrylamide gel. The sample was either in a non-reduced or reduced (+ DTT) state. The PfTERT (raised in rabbit) was used in 1/500 dilution. Two specific bands at a size between 150 and 250 kDa were detected in the reduced sample (expected size ~240 kDa).

IV. DISCUSSION AND FUTURE PERSPECTIVES

IV.1 SIR2 proteins

SIR2 deacetylases mediate silencing at the chromosome ends in the human malaria parasite *Plasmodium falciparum*. The two sirtuins SIR2A and SIR2B were shown to regulate transcription of members of the *var* multigene family, which plays an essential role in the parasite's evasion of the host immune system. Even though *vars* are confined to *P. falciparum,* multigene families encoding predicted surface proteins that share characteristics of the *var* family (defined by the presence of a PEXEL motif, transmembrane domains, signal peptides and clustered location in the subtelomeric regions of the chromosomes) were found in other human and primate *Plasmodium* species. The multigene families found in rodent parasites are not well studied, but are believed to play an analogous role to *var* and other multigene families in escaping the host immune system. The *sir2a* and *sir2b* genes are present in all *Plasmodium* species; therefore it is a plausible assumption that their role in regulating the expression of important parasite antigens is conserved within the *Plasmodium* genus. *P. berghei* is a good model in which to perform a comprehensive study of the two identified *Plasmodium* sirtuins, SIR2A and SIR2B, and determine their role in gene silencing, as well as their consequent impact on parasite development and survival. *P. berghei* offers a highly efficient system for genetic manipulation using a vector recycling strategy (Braks et al, 2006) which enabled the sequential deletion of both *sir2* genes from the genome of a single parasite line. The generated *P. berghei sir2a/sir2b*$^{-/-}$ double deletion clone (1184 m1cl1) was analysed for (1) global changes in gene transcription and (2) ability to survive and propagate *in vivo* in the Brown Norway animal model. All generated deletion lines (*sir2a*$^{-}$, *sir2b*$^{-}$ and *sir2a/b*$^{-/-}$) were assessed for their ability to complete the sporogonic cycle in the *Anopheles* host and to subsequently infect a rodent host. These studies have shown for the first time an unexpected and essential role of SIR2A in the parasite survival in the mosquito host, and a dispensable function of SIR2B. The hypothesised role of SIR2A in the sexual stages has been studied and a mechanism for SIR2A action has been proposed.

IV.1.1 Can SIR2s have combined action of its several counterparts in mammals?

The PfSIR2A has been recently shown to have a dual histone acetyltransferase and ADP-ribosyltransferase function. In mammals there are seven sirtuins, each with different substrate specificity. For instance human SIRT2 was shown to be an NAD+-dependent tubulin deacetylase (North et al., 2003). Interestingly several motility-related genes, including tubulin are significantly

under-expressed in the *Pbsir2a/Pbsir2b*$^{-/-}$ clone at gametocyte stage, as seen from the initial microarray data. Furthermore, in *P. falciparum Δsir2a* alpha tubulin is repressed (in rings) as well. It could be that *Plasmodium* SIR2 proteins have yet another additional function, which in mammals is assigned to a single sirtuin. Furthermore this additional activity could be stage specific and functionally associated with the observed loss of ookinete infectivity associated with absence of SIR2A.

IV.1.1.1 *Plasmodium* SIR2A affects telomere length

The Telomere Restriction Fragment (TRF) analysis of *ΔPbsir2a/b* gDNA extracted from mice infected with BN rat blood showed that the average telomere length of the double knockout parasites was increased by up to 45%. The role of SIR2A in telomere length regulation appears to be a conserved function since *P. falciparum* SIR2A deletion parasites also exhibit longer telomeres (Tonkin et al., 2009). The absence of SIR2 in yeast leads to prolonged acetylation states of the telomere-proximal histones leading to decreased chromatin condensation at these sites (see Fig. 77). Decondensed chromatin would give telomerase (TERT) opportunity to access and elongate the chromosome ends and as a consequence telomeres should be increasing in length as a function of time. Therefore, in the SIR2-mutant parasites TERT protein activity should be restricted exclusively by its timing of expression and its regulatory factors but not by physical inaccessibility to its substrate. Since senescence is directly related to the average length of a telomere, it would be interesting to perform a *tert* deletion in the *Δpbsir2a/b* parasites. The expectation is that those parasites could be observed more readily than in the attempts reported in this thesis since they would senesce and eventually perish more slowly after an increased number of developmental cycles in comparison to the *tert*-parasites of the wt *P. berghei* ANKA strain background.

Another consequence of an open chromatin structure is an increased recombination rate among accessible parts of chromosomes. The subtelomeric regions in the wild type *P. falciparum* parasites were shown to undergo an intensive ectopic recombination (Freitas-Junior et al., 2000). One can imagine that in the absence of SIR2 telomere-proximal regions undergo recombination at an even greater rate since the local chromatin structure is less compact and contains extended telomeres which will promote hybridisation and recombination. In the human fungal pathogen *Candida albicans sir2* deletion leads to a significant increase in recombination rate between various chromosomes (Perez-Martin et al., 1999). In yeast SIR2 loss significantly changes double-strand DNA breaks (DSBs) frequencies of 12% of yeast genes (Mieczkowski et al., 2007).

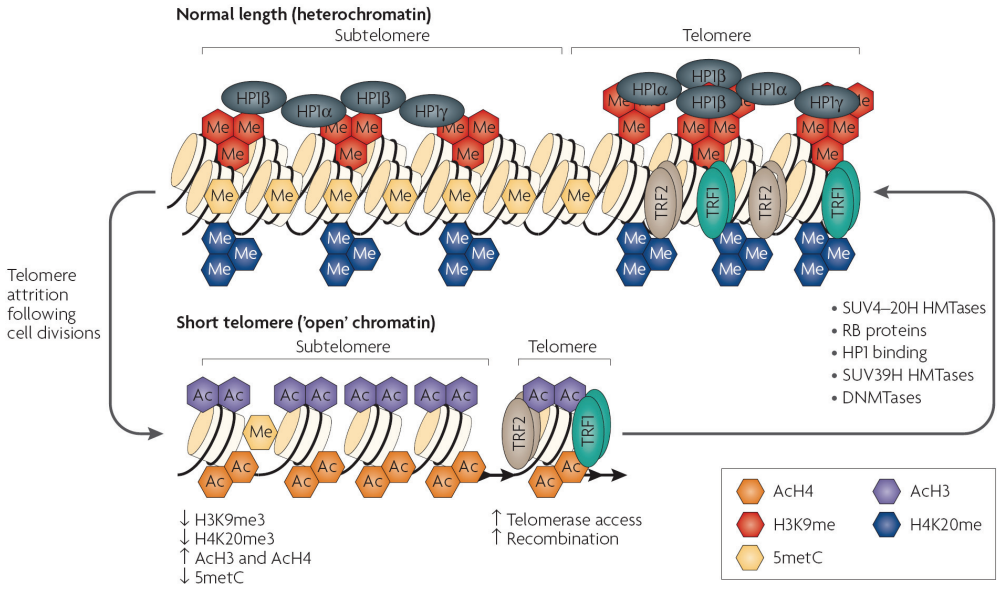

Fig. 77 Schematic represenatation of a condensed and "open" chromatin structure at telomere-proximal regions of a chromosome. Illustration from a review by Blasco, 2007.

Possible major chromosomal rearrangements in *ΔPbsir2a/b* could be examined using a Karyotype and Restriction Display-Pulsed Field Gel Electrophoresis (KARD-2D-PFGE) analysis (Brugere et al., 2000a). The (KARD-PFGE) protocol involves 1-D chromosome separation, digestion with a restriction enzyme(s), Klenow radiolabeling of genomic DNA with [α-^{32}P]dCTP and 2-D separation of restriction fragments followed by autoradiography (see scheme A below). Alternatively single chromosome analysis using a similar technique (developed by the same research group), namely double or multiple-restriction enzyme digestion of isolated chromosomes (DDIC)-2D-PFGE could be performed (see B). The former technique would allow for analysis of specific chromosome regions, here being mainly subtelomeres bearing most of multigene families. A restriction enzyme analysis of chromosomes based on PFGE has been previously developed in *Plasmodium* (van Lin et al., 1997; van Lin et al., 2001). Using this technique Brugere *et al*. showed subtelomeric rearrangements in the genome of the microsporidian parasite *Encephalitozoon cuniculi* (Brugere et al., 2000b).

A **B**

KARD-PFGE

DDIC-PFGE

IV.1.2 Does Sir2 affect cellular localisation of genes within the nucleus by altering their transcriptional status?

A number of studies report that a gene localisation within a nucleus is dependent on its transcriptional status (for recent reviews seeElcock and Bridger, 2010; Zhao et al., 2009). RNA synthesis was shown to be generally more active in the diffused interior euchromatin than in the condensed peripheral heterochromatin (LITTAU et al., 1964). In *P. falciparum* members of the *var* multigene family localise to the nuclear periphery, and these are both silenced and actively transcribed *var* genes although the latter occupies a specialised compartment that contains nucleolar components (Freitas-Junior et al., 2005; Marty et al., 2006, respectively). SIR2A deletion does not affect the positioning of telomere clusters (Marty et al., 2006). However the effect of SIR2A absence on *var* transcripts localisation has not been determined. In support of this observation, recent findings suggest that in general the nuclear pore complex (NPC) plays a functional role in generating and maintaining chromatin boundaries (e.g. Ishii et al., 2002; Schober et al., 2009; Tan-Wong et al., 2009). When a fully completed genome sequence is available, analysis of the location of individual multigene family members in *P. berghei* nuclei as well as other putative SIR2 target genes should provide more insights into gene positioning and transcription within the nucleus. Since SIR2 takes part in transcriptional regulation it is likely that in *Δpbsir2a/b* parasites SIR2-controlled genes would localise to different nuclear sites than in the wild type parasites. For gene localisation studies DNA/RNA Fluorescent *in situ* hybridisation are usually performed and have been for *P. falciparum* (Freitas-Junior et al., 2005; Marty et al., 2006; Mancio-Silva et al., 2008). Unfortunately technical problems did not allow for in-depth study of the chosen candidate genes, within the project time frame. Since this study could be more conclusive with a proper NPC marker, an orthologoue of SUN1 protein was identified in *P. berghei* (PlasmoDB ID: PB001544.02.0; new GeneDB ID: PBANKA_143090). Attempts to tag the putative NPC protein were to date unsuccessful and should be repeated, though SUN1 tagging effects might be hampering its proper function and therefore be deleterious to the parasite it might therefore need to be expressed as a transgene. The role of the nuclear architecture in the complex mechanism of regulation of important *Plasmodium* genes is a yet almost unstudied field of the parasite biology, and is of potential interest in terms of both drug target discovery and broadening of general and parasite-specific gene regulation and organisation processes.

IV.1.3 PbSIR2A and PbSIR2B interaction partners

The determination of the interaction partners of both PbSIR2A and PbSIR2B will allow for further clarification of the epigenetic silencing SIR2-mediated mechanism through identification of the putative transcriptional silencing complex components. Preliminary pull-down experiments using anti-GFP antibody on PbSIR2A::GFP gametocyte extracts, although not entirely conclusive, showed a presence of two of the four ALBA domain-containing proteins (GeneDB IDs: PBANKA_120440 and

PBANKA_136030, respectively; data not shown). These two ALBA proteins both contain a putative but conserved Lys 16 acetylation site (Philip et al., unpublished data). In contrast the highly expressed ALBA 3 (PBANKA_135920), which lacks the conserved Lys 16 and is therefore not predicted to undergo acetylation, was not immunoprecipitated. If this finding is confirmed our hypothesis of SIR2A regulating the ancient ALBA domains remains valid, indicating an active though indirect role of PbSIR2A in the translational repression process through the regulation of the activity of ALBA proteins (see Fig. 78 for schematic representation of SIR2 action). However, in the light of RNA sequencing data generated from gametocytes of wt and *sir2* deletion mutants it appears that ALBA proteins play a non-critical role to repressed mRNA stabilisation, since the steady state transcript levels of the majority of translationally repressed mRNAs remain unchanged in gametocytes (see "SIR2 and translation repression complex" below).

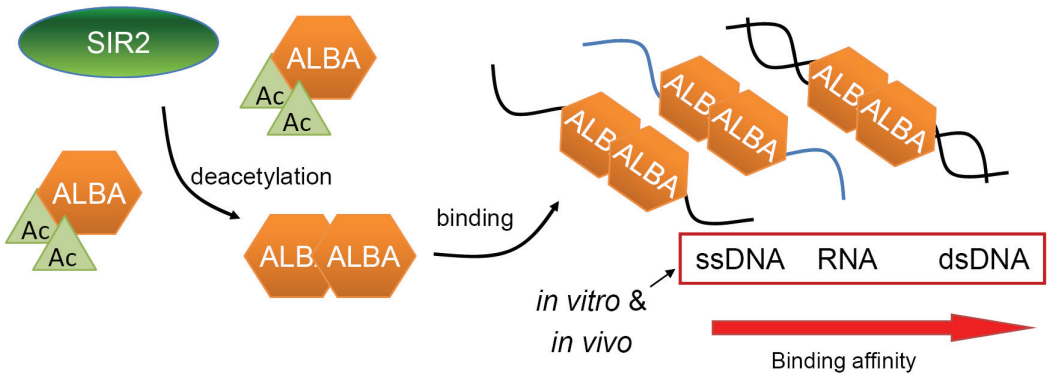

Fig. 78 SIR2 possible mode of action. SIR2 deacetylates ALBA proteins, which then undergo dimerisation and bind with increased affinity to single stranded DNA and RNA, and double-stranded DNA. The red arrow indicates increase in binding affinity to the nucleic acids mentioned, shown both *in vitro* and *in vivo*.

SIR2A::GFP exhibits a highly localised staining pattern in the apical region and nuclear periphery at the ookinete stage (see Results chapter). The intriguing localisation is to date unidentified and not characterised, since the region does not appear morphologically distinctive in light microscopy and transmission electron microscopy images. One way to characterise the region is through the interacting proteins present at the sites of SIR2A::GFP action. No specific proteins were found in the preliminary pull-down experiments of SIR2A::GFP expressing ookinetes. Therefore, although time does not permit, the introduction of a cross-linker, under properly optimised conditions, should increase the chance for immunoprecipitation of temporary SIR2A interactants, providing us with some ideas as to the function and components of the elusive SIR2A sites of action.

The analysis of SIR2A::GFP expressing gametocyte, ookinete and asexual synchronised stages should reveal the different interaction partners, revealing protein complexes potentially specific to each parasite stage. Additionally, PbSIR2B::GFP pull-downs should facilitate uncovering both common and potential distinct processes, in which the two different *Plasmodium* sirtuins participate.

IV.1.4 *In vivo* effects of *sir2a* and *sir2b* deletion

IV.1.4.1 Brown Norway rat experiments

The favoured assumption was that the SIR2s-null parasites would not be able to withstand a host immune response. Therefore, the Brown Norway (BN) rat model was used for phenotype studies of the *Δsir2a/b* parasites (1184m1cl1) using the transgenic GFP::LUC expressing line (676 m1cl1) as reference in four independent infections (total of 8). All animals whether infected with wt or mutant parasite lines controlled the parasitaemia after one month and evidence for continued infection could only be obtained through mechanical passage of blood to naïve mice where all animals developed patent parasitaemias. Blood passaged from BN rats at regular intervals (every week) and even 3 months after initial infection with both 676 and 1184 lines remained infectious to naïve mice suggesting either no or a counterintuitive function(s) of SIR2 proteins function in antigenic variation and/or the role antigenic variation itself.

Considering these findings, at least two questions arise: What is the explanation for the apparently unaffected capacity of the *Pbsir2a/Pbsir2b* double mutant parasites to evade the host immune system? Is long-term survival in the host beneficial to the parasite? Numerous possibilities suggest themselves: if extra antigens are present on the surface of *Δsir2a/b* parasites and are acting as ligands for host protein binding then *sir2* k.o. parasites may have a sequestration advantage and reside at so far unidentified and perhaps additional sites in the host organism. Alternatively, the pattern of recrudescence may be altered in *Δsir2a/b* parasites and the 3 month time point merely represented an episode where *Δpbsir2a/b* parasitaemia was apparent. In order to assess the effects of long-term infection on the cohort of BN rats infected with either *Δpbsir2a/b* or *gfp::luc* parasites in these experiments, the animals were homologously super-infected, 7 months after the initial infections, with high numbers of 1184 *Pbsir2a/Pbsir2b* double knockout and 676 (*gfp::luc*) schizonts and the 676 sequestration pattern assessed with whole animal imaging (Franke-Fayard et al., 2006). Unfortunately 1184 sequestration could not be studied due to lack of luciferase gene expression in these parasites. However, no major differences were observed between the *sir2* mutant and *gfp::luc* parasites by Giemsa-stained blood smears analysis, and as previously observed no changes occurred in the 676 line sequestration patterns (data not shown). In fact some recent findings from homologous infections of mice with wild type and a non-sequestering mutant (SMAC-null parasites) might indicate that sequestration is an advantageous process to *P. berghei* (Franke-Fayard et al., unpublished data). In non-splenectomised mice infected with a mixed population of wt and *smac*$^{-}$ (1:1 ratio) *smac*-null parasites are efficiently removed from the circulation by the spleen. Upon spleen removal *smac* k.o. parasites recover their ability to maintain the infection though still not as efficiently as the wild type. Therefore it appears that the parasite sequestration allows for both spleen avoidance and facilitation of efficient infection and promotion of survival. If that is indeed the case it could be that 1184 asexual parasites are not only fully sequestration competent but exhibit even a prolonged survival time in comparison to wild type because they are withheld from the immune system. At this point it would be

of great interest to generate *sir2a* and *sir2b* single and the double deletion parasites in the *gfp::luc* background in order to characterise the mutant sequestration patterns *in vivo*.

1) Sera collection from the Brown Norway rats

Serum collection from the infected BN rats will permit further investigation of the immune responses to *Δpbsir2a/b* parasites. The specificity of the sera (or antibodies within) collected from both *Δpbsir2a/b*- and GFP::LUC-infected rats should be analysed by Western and Immunofluorescence. It is anticipated that *Δpbsir2a/b* parasites express an increased number of surface antigens due to the absence of SIR2 and failure to repress the expression of SIR2 gene targets (and not due to selection pressure of the host immune system). Therefore the sera from *Δpbsir2a/b*-infected BN rats should react with multiple proteins expressed in *Δpbsir2a/b* parasites as well as all possible surface antigens expressed by the wt parasites at the time. In other words, the wt parasites should undergo efficient switching of their antigens on the red blood cell surface, and as a consequence different antigens should be recognised in wild type parasites cultured in different mice/rats, whereas the *Δpbsir2a/b* antigen repertoire should be global and unchanged assuming the enlarged *Δpbsir2a/b* antigen repertoire is presented to the host immune system.
The protective nature of the collected antibodies can be analysed *in vivo* by passive transfer to naïve rats and/or mice which may indicate that the protein products of SIR2 controlled genes are the targets of protective immune responses.

IV.1.4.2 Mosquito development

Despite no major apparent growth impediments in the asexual blood stages, *ΔPbsir2a/b* parasites cannot be transmitted stalling at the ookinete-to-oocyst stage of the mosquito development; a growth disadvantage not necessarily expected. According to the observations SIR2A$^-$ ookinetes do not cross the midgut epithelium. However based on both light microscopy (toluidine blue staining) and transmission electron microscopy images it is still difficult to assess whether the two knockout line ookinetes attach to the lumen side of the midgut epithelium and cross the peritrophic matrix (PM) or remain trapped within the midgut lumen. Dissections of peritrophic membrane are technically difficult and were not performed in the study. One observation made during mosquito midgut dissections was an atypical characteristic of the midguts themselves infected with the two SIR2A mutants. The midguts were less fragile and appeared uniformly dark in contrast to wild type-infected midguts which were fragile and containing partially clotted blood meal visible as darker regions under a light microscope. To date little is known about molecular factors affecting blood coagulation in *Plasmodium* infections. Several processes have been implicated in changing blood homeostasis in malaria parasite-infected rodent and human hosts (Srichaikul et al., 1975; a recent review by Ghosh and Shetty, 2008). A recent study by Couper et al. has provided evidence for blood plasma-residing microparticles (MPs) as the main inducers of innate pro-inflammatory responses such as TNF-α and IL-6 production in malaria

infection which in turn initiate a complex process of blood coagulation (including platelet activation, aggregation, fibrinogen activation, fibrin strands formation). Microparticles, which arise following cell death, contain parasite material and were shown to be derived almost exclusively from infected red blood cells (Couper et al., 2010). Occasional infection of platelets (=thrombocytes) results in platelet cell death leading to further activation of naive thrombocytes. Furthermore, platelet aggregation is enhanced by exogenous iRBCs-derived adenosine diphosphate, ADP (Inyang et al., 1987), as well as attachment of parasitised cells to blood vessels endothelium causing endothelium damage and subsequent release of von Willebrand Factor (vWF), widely known to trigger blood clot formation (De et al., 2007).

The fact of increased blood clotting in *Plasmodium*-infected blood is consistent with our observations of wild type-infected midguts containing partially clotted blood patches. Interestingly a substantial blood coagulation in concentrated ookinete cultures was observed for the wild type 507 cl1 (GFP_{con}) parasites but not for the *sir2a* (1022 cl2) and *sir2a/b* (1184 m1cl1) mutants. One arguable hypothesis is that SIR2A-null parasites do not excrete sufficient quantities of certain factors, such as e.g. ADP, the reserves of which could be utilised in the purine/pyrimidine pathways seemingly activated in the absence of the SIR2A protein at the gametocyte stage (see Results chapter: “Gametocyte transcriptome analysis of sir2a/b double deletion parasites by RNA-sequencing”. Therefore, it could be that blood coagulation is not activated in 1022 and 1184 parasite infections and that these parasites are in a way less virulent, though still able to successfully infect and propagate through the asexual cycle. Surely, the true biological consequences of SIR2A absence remain to be fully characterised. Nevertheless, this aspect of SIR2A function is intriguing and could bear major insights into *Plasmodium* behaviour in both vertebrate and *Anopheles* hosts.

Another hypothesis for the defective ookinete midgut invasion is an enhanced immune response raised by the *Anopheles* host or that the parasite is more susceptible to the standard innate immune responses elicited by *Plasmodium* parasites. Defence mechanisms of the mosquito against the parasite invasion have recently been studied in more detail, and have emerged as a means to prevent the spread of malaria, for instance by introducing transgenic, *Plasmodium*-resistant mosquitoes with fitness advantages when compared to natural populations (Marrelli et al., 2007). The perspective of a possible enhanced immune response mounted in the mosquito against SIR2A-deficient parasites or that the mutant parasite is less able to survive the normal immune response are yet to be explored.

1) Ookinete motility

SIR2 activity in general affects many cellular pathways and so the effects of *sir2a* deletion might potentially stem not from a single faulty process but from multiple pathways. Ookinete motility in Matrigel™ is decreased 2-2.5 fold in case of *sir2a* and *sir2a*/*sir2b* k.o. parasites compared to wild type. However, the reduction in motility may not be sufficient to be the only cause of the observed complete block in parasite transmission. On the other hand the matrigel-based motility assay has been shown to

give inconsistent results with motility assays performed on glass slides, in insect cells suspension, as is the case for e.g. CDPK3$^-$ parasites (Siden-Kiamos et al., 2006; Ishino et al., 2006; Moon et al., 2009). Motility of the *cdpk3*$^-$ ookinetes in matrigel is between 3 to 6.5 times slower than for the wild type (Moon et al., 2009; Ishino et al., 2006), whereas according to the glass slide motility assay *cdpk3*$^-$ parasites exhibit hardly any movement. Nevertheless, the observed reduction of 98-99% in oocyst numbers for *cdpk3* mutant is consistent in all of these studies. The decrease of 2-2.5 fold noted for SIR2A mutants might therefore significantly contribute to the midgut invasion phenotype reported here. Interestingly, *cdpk3*$^-$ ookinetes aggregate in the vicinity of mosquito midgut epithelium as a result of blood meal digestion process itself. TEM images of the *sir2a*$^-$ parasites were obtained however most probably due to technical problems with tissue penetration by the epoxy resin, it was not possible to assess if the aggregation phenomenon is also observed for *Δsir2a* ookinetes.
One possible explanation for the motility deficiency of the mutants is that *sir2a* affects transcription of motility-associated genes. RNA sequencing data of the gametocyte stage indicates several tubulin-related/kinesin proteins, which are downregulated in the double *sir2a/b* k.o. (see Results, section "Deregulated genes in the *Δsir2a/b* line"). These proteins have been either experimentally confirmed to participate in parasite motility or bioinformatically assigned to the gliding motility functional cluster (Zhou et al., 2008). As previously mentioned one of human sirtuins SIRT2 functions specifically as tubulin deacetylase (North et al., 2003), therefore a SIR2A connection with motility is conceivable.

2) Ookinete surface and secreted proteins

Of the ookinete-specific proteins analysed, Plasmepsin 4 (PM 4) and Pbs28 do not seem to be globally affected. However chitinase could be a good candidate to explain the observed midgut invasion deficiency of *sir2a* mutant ookinetes. Preliminary results from an *in vitro*-based chitinase assay point to reductions in either intracellular chitinase protein levels or a chitinase excretion process. Chitinase is required for chitinous peritrophic matrix digestion and subsequent mosquito midgut epithelium invasion. Furthermore, CTRP, another excreted protein that is essential to cross the midgut epithelium appears to be somewhat depleted in the apical end of *Δsir2a* ookinetes but enriched less towards the apical end when compared to wild type GFP_{con} parasites in an IFA (Fig. 55 in Result chapter). Western analysis (non-reducing conditions) indicates that CTRP content of *sir2* deletion mutant ookinetes is elevated compared to wt. It would appear that delivery of the CTRP to the apical end is affected in the *Δsir2* mutants which again may result in the observed reduction in motility. The different effects of SIR2 absence on two microneme proteins indicates that there may be distinct microneme populations or that there may be different modes of protein insertion into micronemes which are differentially affected by the activity of SIR2A. However. much further and thorough analysis of microneme proteins is needed to fully understand the aspects of SIR2A affecting the action and transport of invasion-facilitating proteins.

3) Is SIR2A essential for sporozoite formation and liver development?

Haemocoel injections have shown that Δ*sir2a* parasites are able to produce oocysts when the midgut barrier is bypassed. The oocysts retain the capacity to mature and produce sporozoites, which are released and found at the site of mosquito salivary glands but appear to develop more slowly. Currently it is unclear whether the sporozoites are able to attach and successfully invade salivary glands (SGs), and subsequently establish a liver and blood stage infection following infected mosquito feeding on a rodent host. It is essential to continue with the study of SIR2A effects on sporozoites, if the observed delay in sporozoite arrival at SGs is confirmed and the invasion ability of sporozoites analysed. It would be fascinating if *sir2a* deletion causes a general invasion phenotype at the ookinete and sporozoite invasive mosquito stages of *P. berghei* development. Sirtuins in *Plasmodium* might indeed play additional highly parasite-specific roles, not observed in other organisms studied to date.

IV.1.5 Analysis of acetylation status of putative substrates of sirtuins in *P. berghei sir2a*$^{-}$ and *sir2b*$^{-}$ clones.

Plasmodium species, like other eukaryotes, have several putative histone deacetylases (according to PlasmoDB data). In other organisms functions of deacetylases overlap, though their gene or genomic region specificity usually differ. At the moment it is not clear if the effects of *Pbsir2a* and *Pbsir2a/Pbsir2b* double deletion are, among others, due to decreased acetylation at putative SIR2 target histones. Using a standard chromatin immunoprecipitation (ChIP) with anti-acetylated histone antibodies and deep sequencing, comparison of the wild type versus all *Δsir2* parasites histone acetylation status can be assessed either globally or at the level of individual genes. This analysis would also allow for a quantitative assessment of the proportion and location of genome association of histones deacetylated by SIR2s with regard to the total histone deacetylation, in addition to the qualitative analysis by IFA already performed. An additional application of telosome pull down could be the identification of telomere-associated proteins (TAPs) by Mass Spectrometry. A comparison of the wt *P. berghei* ANKA strain to the *Δsir2* parasites should possibly reveal differences in the TAPs composition of the generated lines, at the same time also indicating direct SIR2s interaction partners.

Immunofluorescence assay with a global anti-acetylation antibody showing acetylation levels in *Δsir2a* and *Δsir2a/b* ookinete nuclei did not reveal prominent differences from wild type, but the fluorescence signal could not be quantitatively assessed. Interestingly in all analysed ookinetes a “dotty” signal of acetylation antibody was also detected outside the ookinetes nuclei. A similar speckled appearance has been observed in mitochrondrial staining with MitoTracker^{TM} (see Results section, Fig. 35) and partially in microneme staining with α-CTRP and α-PM 4 antibodies (see Results Fig. 55). Interestingly secretory proteins sorting and maturation involves several steps, starting from endoplasmic reticulum

(ER) through Golgi complex where multiple post-translation protein modifications occur, including acetylation. The system of ER, Golgi vesicles and cisternae, and subsequent other vesicular compartments have a progressively acifidifying environment (Anderson and Pathak, 1985; Burgess and Kelly, 1987; see Fig. 79 below). Both pH and acetylation influence the stability and structure of proteins, furthermore the solubility of proteins decreases below their isoelectric point. Therefore, conditions of low pH and increased acetylation (which results in a decrease in local protein charge) may critically destabilise the native state of proteins (Hiraga et al., 1964; Kim et al., 1991; Batra and Uetrecht, 1990) In this kind of environment proteins are usually found in a state termed molten globule (MG), an intermediate state between the native and the denatured state. The MG state is characterised by a native-like secondary structure but with loosely packed amino acids in the interior. Knowledge on post-translation modifications of micronemal proteins is scarce, and to date no micronemal proteins were shown to be acetylated. However, since a multitude of cellular proteins is regulated by acetylation, this modification may well affect microneme-localised proteins as well. SIR2A being a deacetylase is hereby postulated to deacetylate at least some micronemal proteins, thereby increasing their solubility. This event would in turn allow for proper folding and transition into a native state, at which protein function could be executed. The observed apical SIR2A::GFP localisation, as well as “empty” pink-stained apical end indicating local low pH in the SIR2A-null parasites (both 1022 and 1184 lines) is consistent with this proposed model for one SIR2A function (see Results chapter, Fig. 50 for images). It would appear that in the case of CTRP that it is possible that the activity of SIR2A is associated with transport to the apical end of the ookinete which might then depend upon correct folding in an increasingly acidic environment. Therefore, the predominant MG state of micronemal proteins in the *sir2a* mutants could be one explanation for protein presence but non-functionality in these parasites, thereby hindering the mosquito midgut barrier traversal. At this point many analyses including proteome and in particular acetylome and *in situ* structural studies of microneme proteins would be crucial for understanding and confirmation of the proposed mechanism.

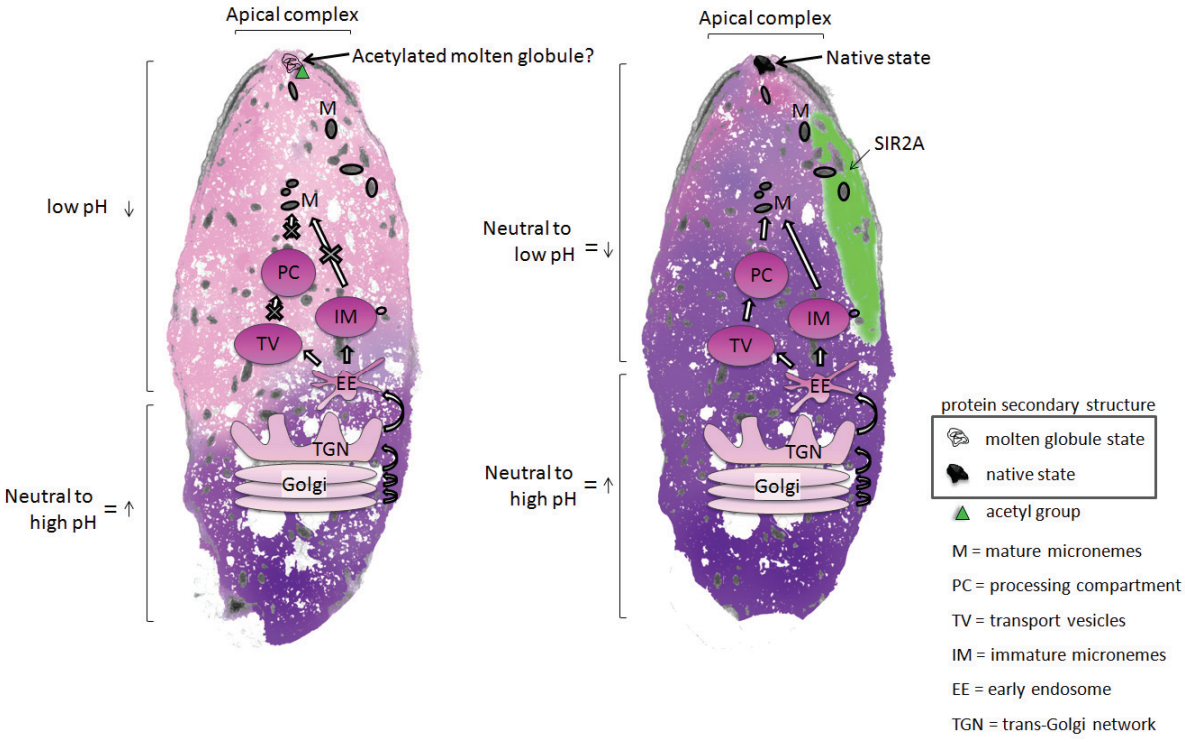

Fig. 79. Model for SIR2A action at the apical end. The model for protein transport in the ookinete is based on a proposed model for *T. gondii* trafficking of micronemal proteins (modified from Huynh et al., 2006). Micronemal polypeptides travel through a number of organelles undergoing post-translational modifications (possibly including acetylation), under increasingly acidic conditions; the proteins pass from Golgi and trans-Golgi network (TGN) through early endosomes (EE) to either transport vesicles (TVs), which fuse with processing compartments (PC) or immature micronemes (IM). The target structures are mature micronemes (M). Right image: In an ookinete expressing SIR2A::GFP (503 cl1) the apical complex is stained by Giemsa similar to wild type (slightly pink), indicating a local decrease in pH. SIR2A::GFP localises to the apical, membrane-proximal region where it deacetylates proteins in a molten globule (MG) state (= a partially native state). Deacetylation causing increased solubility allows for the completion of protein folding resulting in a fully functional native state (black protein pointed with an arrow). The proteins are then ready to perform their action either intracellularly or extracellularly. Left image: SIR2A-null ookinetes stain light pink at a substantial part of the apical region. Polypeptides trafficking through the transport network remain acetylated at their target microneme compartments due to absence of the SIR2A deacetylase. The MG state proteins (arrow pointing to acetylated molten globule) remain non-functional or partially functional, and are either secreted or remain within a mutant ookinete. Alternatively SIR2A could also influence transport of a population(s) of proteins/vesicles, resulting in a depletion of the cargo from the apical end (as seen for CTRP for instance; crossed arrows).

Alternatively the speckled appearance could mark the mRNPs previously identified in gametocytes, which could be present in the ookinete stage as well (Mair et al., 2010; see the point below for more details).

IV.1.6 Sirtuins influence transcription of a number of genes

Since SIR2 is known to function as a deacetylase in transcriptional regulation of genes by controlling the acetylation status of histone tails, deletion of the two SIR2s in *P. berghei* should affect transcriptional status of any SIR2-controlled genes. These we would anticipate are likely to be

organised in the subtelomeric regions but may also occupy preferred locations within the body of a chromosome *e.g.* internal *var* clusters (Gardner et al; Duraisingh et al). In the RMSANGER and Singapore-produced long oligonucleotide DNA array analysis RNA samples from 1184 m1 cl1 and HP parasites at 5 (rings), 10 (early trophs), 16 (late trophs) and 24 (schizonts) hours post infection were analysed in duplicate. The biggest changes were observed at the ring parasite stage, and no major differences were detected at the schizont stage. The majority of analysed genes are annotated as hypothetical, therefore the analysis has been challenging. Some annotated genes included *Pb-fam* and *bir* genes, as well as other multigene family members, found manually by BLAST algorithm search. However, the representation of the upregulated multigene family members is lower than expected based upon their representation in the current annotation of the *P. berghei* genome. This anomaly highlights current difficulties with the use of microarrays to study gene expression and in particular those located in the sub-telomeric regions. Both arrays were designed on the basis of the assembly of the 8x coverage of the *P. berghei* genome. However the data obtained from the probe/signal analysis of the arrays was processed using a lower coverage assembly, and therefore many potentially differentially transcribed genes are suspected to be missing from the final differentially expressed gene list. Furthermore the data obtained from cross chip comparisons revealed major inconsistencies between the two sets of DE genes. Nevertheless both array types showed deregulation of different members of *P. berghei* sub-telomeric multigene families. Unfortunately telomere-proximal regions of the genome might not be well represented on both arrays since sequencing of these regions is highly problematic and reads are difficult to assemble due to the particularly repetitive nature of the *P. berghei* sub-telomeric regions. Taken together these factors have resulted in a poor annotation state of the rodent malaria genomes which has hindered the analysis. The microarray data should possibly be reanalysed using the newest release of the *P. berghei* genome assembly and annotation which might rationalise the discrepancies in the data sets from the two arrays. Nevertheless, the fact that *Pb-fam* and *bir* genes are present on both DE gene lists means there could be more multigene family members on which SIR2 exerts an effect, but their telomere-proximal location renders them impossible to detect with the arrays in their current state of readiness.

In the light of the obtained microarray results we have decided to utilise a newly developed RNA sequencing technology to analyse transcriptional changes in the *sir2a/b* double deletion mutant. Ring, gametocyte and ookinete stages material has been collected. To date only gametocyte samples were processed and transcriptome analysed. The remaining samples await processing.

Of the 100 deregulated genes identified, annotated *birs* and *Pb-fams* contribute 1/3 (n=28, range of deregulation +8 fold change to -13 fold change for *Δsir2a/b* over wt) which favours a function for the *P. berghei* SIR2s in the regulation of multigene families in a manner similar to that of *P. falciparum* sirtuins in *var* gene control. However, despite RNA-seq advantages subtelomeric regions are still problematic to analyse due to exceptionally high gene sequence redundancy and persistent incomplete assembly of the telomere regions of the *P. berghei* genome. Manual assessment of the sequence tags located in the subtelomeres might be possible, however undoubtedly this time-

consuming task would still be hampered by high sequence redundancy of the telomere-proximal regions.

Similarly to microarray results, gametocyte RNA-seq data showed that most of the DE genes in the *sir2a/b* mutant are up-regulated and include several transcription- and translation-related genes, including ribosomal genes (discussed below), as well as some metabolism-related genes. These data support are consistent with PbSIR2s performing a canonical function as general transcriptional repressors and environment-dependent metabolic and translational regulators (through NAD^+ levels sensing).

1) SIR2 and translational repression complex

The possible function of SIR2 in the deacetylation of the ALBA-domain proteins implies that sirtuins might affect RNA stability or deployment disrupting the proper function of translational repression (TR) complex in gametocytes (Mair et al., 2010). However, the fact that SIR2A-null parasites develop into mature at least partially motile ookinetes speaks against SIR2A being a member of the messenger ribonucleoprotein (mRNP) in an essential and global DOZI- or CITH-like manner. Notwithstanding the fact, one cannot exclude SIR2A being a contributor or having an indirect influence on the mRNP at gametocytes stage with an ultimate effect on ookinete phenotype.
Unsurprisingly, RNA-seq data from gametocytes showed that the mRNA species encoding TR complex members themselves were not affected, since their transcripts most likely would have to be affected at an earlier stage in the parasite life cycle in order to prevent protein translation. There is also no direct effect of SIR2A absence at the steady state transcriptional level on most of the translationally repressed genes identified in the gametocyte TR complex. However several (n=9) genes of the top 50 down-regulated list were identified as common to both *Δsir2a/b* and *Δdozi* down-deregulated genes data sets. Interestingly all the annotated genes that were commonly downregulated are linked to the parasite motility process and the *sir2a*$^-$ and *sir2a/b*$^{-/-}$ ookinetes both have reduced motility. It is possible that SIR2A therefore affects the expression of a subset of TR transcripts resulting in a more discrete phenotype than that observed in the *dozi* k.o. mutant.

It is worth mentioning that the composition of mRNPs is thought to be dynamic and that different complexes exist within gametocytes (Mair et al., 2010). Furthermore, it is a plausible theory that TR complexes are not gametocyte-specific but that they are present in other *Plasmodium* stages, such as ookinete (observation by A. Waters group, unpublished data). SIR2A could be an active participant in the hypothesised translational repression process in ookinetes, which could be yet another explanation for its essential role in parasite development in the mosquito. Further work is required to investigate this possibility.

2) SIR2 and ribosomal proteins

Interestingly a number of ribosomal proteins are present on DE gene lists from both asexual stages microarray and gametocyte RNA-seq data; the majority being up-regulated, and some slightly under-expressed in the *P. berghei sir2a/sir2b* double deletion mutant. Numerous studies report evidence for direct ribosomal protein acetylation (Brot and Weisbach, 1972; Liew and Gornall, 1973; Takakura et al., 1992). Acetylation is thought to act as a stabilising factor preventing ubiquitination of lysine residues, which mediates targeting of proteins for proteasomal degradation. N-terminal acetylation is one of the most common protein modifications in eukaryotes and is found on approximately 85% of all mammalian and 50% of all yeast proteins (Polevoda and Sherman, 2003). There are several reports of ribosomal protein deacetylation by HOS2 and RPD3 in yeast *Saccharomyces cerevisiae* (Kurdistani et al., 2002; Robyr et al., 2002). The two yeast proteins share 69% similarity. Interestingly, BLASTing both HOS2 and RPD3 protein sequences against the PlasmoDB protein database of all *Plasmodium* species resulted in identification of the same single orthologoue in each of the species (*P. berghei* orthologoue PB000903.02.0 – 66% similarity to HOS2 and 73% to RPD3). Yeast SIR2 was reported to interact with RPD3 deacetylase, and a number of other deacetylases, including ESA1, GCN5, RPD3, SAS2, as well as some methylases, such as DOT1, SET1, which in turn were shown to influence several acetyltransferases. It may be that *Plasmodium* SIR2s exert an effect on ribosomal proteins through a network of direct or indirect protein interactions. There are precedents for this, a recent report by Yang ey al. (2010) have shown that the mammalian mitochondrial SIRT3 directly associates and deacetylates a mitochondrion ribosomal protein MRPL10 in a NAD^+-dependent manner. This SIRT3 function has apparently a direct effect in mitochondrial protein synthesis levels. Indeed a study by Gazda et al. (2006) provided evidence for a proportional correlation between a ribosomal protein level (here RPS19) and its transcription levels. Interestingly, *rps19* deficiency leads to co-down regulation of a number of other ribosomal genes. Another group found that one of the human ribosomal proteins S13 regulates the expression of its own gene *via* a protein concentration feedback loop (Malygin et al., 2007). An even more captivating fact is a recently shown inverse dependence of yeast life span on ribosomal protein levels (Steffen et al., 2008). This observation is in a perfect accordance with SIR2 function as life-span regulator through, among others, ribosomal proteins.

IV.1.7 Are sirtuin inhibitors/activators potential anti-malarials?

IV.1.7.1 Inhibitors

Sirtuin inhibitors are already available and under development and their effects on parasite survival might be addressed experimentally. Since the SIR2 genes are individually non-essential to both *P. falciparum* and *P. berghei* blood stages the use of SIR2 inhibitors is likely to be restricted to therapeutic strategies that seek to enhance the immunity of the host to the parasite and are unlikely to

be specific mediators of direct parasite killing. However, since PbSIR2A is essential for parasite transmission, sirtuin inhibitors could be a part of anti-malarial therapy, contributing to the reduced transmission of parasites from treated individuals (e.i. transmission-blocking strategy).

Several specific sirtuin inhibitors have been developed to date, including sirtinol (Pallos et al., 2008), AGK2, specific to SIRT2 (Outeiro et al., 2007), splitomycin and several derivatives (Bedalov et al., 2001; Pagans et al., 2005; Posakony et al., 2004), and SIRT5-specific suramin (Schuetz et al., 2007; Trapp et al., 2007). Interestingly suramin was shown to act against sleeping sickness, caused by *Trypanosomes* (Bisaggio et al., 2008). A highly sirtuin-specific inhibitor has been recently developed against a *Leishmania* sirtuin (LiSIR2RP1, Tavares et al., 2010). The inhibitory action of the bisnaphthalimidopropyl (BNIP) is in the low micromolar range and the compound is selective toward the parasite enzyme when compared with human SIRT1.
Of the available sirtuin inhibitors a number have been tested and only nicotinamide is an efficient PfSIR2A inhibitor *in vitro* although acting in the μM range albeit in a dose-dependent manner. Complete inhibition of SIR2 activity was abolished only at a level of 10 mM nicotinamide and therefore pharmacologically unusable (Merrick and Duraisingh, 2007). Although, nicotinamide also showed anti-malarial activity against cultured *P. falciparum* (Prusty et al., 2008), at high IC_{50} value (10 mM) most likely due to off-target in view of the non-essential nature of SIR2 in *Plasmodium*. Similarly a novel competitive PfSIR2A inhibitor surfactin was able to inhibit *P. falciparum* growth in culture at a low concentration (10 μM) (Chakrabarty et al., 2008). However the surfactin inhibitory effect may also be exerted through SIR2-independent effects on the parasite since it was shown to induce apoptosis and cycle arrest-mediated killing of human colon carcinoma cells (Kim et al., 2007). Since genetic deletion of SIR2s shows no major effects on parasite growth in asexual stages, extensive drug tests should be performed on mosquito stages of *Plasmodium* to assess the possible application of sirtuin inhibitors in transmission-blocking anti-malaria therapies.

IV.1.7.2 Activators

Numerous studies indicate that resveratrol, which is the most renowned sirtuin activating compound (STAC), prolongs life-span of nematode worms, fruit flies, rodents and recently chimpanzees ((Baur et al., 2006; Lagouge et al., 2006)) at least in part through SIR2-like protein activation. Resveratrol derivatives have been developed and are highly potent (for a recent review see Alcain and Villalba, 2009). The effects of such activators on *Plasmodium* have yet to be elucidated, though based on evidence from other organisms, including other protozoa sirtuin activation or over-expression e.g. *Leishmania*, *Trypanosoma* and *Dictyostelium* (Vergnes et al., 2002; Garcia-Salcedo et al., 2003; Katayama and Yasukawa, 2008) should be highly advantageous to the parasite, which perhaps points to some commonality of sirtuins functions aside from *Plasmodium*-specific roles of the sirtuin family.

Much remains to be learned about the roles and functions of sirtuins in *Plasmodium*. Uncovering critical parasite-specific roles of SIR2s opens an entire new area of pathogen research which might be crucial to understanding parasite biology as well as provide new insights into the broad features of sirtuin biology.

IV.2 TERT protein

IV.2.1 TERT has an evolutionary conserved function in *Plasmodium*

The TERT deletion clones could not be obtained. Interestingly clone analysis reveals construct integration into the predicted chromosome (FIGE) and the presence of *T. gondii dhfr* selectable marker, as well as wt *Pbtert* gene, whereas the 5' and 3' integration-specific amplifications were unsuccessful. Trials of identification of the integration site of *Tgdhfr-ts* using a novel Tail-PCR approach were so far unsuccessful. PCR-confirmed presence of the wt *tert* gene in the putative *tert*$^-$ clones impels attempts to detect the *Pbtert* transcript presence by both Northern analysis and Reverse Transcriptase-PCR (possible since all putative *tert* deletion clones were stored in liquid N_2).

IV.2.2 TR subunit mutagenesis and deletion.

The next step in the telomerase project could be to perform the telomerase-associated RNA knockout. Since telomerase was shown to interact with many diverse proteins, TERT deletion influences a number of pathways, not necessarily telomere-associated (see section "The effect of telomerase absence"). Abolishing TERT RNA component might not be as severe, though in a number of organisms most dysfunctions resulting from TERT and TR loss overlap (see Introduction). The TR locus has been determined *in silico*. Therefore experimental data is needed to validate the bioinformatically predicted location. Primer extension/RACE experiments can be performed to map the 5' terminus of the TR. Another approach could be deletion of the template region from the TR sequence, resulting in functionally assembled TR with TERT still present, but unable to add telomeric repeats to the 3' telomere end. In addition, as mentioned before, *tert* deletion could also be performed in the *sir*2-null parasites, which exhibit an increased average telomere length. The rate of TERT$^-$ parasites disappearance from the transfected population is then predicted to be slower, and that could possibly allow for isolation and analysis of *Δtert* clones.

IV.2.3 Shelterin complex protein identification

Another aspect of the project is telomerase interactome. To date only several orthologous proteins known to interact with telomerase in other organisms, were found by *in silico* analysis in *Plasmodium*. One possibility in addition to the *in vivo* tagging and affinity purification is *in vitro* TERT expression and subsequent analysis of interacting proteins from the parasite extract by mass spectrometry. A *P. berghei* parasite clone expressing C-terminally tagged TERT (2x MYC tag) has been obtained in this project but recent reports indicated it was unsuitable for canonical TERT function studies (data presented on Telomeres and Telomerase meeting, Ladenburg, Germany, 2008). Recent new wheat-germ cell free expression systems appear to be more efficient than previously developed technologies (Endo and Sawasaki, 2006). Such systems could be used in attempts to express the *P. berghei* TERT protein *in vitro*. The only (and major) drawback is that this approach creates the problem of the need to generate full length clones of the TERT ORF as template for RNA synthesis. Nevertheless, both tagged (e.g. N-terminally) or *in vitro* expressed TERT could be used for previously mentioned telosome pull downs in order to identify and characterise telomere-associated proteins (TAPs).

IV.2.4 Anti-telomerase drugs as auxiliary treatment to existing therapies?

In order to confirm or reject the idea of *Plasmodium* telomerase as a potential drug target anti-telomerase/anti-reverse transcriptase drug testing *in vivo* and *in vitro* (as a proof of principle since cell division is a prerequisite for observation of TERT deletion effects) should be performed. The rationales behind the idea are as follows:

- non-nucleoside reverse transcriptase analogoues (NNRTIs) have been shown by Artur Scherf's group to kill *P. falciparum in vitro* after 3-5 blood stage cycles (unpublished data)

- delavirdine (delavirdine) has been shown to efficiently inhibit *P. yoelii* liver stages *in vitro* (Mahmoudi et al., 2008)
    - ƒ 48hr-treatment of *P. yoelii yoelii* infected mouse hepatocytes *in vitro*

- *P. berghei* TERT k.o. parasites most probably disappear from the transfection populations (within 10-20 days after transfection)

In contrast to other mammals rodents possess highly active telomerase in their somatic cells. However TERT or TR deletion effects are globally observed only in the sixth generation. Therefore the telomerase-inhibitors treatment is not expected to impose any effects on the murine organism itself. Treatment of mice with anti-telomerase drugs , such as G-quadruplex-stabilising compounds like

TMPyP4 analogues (Shi et al., 2001), Abacavir and Lamivirudine (Limoges et al., 2000), Delavirdine (Chang et al., 1997), as well as the nucleoside analogues already tested on *P. falciparum in vitro* culture should provide some data on the *in vivo* effects of anti-telomerase drugs on *P. berghei* parasites (possibly liver and/or blood stages), indicating the direction of the future research.

Reference list

Adam,E., Pierrot,C., Lafitte,S., Godin,C., Saoudi,A., Capron,M., and Khalife,J. (2003). The age-related resistance of rats to Plasmodium berghei infection is associated with differential cellular and humoral immune responses. Int. J. Parasitol. *33*, 1067-1078.

Ahuja,N., Schwer,B., Carobbio,S., Waltregny,D., North,B.J., Castronovo,V., Maechler,P., and Verdin,E. (2007). Regulation of insulin secretion by SIRT4, a mitochondrial ADP-ribosyltransferase. J. Biol. Chem. *282*, 33583-33592.

Aigner,S. and Cech,T.R. (2004). The Euplotes telomerase subunit p43 stimulates enzymatic activity and processivity in vitro. RNA. *10*, 1108-1118.

Aigner,S., Lingner,J., Goodrich,K.J., Grosshans,C.A., Shevchenko,A., Mann,M., and Cech,T.R. (2000). Euplotes telomerase contains an La motif protein produced by apparent translational frameshifting. EMBO J. *19*, 6230-6239.

Aikawa,M., Carter,R., Ito,Y., and Nijhout,M.M. (1984). New observations on gametogenesis, fertilization, and zygote transformation in Plasmodium gallinaceum. J. Protozool. *31*, 403-413.

Akhtar,A. and Gasser,S.M. (2007). The nuclear envelope and transcriptional control. Nat. Rev. Genet. *8*, 507-517.

Alcain,F.J. and Villalba,J.M. (2009). Sirtuin activators. Expert. Opin. Ther. Pat *19*, 403-414.

Allis,C.D., Richman,R., Gorovsky,M.A., Ziegler,Y.S., Touchstone,B., Bradley,W.A., and Cook,R.G. (1986). hv1 is an evolutionarily conserved H2A variant that is preferentially associated with active genes. J. Biol. Chem. *261*, 1941-1948.

Allsopp,R.C., Chang,E., Kashefi-Aazam,M., Rogaev,E.I., Piatyszek,M.A., Shay,J.W., and Harley,C.B. (1995). Telomere shortening is associated with cell division in vitro and in vivo. Exp. Cell Res. *220*, 194-200.

Altaf,M., Auger,A., Covic,M., and Cote,J. (2009). Connection between histone H2A variants and chromatin remodeling complexes. Biochem. Cell Biol. *87*, 35-50.

Aly,A.S. and Matuschewski,K. (2005). A malarial cysteine protease is necessary for Plasmodium sporozoite egress from oocysts. J. Exp. Med. *202*, 225-230.

Anderson,R.G. and Pathak,R.K. (1985). Vesicles and cisternae in the trans Golgi apparatus of human fibroblasts are acidic compartments. Cell *40*, 635-643.

Angelov,D., Molla,A., Perche,P.Y., Hans,F., Cote,J., Khochbin,S., Bouvet,P., and Dimitrov,S. (2003). The histone variant macroH2A interferes with transcription factor binding and SWI/SNF nucleosome remodeling. Mol. Cell *11*, 1033-1041.

Aparicio,O.M., Billington,B.L., and Gottschling,D.E. (1991). Modifiers of position effect are shared between telomeric and silent mating-type loci in S. cerevisiae. Cell *66*, 1279-1287.

Artandi,S.E., Chang,S., Lee,S.L., Alson,S., Gottlieb,G.J., Chin,L., and DePinho,R.A. (2000). Telomere dysfunction promotes non-reciprocal translocations and epithelial cancers in mice. Nature *406*, 641-645.

Autexier,C. and Lue,N.F. (2006). The Structure and Function of Telomerase Reverse Transcriptase. Annu. Rev. Biochem.

Azzalin,C.M., Reichenbach,P., Khoriauli,L., Giulotto,E., and Lingner,J. (2007). Telomeric repeat containing RNA and RNA surveillance factors at mammalian chromosome ends. Science *318*, 798-801.

Bahl,A., Brunk,B., Coppel,R.L., Crabtree,J., Diskin,S.J., Fraunholz,M.J., Grant,G.R., Gupta,D., Huestis,R.L., Kissinger,J.C., Labo,P., Li,L., McWeeney,S.K., Milgram,A.J., Roos,D.S., Schug,J., and Stoeckert,C.J., Jr. (2002). PlasmoDB: the Plasmodium genome resource. An integrated database providing tools for accessing, analyzing and mapping expression and sequence data (both finished and unfinished). Nucleic Acids Res. *30*, 87-90.

Banerjee,R., Liu,J., Beatty,W., Pelosof,L., Klemba,M., and Goldberg,D.E. (2002). Four plasmepsins are active in the Plasmodium falciparum food vacuole, including a protease with an active-site histidine. Proc. Natl. Acad. Sci. U. S. A *99*, 990-995.

Bao,Y., Konesky,K., Park,Y.J., Rosu,S., Dyer,P.N., Rangasamy,D., Tremethick,D.J., Laybourn,P.J., and Luger,K. (2004). Nucleosomes containing the histone variant H2A.Bbd organize only 118 base pairs of DNA. EMBO J. *23*, 3314-3324.

Baran,N., Haviv,Y., Paul,B., and Manor,H. (2002). Studies on the minimal lengths required for DNA primers to be extended by the Tetrahymena telomerase: implications for primer positioning by the enzyme. Nucleic Acids Res. *30*, 5570-5578.

Batra,P.P. and Uetrecht,D. (1990). Helix stability in succinylated and acetylated ovalbumins: effect of high pH, urea and guanidine hydrochloride. Biochim. Biophys. Acta *1040*, 102-108.

Baur,J.A., Pearson,K.J., Price,N.L., Jamieson,H.A., Lerin,C., Kalra,A., Prabhu,V.V., Allard,J.S., Lopez-Lluch,G., Lewis,K., Pistell,P.J., Poosala,S., Becker,K.G., Boss,O., Gwinn,D., Wang,M., Ramaswamy,S., Fishbein,K.W., Spencer,R.G., Lakatta,E.G., Le,C.D., Shaw,R.J., Navas,P., Puigserver,P., Ingram,D.K., de,C.R., and Sinclair,D.A. (2006). Resveratrol improves health and survival of mice on a high-calorie diet. Nature *444*, 337-342.

Baur,J.A., Wright,W.E., and Shay,J.W. (2004). Analysis of mammalian telomere position effect. Methods Mol. Biol. *287*, 121-136.

Baur,J.A., Zou,Y., Shay,J.W., and Wright,W.E. (2001). Telomere position effect in human cells. Science *292*, 2075-2077.

Bedalov,A., Gatbonton,T., Irvine,W.P., Gottschling,D.E., and Simon,J.A. (2001). Identification of a small molecule inhibitor of Sir2p. Proc. Natl. Acad. Sci. U. S. A *98*, 15113-15118.

Bednenko,J., Melek,M., Greene,E.C., and Shippen,D.E. (1997). Developmentally regulated initiation of DNA synthesis by telomerase: evidence for factor-assisted de novo telomere formation. EMBO J. *16*, 2507-2518.

Beernink,H.T., Miller,K., Deshpande,A., Bucher,P., and Cooper,J.P. (2003). Telomere maintenance in fission yeast requires an Est1 ortholog. Curr. Biol. *13*, 575-580.

Beetsma,A.L., van de Wiel,T.J., Sauerwein,R.W., and Eling,W.M. (1998). Plasmodium berghei ANKA: purification of large numbers of infectious gametocytes. Exp. Parasitol. *88*, 69-72.

Bell,S.D., Botting,C.H., Wardleworth,B.N., Jackson,S.P., and White,M.F. (2002). The interaction of Alba, a conserved archaeal chromatin protein, with Sir2 and its regulation by acetylation. Science *296*, 148-151.

Berman,J., Tachibana,C.Y., and Tye,B.K. (1986). Identification of a telomere-binding activity from yeast. Proc. Natl. Acad. Sci. U. S. A *83*, 3713-3717.

Bhattacharyya,A. and Blackburn,E.H. (1994). Architecture of telomerase RNA. EMBO J. *13*, 5721-5731.

Bisaggio,D.F., Adade,C.M., and Souto-Padron,T. (2008). In vitro effects of suramin on Trypanosoma cruzi. Int. J. Antimicrob. Agents *31*, 282-286.

Blackburn,E.H. and Gall,J.G. (1978). A tandemly repeated sequence at the termini of the extrachromosomal ribosomal RNA genes in Tetrahymena. J. Mol. Biol. *120*, 33-53.

Blander,G. and Guarente,L. (2004). The Sir2 family of protein deacetylases. Annu. Rev. Biochem. *73*, 417-435.

Blandin,S., Shiao,S.H., Moita,L.F., Janse,C.J., Waters,A.P., Kafatos,F.C., and Levashina,E.A. (2004). Complement-like protein TEP1 is a determinant of vectorial capacity in the malaria vector Anopheles gambiae. Cell *116*, 661-670.

Blasco,M.A. (2007). The epigenetic regulation of mammalian telomeres. Nat. Rev. Genet. *8*, 299-309.

Blasco,M.A., Lee,H.W., Hande,M.P., Samper,E., Lansdorp,P.M., DePinho,R.A., and Greider,C.W. (1997). Telomere shortening and tumor formation by mouse cells lacking telomerase RNA. Cell *91*, 25-34.

Bodnar,A.G., Ouellette,M., Frolkis,M., Holt,S.E., Chiu,C.P., Morin,G.B., Harley,C.B., Shay,J.W., Lichtsteiner,S., and Wright,W.E. (1998). Extension of life-span by introduction of telomerase into normal human cells. Science *279*, 349-352.

Bosoy,D., Peng,Y., Mian,I.S., and Lue,N.F. (2003). Conserved N-terminal motifs of telomerase reverse transcriptase required for ribonucleoprotein assembly in vivo. J. Biol. Chem. *278*, 3882-3890.

Bottius,E., Bakhsis,N., and Scherf,A. (1998). Plasmodium falciparum telomerase: de novo telomere addition to telomeric and nontelomeric sequences and role in chromosome healing. Mol. Cell Biol. *18*, 919-925.

Boulton,S.J. and Jackson,S.P. (1998). Components of the Ku-dependent non-homologous end-joining pathway are involved in telomeric length maintenance and telomeric silencing. EMBO J. *17*, 1819-1828.

Braks,J.A., Franke-Fayard,B., Kroeze,H., Janse,C.J., and Waters,A.P. (2006). Development and application of a positive-negative selectable marker system for use in reverse genetics in Plasmodium. Nucleic Acids Res. *34*, e39.

BRAY,R.S. (1954). The mosquito transmission of Plasmodium berghei. Indian J. Malariol. *8*, 263-274.

Broccoli,D., Smogorzewska,A., Chong,L., and de Lange,T. (1997). Human telomeres contain two distinct Myb-related proteins, TRF1 and TRF2. Nat. Genet. *17*, 231-235.

Brot,N. and Weisbach,H. (1972). The enzymatic acetylation of E. coli ribosomal protein L 12. Biochem. Biophys. Res. Commun. *49*, 673-679.

Brugere,J.F., Cornillot,E., Metenier,G., and Vivares,C.P. (2000a). In-gel DNA radiolabelling and two-dimensional pulsed field gel electrophoresis procedures suitable for fingerprinting and mapping small eukaryotic genomes. Nucleic Acids Res. *28*, E48.

Brugere,J.F., Cornillot,E., Metenier,G., and Vivares,C.P. (2000b). Occurence of subtelomeric rearrangements in the genome of the microsporidian parasite Encephalitozoon cuniculi, as revealed by a new fingerprinting procedure based on two-dimensional pulsed field gel electrophoresis. Electrophoresis *21*, 2576-2581.

Bryan,T.M., Goodrich,K.J., and Cech,T.R. (2000). Telomerase RNA bound by protein motifs specific to telomerase reverse transcriptase. Mol. Cell *6*, 493-499.

Buchman,A.R., Kimmerly,W.J., Rine,J., and Kornberg,R.D. (1988). Two DNA-binding factors recognize specific sequences at silencers, upstream activating sequences, autonomously replicating sequences, and telomeres in Saccharomyces cerevisiae. Mol. Cell Biol. *8*, 210-225.

Burgess,T.L. and Kelly,R.B. (1987). Constitutive and regulated secretion of proteins. Annu. Rev. Cell Biol. *3*, 243-293.

Calderwood,M.S., Gannoun-Zaki,L., Wellems,T.E., and Deitsch,K.W. (2003). Plasmodium falciparum var genes are regulated by two regions with separate promoters, one upstream of the coding region and a second within the intron. J. Biol. Chem. *278*, 34125-34132.

Carey,V.J., Gentry,J., Whalen,E., and Gentleman,R. (2005). Network structures and algorithms in Bioconductor. Bioinformatics. *21*, 135-136.

Carlton,J.M., Angiuoli,S.V., Suh,B.B., Kooij,T.W., Pertea,M., Silva,J.C., Ermolaeva,M.D., Allen,J.E., Selengut,J.D., Koo,H.L., Peterson,J.D., Pop,M., Kosack,D.S., Shumway,M.F., Bidwell,S.L., Shallom,S.J., van Aken,S.E., Riedmuller,S.B., Feldblyum,T.V., Cho,J.K., Quackenbush,J., Sedegah,M., Shoaibi,A., Cummings,L.M., Florens,L., Yates,J.R., Raine,J.D., Sinden,R.E., Harris,M.A., Cunningham,D.A., Preiser,P.R., Bergman,L.W., Vaidya,A.B., van Lin,L.H., Janse,C.J., Waters,A.P., Smith,H.O., White,O.R., Salzberg,S.L., Venter,J.C., Fraser,C.M., Hoffman,S.L., Gardner,M.J., and Carucci,D.J. (2002). Genome sequence and comparative analysis of the model rodent malaria parasite Plasmodium yoelii yoelii. Nature *419*, 512-519.

Carruthers,L.M., Bednar,J., Woodcock,C.L., and Hansen,J.C. (1998). Linker histones stabilize the intrinsic salt-dependent folding of nucleosomal arrays: mechanistic ramifications for higher-order chromatin folding. Biochemistry *37*, 14776-14787.

Chakrabarti,K., Pearson,M., Grate,L., Sterne-Weiler,T., Deans,J., Donohue,J.P., and Ares,M., Jr. (2007). Structural RNAs of known and unknown function identified in malaria parasites by comparative genomics and RNA analysis. RNA.

Chakrabarty,S.P., Saikumari,Y.K., Bopanna,M.P., and Balaram,H. (2008). Biochemical characterization of Plasmodium falciparum Sir2, a NAD+-dependent deacetylase. Mol. Biochem. Parasitol. *158*, 139-151.

Chakravarthy,S. and Luger,K. (2006). The histone variant macro-H2A preferentially forms "hybrid nucleosomes". J. Biol. Chem. *281*, 25522-25531.

Chang,M., Sood,V.K., Wilson,G.J., Kloosterman,D.A., Sanders,P.E., Hauer,M.J., Zhang,W., and Branstetter,D.G. (1997). Metabolism of the HIV-1 reverse transcriptase inhibitor delavirdine in mice. Drug Metab Dispos. *25*, 828-839.

Chen,J.L., Blasco,M.A., and Greider,C.W. (2000). Secondary structure of vertebrate telomerase RNA. Cell *100*, 503-514.

Chen,J.L. and Greider,C.W. (2003). Template boundary definition in mammalian telomerase. Genes Dev. *17*, 2747-2752.

Chookajorn,T., Dzikowski,R., Frank,M., Li,F., Jiwani,A.Z., Hartl,D.L., and Deitsch,K.W. (2007). Epigenetic memory at malaria virulence genes. Proc. Natl. Acad. Sci. U. S. A *104*, 899-902.

Choudhary,C., Kumar,C., Gnad,F., Nielsen,M.L., Rehman,M., Walther,T.C., Olsen,J.V., and Mann,M. (2009). Lysine acetylation targets protein complexes and co-regulates major cellular functions. Science *325*, 834-840.

Claudianos,C., Dessens,J.T., Trueman,H.E., Arai,M., Mendoza,J., Butcher,G.A., Crompton,T., and Sinden,R.E. (2002). A malaria scavenger receptor-like protein essential for parasite development. Mol. Microbiol. *45*, 1473-1484.

Cohen,D.E., Supinski,A.M., Bonkowski,M.S., Donmez,G., and Guarente,L.P. (2009). Neuronal SIRT1 regulates endocrine and behavioral responses to calorie restriction. Genes Dev. *23*, 2812-2817.

Cohn,M. and Blackburn,E.H. (1995). Telomerase in yeast. Science *269*, 396-400.

Collingwood,T.N., Urnov,F.D., and Wolffe,A.P. (1999). Nuclear receptors: coactivators, corepressors and chromatin remodeling in the control of transcription. J. Mol. Endocrinol. *23*, 255-275.

Collins,K. (1999). Ciliate telomerase biochemistry. Annu. Rev. Biochem. *68*, 187-218.

Collins,K. and Gandhi,L. (1998). The reverse transcriptase component of the Tetrahymena telomerase ribonucleoprotein complex. Proc. Natl. Acad. Sci. U. S. A *95*, 8485-8490.

Collins,K. and Greider,C.W. (1993). Tetrahymena telomerase catalyzes nucleolytic cleavage and nonprocessive elongation. Genes Dev. *7*, 1364-1376.

Colman,R.J., Anderson,R.M., Johnson,S.C., Kastman,E.K., Kosmatka,K.J., Beasley,T.M., Allison,D.B., Cruzen,C., Simmons,H.A., Kemnitz,J.W., and Weindruch,R. (2009). Caloric restriction delays disease onset and mortality in rhesus monkeys. Science *325*, 201-204.

Conrad,M.N., Wright,J.H., Wolf,A.J., and Zakian,V.A. (1990). RAP1 protein interacts with yeast telomeres in vivo: overproduction alters telomere structure and decreases chromosome stability. Cell *63*, 739-750.

Cooper,H.M. and Spelbrink,J.N. (2008). The human SIRT3 protein deacetylase is exclusively mitochondrial. Biochem. J. *411*, 279-285.

Copeland,C.C., Marz,M., Rose,D., Hertel,J., Brindley,P.J., Santana,C.B., Kehr,S., Attolini,C.S., and Stadler,P.F. (2009). Homology-based annotation of non-coding RNAs in the genomes of Schistosoma mansoni and Schistosoma japonicum. BMC. Genomics *10*, 464.

Costanzi,C. and Pehrson,J.R. (1998). Histone macroH2A1 is concentrated in the inactive X chromosome of female mammals. Nature *393*, 599-601.

Couper,K.N., Barnes,T., Hafalla,J.C., Combes,V., Ryffel,B., Secher,T., Grau,G.E., Riley,E.M., and de Souza,J.B. (2010). Parasite-derived plasma microparticles contribute significantly to malaria infection-induced inflammation through potent macrophage stimulation. PLoS. Pathog. *6*, e1000744.

Cristofari,G. and Darlix,J.L. (2002). The ubiquitous nature of RNA chaperone proteins. Prog. Nucleic Acid Res. Mol. Biol. *72*, 223-268.

Cubizolles,F., Martino,F., Perrod,S., and Gasser,S.M. (2006). A homotrimer-heterotrimer switch in Sir2 structure differentiates rDNA and telomeric silencing. Mol. Cell *21*, 825-836.

Dame,J.B., Yowell,C.A., Omara-Opyene,L., Carlton,J.M., Cooper,R.A., and Li,T. (2003). Plasmepsin 4, the food vacuole aspartic proteinase found in all Plasmodium spp. infecting man. Mol. Biochem. Parasitol. *130*, 1-12.

Dandjinou,A.T., Levesque,N., Larose,S., Lucier,J.F., Abou,E.S., and Wellinger,R.J. (2004). A phylogenetically based secondary structure for the yeast telomerase RNA. Curr. Biol. *14*, 1148-1158.

de la Barre,A.E., Angelov,D., Molla,A., and Dimitrov,S. (2001). The N-terminus of histone H2B, but not that of histone H3 or its phosphorylation, is essential for chromosome condensation. EMBO J. *20*, 6383-6393.

de la,C.T., Herrero,P., Moreno-Herrero,F., Chaves,R.S., and Moreno,F. (2002). Mediator factor Med8p interacts with the hexokinase 2: implication in the glucose signalling pathway of Saccharomyces cerevisiae. J. Mol. Biol. *319*, 703-714.

de Lange,T. (2004). T-loops and the origin of telomeres. Nat. Rev. Mol. Cell Biol. *5*, 323-329.

de Lange,T., Shiue,L., Myers,R.M., Cox,D.R., Naylor,S.L., Killery,A.M., and Varmus,H.E. (1990). Structure and variability of human chromosome ends. Mol. Cell Biol. *10*, 518-527.

De,M.Q., Groot,E., Lenting,P.J., de Groot,P.G., McCall,M., Sauerwein,R.W., Fijnheer,R., and van,d., V (2007). Thrombocytopenia and release of activated von Willebrand Factor during early Plasmodium falciparum malaria. J. Infect. Dis. *196*, 622-628.

Deitsch,K.W., del Pinal,A., and Wellems,T.E. (1999). Intra-cluster recombination and var transcription switches in the antigenic variation of Plasmodium falciparum. Mol. Biochem. Parasitol. *101*, 107-116.

Deitsch,K.W. and Hviid,L. (2004). Variant surface antigens, virulence genes and the pathogenesis of malaria. Trends Parasitol. *20*, 562-566.

Deng,Z., Norseen,J., Wiedmer,A., Riethman,H., and Lieberman,P.M. (2009). TERRA RNA binding to TRF2 facilitates heterochromatin formation and ORC recruitment at telomeres. Mol. Cell *35*, 403-413.

Dessens,J.T., Beetsma,A.L., Dimopoulos,G., Wengelnik,K., Crisanti,A., Kafatos,F.C., and Sinden,R.E. (1999). CTRP is essential for mosquito infection by malaria ookinetes. EMBO J. *18*, 6221-6227.

Dessens,J.T., Mendoza,J., Claudianos,C., Vinetz,J.M., Khater,E., Hassard,S., Ranawaka,G.R., and Sinden,R.E. (2001). Knockout of the rodent malaria parasite chitinase pbCHT1 reduces infectivity to mosquitoes. Infect. Immun. *69*, 4041-4047.

Dessens,J.T., Siden-Kiamos,I., Mendoza,J., Mahairaki,V., Khater,E., Vlachou,D., Xu,X.J., Kafatos,F.C., Louis,C., Dimopoulos,G., and Sinden,R.E. (2003). SOAP, a novel malaria ookinete protein involved in mosquito midgut invasion and oocyst development. Mol. Microbiol. *49*, 319-329.

Dessens,J.T., Sinden,R.E., and Claudianos,C. (2004). LCCL proteins of apicomplexan parasites. Trends Parasitol. *20*, 102-108.

Dokal,I. (2000). Dyskeratosis congenita in all its forms. Br. J. Haematol. *110*, 768-779.

Dokal,I. (2001). Dyskeratosis congenita. A disease of premature ageing. Lancet *358 Suppl*, S27.

Doolan,D.L. and Hoffman,S.L. (1999). IL-12 and NK cells are required for antigen-specific adaptive immunity against malaria initiated by CD8+ T cells in the Plasmodium yoelii model. J. Immunol. *163*, 884-892.

Dore,E., Pace,T., Ponzi,M., Picci,L., and Frontali,C. (1990). Organization of subtelomeric repeats in Plasmodium berghei. Mol. Cell Biol. *10*, 2423-2427.

Dore,E., Pace,T., Ponzi,M., Scotti,R., and Frontali,C. (1986). Homologous telomeric sequences are present in different species of the genus Plasmodium. Mol. Biochem. Parasitol. *21*, 121-127.

Dreesen,O., Li,B., and Cross,G.A. (2005). Telomere structure and shortening in telomerase-deficient Trypanosoma brucei. Nucleic Acids Res. *33*, 4536-4543.

Drosopoulos,W.C. and Prasad,V.R. (2010). The telomerase-specific T motif is a restrictive determinant of repetitive reverse transcription by human telomerase. Mol. Cell Biol. *30*, 447-459.

Du,J., Jiang,H., and Lin,H. (2009). Investigating the ADP-ribosyltransferase activity of sirtuins with NAD analogues and 32P-NAD. Biochemistry *48*, 2878-2890.

Duraisingh,M.T., Voss,T.S., Marty,A.J., Duffy,M.F., Good,R.T., Thompson,J.K., Freitas-Junior,L.H., Scherf,A., Crabb,B.S., and Cowman,A.F. (2005). Heterochromatin silencing and locus repositioning linked to regulation of virulence genes in Plasmodium falciparum. Cell *121*, 13-24.

Dzikowski,R., Li,F., Amulic,B., Eisberg,A., Frank,M., Patel,S., Wellems,T.E., and Deitsch,K.W. (2007). Mechanisms underlying mutually exclusive expression of virulence genes by malaria parasites. EMBO Rep. *8*, 959-965.

Ecker,A., Bushell,E.S., Tewari,R., and Sinden,R.E. (2008). Reverse genetics screen identifies six proteins important for malaria development in the mosquito. Mol. Microbiol. *70*, 209-220.

Eksi,S., Czesny,B., Greenbaum,D.C., Bogyo,M., and Williamson,K.C. (2004). Targeted disruption of Plasmodium falciparum cysteine protease, falcipain 1, reduces oocyst production, not erythrocytic stage growth. Mol. Microbiol. *53*, 243-250.

Elcock,L.S. and Bridger,J.M. (2010). Exploring the relationship between interphase gene positioning, transcriptional regulation and the nuclear matrix. Biochem. Soc. Trans. *38*, 263-267.

Emery,H.S. and Weiner,A.M. (1981). An irregular satellite sequence is found at the termini of the linear extrachromosomal rDNA in Dictyostelium discoideum. Cell *26*, 411-419.

Endo,Y. and Sawasaki,T. (2006). Cell-free expression systems for eukaryotic protein production. Curr. Opin. Biotechnol. *17*, 373-380.

Fahie,K., Hu,P., Swatkoski,S., Cotter,R.J., Zhang,Y., and Wolberger,C. (2009). Side chain specificity of ADP-ribosylation by a sirtuin. FEBS J. *276*, 7159-7176.

Fang,J., Chen,T., Chadwick,B., Li,E., and Zhang,Y. (2004). Ring1b-mediated H2A ubiquitination associates with inactive X chromosomes and is involved in initiation of X inactivation. J. Biol. Chem. *279*, 52812-52815.

Figueiredo,L.M., Freitas-Junior,L.H., Bottius,E., Olivo-Marin,J.C., and Scherf,A. (2002). A central role for Plasmodium falciparum subtelomeric regions in spatial positioning and telomere length regulation. EMBO J. *21*, 815-824.

Figueiredo,L.M., Rocha,E.P., Mancio-Silva,L., Prevost,C., Hernandez-Verdun,D., and Scherf,A. (2005). The unusually large Plasmodium telomerase reverse-transcriptase localizes in a discrete compartment associated with the nucleolus. Nucleic Acids Res. *33*, 1111-1122.

Fingerman,I.M., Du,H.N., and Briggs,S.D. (2008). Controlling histone methylation via trans-histone pathways. Epigenetics. *3*, 237-242.

Fischer,K., Chavchich,M., Huestis,R., Wilson,D.W., Kemp,D.J., and Saul,A. (2003). Ten families of variant genes encoded in subtelomeric regions of multiple chromosomes of Plasmodium chabaudi, a malaria species that undergoes antigenic variation in the laboratory mouse. Mol. Microbiol. *48*, 1209-1223.

Fischer,T., Strasser,K., Racz,A., Rodriguez-Navarro,S., Oppizzi,M., Ihrig,P., Lechner,J., and Hurt,E. (2002). The mRNA export machinery requires the novel Sac3p-Thp1p complex to dock at the nucleoplasmic entrance of the nuclear pores. EMBO J. *21*, 5843-5852.

Fisher,T.S., Taggart,A.K., and Zakian,V.A. (2004). Cell cycle-dependent regulation of yeast telomerase by Ku. Nat. Struct. Mol. Biol. *11*, 1198-1205.

Flick,K. and Chen,Q. (2004). var genes, PfEMP1 and the human host. Mol. Biochem. Parasitol. *134*, 3-9.

Ford,E., Voit,R., Liszt,G., Magin,C., Grummt,I., and Guarente,L. (2006). Mammalian Sir2 homolog SIRT7 is an activator of RNA polymerase I transcription. Genes Dev. *20*, 1075-1080.

Ford,L.P., Shay,J.W., and Wright,W.E. (2001). The La antigen associates with the human telomerase ribonucleoprotein and influences telomere length in vivo. RNA. *7*, 1068-1075.

Forney,J., Henderson,E.R., and Blackburn,E.H. (1987). Identification of the telomeric sequence of the acellular slime molds Didymium iridis and Physarum polycephalum. Nucleic Acids Res. *15*, 9143-9152.

Forsyth,N.R., Wright,W.E., and Shay,J.W. (2002). Telomerase and differentiation in multicellular organisms: turn it off, turn it on, and turn it off again. Differentiation *69*, 188-197.

Fraiture,M., Baxter,R.H., Steinert,S., Chelliah,Y., Frolet,C., Quispe-Tintaya,W., Hoffmann,J.A., Blandin,S.A., and Levashina,E.A. (2009). Two mosquito LRR proteins function as complement control factors in the TEP1-mediated killing of Plasmodium. Cell Host. Microbe *5*, 273-284.

Frank,M., Dzikowski,R., Costantini,D., Amulic,B., Berdougo,E., and Deitsch,K. (2006). Strict pairing of var promoters and introns is required for var gene silencing in the malaria parasite Plasmodium falciparum. J. Biol. Chem. *281*, 9942-9952.

Franke-Fayard,B., Trueman,H., Ramesar,J., Mendoza,J., van der,K.M., van der,L.R., Sinden,R.E., Waters,A.P., and Janse,C.J. (2004). A Plasmodium berghei reference line that constitutively expresses GFP at a high level throughout the complete life cycle. Mol. Biochem. Parasitol. *137*, 23-33.

Franke-Fayard,B., Waters,A.P., and Janse,C.J. (2006). Real-time in vivo imaging of transgenic bioluminescent blood stages of rodent malaria parasites in mice. Nat. Protoc. *1*, 476-485.

Freitas-Junior,L.H., Bottius,E., Pirrit,L.A., Deitsch,K.W., Scheidig,C., Guinet,F., Nehrbass,U., Wellems,T.E., and Scherf,A. (2000). Frequent ectopic recombination of virulence factor genes in telomeric chromosome clusters of P. falciparum. Nature *407*, 1018-1022.

Freitas-Junior,L.H., Hernandez-Rivas,R., Ralph,S.A., Montiel-Condado,D., Ruvalcaba-Salazar,O.K., Rojas-Meza,A.P., Mancio-Silva,L., Leal-Silvestre,R.J., Gontijo,A.M., Shorte,S., and Scherf,A. (2005). Telomeric heterochromatin propagation and histone acetylation control mutually exclusive expression of antigenic variation genes in malaria parasites. Cell *121*, 25-36.

French,J.B., Cen,Y., and Sauve,A.A. (2008). Plasmodium falciparum Sir2 is an NAD(+)-Dependent Deacetylase and an Acetyllysine-Dependent and Acetyllysine-Independent NAD(+) Glycohydrolase. Biochemistry.

Frolet,C., Thoma,M., Blandin,S., Hoffmann,J.A., and Levashina,E.A. (2006). Boosting NF-kappaB-dependent basal immunity of Anopheles gambiae aborts development of Plasmodium berghei. Immunity. *25*, 677-685.

Fulton,T.B. and Blackburn,E.H. (1998). Identification of Kluyveromyces lactis telomerase: discontinuous synthesis along the 30-nucleotide-long templating domain. Mol. Cell Biol. *18*, 4961-4970.

Funk,W.D., Wang,C.K., Shelton,D.N., Harley,C.B., Pagon,G.D., and Hoeffler,W.K. (2000). Telomerase expression restores dermal integrity to in vitro-aged fibroblasts in a reconstituted skin model. Exp. Cell Res. *258*, 270-278.

Garcia-Salcedo,J.A., Gijon,P., Nolan,D.P., Tebabi,P., and Pays,E. (2003). A chromosomal SIR2 homologue with both histone NAD-dependent ADP-ribosyltransferase and deacetylase activities is involved in DNA repair in Trypanosoma brucei. EMBO J. *22*, 5851-5862.

Gardner,M.J., Hall,N., Fung,E., White,O., Berriman,M., Hyman,R.W., Carlton,J.M., Pain,A., Nelson,K.E., Bowman,S., Paulsen,I.T., James,K., Eisen,J.A., Rutherford,K., Salzberg,S.L., Craig,A., Kyes,S., Chan,M.S., Nene,V., Shallom,S.J., Suh,B., Peterson,J., Angiuoli,S., Pertea,M., Allen,J., Selengut,J., Haft,D., Mather,M.W., Vaidya,A.B., Martin,D.M., Fairlamb,A.H., Fraunholz,M.J., Roos,D.S., Ralph,S.A., McFadden,G.I., Cummings,L.M., Subramanian,G.M., Mungall,C., Venter,J.C., Carucci,D.J., Hoffman,S.L., Newbold,C., Davis,R.W., Fraser,C.M., and Barrell,B. (2002). Genome sequence of the human malaria parasite Plasmodium falciparum. Nature *419*, 498-511.

Gautier,T., Abbott,D.W., Molla,A., Verdel,A., Ausio,J., and Dimitrov,S. (2004). Histone variant H2ABbd confers lower stability to the nucleosome. EMBO Rep. *5*, 715-720.

Gazda,H.T., Kho,A.T., Sanoudou,D., Zaucha,J.M., Kohane,I.S., Sieff,C.A., and Beggs,A.H. (2006). Defective ribosomal protein gene expression alters transcription, translation, apoptosis, and oncogenic pathways in Diamond-Blackfan anemia. Stem Cells *24*, 2034-2044.

George,J.A., DeBaryshe,P.G., Traverse,K.L., Celniker,S.E., and Pardue,M.L. (2006). Genomic organization of the Drosophila telomere retrotransposable elements. Genome Res. *16*, 1231-1240.

Gertz,M. and Steegborn,C. (2009). Function and regulation of the mitochondrial Sirtuin isoform Sirt5 in Mammalia. Biochim. Biophys. Acta.

Ghosh,K. and Shetty,S. (2008). Blood coagulation in falciparum malaria--a review. Parasitol. Res. *102*, 571-576.

Gotta,M. and Gasser,S.M. (1996). Nuclear organization and transcriptional silencing in yeast. Experientia *52*, 1136-1147.

Gotta,M., Laroche,T., Formenton,A., Maillet,L., Scherthan,H., and Gasser,S.M. (1996a). The clustering of telomeres and colocalization with Rap1, Sir3, and Sir4 proteins in wild-type Saccharomyces cerevisiae. J. Cell Biol. *134*, 1349-1363.

Gotta,M., Laroche,T., Formenton,A., Maillet,L., Scherthan,H., and Gasser,S.M. (1996b). The clustering of telomeres and colocalization with Rap1, Sir3, and Sir4 proteins in wild-type Saccharomyces cerevisiae. J. Cell Biol. *134*, 1349-1363.

Gottlieb,S. and Esposito,R.E. (1989). A new role for a yeast transcriptional silencer gene, SIR2, in regulation of recombination in ribosomal DNA. Cell *56*, 771-776.

Gottschling,D.E., Aparicio,O.M., Billington,B.L., and Zakian,V.A. (1990). Position effect at S. cerevisiae telomeres: reversible repression of Pol II transcription. Cell *63*, 751-762.

Greene,E.C. and Shippen,D.E. (1998). Developmentally programmed assembly of higher order telomerase complexes with distinct biochemical and structural properties. Genes Dev. *12*, 2921-2931.

Greider,C.W. (1991). Telomerase is processive. Mol. Cell Biol. *11*, 4572-4580.

Greider,C.W. and Blackburn,E.H. (1985). Identification of a specific telomere terminal transferase activity in Tetrahymena extracts. Cell *43*, 405-413.

Griffith,J.D., Comeau,L., Rosenfield,S., Stansel,R.M., Bianchi,A., Moss,H., and de Lange,T. (1999). Mammalian telomeres end in a large duplex loop. Cell *97*, 503-514.

Grubisha,O., Rafty,L.A., Takanishi,C.L., Xu,X., Tong,L., Perraud,A.L., Scharenberg,A.M., and Denu,J.M. (2006). Metabolite of SIR2 reaction modulates TRPM2 ion channel. J. Biol. Chem. *281*, 14057-14065.

Gupta,L., Kumar,S., Han,Y.S., Pimenta,P.F., and Barillas-Mury,C. (2005). Midgut epithelial responses of different mosquito-Plasmodium combinations: the actin cone zipper repair mechanism in Aedes aegypti. Proc. Natl. Acad. Sci. U. S. A *102*, 4010-4015.

Haigis,M.C., Mostoslavsky,R., Haigis,K.M., Fahie,K., Christodoulou,D.C., Murphy,A.J., Valenzuela,D.M., Yancopoulos,G.D., Karow,M., Blander,G., Wolberger,C., Prolla,T.A., Weindruch,R., Alt,F.W., and Guarente,L. (2006). SIRT4 inhibits glutamate dehydrogenase and opposes the effects of calorie restriction in pancreatic beta cells. Cell *126*, 941-954.

Hall,N., Karras,M., Raine,J.D., Carlton,J.M., Kooij,T.W., Berriman,M., Florens,L., Janssen,C.S., Pain,A., Christophides,G.K., James,K., Rutherford,K., Harris,B., Harris,D., Churcher,C., Quail,M.A., Ormond,D., Doggett,J., Trueman,H.E., Mendoza,J., Bidwell,S.L., Rajandream,M.A., Carucci,D.J., Yates,J.R., III, Kafatos,F.C., Janse,C.J., Barrell,B., Turner,C.M., Waters,A.P., and Sinden,R.E. (2005). A comprehensive survey of the Plasmodium life cycle by genomic, transcriptomic, and proteomic analyses. Science *307*, 82-86.

Happel,N. and Doenecke,D. (2009). Histone H1 and its isoforms: contribution to chromatin structure and function. Gene *431*, 1-12.

Hayflick,L. (1965). THE LIMITED IN VITRO LIFETIME OF HUMAN DIPLOID CELL STRAINS. Exp. Cell Res. *37*, 614-636.

Hearn,J., Rayment,N., Landon,D.N., Katz,D.R., and de Souza,J.B. (2000). Immunopathology of cerebral malaria: morphological evidence of parasite sequestration in murine brain microvasculature. Infect. Immun. *68*, 5364-5376.

Hemann,M.T. and Greider,C.W. (2000). Wild-derived inbred mouse strains have short telomeres. Nucleic Acids Res. *28*, 4474-4478.

Henckel,A., Nakabayashi,K., Sanz,L.A., Feil,R., Hata,K., and Arnaud,P. (2009). Histone methylation is mechanistically linked to DNA methylation at imprinting control regions in mammals. Hum. Mol. Genet. *18*, 3375-3383.

Hernandez-Rivas,R., Mattei,D., Sterkers,Y., Peterson,D.S., Wellems,T.E., and Scherf,A. (1997). Expressed var genes are found in Plasmodium falciparum subtelomeric regions. Mol. Cell Biol. *17*, 604-611.

Herrera,E., Samper,E., Martin-Caballero,J., Flores,J.M., Lee,H.W., and Blasco,M.A. (1999). Disease states associated with telomerase deficiency appear earlier in mice with short telomeres. EMBO J. *18*, 2950-2960.

Herrero-Yraola,A., Bakhit,S.M., Franke,P., Weise,C., Schweiger,M., Jorcke,D., and Ziegler,M. (2001). Regulation of glutamate dehydrogenase by reversible ADP-ribosylation in mitochondria. EMBO J. *20*, 2404-2412.

Hertz-Fowler,C., Peacock,C.S., Wood,V., Aslett,M., Kerhornou,A., Mooney,P., Tivey,A., Berriman,M., Hall,N., Rutherford,K., Parkhill,J., Ivens,A.C., Rajandream,M.A., and Barrell,B. (2004). GeneDB: a resource for prokaryotic and eukaryotic organisms. Nucleic Acids Res. *32*, D339-D343.

Hetzer,M.W. and Wente,S.R. (2009). Border control at the nucleus: biogenesis and organization of the nuclear membrane and pore complexes. Dev. Cell *17*, 606-616.

Hillyer,J.F., Barreau,C., and Vernick,K.D. (2007). Efficiency of salivary gland invasion by malaria sporozoites is controlled by rapid sporozoite destruction in the mosquito haemocoel. Int. J. Parasitol. *37*, 673-681.

Hillyer,J.F., Schmidt,S.L., and Christensen,B.M. (2003). Rapid phagocytosis and melanization of bacteria and Plasmodium sporozoites by hemocytes of the mosquito Aedes aegypti. J. Parasitol. *89*, 62-69.

HIRAGA,M., ANAN,F.K., and ABE,K. (1964). THE EFFECT OF ACETYLATION ON THE PROPERTIES OF BEEF LIVER CATALASE. J. Biochem. *56*, 416-423.

Hirai,M., Arai,M., Kawai,S., and Matsuoka,H. (2006). PbGCbeta is essential for Plasmodium ookinete motility to invade midgut cell and for successful completion of parasite life cycle in mosquitoes. J. Biochem. *140*, 747-757.

Ho,M. and White,N.J. (1999). Molecular mechanisms of cytoadherence in malaria. Am. J. Physiol *276*, C1231-C1242.

Holt,S.E., Aisner,D.L., Baur,J., Tesmer,V.M., Dy,M., Ouellette,M., Trager,J.B., Morin,G.B., Toft,D.O., Shay,J.W., Wright,W.E., and White,M.A. (1999). Functional requirement of p23 and Hsp90 in telomerase complexes. Genes Dev. *13*, 817-826.

Horrocks,P., Wong,E., Russell,K., and Emes,R.D. (2009). Control of gene expression in Plasmodium falciparum - ten years on. Mol. Biochem. Parasitol. *164*, 9-25.

Huard,S., Moriarty,T.J., and Autexier,C. (2003). The C terminus of the human telomerase reverse transcriptase is a determinant of enzyme processivity. Nucleic Acids Res. *31*, 4059-4070.

Huynh,M.H., Harper,J.M., and Carruthers,V.B. (2006). Preparing for an invasion: charting the pathway of adhesion proteins to Toxoplasma micronemes. Parasitol. Res. *98*, 389-395.

Imai,S., Armstrong,C.M., Kaeberlein,M., and Guarente,L. (2000). Transcriptional silencing and longevity protein Sir2 is an NAD-dependent histone deacetylase. Nature *403*, 795-800.

Inyang,A.L., Sodeinde,O., Okpako,D.T., and Essien,E.M. (1987). Platelet reactions after interaction with cultured Plasmodium falciparum infected erythrocytes. Br. J. Haematol. *66*, 375-378.

Ishii,K., Arib,G., Lin,C., Van,H.G., and Laemmli,U.K. (2002). Chromatin boundaries in budding yeast: the nuclear pore connection. Cell *109*, 551-562.

Ishino,T., Orito,Y., Chinzei,Y., and Yuda,M. (2006). A calcium-dependent protein kinase regulates Plasmodium ookinete access to the midgut epithelial cell. Mol. Microbiol. *59*, 1175-1184.

Issar,N., Ralph,S.A., Mancio-Silva,L., Keeling,C., and Scherf,A. (2009). Differential sub-nuclear localisation of repressive and activating histone methyl modifications in P. falciparum. Microbes. Infect. *11*, 403-407.

Issar,N., Roux,E., Mattei,D., and Scherf,A. (2008). Identification of a novel post-translational modification in Plasmodium falciparum: protein sumoylation in different cellular compartments. Cell Microbiol. *10*, 1999-2011.

Janse,C.J., Franke-Fayard,B., Mair,G.R., Ramesar,J., Thiel,C., Engelmann,S., Matuschewski,K., van Gemert,G.J., Sauerwein,R.W., and Waters,A.P. (2006a). High efficiency transfection of Plasmodium berghei facilitates novel selection procedures. Mol. Biochem. Parasitol. *145*, 60-70.

Janse,C.J., Ramesar,J., and Waters,A.P. (2006b). High-efficiency transfection and drug selection of genetically transformed blood stages of the rodent malaria parasite Plasmodium berghei. Nat. Protoc. *1*, 346-356.

Janse,C.J. and Waters,A.P. (1995). Plasmodium berghei: the application of cultivation and purification techniques to molecular studies of malaria parasites. Parasitol. Today *11*, 138-143.

Janssen,C.S., Phillips,R.S., Turner,C.M., and Barrett,M.P. (2004). Plasmodium interspersed repeats: the major multigene superfamily of malaria parasites. Nucleic Acids Res. *32*, 5712-5720.

Jeong,Y.S., Cho,S., Park,J.S., Ko,Y., and Kang,Y.K. (2010). Phosphorylation of serine-10 of histone H3 shields modified lysine-9 selectively during mitosis. Genes Cells.

Johnson,A., Li,G., Sikorski,T.W., Buratowski,S., Woodcock,C.L., and Moazed,D. (2009). Reconstitution of heterochromatin-dependent transcriptional gene silencing. Mol. Cell *35*, 769-781.

Kachouri-Lafond,R., Dujon,B., Gilson,E., Westhof,E., Fairhead,C., and Teixeira,M.T. (2009). Large telomerase RNA, telomere length heterogeneity and escape from senescence in Candida glabrata. FEBS Lett. *583*, 3605-3610.

Kadota,K., Ishino,T., Matsuyama,T., Chinzei,Y., and Yuda,M. (2004). Essential role of membrane-attack protein in malarial transmission to mosquito host. Proc. Natl. Acad. Sci. U. S. A *101*, 16310-16315.

Kaestli,M., Cockburn,I.A., Cortes,A., Baea,K., Rowe,J.A., and Beck,H.P. (2006). Virulence of malaria is associated with differential expression of Plasmodium falciparum var gene subgroups in a case-control study. J. Infect. Dis. *193*, 1567-1574.

Kariu,T., Ishino,T., Yano,K., Chinzei,Y., and Yuda,M. (2006). CelTOS, a novel malarial protein that mediates transmission to mosquito and vertebrate hosts. Mol. Microbiol. *59*, 1369-1379.

Katayama,T. and Yasukawa,H. (2008). Analysis of Sir2E in the cellular slime mold Dictyostelium discoideum: cellular localization, spatial expression and overexpression. Dev. Growth Differ. *50*, 645-652.

Khan,S.M., Franke-Fayard,B., Mair,G.R., Lasonder,E., Janse,C.J., Mann,M., and Waters,A.P. (2005). Proteome analysis of separated male and female gametocytes reveals novel sex-specific Plasmodium biology. Cell *121*, 675-687.

Kim,S.C., Sprung,R., Chen,Y., Xu,Y., Ball,H., Pei,J., Cheng,T., Kho,Y., Xiao,H., Xiao,L., Grishin,N.V., White,M., Yang,X.J., and Zhao,Y. (2006). Substrate and functional diversity of lysine acetylation revealed by a proteomics survey. Mol. Cell *23*, 607-618.

Kim,S.Y., Kim,J.Y., Kim,S.H., Bae,H.J., Yi,H., Yoon,S.H., Koo,B.S., Kwon,M., Cho,J.Y., Lee,C.E., and Hong,S. (2007). Surfactin from Bacillus subtilis displays anti-proliferative effect via apoptosis induction, cell cycle arrest and survival signaling suppression. FEBS Lett. *581*, 865-871.

Kipling,D. and Cooke,H.J. (1990). Hypervariable ultra-long telomeres in mice. Nature *347*, 400-402.

Kirwan,M. and Dokal,I. (2009). Dyskeratosis congenita, stem cells and telomeres. Biochim. Biophys. Acta *1792*, 371-379.

Klobutcher,L.A., Swanton,M.T., Donini,P., and Prescott,D.M. (1981). All gene-sized DNA molecules in four species of hypotrichs have the same terminal sequence and an unusual 3' terminus. Proc. Natl. Acad. Sci. U. S. A *78*, 3015-3019.

Kooij,T.W., Carlton,J.M., Bidwell,S.L., Hall,N., Ramesar,J., Janse,C.J., and Waters,A.P. (2005). A Plasmodium whole-genome synteny map: indels and synteny breakpoints as foci for species-specific genes. PLoS. Pathog. *1*, e44.

Kowieski,T.M., Lee,S., and Denu,J.M. (2008). Acetylation-dependent ADP-ribosylation by Trypanosoma brucei Sir2. J. Biol. Chem. *283*, 5317-5326.

Kubo,Y., Okazaki,S., Anzai,T., and Fujiwara,H. (2001). Structural and phylogenetic analysis of TRAS, telomeric repeat-specific non-LTR retrotransposon families in Lepidopteran insects. Mol. Biol. Evol. *18*, 848-857.

Kurdistani,S.K., Robyr,D., Tavazoie,S., and Grunstein,M. (2002). Genome-wide binding map of the histone deacetylase Rpd3 in yeast. Nat. Genet. *31*, 248-254.

Kustatscher,G., Hothorn,M., Pugieux,C., Scheffzek,K., and Ladurner,A.G. (2005). Splicing regulates NAD metabolite binding to histone macroH2A. Nat. Struct. Mol. Biol. *12*, 624-625.

Kyrion,G., Liu,K., Liu,C., and Lustig,A.J. (1993). RAP1 and telomere structure regulate telomere position effects in Saccharomyces cerevisiae. Genes Dev. *7*, 1146-1159.

Lagouge,M., Argmann,C., Gerhart-Hines,Z., Meziane,H., Lerin,C., Daussin,F., Messadeq,N., Milne,J., Lambert,P., Elliott,P., Geny,B., Laakso,M., Puigserver,P., and Auwerx,J. (2006). Resveratrol improves mitochondrial function and protects against metabolic disease by activating SIRT1 and PGC-1alpha. Cell *127*, 1109-1122.

Lai,C.K., Miller,M.C., and Collins,K. (2002). Template boundary definition in Tetrahymena telomerase. Genes Dev. *16*, 415-420.

Lai,C.K., Mitchell,J.R., and Collins,K. (2001). RNA binding domain of telomerase reverse transcriptase. Mol. Cell Biol. *21*, 990-1000.

Landry,J., Slama,J.T., and Sternglanz,R. (2000). Role of NAD(+) in the deacetylase activity of the SIR2-like proteins. Biochem. Biophys. Res. Commun. *278*, 685-690.

Lee,H.S., Park,J.H., Kim,S.J., Kwon,S.J., and Kwon,J. (2010). A cooperative activation loop among SWI/SNF, gamma-H2AX and H3 acetylation for DNA double-strand break repair. EMBO J.

Lee,S., Tong,L., and Denu,J.M. (2008). Quantification of endogenous sirtuin metabolite O-acetyl-ADP-ribose. Anal. Biochem. *383*, 174-179.

Leeper,T.C., Athanassiou,Z., Dias,R.L., Robinson,J.A., and Varani,G. (2005). TAR RNA recognition by a cyclic peptidomimetic of Tat protein. Biochemistry *44*, 12362-12372.

Lei,M., Zaug,A.J., Podell,E.R., and Cech,T.R. (2005). Switching human telomerase on and off with hPOT1 protein in vitro. J. Biol. Chem. *280*, 20449-20456.

Lendvay,T.S., Morris,D.K., Sah,J., Balasubramanian,B., and Lundblad,V. (1996). Senescence mutants of Saccharomyces cerevisiae with a defect in telomere replication identify three additional EST genes. Genetics *144*, 1399-1412.

Lewis,M.S. and Pikaard,C.S. (2001). Restricted chromosomal silencing in nucleolar dominance. Proc. Natl. Acad. Sci. U. S. A *98*, 14536-14540.

Li,F., Patra,K.P., Yowell,C.A., Dame,J.B., Chin,K., and Vinetz,J.M. (2010). Apical surface expression of aspartic protease Plasmepsin 4, a potential transmission-blocking target of the plasmodium ookinete. J. Biol. Chem. *285*, 8076-8083.

li-Youcef,N., Lagouge,M., Froelich,S., Koehl,C., Schoonjans,K., and Auwerx,J. (2007). Sirtuins: the 'magnificent seven', function, metabolism and longevity. Ann. Med. *39*, 335-345.

Liew,C.C. and Gornall,A.G. (1973). Acetylation of ribosomal proteins. I. Characterization and properties of rat liver ribosomal proteins. J. Biol. Chem. *248*, 977-983.

Limoges,J., Persidsky,Y., Poluektova,L., Rasmussen,J., Ratanasuwan,W., Zelivyanskaya,M., McClernon,D.R., Lanier,E.R., and Gendelman,H.E. (2000). Evaluation of antiretroviral drug efficacy for HIV-1 encephalitis in SCID mice. Neurology *54*, 379-389.

Lingner,J., Hendrick,L.L., and Cech,T.R. (1994). Telomerase RNAs of different ciliates have a common secondary structure and a permuted template. Genes Dev. *8*, 1984-1998.

Lingner,J., Hughes,T.R., Shevchenko,A., Mann,M., Lundblad,V., and Cech,T.R. (1997). Reverse transcriptase motifs in the catalytic subunit of telomerase. Science *276*, 561-567.

Liou,G.G., Tanny,J.C., Kruger,R.G., Walz,T., and Moazed,D. (2005). Assembly of the SIR complex and its regulation by O-acetyl-ADP-ribose, a product of NAD-dependent histone deacetylation. Cell *121*, 515-527.

Liszt,G., Ford,E., Kurtev,M., and Guarente,L. (2005). Mouse Sir2 homolog SIRT6 is a nuclear ADP-ribosyltransferase. J. Biol. Chem. *280*, 21313-21320.

LITTAU,V.C., ALLFREY,V.G., FRENSTER,J.H., and MIRSKY,A.E. (1964). ACTIVE AND INACTIVE REGIONS OF NUCLEAR CHROMATIN AS REVEALED BY ELECTRON MICROSCOPE AUTORADIOGRAPHY. Proc. Natl. Acad. Sci. U. S. A *52*, 93-100.

Lopez-Rubio,J.J., Gontijo,A.M., Nunes,M.C., Issar,N., Hernandez,R.R., and Scherf,A. (2007). 5' flanking region of var genes nucleate histone modification patterns linked to phenotypic inheritance of virulence traits in malaria parasites. Mol. Microbiol. *66*, 1296-1305.

Lopez-Rubio,J.J., Mancio-Silva,L., and Scherf,A. (2009). Genome-wide analysis of heterochromatin associates clonally variant gene regulation with perinuclear repressive centers in malaria parasites. Cell Host. Microbe *5*, 179-190.

Lue,N.F. (2004). Adding to the ends: what makes telomerase processive and how important is it? Bioessays *26*, 955-962.

Lue,N.F. and Peng,Y. (1997). Identification and characterization of a telomerase activity from Schizosaccharomyces pombe. Nucleic Acids Res. *25*, 4331-4337.

Lundblad,V. and Szostak,J.W. (1989). A mutant with a defect in telomere elongation leads to senescence in yeast. Cell *57*, 633-643.

Lustig,A.J. (1998). Mechanisms of silencing in Saccharomyces cerevisiae. Curr. Opin. Genet. Dev. *8*, 233-239.

Lyst,M.J. and Stancheva,I. (2007). A role for SUMO modification in transcriptional repression and activation. Biochem. Soc. Trans. *35*, 1389-1392.

MacDonald,V.E. and Howe,L.J. (2009). Histone acetylation: where to go and how to get there. Epigenetics. *4*, 139-143.

Mahairaki,V., Voyatzi,T., Siden-Kiamos,I., and Louis,C. (2005). The Anopheles gambiae gamma1 laminin directly binds the Plasmodium berghei circumsporozoite- and TRAP-related protein (CTRP). Mol. Biochem. Parasitol. *140*, 119-121.

Mahmoudi,N., Garcia-Domenech,R., Galvez,J., Farhati,K., Franetich,J.F., Sauerwein,R., Hannoun,L., Derouin,F., Danis,M., and Mazier,D. (2008). New active drugs against liver stages of Plasmodium predicted by Molecular Topology. Antimicrob. Agents Chemother.

Maillet,L., Boscheron,C., Gotta,M., Marcand,S., Gilson,E., and Gasser,S.M. (1996). Evidence for silencing compartments within the yeast nucleus: a role for telomere proximity and Sir protein concentration in silencer-mediated repression. Genes Dev. *10*, 1796-1811.

Mair,G.R., Braks,J.A., Garver,L.S., Wiegant,J.C., Hall,N., Dirks,R.W., Khan,S.M., Dimopoulos,G., Janse,C.J., and Waters,A.P. (2006). Regulation of sexual development of Plasmodium by translational repression. Science *313*, 667-669.

Mair,G.R., Lasonder,E., Garver,L.S., Franke-Fayard,B.M., Carret,C.K., Wiegant,J.C., Dirks,R.W., Dimopoulos,G., Janse,C.J., and Waters,A.P. (2010). Universal features of post-transcriptional gene regulation are critical for Plasmodium zygote development. PLoS. Pathog. *6*, e1000767.

Malygin,A.A., Parakhnevitch,N.M., Ivanov,A.V., Eperon,I.C., and Karpova,G.G. (2007). Human ribosomal protein S13 regulates expression of its own gene at the splicing step by a feedback mechanism. Nucleic Acids Res. *35*, 6414-6423.

Mancio-Silva,L., Rojas-Meza,A.P., Vargas,M., Scherf,A., and Hernandez-Rivas,R. (2008). Differential association of Orc1 and Sir2 proteins to telomeric domains in Plasmodium falciparum. J. Cell Sci. *121*, 2046-2053.

Marrelli,M.T., Li,C., Rasgon,J.L., and Jacobs-Lorena,M. (2007). Transgenic malaria-resistant mosquitoes have a fitness advantage when feeding on Plasmodium-infected blood. Proc. Natl. Acad. Sci. U. S. A *104*, 5580-5583.

Martin-Ruiz,C., Saretzki,G., Petrie,J., Ladhoff,J., Jeyapalan,J., Wei,W., Sedivy,J., and von,Z.T. (2004). Stochastic variation in telomere shortening rate causes heterogeneity of human fibroblast replicative life span. J. Biol. Chem. *279*, 17826-17833.

Marty,A.J., Thompson,J.K., Duffy,M.F., Voss,T.S., Cowman,A.F., and Crabb,B.S. (2006). Evidence that Plasmodium falciparum chromosome end clusters are cross-linked by protein and are the sites of both virulence gene silencing and activation. Mol. Microbiol. *62*, 72-83.

Mason,J.M. and Biessmann,H. (1995). The unusual telomeres of Drosophila. Trends Genet. *11*, 58-62.

Masutomi,K., Kaneko,S., Hayashi,N., Yamashita,T., Shirota,Y., Kobayashi,K., and Murakami,S. (2000). Telomerase activity reconstituted in vitro with purified human telomerase reverse transcriptase and human telomerase RNA component. J. Biol. Chem. *275*, 22568-22573.

Mattei,D. and Scherf,A. (1994). Subtelomeric chromosome instability in Plasmodium falciparum: short telomere-like sequence motifs found frequently at healed chromosome breakpoints. Mutat. Res. *324*, 115-120.

Meding,S.J. and Langhorne,J. (1991). CD4+ T cells and B cells are necessary for the transfer of protective immunity to Plasmodium chabaudi chabaudi. Eur. J. Immunol. *21*, 1433-1438.

Melek,M., Davis,B.T., and Shippen,D.E. (1994). Oligonucleotides complementary to the Oxytricha nova telomerase RNA delineate the template domain and uncover a novel mode of primer utilization. Mol. Cell Biol. *14*, 7827-7838.

Menard,R., Sultan,A.A., Cortes,C., Altszuler,R., van Dijk,M.R., Janse,C.J., Waters,A.P., Nussenzweig,R.S., and Nussenzweig,V. (1997). Circumsporozoite protein is required for development of malaria sporozoites in mosquitoes. Nature *385*, 336-340.

Menon,B.B., Sarma,N.J., Pasula,S., Deminoff,S.J., Willis,K.A., Barbara,K.E., Andrews,B., and Santangelo,G.M. (2005). Reverse recruitment: the Nup84 nuclear pore subcomplex mediates Rap1/Gcr1/Gcr2 transcriptional activation. Proc. Natl. Acad. Sci. U. S. A *102*, 5749-5754.

Merrick,C.J. and Duraisingh,M.T. (2007). Plasmodium falciparum Sir2: an unusual sirtuin with dual histone deacetylase and ADP-ribosyltransferase activity. Eukaryot. Cell *6*, 2081-2091.

Merrick,C.J., Dzikowski,R., Imamura,H., Chuang,J., Deitsch,K., and Duraisingh,M.T. (2010). The effect of Plasmodium falciparum Sir2a histone deacetylase on clonal and longitudinal variation in expression of the var family of virulence genes. Int. J. Parasitol. *40*, 35-43.

Michel,K., Budd,A., Pinto,S., Gibson,T.J., and Kafatos,F.C. (2005). Anopheles gambiae SRPN2 facilitates midgut invasion by the malaria parasite Plasmodium berghei. EMBO Rep. *6*, 891-897.

Michishita,E., Park,J.Y., Burneskis,J.M., Barrett,J.C., and Horikawa,I. (2005). Evolutionarily conserved and nonconserved cellular localizations and functions of human SIRT proteins. Mol. Biol. Cell *16*, 4623-4635.

Mieczkowski,P.A., Dominska,M., Buck,M.J., Lieb,J.D., and Petes,T.D. (2007). Loss of a histone deacetylase dramatically alters the genomic distribution of Spo11p-catalyzed DNA breaks in Saccharomyces cerevisiae. Proc. Natl. Acad. Sci. U. S. A *104*, 3955-3960.

Miyoshi,K., Shirai,C., and Mizuta,K. (2003). Transcription of genes encoding trans-acting factors required for rRNA maturation/ribosomal subunit assembly is coordinately regulated with ribosomal protein genes and involves Rap1 in Saccharomyces cerevisiae. Nucleic Acids Res. *31*, 1969-1973.

Moehle,C.M. and Hinnebusch,A.G. (1991). Association of RAP1 binding sites with stringent control of ribosomal protein gene transcription in Saccharomyces cerevisiae. Mol. Cell Biol. *11*, 2723-2735.

Moon,R.W., Taylor,C.J., Bex,C., Schepers,R., Goulding,D., Janse,C.J., Waters,A.P., Baker,D.A., and Billker,O. (2009). A cyclic GMP signalling module that regulates gliding motility in a malaria parasite. PLoS. Pathog. *5*, e1000599.

Morahan,B.J., Wang,L., and Coppel,R.L. (2009). No TRAP, no invasion. Trends Parasitol. *25*, 77-84.

Moriarty,T.J., Marie-Egyptienne,D.T., and Autexier,C. (2004). Functional organization of repeat addition processivity and DNA synthesis determinants in the human telomerase multimer. Mol. Cell Biol. *24*, 3720-3733.

Morin,G.B. (1989). The human telomere terminal transferase enzyme is a ribonucleoprotein that synthesizes TTAGGG repeats. Cell *59*, 521-529.

Morin,G.B. (1991). Recognition of a chromosome truncation site associated with alpha-thalassaemia by human telomerase. Nature *353*, 454-456.

Mostoslavsky,R., Chua,K.F., Lombard,D.B., Pang,W.W., Fischer,M.R., Gellon,L., Liu,P., Mostoslavsky,G., Franco,S., Murphy,M.M., Mills,K.D., Patel,P., Hsu,J.T., Hong,A.L., Ford,E., Cheng,H.L., Kennedy,C., Nunez,N., Bronson,R., Frendewey,D., Auerbach,W., Valenzuela,D., Karow,M., Hottiger,M.O., Hursting,S., Barrett,J.C., Guarente,L., Mulligan,R., Demple,B., Yancopoulos,G.D., and Alt,F.W. (2006). Genomic instability and aging-like phenotype in the absence of mammalian SIRT6. Cell *124*, 315-329.

Moyzis,R.K., Buckingham,J.M., Cram,L.S., Dani,M., Deaven,L.L., Jones,M.D., Meyne,J., Ratliff,R.L., and Wu,J.R. (1988). A highly conserved repetitive DNA sequence, (TTAGGG)n, present at the telomeres of human chromosomes. Proc. Natl. Acad. Sci. U. S. A *85*, 6622-6626.

Muhle,R.A., Adjalley,S., Falkard,B., Nkrumah,L.J., Muhle,M.E., and Fidock,D.A. (2009). A var gene promoter implicated in severe malaria nucleates silencing and is regulated by 3' untranslated region and intronic cis-elements. Int. J. Parasitol. *39*, 1425-1439.

Muller,H.M., Reckmann,I., Hollingdale,M.R., Bujard,H., Robson,K.J., and Crisanti,A. (1993). Thrombospondin related anonymous protein (TRAP) of Plasmodium falciparum binds specifically to sulfated glycoconjugates and to HepG2 hepatoma cells suggesting a role for this molecule in sporozoite invasion of hepatocytes. EMBO J. *12*, 2881-2889.

Nagata,T., Takada,Y., Ono,A., Nagata,K., Konishi,Y., Nukina,T., Ono,M., Matsugami,A., Furukawa,A., Fujimoto,N., Fukuda,H., Nakagama,H., and Katahira,M. (2008). Elucidation of the mode of interaction in the UP1-telomerase RNA-telomeric DNA ternary complex which serves to recruit telomerase to telomeric DNA and to enhance the telomerase activity. Nucleic Acids Res. *36*, 6816-6824.

Nakayama,J., Rice,J.C., Strahl,B.D., Allis,C.D., and Grewal,S.I. (2001). Role of histone H3 lysine 9 methylation in epigenetic control of heterochromatin assembly. Science *292*, 110-113.

Nakayama,J., Tahara,H., Tahara,E., Saito,M., Ito,K., Nakamura,H., Nakanishi,T., Tahara,E., Ide,T., and Ishikawa,F. (1998). Telomerase activation by hTRT in human normal fibroblasts and hepatocellular carcinomas. Nat. Genet. *18*, 65-68.

North,B.J., Marshall,B.L., Borra,M.T., Denu,J.M., and Verdin,E. (2003). The human Sir2 ortholog, SIRT2, is an NAD+-dependent tubulin deacetylase. Mol. Cell *11*, 437-444.

Nowak,S.J. and Corces,V.G. (2004). Phosphorylation of histone H3: a balancing act between chromosome condensation and transcriptional activation. Trends Genet. *20*, 214-220.

Oeseburg,H., de Boer,R.A., van Gilst,W.H., and van der Harst,P. (2010). Telomere biology in healthy aging and disease. Pflugers Arch. *459*, 259-268.

Okazaki,S., Tsuchida,K., Maekawa,H., Ishikawa,H., and Fujiwara,H. (1993). Identification of a pentanucleotide telomeric sequence, (TTAGG)n, in the silkworm Bombyx mori and in other insects. Mol. Cell Biol. *13*, 1424-1432.

Orphanides,G. and Reinberg,D. (2000). RNA polymerase II elongation through chromatin. Nature *407*, 471-475.

Osanai,M., Kojima,K.K., Futahashi,R., Yaguchi,S., and Fujiwara,H. (2006). Identification and characterization of the telomerase reverse transcriptase of Bombyx mori (silkworm) and Tribolium castaneum (flour beetle). Gene *376*, 281-289.

Osta,M.A., Christophides,G.K., and Kafatos,F.C. (2004). Effects of mosquito genes on Plasmodium development. Science *303*, 2030-2032.

Outeiro,T.F., Kontopoulos,E., Altmann,S.M., Kufareva,I., Strathearn,K.E., Amore,A.M., Volk,C.B., Maxwell,M.M., Rochet,J.C., McLean,P.J., Young,A.B., Abagyan,R., Feany,M.B., Hyman,B.T., and

Kazantsev,A.G. (2007). Sirtuin 2 inhibitors rescue alpha-synuclein-mediated toxicity in models of Parkinson's disease. Science *317*, 516-519.

Pagans,S., Pedal,A., North,B.J., Kaehlcke,K., Marshall,B.L., Dorr,A., Hetzer-Egger,C., Henklein,P., Frye,R., McBurney,M.W., Hruby,H., Jung,M., Verdin,E., and Ott,M. (2005). SIRT1 regulates HIV transcription via Tat deacetylation. PLoS. Biol. *3*, e41.

Pallos,J., Bodai,L., Lukacsovich,T., Purcell,J.M., Steffan,J.S., Thompson,L.M., and Marsh,J.L. (2008). Inhibition of specific HDACs and sirtuins suppresses pathogenesis in a Drosophila model of Huntington's disease. Hum. Mol. Genet. *17*, 3767-3775.

Palm,W. and de,L.T. (2008). How shelterin protects mammalian telomeres. Annu. Rev. Genet. *42*, 301-334.

Paton,M.G., Barker,G.C., Matsuoka,H., Ramesar,J., Janse,C.J., Waters,A.P., and Sinden,R.E. (1993). Structure and expression of a post-transcriptionally regulated malaria gene encoding a surface protein from the sexual stages of Plasmodium berghei. Mol. Biochem. Parasitol. *59*, 263-275.

Pennock,E., Buckley,K., and Lundblad,V. (2001). Cdc13 delivers separate complexes to the telomere for end protection and replication. Cell *104*, 387-396.

Perez-Martin,J., Uria,J.A., and Johnson,A.D. (1999). Phenotypic switching in Candida albicans is controlled by a SIR2 gene. EMBO J. *18*, 2580-2592.

Polevoda,B. and Sherman,F. (2003). Composition and function of the eukaryotic N-terminal acetyltransferase subunits. Biochem. Biophys. Res. Commun. *308*, 1-11.

Ponzi,M., Janse,C.J., Dore,E., Scotti,R., Pace,T., Reterink,T.J., van der Berg,F.M., and Mons,B. (1990). Generation of chromosome size polymorphism during in vivo mitotic multiplication of Plasmodium berghei involves both loss and addition of subtelomeric repeat sequences. Mol. Biochem. Parasitol. *41*, 73-82.

Ponzi,M., Pace,T., Dore,E., and Frontali,C. (1985). Identification of a telomeric DNA sequence in Plasmodium berghei. EMBO J. *4*, 2991-2995.

Posakony,J., Hirao,M., Stevens,S., Simon,J.A., and Bedalov,A. (2004). Inhibitors of Sir2: evaluation of splitomicin analogues. J. Med. Chem. *47*, 2635-2644.

Povelones,M., Waterhouse,R.M., Kafatos,F.C., and Christophides,G.K. (2009). Leucine-rich repeat protein complex activates mosquito complement in defense against Plasmodium parasites. Science *324*, 258-261.

Prowse,K.R., Avilion,A.A., and Greider,C.W. (1993). Identification of a nonprocessive telomerase activity from mouse cells. Proc. Natl. Acad. Sci. U. S. A *90*, 1493-1497.

Prowse,K.R. and Greider,C.W. (1995). Developmental and tissue-specific regulation of mouse telomerase and telomere length. Proc. Natl. Acad. Sci. U. S. A *92*, 4818-4822.

Prozorovski,T., Schulze-Topphoff,U., Glumm,R., Baumgart,J., Schroter,F., Ninnemann,O., Siegert,E., Bendix,I., Brustle,O., Nitsch,R., Zipp,F., and Aktas,O. (2008). Sirt1 contributes critically to the redox-dependent fate of neural progenitors. Nat. Cell Biol. *10*, 385-394.

Prusty,D., Mehra,P., Srivastava,S., Shivange,A.V., Gupta,A., Roy,N., and Dhar,S.K. (2008). Nicotinamide inhibits Plasmodium falciparum Sir2 activity in vitro and parasite growth. FEMS Microbiol. Lett.

Ralph,S.A., Scheidig-Benatar,C., and Scherf,A. (2005). Antigenic variation in Plasmodium falciparum is associated with movement of var loci between subnuclear locations. Proc. Natl. Acad. Sci. U. S. A *102*, 5414-5419.

Rangasamy,D., Greaves,I., and Tremethick,D.J. (2004). RNA interference demonstrates a novel role for H2A.Z in chromosome segregation. Nat. Struct. Mol. Biol. *11*, 650-655.

Renauld,H., Aparicio,O.M., Zierath,P.D., Billington,B.L., Chhablani,S.K., and Gottschling,D.E. (1993). Silent domains are assembled continuously from the telomere and are defined by promoter distance and strength, and by SIR3 dosage. Genes Dev. *7*, 1133-1145.

Rice,J.C., Briggs,S.D., Ueberheide,B., Barber,C.M., Shabanowitz,J., Hunt,D.F., Shinkai,Y., and Allis,C.D. (2003). Histone methyltransferases direct different degrees of methylation to define distinct chromatin domains. Mol. Cell *12*, 1591-1598.

Richards,E.J. and Ausubel,F.M. (1988). Isolation of a higher eukaryotic telomere from Arabidopsis thaliana. Cell *53*, 127-136.

Riehle,M.M., Markianos,K., Niare,O., Xu,J., Li,J., Toure,A.M., Podiougou,B., Oduol,F., Diawara,S., Diallo,M., Coulibaly,B., Ouatara,A., Kruglyak,L., Traore,S.F., and Vernick,K.D. (2006). Natural malaria infection in Anopheles gambiae is regulated by a single genomic control region. Science *312*, 577-579.

Rine,J., Strathern,J.N., Hicks,J.B., and Herskowitz,I. (1979). A suppressor of mating-type locus mutations in Saccharomyces cerevisiae: evidence for and identification of cryptic mating-type loci. Genetics *93*, 877-901.

RITOSSA,F.M. and SPIEGELMAN,S. (1965). LOCALIZATION OF DNA COMPLEMENTARY TO RIBOSOMAL RNA IN THE NUCLEOLUS ORGANIZER REGION OF DROSOPHILA MELANOGASTER. Proc. Natl. Acad. Sci. U. S. A *53*, 737-745.

Robyr,D., Suka,Y., Xenarios,I., Kurdistani,S.K., Wang,A., Suka,N., and Grunstein,M. (2002). Microarray deacetylation maps determine genome-wide functions for yeast histone deacetylases. Cell *109*, 437-446.

Rodriguez-Navarro,S., Fischer,T., Luo,M.J., Antunez,O., Brettschneider,S., Lechner,J., Perez-Ortin,J.E., Reed,R., and Hurt,E. (2004). Sus1, a functional component of the SAGA histone acetylase complex and the nuclear pore-associated mRNA export machinery. Cell *116*, 75-86.

Rogakou,E.P., Pilch,D.R., Orr,A.H., Ivanova,V.S., and Bonner,W.M. (1998). DNA double-stranded breaks induce histone H2AX phosphorylation on serine 139. J. Biol. Chem. *273*, 5858-5868.

Rogina,B. and Helfand,S.L. (2004). Sir2 mediates longevity in the fly through a pathway related to calorie restriction. Proc. Natl. Acad. Sci. U. S. A *101*, 15998-16003.

Romero,D.P. and Blackburn,E.H. (1991). A conserved secondary structure for telomerase RNA. Cell *67*, 343-353.

Roth,C.W., Kobeski,F., Walter,M.F., and Biessmann,H. (1997). Chromosome end elongation by recombination in the mosquito Anopheles gambiae. Mol. Cell Biol. *17*, 5176-5183.

Rottmann,M., Lavstsen,T., Mugasa,J.P., Kaestli,M., Jensen,A.T., Muller,D., Theander,T., and Beck,H.P. (2006). Differential expression of var gene groups is associated with morbidity caused by Plasmodium falciparum infection in Tanzanian children. Infect. Immun. *74*, 3904-3911.

Rubin,G.M. (1978). Isolation of a telomeric DNA sequence from Drosophila melanogaster. Cold Spring Harb. Symp. Quant. Biol. *42 Pt 2*, 1041-1046.

Rubio,J.P., Thompson,J.K., and Cowman,A.F. (1996). The var genes of Plasmodium falciparum are located in the subtelomeric region of most chromosomes. EMBO J. *15*, 4069-4077.

Salanti,A., Staalsoe,T., Lavstsen,T., Jensen,A.T., Sowa,M.P., Arnot,D.E., Hviid,L., and Theander,T.G. (2003). Selective upregulation of a single distinctly structured var gene in chondroitin sulphate A-

adhering Plasmodium falciparum involved in pregnancy-associated malaria. Mol. Microbiol. *49*, 179-191.

Salcedo-Amaya,A.M., van Driel,M.A., Alako,B.T., Trelle,M.B., van den Elzen,A.M., Cohen,A.M., Janssen-Megens,E.M., van,d., V, Selzer,R.R., Iniguez,A.L., Green,R.D., Sauerwein,R.W., Jensen,O.N., and Stunnenberg,H.G. (2009). Dynamic histone H3 epigenome marking during the intraerythrocytic cycle of Plasmodium falciparum. Proc. Natl. Acad. Sci. U. S. A.

Sasaki,T., Maier,B., Koclega,K.D., Chruszcz,M., Gluba,W., Stukenberg,P.T., Minor,W., and Scrable,H. (2008). Phosphorylation regulates SIRT1 function. PLoS. One. *3*, e4020.

Scherf,A., Hernandez-Rivas,R., Buffet,P., Bottius,E., Benatar,C., Pouvelle,B., Gysin,J., and Lanzer,M. (1998). Antigenic variation in malaria: in situ switching, relaxed and mutually exclusive transcription of var genes during intra-erythrocytic development in Plasmodium falciparum. EMBO J. *17*, 5418-5426.

Schlissel,M.S. and Brown,D.D. (1984). The transcriptional regulation of Xenopus 5s RNA genes in chromatin: the roles of active stable transcription complexes and histone H1. Cell *37*, 903-913.

Schmid,M., Arib,G., Laemmli,C., Nishikawa,J., Durussel,T., and Laemmli,U.K. (2006). Nup-PI: the nucleopore-promoter interaction of genes in yeast. Mol. Cell *21*, 379-391.

Schober,H., Ferreira,H., Kalck,V., Gehlen,L.R., and Gasser,S.M. (2009). Yeast telomerase and the SUN domain protein Mps3 anchor telomeres and repress subtelomeric recombination. Genes Dev. *23*, 928-938.

Schuetz,A., Min,J., Antoshenko,T., Wang,C.L., Allali-Hassani,A., Dong,A., Loppnau,P., Vedadi,M., Bochkarev,A., Sternglanz,R., and Plotnikov,A.N. (2007). Structural basis of inhibition of the human NAD+-dependent deacetylase SIRT5 by suramin. Structure. *15*, 377-389.

Schwer,B., North,B.J., Frye,R.A., Ott,M., and Verdin,E. (2002). The human silent information regulator (Sir)2 homologue hSIRT3 is a mitochondrial nicotinamide adenine dinucleotide-dependent deacetylase. J. Cell Biol. *158*, 647-657.

Sealey,D.C., Zheng,L., Taboski,M.A., Cruickshank,J., Ikura,M., and Harrington,L.A. (2010). The N-terminus of hTERT contains a DNA-binding domain and is required for telomerase activity and cellular immortalization. Nucleic Acids Res. *38*, 2019-2035.

Serakinci,N., Graakjaer,J., and Kolvraa,S. (2008). Telomere stability and telomerase in mesenchymal stem cells. Biochimie *90*, 33-40.

Seto,A.G., Livengood,A.J., Tzfati,Y., Blackburn,E.H., and Cech,T.R. (2002). A bulged stem tethers Est1p to telomerase RNA in budding yeast. Genes Dev. *16*, 2800-2812.

Seto,A.G., Umansky,K., Tzfati,Y., Zaug,A.J., Blackburn,E.H., and Cech,T.R. (2003). A template-proximal RNA paired element contributes to Saccharomyces cerevisiae telomerase activity. RNA. *9*, 1323-1332.

Shahabuddin,M. and Pimenta,P.F. (1998). Plasmodium gallinaceum preferentially invades vesicular ATPase-expressing cells in Aedes aegypti midgut. Proc. Natl. Acad. Sci. U. S. A *95*, 3385-3389.

Shahabuddin,M., Toyoshima,T., Aikawa,M., and Kaslow,D.C. (1993). Transmission-blocking activity of a chitinase inhibitor and activation of malarial parasite chitinase by mosquito protease. Proc. Natl. Acad. Sci. U. S. A *90*, 4266-4270.

Shampay,J. and Blackburn,E.H. (1988). Generation of telomere-length heterogeneity in Saccharomyces cerevisiae. Proc. Natl. Acad. Sci. U. S. A *85*, 534-538.

Shampay,J., Szostak,J.W., and Blackburn,E.H. (1984). DNA sequences of telomeres maintained in yeast. Nature *310*, 154-157.

Sherman,I.W., Eda,S., and Winograd,E. (2003). Cytoadherence and sequestration in Plasmodium falciparum: defining the ties that bind. Microbes. Infect. *5*, 897-909.

Shi,D.F., Wheelhouse,R.T., Sun,D., and Hurley,L.H. (2001). Quadruplex-interactive agents as telomerase inhibitors: synthesis of porphyrins and structure-activity relationship for the inhibition of telomerase. J. Med. Chem. *44*, 4509-4523.

Shiao,S.H., Whitten,M.M., Zachary,D., Hoffmann,J.A., and Levashina,E.A. (2006). Fz2 and cdc42 mediate melanization and actin polymerization but are dispensable for Plasmodium killing in the mosquito midgut. PLoS. Pathog. *2*, e133.

Shiio,Y. and Eisenman,R.N. (2003). Histone sumoylation is associated with transcriptional repression. Proc. Natl. Acad. Sci. U. S. A *100*, 13225-13230.

Shukla,A., Chaurasia,P., and Bhaumik,S.R. (2009). Histone methylation and ubiquitination with their cross-talk and roles in gene expression and stability. Cell Mol. Life Sci. *66*, 1419-1433.

Siden-Kiamos,I., Ecker,A., Nyback,S., Louis,C., Sinden,R.E., and Billker,O. (2006). Plasmodium berghei calcium-dependent protein kinase 3 is required for ookinete gliding motility and mosquito midgut invasion. Mol. Microbiol. *60*, 1355-1363.

Siden-Kiamos,I., Vlachou,D., Margos,G., Beetsma,A., Waters,A.P., Sinden,R.E., and Louis,C. (2000). Distinct roles for pbs21 and pbs25 in the in vitro ookinete to oocyst transformation of Plasmodium berghei. J. Cell Sci. *113 Pt 19*, 3419-3426.

Silva,M., Pereira,H.S., Bento,M., Santos,A.P., Shaw,P., Delgado,M., Neves,N., and Viegas,W. (2008). Interplay of ribosomal DNA loci in nucleolar dominance: dominant NORs are up-regulated by chromatin dynamics in the wheat-rye system. PLoS. One. *3*, e3824.

Smalley,M.E. (1975). The nature of age immunity to Plasmodium berghei in the rat. Parasitology *71*, 337-347.

Smith,C.L. and Hager,G.L. (1997). Transcriptional regulation of mammalian genes in vivo. A tale of two templates. J. Biol. Chem. *272*, 27493-27496.

Smith,J.S. and Boeke,J.D. (1997). An unusual form of transcriptional silencing in yeast ribosomal DNA. Genes Dev. *11*, 241-254.

Sperger,J.M. and Cech,T.R. (2001). A stem-loop of Tetrahymena telomerase RNA distant from the template potentiates RNA folding and telomerase activity. Biochemistry *40*, 7005-7016.

Sprung,C.N., Sabatier,L., and Murnane,J.P. (1996). Effect of telomere length on telomeric gene expression. Nucleic Acids Res. *24*, 4336-4340.

Srichaikul,T., Puwasatien,P., Karnjanajetanee,J., Bokisch,V.A., and Pawasatien,P. (1975). Complement changes and disseminated intravascular coagulation in Plasmodium falciparum malaria. Lancet *1*, 770-772.

Steffen,K.K., MacKay,V.L., Kerr,E.O., Tsuchiya,M., Hu,D., Fox,L.A., Dang,N., Johnston,E.D., Oakes,J.A., Tchao,B.N., Pak,D.N., Fields,S., Kennedy,B.K., and Kaeberlein,M. (2008). Yeast life span extension by depletion of 60s ribosomal subunits is mediated by Gcn4. Cell *133*, 292-302.

Stellwagen,A.E., Haimberger,Z.W., Veatch,J.R., and Gottschling,D.E. (2003). Ku interacts with telomerase RNA to promote telomere addition at native and broken chromosome ends. Genes Dev. *17*, 2384-2395.

Stewart,S.A. and Weinberg,R.A. (2006). Telomeres: cancer to human aging. Annu. Rev. Cell Dev. Biol. *22*, 531-557.

Stoppler,H., Hartmann,D.P., Sherman,L., and Schlegel,R. (1997). The human papillomavirus type 16 E6 and E7 oncoproteins dissociate cellular telomerase activity from the maintenance of telomere length. J. Biol. Chem. *272*, 13332-13337.

Su,Z. and Stevenson,M.M. (2002). IL-12 is required for antibody-mediated protective immunity against blood-stage Plasmodium chabaudi AS malaria infection in mice. J. Immunol. *168*, 1348-1355.

Sultan,A.A., Thathy,V., Frevert,U., Robson,K.J., Crisanti,A., Nussenzweig,V., Nussenzweig,R.S., and Menard,R. (1997). TRAP is necessary for gliding motility and infectivity of plasmodium sporozoites. Cell *90*, 511-522.

Taggart,A.K., Teng,S.C., and Zakian,V.A. (2002). Est1p as a cell cycle-regulated activator of telomere-bound telomerase. Science *297*, 1023-1026.

Takakura,H., Tsunasawa,S., Miyagi,M., and Warner,J.R. (1992). NH2-terminal acetylation of ribosomal proteins of Saccharomyces cerevisiae. J. Biol. Chem. *267*, 5442-5445.

Tan-Wong,S.M., Wijayatilake,H.D., and Proudfoot,N.J. (2009). Gene loops function to maintain transcriptional memory through interaction with the nuclear pore complex. Genes Dev. *23*, 2610-2624.

Tanner,K.G., Landry,J., Sternglanz,R., and Denu,J.M. (2000). Silent information regulator 2 family of NAD- dependent histone/protein deacetylases generates a unique product, 1-O-acetyl-ADP-ribose. Proc. Natl. Acad. Sci. U. S. A *97*, 14178-14182.

Tanno,M., Sakamoto,J., Miura,T., Shimamoto,K., and Horio,Y. (2007). Nucleocytoplasmic shuttling of the NAD+-dependent histone deacetylase SIRT1. J. Biol. Chem. *282*, 6823-6832.

Tavares,J., Ouaissi,A., Kong Thoo,L.P., Loureiro,I., Kaur,S., Roy,N., and Cordeiro-da-Silva,A. (2010). Bisnaphthalimidopropyl derivatives as inhibitors of Leishmania SIR2 related protein 1. ChemMedChem. *5*, 140-147.

Taylor,C.J., McRobert,L., and Baker,D.A. (2008a). Disruption of a Plasmodium falciparum cyclic nucleotide phosphodiesterase gene causes aberrant gametogenesis. Mol. Microbiol. *69*, 110-118.

Taylor,D.M., Maxwell,M.M., Luthi-Carter,R., and Kazantsev,A.G. (2008b). Biological and potential therapeutic roles of sirtuin deacetylases. Cell Mol. Life Sci. *65*, 4000-4018.

Taylor,J.E. and Rudenko,G. (2006). Switching trypanosome coats: what's in the wardrobe? Trends Genet. *22*, 614-620.

Tham,W.H. and Zakian,V.A. (2002). Transcriptional silencing at Saccharomyces telomeres: implications for other organisms. Oncogene *21*, 512-521.

Theimer,C.A., Finger,L.D., Trantirek,L., and Feigon,J. (2003). Mutations linked to dyskeratosis congenita cause changes in the structural equilibrium in telomerase RNA. Proc. Natl. Acad. Sci. U. S. A *100*, 449-454.

Thompson,J. and Sinden,R.E. (1994). In situ detection of Pbs21 mRNA during sexual development of Plasmodium berghei. Mol. Biochem. Parasitol. *68*, 189-196.

Tissenbaum,H.A. and Guarente,L. (2001). Increased dosage of a sir-2 gene extends lifespan in Caenorhabditis elegans. Nature *410*, 227-230.

Tomas,A.M., Margos,G., Dimopoulos,G., van Lin,L.H., de Koning-Ward,T.F., Sinha,R., Lupetti,P., Beetsma,A.L., Rodriguez,M.C., Karras,M., Hager,A., Mendoza,J., Butcher,G.A., Kafatos,F., Janse,C.J., Waters,A.P., and Sinden,R.E. (2001). P25 and P28 proteins of the malaria ookinete surface have multiple and partially redundant functions. EMBO J. *20*, 3975-3983.

Tonkin,C.J., Carret,C.K., Duraisingh,M.T., Voss,T.S., Ralph,S.A., Hommel,M., Duffy,M.F., Silva,L.M., Scherf,A., Ivens,A., Speed,T.P., Beeson,J.G., and Cowman,A.F. (2009). Sir2 paralogues cooperate to regulate virulence genes and antigenic variation in Plasmodium falciparum. PLoS. Biol. *7*, e84.

Towbin,B.D., Meister,P., and Gasser,S.M. (2009). The nuclear envelope--a scaffold for silencing? Curr. Opin. Genet. Dev. *19*, 180-186.

Trapp,J., Meier,R., Hongwiset,D., Kassack,M.U., Sippl,W., and Jung,M. (2007). Structure-activity studies on suramin analogues as inhibitors of NAD+-dependent histone deacetylases (sirtuins). ChemMedChem. *2*, 1419-1431.

Trueman,H.E., Raine,J.D., Florens,L., Dessens,J.T., Mendoza,J., Johnson,J., Waller,C.C., Delrieu,I., Holders,A.A., Langhorne,J., Carucci,D.J., Yates,J.R., III, and Sinden,R.E. (2004). Functional characterization of an LCCL-lectin domain containing protein family in Plasmodium berghei. J. Parasitol. *90*, 1062-1071.

Trujillo,K.M., Bunch,J.T., and Baumann,P. (2005). Extended DNA binding site in Pot1 broadens sequence specificity to allow recognition of heterogeneous fission yeast telomeres. J. Biol. Chem. *280*, 9119-9128.

Tsai,Y.L., Hayward,R.E., Langer,R.C., Fidock,D.A., and Vinetz,J.M. (2001). Disruption of Plasmodium falciparum chitinase markedly impairs parasite invasion of mosquito midgut. Infect. Immun. *69*, 4048-4054.

Ujike-Asai,A., Okada,A., Du,Y., Maruyama,M., Yuan,X., Ishikawa,F., Motoo,Y., Isobe,K., and Nakajima,H. (2007). Large defects of type I allergic response in telomerase reverse transcriptase knockout mice. J. Leukoc. Biol. *82*, 429-435.

van Dijk,M.R., Janse,C.J., and Waters,A.P. (1996). Expression of a Plasmodium gene introduced into subtelomeric regions of Plasmodium berghei chromosomes. Science *271*, 662-665.

van Dijk,M.R., Waters,A.P., and Janse,C.J. (1995). Stable transfection of malaria parasite blood stages. Science *268*, 1358-1362.

van Lin,L.H., Pace,T., Janse,C.J., Birago,C., Ramesar,J., Picci,L., Ponzi,M., and Waters,A.P. (2001). Interspecies conservation of gene order and intron-exon structure in a genomic locus of high gene density and complexity in Plasmodium. Nucleic Acids Res. *29*, 2059-2068.

van Lin,L.H., Pace,T., Janse,C.J., Scotti,R., and Ponzi,M. (1997). A long range restriction map of chromosome 5 of Plasmodium berghei demonstrates a chromosome specific symmetrical subtelomeric organisation. Mol. Biochem. Parasitol. *86*, 111-115.

Vaquero,A. and Reinberg,D. (2009). Calorie restriction and the exercise of chromatin. Genes Dev. *23*, 1849-1869.

Vergnes,B., Sereno,D., Madjidian-Sereno,N., Lemesre,J.L., and Ouaissi,A. (2002). Cytoplasmic SIR2 homologue overexpression promotes survival of Leishmania parasites by preventing programmed cell death. Gene *296*, 139-150.

Vermeulen,A.N., Ponnudurai,T., Beckers,P.J., Verhave,J.P., Smits,M.A., and Meuwissen,J.H. (1985). Sequential expression of antigens on sexual stages of Plasmodium falciparum accessible to transmission-blocking antibodies in the mosquito. J. Exp. Med. *162*, 1460-1476.

Vervenne,R.A., Dirks,R.W., Ramesar,J., Waters,A.P., and Janse,C.J. (1994). Differential expression in blood stages of the gene coding for the 21-kilodalton surface protein of ookinetes of Plasmodium berghei as detected by RNA in situ hybridisation. Mol. Biochem. Parasitol. *68*, 259-266.

Vinetz,J.M., Valenzuela,J.G., Specht,C.A., Aravind,L., Langer,R.C., Ribeiro,J.M., and Kaslow,D.C. (2000). Chitinases of the avian malaria parasite Plasmodium gallinaceum, a class of enzymes necessary for parasite invasion of the mosquito midgut. J. Biol. Chem. *275*, 10331-10341.

Vlachou,D., Lycett,G., Siden-Kiamos,I., Blass,C., Sinden,R.E., and Louis,C. (2001). Anopheles gambiae laminin interacts with the P25 surface protein of Plasmodium berghei ookinetes. Mol. Biochem. Parasitol. *112*, 229-237.

Volz,J., Muller,H.M., Zdanowicz,A., Kafatos,F.C., and Osta,M.A. (2006). A genetic module regulates the melanization response of Anopheles to Plasmodium. Cell Microbiol. *8*, 1392-1405.

Volz,J., Osta,M.A., Kafatos,F.C., and Muller,H.M. (2005). The roles of two clip domain serine proteases in innate immune responses of the malaria vector Anopheles gambiae. J. Biol. Chem. *280*, 40161-40168.

Voss,T.S., Healer,J., Marty,A.J., Duffy,M.F., Thompson,J.K., Beeson,J.G., Reeder,J.C., Crabb,B.S., and Cowman,A.F. (2006). A var gene promoter controls allelic exclusion of virulence genes in Plasmodium falciparum malaria. Nature *439*, 1004-1008.

Vreden,S.G., Sauerwein,R.W., Verhave,J.P., Van,R.N., Meuwissen,J.H., and van den Broek,M.F. (1993). Kupffer cell elimination enhances development of liver schizonts of Plasmodium berghei in rats. Infect. Immun. *61*, 1936-1939.

Vreden,S.G., van den Broek,M.F., Oettinger,M.C., Verhave,J.P., Meuwissen,J.H., and Sauerwein,R.W. (1992). Cytokines inhibit the development of liver schizonts of the malaria parasite Plasmodium berghei in vivo. Eur. J. Immunol. *22*, 2271-2275.

Vulliamy,T., Beswick,R., Kirwan,M., Marrone,A., Digweed,M., Walne,A., and Dokal,I. (2008). Mutations in the telomerase component NHP2 cause the premature ageing syndrome dyskeratosis congenita. Proc. Natl. Acad. Sci. U. S. A *105*, 8073-8078.

Vulliamy,T., Marrone,A., Goldman,F., Dearlove,A., Bessler,M., Mason,P.J., and Dokal,I. (2001). The RNA component of telomerase is mutated in autosomal dominant dyskeratosis congenita. Nature *413*, 432-435.

Walter,M.F., Bozorgnia,L., Maheshwari,A., and Biessmann,H. (2001). The rate of terminal nucleotide loss from a telomere of the mosquito Anopheles gambiae. Insect Mol. Biol. *10*, 105-110.

Wang,H., Wang,L., Erdjument-Bromage,H., Vidal,M., Tempst,P., Jones,R.S., and Zhang,Y. (2004). Role of histone H2A ubiquitination in Polycomb silencing. Nature *431*, 873-878.

Wang,Z., Gerstein,M., and Snyder,M. (2009). RNA-Seq: a revolutionary tool for transcriptomics. Nat. Rev. Genet. *10*, 57-63.

Warimwe,G.M., Keane,T.M., Fegan,G., Musyoki,J.N., Newton,C.R., Pain,A., Berriman,M., Marsh,K., and Bull,P.C. (2009). Plasmodium falciparum var gene expression is modified by host immunity. Proc. Natl. Acad. Sci. U. S. A *106*, 21801-21806.

Watson,J.D. (1972). Origin of concatemeric T7 DNA. Nat. New Biol. *239*, 197-201.

WEATHERSBY,A.B. (1952). The role of the stomach wall in the exogenous development of Plasmodium gallinaceum as studies by means of haemocoel injections of susceptible and refractory mosquitoes. J. Infect. Dis. *91*, 198-205.

Weinrich,S.L., Pruzan,R., Ma,L., Ouellette,M., Tesmer,V.M., Holt,S.E., Bodnar,A.G., Lichtsteiner,S., Kim,N.W., Trager,J.B., Taylor,R.D., Carlos,R., Andrews,W.H., Wright,W.E., Shay,J.W., Harley,C.B., and Morin,G.B. (1997). Reconstitution of human telomerase with the template RNA component hTR and the catalytic protein subunit hTRT. Nat. Genet. *17*, 498-502.

Wiley,E.A. and Zakian,V.A. (1995). Extra telomeres, but not internal tracts of telomeric DNA, reduce transcriptional repression at Saccharomyces telomeres. Genetics *139*, 67-79.

Witkin,K.L. and Collins,K. (2004). Holoenzyme proteins required for the physiological assembly and activity of telomerase. Genes Dev. *18*, 1107-1118.

Wright,W.E. and Shay,J.W. (1992). Telomere positional effects and the regulation of cellular senescence. Trends Genet. *8*, 193-197.

Wu,W.H., Wu,C.H., Ladurner,A., Mizuguchi,G., Wei,D., Xiao,H., Luk,E., Ranjan,A., and Wu,C. (2009). N terminus of Swr1 binds to histone H2AZ and provides a platform for subunit assembly in the chromatin remodeling complex. J. Biol. Chem. *284*, 6200-6207.

Xie,M., Mosig,A., Qi,X., Li,Y., Stadler,P.F., and Chen,J.J. (2008). Structure and function of the smallest vertebrate telomerase RNA from teleost fish. J. Biol. Chem. *283*, 2049-2059.

Yang,Y., Cimen,H., Han,M.J., Shi,T., Deng,J.H., Koc,H., Palacios,O.M., Montier,L., Bai,Y., Tong,Q., and Koc,E.C. (2010). NAD+-dependent deacetylase SIRT3 regulates mitochondrial protein synthesis by deacetylation of the ribosomal protein MRPL10. J. Biol. Chem. *285*, 7417-7429.

Yang,Y., Fu,W., Chen,J., Olashaw,N., Zhang,X., Nicosia,S.V., Bhalla,K., and Bai,W. (2007). SIRT1 sumoylation regulates its deacetylase activity and cellular response to genotoxic stress. Nat. Cell Biol. *9*, 1253-1262.

YOELI,M., Vanderberg,J., Nawrot,R., and Most,H. (1965). Studies on sporozoite-induced infections of rodent malaria. II. Anopheles stephensi as an experimental vector of Plasmodium berghei. Am. J. Trop. Med. Hyg. *14*, 927-930.

Yu,G.L., Bradley,J.D., Attardi,L.D., and Blackburn,E.H. (1990). In vivo alteration of telomere sequences and senescence caused by mutated Tetrahymena telomerase RNAs. Nature *344*, 126-132.

Yuan,X., Ishibashi,S., Hatakeyama,S., Saito,M., Nakayama,J., Nikaido,R., Haruyama,T., Watanabe,Y., Iwata,H., Iida,M., Sugimura,H., Yamada,N., and Ishikawa,F. (1999). Presence of telomeric G-strand tails in the telomerase catalytic subunit TERT knockout mice. Genes Cells *4*, 563-572.

Yuan,Z. and Seto,E. (2007). A functional link between SIRT1 deacetylase and NBS1 in DNA damage response. Cell Cycle *6*, 2869-2871.

Yuda,M., Sakaida,H., and Chinzei,Y. (1999). Targeted disruption of the plasmodium berghei CTRP gene reveals its essential role in malaria infection of the vector mosquito. J. Exp. Med. *190*, 1711-1716.

Zappulla,D.C. and Cech,T.R. (2004). Yeast telomerase RNA: a flexible scaffold for protein subunits. Proc. Natl. Acad. Sci. U. S. A *101*, 10024-10029.

Zhao,K., Chai,X., and Marmorstein,R. (2004). Structure and substrate binding properties of cobB, a Sir2 homolog protein deacetylase from Escherichia coli. J. Mol. Biol. *337*, 731-741.

Zhao,R., Bodnar,M.S., and Spector,D.L. (2009). Nuclear neighborhoods and gene expression. Curr. Opin. Genet. Dev. *19*, 172-179.

Zhou,Y., Ramachandran,V., Kumar,K.A., Westenberger,S., Refour,P., Zhou,B., Li,F., Young,J.A., Chen,K., Plouffe,D., Henson,K., Nussenzweig,V., Carlton,J., Vinetz,J.M., Duraisingh,M.T., and Winzeler,E.A. (2008). Evidence-based annotation of the malaria parasite's genome using comparative expression profiling. PLoS. One. *3*, e1570.

ZUCKERMAN,A. and YOELI,M. (1954). Age and sex as factors influencing Plasmodium berghei infections in intact and splenectomized rats. J. Infect. Dis. *94*, 225-236.

Appendix

RNA sequencing of *Δsir2a/b* vs. wild type gametocyte samples

Table A1. Top 50 down-regulated genes in the *Δsir2a/b* gametocytes. Highlighted are the genes significantly deregulated in the DOZI^{-} gametocytes.

New ID	Prev systematic ID	Log2 fold change	Fold change	WT tags/gene	*Δsir2a/b* tags/gene	Description
PBANKA_094390	PB104816.00.0	-3.70044	-13.00	13	1	PBANKA_094390 Pb-fam protein 8125965:8128041 forward
PBANKA_072260	PB103795.00.0	-3.21501	-9.29	325	35	PBANKA_072260 Plasmodium exported protein, unknown function 5115168:5116107 forward
PBANKA_100220	PB000891.00.0	-2.32193	-5.00	5	1	Pbs36p p36 protein 8236255:8237673 reverse
PBANKA_021600	PB402983.00.0	-2.16993	-4.50	45	10	PBANKA_021600 BIR protein, pseudogene 1114138:1116059 forward
PBANKA_146570	#N/A	-2	-4.00	4	1	PBANKA_146570 Pb-fam-1 protein, pseudogene 18164579:18165613 reverse
PBANKA_050020	PB500042.00.0	-1.96347	-3.90	117	30	PBANKA_050020 BIR protein 2456207:2457318 reverse
PBANKA_050060	PB101599.00.1	-1.82312	-3.54	46	13	PBANKA_050060 Plasmodium exported protein, unknown function 2474948:2475861 reverse
PBANKA_050090	#N/A	-1.73697	-3.33	10	3	PBANKA_050090 Pb-fam protein 2485773:2487849 reverse
PBANKA_000120	#N/A	-1.58496	-3.00	3	1	PBANKA_000120 Pb-fam-1 protein 18220483:18221157 forward
PBANKA_130020	PB401775.00.0	-1.57901	-2.99	242	81	PBANKA_130020 BIR protein 13228605:13229741 reverse
PBANKA_000640	#N/A	-1.32193	-2.50	5	2	PBANKA_000640 BIR protein, fragment 18430428:18430922 forward
PBANKA_113310	PB100542.00.0	-1.21186	-2.32	1501	648	PBANKA_113310 serine/threonine protein kinase, putative 10936819:10947846 forward
PBANKA_030010	PB200066.00.1	-1.1375	-2.20	11	5	PBANKA_030010 Pb-fam protein 1125921:1128605 reverse
PBANKA_062370	#N/A	-1.1375	-2.20	11	5	PBANKA_062370 Pb-fam protein, fragment 4299326:4301773 forward
PBANKA_100600	PB000740.01.0	-1.1375	-2.20	33	15	PBANKA_100600 conserved Plasmodium protein, unknown function 8396119:8397980 reverse
PBANKA_000280	PB000487.00.0	-1.11548	-2.17	13	6	PBANKA_000280 reticulocyte binding protein, putative, fragment 18284314:18286360 forward
PBANKA_142790	PB000198.03.0	-1.06711	-2.10	44	21	PBANKA_142790 conserved Plasmodium protein, unknown function 16761770:16762084 forward
PBANKA_000460	#N/A	-1	-2.00	14	7	PBANKA_000460 BIR protein, fragment 18364377:18364460 forward
PBANKA_011050	PB105848.00.0	-0.997881	-2.00	2041	1022	PBANKA_011050 leucine-rich repeat protein 5, putative 398038:404879 reverse
PBANKA_122830	PB000759.02.0	-0.997375	-2.00	1098	550	PBANKA_122830 conserved Plasmodium protein, unknown function 12510829:12523956 reverse
PBANKA_145420	PB000959.01.0	-0.980721	-1.97	223	113	PBANKA_145420 conserved Plasmodium protein, unknown function 17763075:17780270 forward
PBANKA_110850	PB000033.03.0	-0.971356	-1.96	2643	1348	PBANKA_110850 conserved Plasmodium protein, unknown function 10020941:10028587 forward
PBANKA_072290	#N/A	-0.954196	-1.94	31	16	PBANKA_072290 BIR protein, pseudogene 5127953:5128999 forward
PBANKA_072280	PB102443.00.0	-0.921997	-1.89	36	19	PBANKA_072280 Plasmodium exported protein, unknown function 5122107:5123028 forward
PBANKA_081750	PB001013.03.0	-0.917538	-1.89	34	18	PBANKA_081750 conserved Plasmodium protein, unknown function 5837179:5838947 reverse

PBANKA_090790	PB000242.01.0	-0.917446	-1.89	6996	3704	PBANKA_090790 conserved Plasmodium protein, unknown function 6785801:6792283 reverse
PBANKA_070130	PB000506.01.0	-0.893085	-1.86	26	14	PBANKA_070130 conserved Plasmodium protein, unknown function 4372550:4373914 forward
PBANKA_000060	PB500044.00.0	-0.893085	-1.86	13	7	PBANKA_000060 BIR protein 18201269:18202314 reverse
PBANKA_133050	PB000947.02.0	-0.893085	-1.86	13	7	PBANKA_133050 conserved Plasmodium protein, unknown function 14450262:14451887 forward
PBANKA_090190	PB000497.00.0	-0.892722	-1.86	4547	2449	PBANKA_090190 tubulin-tyrosine ligase, putative 6578032:6586572 reverse
PBANKA_102310	PB000432.02.0	-0.886542	-1.85	220	119	PBANKA_102310 conserved Plasmodium protein, unknown function 9021867:9026438 forward
PBANKA_114660	PB402997.00.0	-0.879706	-1.84	46	25	PBANKA_114660 Plasmodium exported protein, unknown function 11441266:11442183 forward
PBANKA_010890	PB000307.03.0	-0.877516	-1.84	79	43	PBANKA_010890 conserved Plasmodium protein, unknown function 343565:344138 reverse
PBANKA_050330	PB000784.01.0	-0.873976	-1.83	4875	2660	PBANKA_050330 conserved Plasmodium protein, unknown function 2582865:2587271 reverse
PBANKA_124660	PB403061.00.0	-0.863938	-1.82	91	50	PBANKA_124660 Plasmodium exported protein, unknown function 13201165:13202095 forward
PBANKA_000220	#N/A	-0.847997	-1.80	36	20	PBANKA_000220 reticulocyte binding protein, putative, fragment 18250694:18253770 reverse
PBANKA_080180	PB000303.01.0	-0.83736	-1.79	3000	1679	PBANKA_080180 conserved Plasmodium protein, unknown function 5220988:5229939 forward
PBANKA_040940	PB105688.00.0	-0.83251	-1.78	1186	666	PBANKA_040940 protein kinase, putative 2082184:2090447 forward
PBANKA_070120	PB101523.00.0	-0.830075	-1.78	144	81	PBANKA_070120 conserved Plasmodium protein, unknown function 4364489:4371970 forward
PBANKA_146260	PB000546.02.0	-0.830075	-1.78	32	18	PBANKA_146260 conserved Plasmodium protein, unknown function 18036818:18039031 reverse
PBANKA_136565.1	#N/A	-0.823122	-1.77	23	13	PBANKA_136565.1 Pb-fam-1 protein, pseudogene 15715529:15717005 reverse
PBANKA_060950	PB000464.00.0	-0.812124	-1.76	12273	6990	PBANKA_060950 kinesin-related protein, putative 3751234:3756331 forward
PBANKA_120060	PB000622.02.0	-0.808776	-1.75	254	145	PBANKA_120060 Plasmodium exported protein, unknown function 11470381:11477134 reverse
PBANKA_135340	PB000652.03.0	-0.786293	-1.72	119	69	PSOP7 secreted ookinete protein, putative 15241844:15244282 reverse
PBANKA_141720	PB000157.01.0	-0.78236	-1.72	8383	4874	PBANKA_141720 conserved Plasmodium protein, unknown function 16357783:16360203 reverse
PBANKA_082010	PB000018.00.0	-0.780069	-1.72	419	244	PBANKA_082010 PPPDE peptidase, putative 5927549:5928409 reverse
PBANKA_070560	PB000662.02.0	-0.776925	-1.71	5430	3169	PBANKA_070560 conserved Plasmodium protein, unknown function 4526219:4531004 reverse
PBANKA_052130	PB000684.01.0	-0.772399	-1.71	316	185	PBANKA_052130 zinc finger protein, putative 3234218:3242626 reverse
PBANKA_134250	PB401942.00.0	-0.765595	-1.70	12011	7065	PBANKA_134250 conserved Plasmodium protein, unknown function 14883564:14888129 forward
PBANKA_141120	PB000679.00.0	-0.76457	-1.70	897	528	PBANKA_141120 conserved Plasmodium protein, unknown function 16136891:16142767 reverse

Table A2. Top 50 up-regulated genes in the *Δsir2a/b* gametocytes.

New ID	Prev systematic ID	Log2 fold change	Fold change	WT tags/gene	SIR2dKO tags/gene	Description
PBANKA_001030	#N/A	3	8.00	1	8	PBANKA_001030:exon:3 BIR protein 18518183:18519188 reverse
PBANKA_110030	#N/A	1.73697	3.33	3	10	PBANKA_110030 BIR protein, pseudogene 9727706:9728524 reverse
PBANKA_062390	PB200040.00.0	1.67807	3.20	50	160	PBANKA_062390 BIR protein 4312785:4313872 forward
PBANKA_000040	PB402264.00.0	1.66297	3.17	6	19	PBANKA_000040 Pb-fam protein, fragment 18194955:18196366 reverse
PBANKA_131510	PB000549.02.0	1.44508	2.72	202	550	Sir2b transcriptional regulatory protein sir2b 13843507:13846992 forward
PBANKA_123700	PB300071.00.0	1.42623	2.69	899	2416	PBANKA_123700 S-adenosylmethionine-dependent methyltransferase, putative 12826039:12828107 reverse
PBANKA_140840	PB300794.00.0	1.35364	2.56	18	46	PBANKA_140840 conserved Plasmodium protein, unknown function 16057799:16058410 forward
PBANKA_130210	PB000725.02.0	1.32193	2.50	16	40	PBANKA_130210 50S ribosomal protein L20, putative 13333782:13334307 reverse
PBANKA_113600	PB000284.03.0	1.31774	2.49	69	172	PBANKA_113600 ADP-ribosylation factor, putative 11056164:11056999 forward
PBANKA_101700	PB300290.00.0	1.25634	2.39	18	43	PBANKA_101700 CorA-like Mg2+ transporter protein, putative 8817265:8818701 reverse
PBANKA_030600	PB000214.00.0	1.25572	2.39	972	2321	PBANKA_030600 transmission-blocking target antigen, putative 1329389:1336252 forward
PBANKA_110690	PB001289	1.23133	2.35	46	108	PBANKA_110690 conserved Plasmodium protein, unknown function 9962758:9965268 reverse
PBANKA_061120	PB000028.03.0	1.22571	2.34	62	145	PBANKA_061120 conserved Plasmodium protein, unknown function 3818092:3819738 reverse
PBANKA_130120	PB000767.03.0	1.22239	2.33	3	7	PBANKA_130120 mediator complex subunit 31, putative 13287069:13287473 reverse
PBANKA_112760	#N/A	1.22239	2.33	9	21	PBANKA_112760 conserved Plasmodium protein, unknown function 10734507:10735391 reverse
PBANKA_000470	#N/A	1.22239	2.33	6	14	PBANKA_000470 Pb-fam protein, pseudogene 18367196:18369417 forward
PBANKA_146410	PB102669.00.0	1.20163	2.30	20	46	PBANKA_146410 coronin, putative 18096683:18098555 forward
PBANKA_000150	#N/A	1.16993	2.25	16	36	PBANKA_000150 BIR protein, fragment 18229031:18229120 forward
PBANKA_071140	PB000100.01.0	1.16439	2.24	58	130	PPLP4 perforin like protein 4 4718221:4720269 reverse
PBANKA_123530	#N/A	1.12707	2.18	467	1020	PBANKA_123530 BIS(5'-nucleosyl)-tetraphosphatase (diadenosine tetraphosphatase), putative 12771232:12772384 reverse
PBANKA_110080	PB500009.00.0	1.12553	2.18	33	72	PBANKA_110080 BIR protein 9749310:9750431 reverse
PBANKA_143050	PB001271.02.0	1.11321	2.16	49	106	PBANKA_143050 conserved Plasmodium protein, unknown function 16843606:16844070 forward
PBANKA_141800	PB000809.02.0	1.10069	2.14	83	178	PBANKA_141800 conserved Plasmodium protein, unknown function 16392519:16392743 forward
PBANKA_121210	PB000913.03.0	1.09311	2.13	15	32	PBANKA_121210 conserved Plasmodium protein, unknown function 11878196:11879377 forward
PBANKA_051560	PB300810.00.0	1.08246	2.12	17	36	PBANKA_051560 conserved Plasmodium protein, unknown function 3039137:3040793 reverse
PBANKA_021590	#N/A	1.07039	2.10	10	21	PBANKA_021590 BIR protein, pseudogene 1110891:1112140 forward
PBANKA_031670	#N/A	1.06054	2.09	35	73	PBANKA_031670 Plasmodium exported protein, unknown function 1709465:1710219 forward
PBANKA_091650	#N/A	1.04731	2.07	30	62	PBANKA_091650 conserved Plasmodium protein, unknown function 7150506:7152662 forward

PBANKA_010010	PB108427.00.0	1.04406	2.06	129	266	PBANKA_010010 Pb-fam-1 protein 2964:4509 forward
PBANKA_031130	PB000192.00.0	1.0435	2.06	49	101	PBANKA_031130 conserved Plasmodium protein, unknown function 1518548:1519453 forward
PBANKA_132570	PB001018.01.0	1.0346	2.05	206	422	PBANKA_132570 thioredoxin-like protein, putative 14218840:14219205 reverse
PBANKA_020050	#N/A	1.02975	2.04	48	98	PBANKA_020050 BIR protein, pseudogene 502420:503512 reverse
PBANKA_130580	PB000215.03.0	1.02857	2.04	50	102	PBANKA_130580 transcription factor TFIIH complex subunit Tfb5, putative 13490720:13490923 forward
PBANKA_132210	PB000293.01.0	1.026	2.04	55	112	PBANKA_132210 conserved Plasmodium protein, unknown function 14115068:14116018 reverse
PBANKA_135360	#N/A	1	2.00	2	4	PBANKA_135360 conserved Plasmodium protein, unknown function 15246592:15246768 reverse
PBANKA_120920	PB000040.00.0	1	2.00	89	178	PBANKA_120920 ribosomal protein, putative 11773657:11774523 reverse
PBANKA_103080	PB000952.01.0	1	2.00	20	40	PBANKA_103080 conserved Plasmodium protein, unknown function 9338275:9339936 reverse
PBANKA_080740	PB001065.01.0	1	2.00	14	28	PBANKA_080740 proteasome regulatory protein, putative 5480940:5481614 forward
PBANKA_000510	PB001659.02.0	1	2.00	9	18	PBANKA_000510 reticulocyte binding protein, putative, fragment 18385897:18388411 forward
PBANKA_021570	PB200055.00.0	1	2.00	21	42	PBANKA_021570 BIR protein 1104340:1105457 forward
PBANKA_030050	#N/A	1	2.00	17	34	PBANKA_030050 BIR protein, pseudogene 1142577:1144048 reverse
PBANKA_040020	#N/A	1	2.00	6	12	PBANKA_040020 BIR protein, pseudogene 1735101:1736135 reverse
PBANKA_114650	#N/A	1	2.00	2	4	PBANKA_114650 BIR protein, pseudogene 11434384:11435573 forward
PBANKA_092310	PB108296.00.0	0.991685	1.99	87	173	PBANKA_092310 conserved Plasmodium protein, unknown function 7369949:7371261 forward
PBANKA_142260	#N/A	0.991067	1.99	81	161	Sel3 selenoprotein, putative 16561925:16562944 forward
PBANKA_121640	PB301249.00.0	0.982722	1.98	42	83	PBANKA_121640 RNA triphosphatase, putative 12039988:12041907 forward
PBANKA_060650	#N/A	0.971986	1.96	78	153	PBANKA_060650 50S ribosomal protein L29, putative 3629462:3630055 forward
PBANKA_136190	PB102634.00.0	0.965235	1.95	42	82	PBANKA_136190 nucleoside diphosphate hydrolase, putative 15577867:15578773 reverse
PBANKA_082050	PB000160.03.0	0.965235	1.95	42	82	PBANKA_082050 dolichyl-diphosphooligosaccharide--protein-glycosyltransferase, putative 5938099:5939655 forward
PBANKA_135710	#N/A	0.965082	1.95	230	449	PBANKA_135710 conserved Plasmodium protein, unknown function, pseudogene 15389705:15391952 forward

Fig. A1 Transcript levels in *P. berghei* wild type gametocytes. X axis represents the currently defined 4898 genes. The Y axis shows the number of tags/gene in a $\log_{10}$ scale. The most abundant transcript in wild type gametocytes is *p28* (PBANKA_051490; gene product = 28 kDa ookinete surface protein), the least abundant two transcripts (1 tag/gene) are PBANKA_112800 (annotated as conserved *Plasmodium* protein) and PBANKA_001030 (*bir*).

Table A3. Primers used in the experiments presented in this thesis.

Used for knockouts generation, integration analysis

Primer	Sequence (5' to 3')
190D	CGGGATCCATGCATAAACCGGTGTGTC
191D	CGGGATCCAAGCTTCTGTATTTCCGC
695	AATATTCATAACACACTTTTAAGC
1419	AGATCTGGGACAAGAATGTG
1420	ACTAGTGACAGCCATCTCCATCTG
1662	GATTCATAAATAGTTGGACTTG
2121	CGTCGCCGTCCAGCTCG
2128	GCTAGCGTGACAGGGGGAATGGC
2160	CCGGGCCCGACACAACCGTAAATAGC
2161	CCCAAGCTTGATAAAGCTACATGTCC
2162	CGGGTACCACCCGAATGTCCATG
2163	GCTCTAGACAAAGATCGGACTAGC
2312	CATGGTGAGTACCTTCCC
2313	CACAATTAGGTGAATCCCAAG
3071	TGCTTTGAGGGGTGAGC
3368	AAAAAGCTTCGCTATTATTCCAAATGC
3369	AGAATGCGGCCGCATAATCAAACATAGTACG
3370	AAACTCGAGGGATATGATGATGTTATTTC
3371	AAAGAATTCGATAGAATTGGATAACTC
3435	GTCAGAACATAGAATTAGTTATG
3436	CATGGAATAATTAACAAACTCG
3542	CCCATAAGATATCATTATTTAG
3543	GTTGGATGATATACTTAAATACC
3544	CTAGTTCAGGACTGCAAG
3545	GCAGTTCTTATAGCAAGAG
L307C	GCTTAATTCTTTTCGAGCTC
L886	GGAAGATCTATGGTTGGTTCGCTAAACTGCATCG
L887	GGAAGATCTTTAATCATTCTTCTCATATACTTC
L1511	CGATTCACCAGCTCTGAC

Used for qPCR for cDNA presence in the analysed RNA-seq gametocytes samples

Primer	Sequence (5' to 3')
4834	TGAGGTAACCCCAACTGAAGGA
4835	CATCAATGGCGTGTTTTCCC
4836	GGAGGTATGACAAGAATGCCAA
4837	CTTGTATAGCAGCGCCTAATGC
4838	CCATGGCCATTTATAAGTCATGATG
4839	GGCATTTTTGATTGACCGATTAAC
4840	TTTCAGAGCCTGTGTCTCAACA
4841	CATTGGTTGGACTGTCTTGGC
5171	GGGGATTGGTTTTGACGTTTTTGCG
5172	AAGCATTAAATAAAGCGAATACATCCTTAT
5173	AATCTCGACCCCCTATCTAGCG
5174	CGAAGTGCCTACCAATTT TTGG
5175	CTTATGCTGCTGCACCTGTTG
5176	CCCATGAATCCATCTTCCTCTT
5177	ACCCACCATTAGGAAGATTTGC
5178	AGCTGAGACAGCTCCAGGTTCT
5179	AGCAATGCCATTCAATAGCACC
5180	TTTGCTCATCCCCGCTGTT

Acknowledgments

The research leading to these results has received funding from MalParTraining, an FP6-funded Marie Curie Action under contract number MEST-CT-2005-020492.

I would like to express my gratitude to all my supervisors:

Prof. Andy Waters for his guidance, insights, limitless patience, understanding and open-mindedness, ability to motivate and inspire me. Thank you for your kindness, trust and generosity.

Dr. Chris Janse for his guidance, devotion, insightful advice, and his immeasurable energy that has propelled both the project and my own scientific development.

Prof. Artur Scherf for his guidance, power of motivation, and for the opportunity to work on this project.

Prof. Michael Lanzer for his guidance and scientific supervision.

Thank you to all the collaborators.

Thank you to all the members of the C.J. Janse lab (Leiden University Medical Centre, Leiden, the Netherlands) for all the advice and for making my stay in the Netherlands deeply memorable.

Thank you to all the members of the A.P. Waters lab (Glasgow Biomedical Research Centre, University of Glasgow, Scotland, UK) for making me feel part of the group for the short period of time, and for all their scientific advice.

I would like to thank all the MalParTraining and Antimal PhD students who have made the time of my PhD one of the best periods of all.

Last but not least, I would like to thank my family, my brother Wojciech, and my parents Anna and Jerzy, who have put an enormous amount of energy into giving me the best possibilities. Thank you for your continuous support and faith.